Distinct circadian mechanisms govern rhythms in cardiac electrophysiology and susceptibility to arrhythmia

A thesis submitted to the University of Manchester for the degree of Doctor of Philosophy (PhD)
in the Faculty of Biology, Medicine and Health

2021

Edward A Hayter

School of Medical Sciences

Division of Diabetes, Endocrinology and Gastroenterology

Table of contents

Word count: 59484

List of Figures

List of Tables

List of abbreviations

Abbreviation	Definition
ACTH	Adrenocorticotropic hormone
ATP	Adenosine triphosphate
AV	Atrioventricular
AVP	Arginine vasopressin
BVT	Bidirectional ventricular tachycardia
CK1ε/δ	Casein kinase 1 ε/δ
CPVT	Catecholaminergic polymorphic ventricular tachycardia
Cre	Cre recombinase
CRH	corticotrophin releasing hormone
DAD	Delayed afterdepolarisation
DMH	Dorsomedial hypothalamus
EAD	Early afterdepolarisation
ECG	Electrocardiogram
FDR	False discovery rate
GABA	Gamma-aminobutyric acid
GHT	Geniculohypothalamic tract
GnRH	Gonadotrophin releasing hormone
GRP	Gastrin releasing peptide
HCN	Hyperpolarisation-activated cyclic nucleotide-gated
HPA	Hypothalamus-pituitary-adrenal
HR	Heart rate
HRV	Heart rate variability
IGL	Intergeniculate leaflet
ipRGC	Intrinsically photosensitive retinal ganglion cell
LD	Light/dark
LF:HF	Low to high frequency power ratio
LH	Lateral hypothalamus
mRNA	messenger ribonucleic acid
NCX	Sodium-calcium exchanger
NTS	Nucleus tractus solitarius
PCA	Principal component analysis
POA	Pre-optic area
PRC	Phase response curve
PVC	Premature ventricular complex
PVN	Paraventricular nucleus
RGC	Retinal ganglion cell
RHT	Retinohypothalamic tract
RNA	Ribonucleic acid
RORE	retinoic acid-related orphan receptor response element
rrHRV	Relative RR interval HRV
RyR	ryanodine receptor
SA	Sinoatrial
SCF	Skp, cullin, F-box containing complex

SCN	Suprachiasmatic Nucleus
SDNN	Standard deviation of valid RR intervals
SPZ	Subparaventricular zone
SR	Sarcoplasmic reticulum
TRH	Thyroid releasing hormone
TSD	Total sleep deprivation
TTFL	Transcriptional/translational feedback loop
VIP	Vasoactive intestinal polypeptide
VT	Ventricular tachycardia
αMHC	α myosin heavy chain

Abstract

In mammals, cardiac functions, such as heart rate, exhibit pronounced daily rhythms to facilitate the changing energy demands of the body across the day and night. Moreover, potentially fatal cardiac arrhythmias are more likely to occur at certain times of day, with many types of arrhythmia occurring most frequently in the morning hours. Importantly, fluctuations in heart activity are not simply determined by changes in our behavioural state, with recent evidence revealing an important role for the circadian timing system (our internal body clock). The circadian system is hierarchical in nature, orchestrated by a dominant clock within the suprachiasmatic nuclei (SCN) in the hypothalamus, yet influential molecular clocks are located in cells throughout the body, including muscle and pacing cells of the heart (cardiomyocytes). Evidence suggests a role for the cardiomyocyte clock in dictating rhythms in metabolic processes and aspects of ionic conduction. However, it remains unclear how timing information from central (SCN) and local tissue clocks is integrated with changes in behavioural state to impart daily rhythms in electrical properties of the heart and arrhythmia susceptibility; here lies the central objective of this PhD.

To examine circadian dynamics in cardiac electrophysiology, we first developed a robust method for automated analysis of longitudinal electrocardiographic (ECG) recordings. Using this approach, we demonstrate in two tightly controlled human laboratory studies that activity at key sites of the cardiac conduction system, namely the sinoatrial (SA) and atrioventricular (AV) nodes, are strongly rhythmic, yet are differentially responsive to behavioural and sleep states. This renders them susceptible to misalignment in response to abrupt changes in behavioural routine. We go on to show that mice exhibit similar conduction dynamics, and define the relative contributions of behavioural state, and central and peripheral clocks in dictating rhythms in electrophysiology. We show that the balance of circadian inputs to the SA and AV nodes differ; while rhythms in SA nodal pacemaking are driven by central and local clocks, and behavioural state, rhythms in AV nodal delay are dictated principally by central clocks via parasympathetic signalling. Remarkably, we observed a time-of-day dependent susceptibility to ventricular tachycardia, and demonstrate that cardiomyocyte clocks drive rhythms in excitability at the cost of increased arrhythmia susceptibility at the start of the active phase. This work reveals fundamental new understanding regarding circadian influences over cardiac physiology.

Declaration

I, Edward Hayter, declare that no portion of the work referred to in this thesis has been submitted in support of an application for another degree or qualification of this or any other university or other institute of learning.

Copyright Statement

i. The author of this thesis (including any appendices and/or schedules to this thesis) owns certain copyright or related rights in it (the "Copyright") and s/he has given the University of Manchester certain rights to use such Copyright, including for administrative purposes.

ii. Copies of this thesis, either in full or in extracts and whether in hard or electronic copy, may be made **only** in accordance with the Copyright, Designs and Patents Act 1988 (as amended) and regulations issued under it or, where appropriate, in accordance with licensing agreements which the University has from time to time. This page must form part of any such copies made.

iii. The ownership of certain Copyright, patents, designs, trademarks and other intellectual property (the "Intellectual Property") and any reproductions of copyright works in the thesis, for example graphs and tables ("Reproductions"), which may be described in this thesis, may not be owned by the author and may be owned by third parties. Such Intellectual Property and Reproductions cannot and must not be made available for use without the prior written permission of the owner(s) of the relevant Intellectual Property and/or Reproductions

iv. Further information on the conditions under which disclosure, publication and commercialisation of this thesis, the Copyright and any Intellectual Property and/or Reproductions described in it may take place is available in the University IP Policy (see http://documents.manchester.ac.uk/DocuInfo.aspx?DocID=2442 0), in any relevant Thesis restriction declarations deposited in the University Library, the University Library's regulations (see http://www.library.manchester.ac.uk/about/regulations/) and in the University's policy on Presentation of Theses.

Acknowledgements

I have been fortunate enough to be surrounded by individuals who have provided much guidance, support and seemingly endless patience, without whom this PhD work and thesis would not have been possible. I am thankful to all those who have helped me along the way, both academically and personally, and to those who have been there for me through the peaks and troughs of the last four years.

First and foremost I wish to express an enormous gratitude to my supervisor David Bechtold, who not only guided me through scientific research, but has provided me with a great deal of life and career advice. David has been an excellent role model, both scientifically and as a supervisor, for which I am grateful. I would also like to thank my co-supervisors, Tim Brown and Andrew Trafford, who have always been there to advise me and provide insight and expertise. Likewise, I thank my advisors, Holly Shiels and Hugh Piggins, who have been there to offer support when required.

An immense thanks is due to my wonderful wife Sarah, who has been relentlessly supportive in my PhD endeavours. I would have never made it this far without her.

I would also like to thank my parents who, despite not living in the academic world, have read, and proofread, everything I've written, and provided me with the skills and opportunities in life to make it here. Also to my parents in law, sisters, brothers in law, nieces and nephews for their support.

Finally I would like to thank my friends and colleagues, who not only have made this PhD such an enjoyable experience, but provided emotional support and advice to help me through: Josh, Sarika, Dave, Mike, Becca, Abi, Liz, Nichola, Nicola and the rest of the Bechtold, Brown and Gibbs labs.

I would also like to acknowledge the Biotechnology and Biological Sciences Research Council, who provided funding for this PhD.

Chapter 1: Introduction

Due to the rotation of the earth, most organisms on the planet are subject to daily oscillations in external influences, including light, temperature, and nutrient availability. On account of these changing conditions across the day, organisms have evolved a remarkably accurate endogenous biological clock with a period of approximately 24hrs, collectively referred to as the circadian system (from *circa* meaning "about" and *dies* meaning "day"). The endogenous clock synchronises with external timing cues and influences almost all aspects of physiology, from sleep/wake state in humans to photosynthesis in plants (Takahashi *et al.*, 2008).

The earliest accounts of circadian processes originate at least 2300 years ago when a ship's captain serving under Alexander the Great, named Androsthenes, described the daily rhythm of leaf movements of the tamarind tree, *Tamarindus indica* (Phillips, 2005). In 1729, a French biologist de Mairan recorded daily rhythms in leaf movement of the *Mimosa* plant that persist even in constant darkness (Gardner *et al.*, 2006). Despite this evidence of endogenous biological timing, it was not until 1918 that it was demonstrated that animals could maintain 24 hour rhythms in locomotor activity without need for external influence of light and temperature cycles, and 1935 when an endogenous rhythm in activity was first demonstrated in *Drosophila Melanogaster,* and attributed to the circadian timing system (Bruce and Pittendrigh, 1957; Singh *et al.*, 2012). From 1966 into the early 1980s, Jürgen Aschoff and Rütger Weaver performed experiments on students in an underground bunker, again void of cues, to demonstrate the endogenous 24hr circadian rhythm in a range of physiological parameters in humans (Aschoff, 1965; Wirz-Justice *et al.*, 2005). Since then, there has been a great advance of scientific discovery in the field, with circadian rhythms having been identified in almost all species, across a wide range of physiological processes and involved in many aspects of health and wellbeing.

The circadian system in mammals is hierarchical in nature and is governed by the Suprachiasmatic Nuclei (SCN), a compact structure in the anterior hypothalamus which provides both robust timing and entrainment to environmental rhythms via external timing cues, such as light/dark (LD) cycles. In turn, SCN activity dictates gross rhythms in physiology such as sleep/wake state and body temperature. Virtually every cell in the body

possesses the machinery for circadian timekeeping and are kept in alignment by the SCN. On a molecular level, circadian timing is driven by coupled transcriptional-translational feedback loops in which core 'clock' genes are expressed rhythmically to regulate expression of circadian-associated genes and thus impact physiology. A prime example of how the circadian system exerts influence over physiology is in the heart. The rhythmicity of cardiac physiology and organ function across the day is a product of behavioural patterns, and central clock and local tissue clock activity (Scheer *et al.*, 2001; Young *et al.*, 2014; Hayter *et al.*, 2021a). How central and local clock function is integrated to control cardiac physiology currently remains unclear, and this is the primary focus of this PhD.

1.1 Mammalian circadian organisation

1.1.1 The Suprachiasmatic Nuclei

Seated in the anteroventral hypothalamus, just above the optic chiasm and either side of the third ventricle, lie the SCN which together comprise the orchestrating circadian pacemaker of the mammalian body (Welsh *et al.*, 2010). Early lesioning studies established the SCN as the principal pacemaker of the body. For example, SCN lesioned rats exhibit arrhythmic patterns of locomotor activity and drinking behaviour, and display a loss of normal corticosterone rhythms (Moore and Eichler, 1972; Stephen and Irving, 1972). Remarkably, implantation of foetal SCN tissue to previously lesioned animals can restore behavioural rhythms, or produce behavioural rhythms in genetically arrhythmic animals. Indeed, rescued rhythms after SCN tissue implantation present with the circadian characteristics (period) of the donor animal, rather than that shown previously by the recipient animal (Lehman *et al.*, 1987; Ralph *et al.*, 1990; Sujino *et al.*, 2003).

In mice, the SCN consist of approximately 20000 neurons, which are distributed anatomically into ventral 'core' and dorsal 'shell' regions. The core region receives neural input directly from the retina, allowing for a link to the outside environment. The core region feeds densely into the shell which in turn feeds out to peripheral oscillators to ultimately coordinate phasing around the body (Leak *et al.*, 1999; Abrahamson and Moore, 2001; Evans *et al.*, 2015). Most SCN neurons are GABAergic with few glutamatergic cells, and many are colocalised with other neurotransmitters including vasoactive intestinal polypeptide (VIP), gastrin releasing peptide (GRP) and arginine vasopressin (AVP) (Moore

and Speh, 1993; Cui *et al.*, 2001). Across the SCN each of these neuropeptides displays a non-uniform, complex distribution, resulting in nuclei which are remarkably heterogeneous (Abrahamson and Moore, 2001). It is this heterogeneity (and heterogeneities in electrical properties across the SCN) that likely underpin the ability of the SCN to control multiple physiological process across different temporal phases simultaneously.

Neurons of the SCN display remarkably strong intracellular coupling via interneural electrical communication to form a cohesive network. SCN neurons display rhythms when dispersed individually *in vitro*, but when part of a greater network they couple tightly to synchronise and produce robust, coherent circadian oscillations at the tissue level (Webb *et al.*, 2009). A core feature of the SCN is that under the right *in vitro* culture conditions, cycling can be maintained almost indefinitely. Unlike the SCN, peripheral oscillators quickly lose amplitude and phase coherence between cells after a few days in culture (Patton and Hastings, 2018). The core region of the SCN has a vital role in maintaining synchrony within the SCN. Specific legions of the core, but not the shell, result in loss of physiological rhythms (e.g. body temperature, locomotor activity) and in vitro slices that have been bisected into core and shell regions retain synchrony only in the core (Silver *et al.*, 1996; Yamaguchi *et al.*, 2003; Kriegsfeld *et al.*, 2004). VIP is the predominant neurotransmitter in the core region and is crucial for SCN coupling. Mice that lack VIP or associated receptor VIPR2 have weak behavioural rhythms and SCN slices from these animals display marked desynchrony between cells (Harmar *et al.*, 2002; Colwell *et al.*, 2003; Cutler *et al.*, 2003; Brown *et al.*, 2007). Similarly, application of VIP to SCN slices or microinjection into the SCN *in vivo* results in phase shifts similar to those induced by light (Piggins *et al.*, 1995; Watanabe *et al.*, 2000). While VIP is the dominant entraining neurotransmitter within the SCN, other neurotransmitters such as GRP, neurotensin and GABA may also contribute to, or perform a modulatory role in SCN coordination and timekeeping (Welsh *et al.*, 2010).

1.1.2 Circadian entrainment

In order for the SCN to accurately synchronise with the changing conditions across the day it must be responsive to the external environment. Under constant conditions, behavioural rhythms remain cyclic with a period dictated by the animal's endogenous clock, a process known as 'free-running' (**Fig 1.1A**). Individual circadian period can vary largely, but on average is slightly longer than 24hrs in humans, and slightly shorter than 24hrs in normal

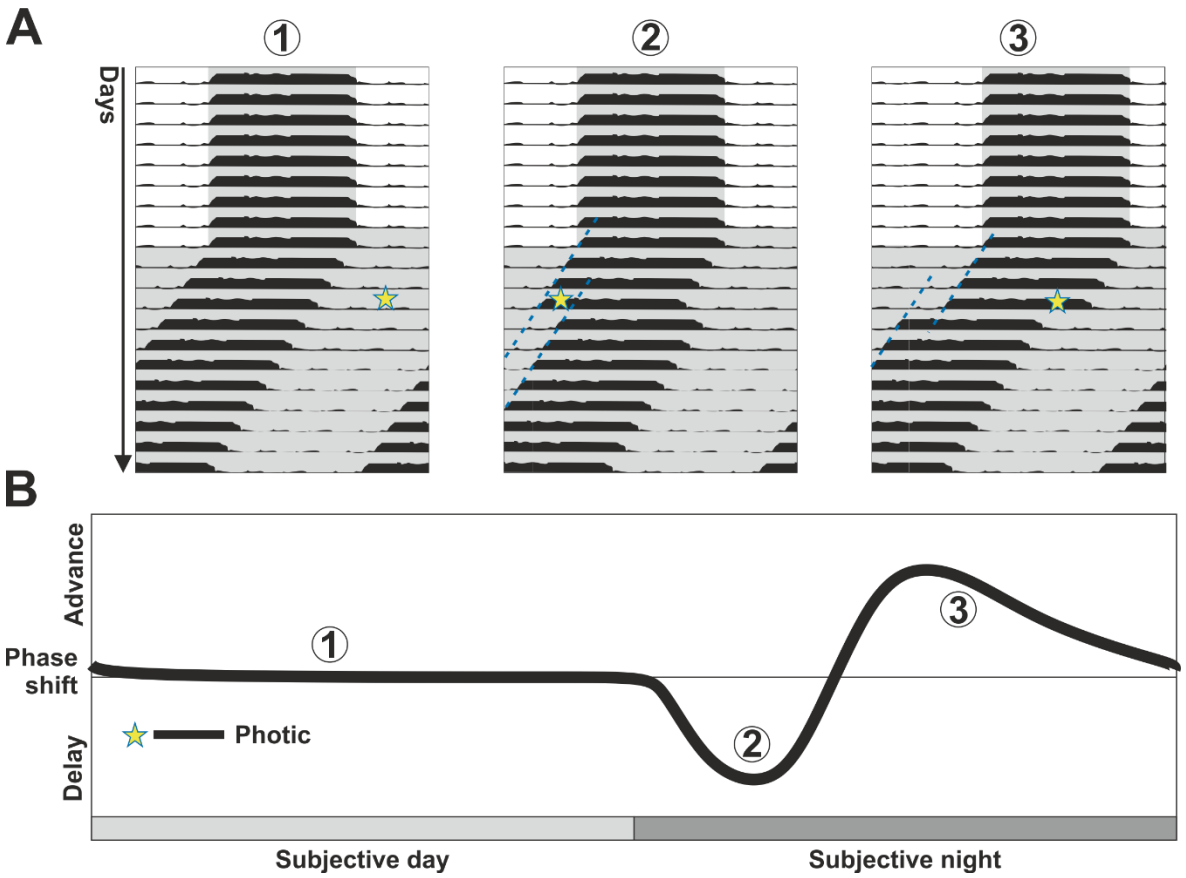

Figure 1.1. Circadian entrainment and free running shifts. A. Actogram schematics of mouse locomotor activity during light-dark and constant darkness conditions, and shifts resulting from photic cues (e.g. light pulse) given at different times of day. Each row represents a day and grey bars indicate darkness. Inset yellow stars indicate timing of light pulse and blue dashed lines indicate trend of locomotor activity onset pre and post light pulse. Numbers correspond to timing of light pulse in **B. B.** Phase response curve for photic cues. A photic cue given during early subjective night (i.e. near the start of locomotor activity onset) results in a phase delay (2) and at the end of the subjective night results in a phase advance (3). Figure adapted from (Golombek and Rosenstein, 2010).

laboratory mice. To maintain synchrony with the environment the circadian clock in the SCN receives external cues known as zeitgebers ('time-givers' in German). The dominant zeitgeber in most species including mammals is light, but other cues such as rhythms in feeding, exercise or even social interaction can provide timing cues in to the circadian system. Under stable, 24hr conditions these zeitgebers provide minor adjustments to the circadian clock, akin to manual daily adjustments made to a poorly timed watch to maintain accurate time (Golombek and Rosenstein, 2010). Photic cues reach the SCN through the retina and have a different impact on the clock dependent on the time of day provided (**Fig 1.1A, B**). In darkness, a pulse of light given during the subjective day has little impact on the clock. A light pulse given in what would be the early night causes a delayed phase in nocturnal animals and a pulse given at the end of the night advances the clock. The magnitude and direction of phase response can be plotted as a function of time of light pulse in a phase response curve (PRC; **Fig 1.1B**). PRCs can vary largely between animals, with clear differences between diurnal and nocturnal animals. It is this adaptive mechanism by which the endogenous clock can accurately entrain to external cues.

Upon a major shift in LD cycle, such as experienced following a transatlantic flight, the circadian system becomes transiently misaligned with the environment. During this 'jetlag' period, the SCN receives photic cues at times which elicit a phase shift. Accordingly, each day the phasing of the SCN moves closer to that of the environment, eventually becoming aligned with the LD cycle. This process usually takes many days, with the SCN shifting by approximately 1hr per day, although this is dependent on the intensity of the photic stimuli. Depending on the magnitude of the phase shift, the SCN can advance or delay its phase to entrain. Under DD conditions, some non-photic cues, such as feeding, can also entrain the SCN, though as a much weaker entraining stimulus (Golombek and Rosenstein, 2010).

1.1.3 SCN inputs

The SCN receives information from the outside world through light entering the eye and being absorbed by photoreceptors in the retina, principally done by 'classic' rod and cone photoreception which plays a major role in image forming visual responses. Another critical cell in the retina are retinal ganglion cells (RGCs), which integrate signals from rod and cone photoreceptors before projecting to the brain, forming the optic tracts. A small subset of RGCs (1-2%) also express the photopigment melanopsin, rendering them intrinsically

photosensitive (ipRGCs), with maximal sensitivity to light on the blue end of the spectrum (Berson *et al.*, 2002; Hattar *et al.*, 2002). ipRGCs are critical to the circadian effects of light on the SCN (e.g. entrainment). Axons of ipRGCs form the retinohypothalamic tract (RHT) and predominantly coexpress glutamate and PACAP. They project to the SCN and other brain regions including the intergeniculate leaflet (IGL), a centre for integration of photic and non-photic cues, and the olivary pretectal nucleus, the brain region responsible for the pupillary light reflex (Hannibal, 2002; Gooley *et al.*, 2003; Hattar *et al.*, 2006). The RHT is the primary avenue by which the SCN receives information from the outside world. As ipRGCs integrate signals from rods and cones, this information is also relayed to the SCN. Rods are particularly sensitive to low light levels and provide scotopic excitation to the SCN, while cones respond differently to light of different wavelengths, thus providing information on the spectral composition of the light (Hatori *et al.*, 2008). The SCN primarily uses the brightness of light (signalled by ipRGCs) to establish time of day, but can also use cone-dependent spectral information to aid entrainment to the changing spectra of light across the day (Walmsley *et al.*, 2015).

The SCN also receive mono- and poly-synaptic projections from an array of other brain structures (Pickard, 1982; Moga and Moore, 1997; Krout *et al.*, 2002). It is thought that these connections provide non-photic information on physiological state to the SCN, such as satiety and body temperature (Hastings *et al.*, 1997; Abe *et al.*, 2007; Refinetti, 2010). While many of the connections to the SCN are sparse and poorly understood, there exists a robust innervation from the IGL, via the geniculohypothalamic tract (GHT; **Fig 1.2**) (Moore and Card, 1994). Ablation of the GHT abolishes the ability for mice to entrain to forced or scheduled wheel running, arousal stimuli and to benzodiazepine-induced phase shifts, suggesting that the IGL is an integrator and relay of circadian information (Johnson *et al.*, 1988; Biello *et al.*, 1994; Janik and Mrosovsky, 1994; Hastings *et al.*, 1997; Marchant *et al.*, 1997). Together the SCN and IGL form the centre of a vast, interconnected network of brain regions, likely centred on circadian control by photic and non-photic cues (Morin, 2013).

1.1.4 SCN outputs

The SCN exerts rhythmic control over peripheral physiology by direct neural projections to modulate the endocrine system and the autonomic nervous system (Meyer-Bernstein *et al.*, 1999; Buijs *et al.*, 2003). Neural projections from the SCN primarily target hypothalamic

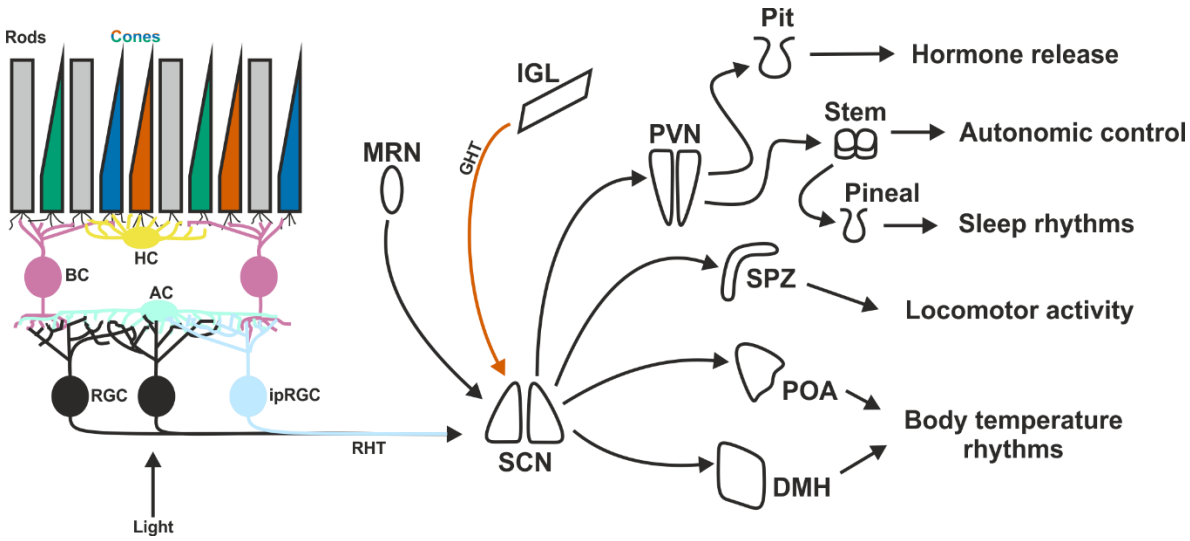

Figure 1.2. Inputs and outputs of the SCN. The primary input to the SCN is from the retina in which light is absorbed by rod, cone and ipRGC photoreceptors. Pre-processing of signals in the retina occurs through bipolar cells (BC), horizontal cells (HC) and amacrine cells (AC) before RGC compile the information to send to the SCN via the retinohypothalamic tract (RHT) (and other brain regions through the optic tract). The SCN also receives input from the IGL down the geniculohypothalamic tract (GHT), likely signalling broad circadian information, and from the median raphe nucleus (MRN), likely providing information about circadian phase. The SCN projects to a host of hypothalamic regions to dictate rhythmicity across physiology including the subparaventricular zone (SPZ) to control locomotor activity, preoptic area (POA) and dorsomedial hypothalamus (DMH) to dictate rhythms in body temperature and the paraventricular nucleus (PVN) to ultimately control hormone release, dictate autonomic control across the body and promote sleep through downstream projections.

regions involved in homeostatic control such as the paraventricular (PVN), subparaventricular (SPZ), pre-optic (POA), dorsomedial (DMH) and lateral (LH) nuclei (**Fig 1.2**) (Morin, 2013). The SCN directly drives rhythms in body temperature through projections to thermoregulatory centres such as the POA and DMH, locomotor activity through projections to the SPZ and sleep/wake cycles through projections to the PVN to regulate melatonin secretion from the pineal gland, and through projections to the POA and LH (Kramer *et al.*, 2001; Moore, 2007; Clapham, 2012). To directly influence endocrine release, the SCN projects to number of hormone-secreting neurons including gonadotrophin releasing hormone (GnRH) in the POA, corticotrophin releasing hormone (CRH) and thyroid releasing hormone (TRH) in the PVN to influence daily rhythms in hormone release (Kalsbeek and Buijs, 2002; Kalsbeek *et al.*, 2006). Within the PVN there are also subpopulations of neurons that project to sympathetic and parasympathetic motor neurons, providing a potent mechanism through which the SCN influence autonomic control of physiology across day and night (Buijs *et al.*, 2013). For example, this pathway (SCN-PVN-autonomic nervous system) has been shown to influence corticosterone secretion from the adrenal gland, plasma glucose homeostasis and heart rate (HR) (Kalsbeek *et al.*, 2004; Paul *et al.*, 2020). In practise, these systems (neural control of gross physiology, endocrine release and autonomic signalling) act in parallel, providing coordinated control of rhythmic behaviour and physiology. An elegant example of this is through the hypothalamus-pituitary-adrenal (HPA) axis in which the SCN drives CRH release from the PVN, which drives adrenocorticotropic hormone (ACTH) release from the pituitary gland which results in release of corticosterone from the adrenal gland. Corticosterone then feeds back to regulate the release of CRH and ACTH. Meanwhile, the SCN also regulates the adrenal sensitivity to ACTH via autonomic signalling, highlighting how the SCN exerts control over glucocorticoid release in two ways: neuroendocrine control and autonomic signalling. Glucocorticoid signalling is also itself a major internal zeitgeber, acting on peripheral clocks (Ishida *et al.*, 2005; Oster *et al.*, 2006; Son *et al.*, 2008; Astiz *et al.*, 2019; Paul and Brown, 2019).

1.1.5 Peripheral clock synchronisation

The circadian clocks around the body can be thought of as an orchestra, with clocks in peripheral tissues acting as individual musicians and the SCN as the conductor. The

conductor ensures the orchestra remain in synchrony to perform the symphony. Without a conductor, the musicians play at their own tempo, resulting in a cacophony. The SCN orchestrates major behavioural and physiological rhythms (e.g. sleep/wake cycle, body temperature) as well as synchronises peripheral tissue clocks to ensure proper rhythmic functioning of the body (Astiz *et al.*, 2019). The SCN synchronises peripheral clocks in a variety of methods including signalling by both branches of the autonomic nervous system, driving rhythms in circulating hormones such as glucocorticoids (GC), and dictating rhythms in body temperature (**Fig 1.3**) (Mohawk *et al.*, 2012). Furthermore, the SCN coordinate rhythmic and circadian function in many organ systems and peripheral tissues indirectly by driving rhythms in gross behavioural processes such as locomotor activity and feeding. Feeding is a strong, non-photic signal to peripheral tissue clocks, which can act independently from the SCN, possibly through insulin signalling (Crosby *et al.*, 2019). An imposed feeding schedule can entrain peripheral clocks while independent of the SCN. Food entrainment of peripheral tissues can occur in the absence of the SCN, while in animals with an intact SCN, the phasing of the SCN remains temporally locked to the LD cycle while peripheral tissues entrain to the feeding schedule (Damiola *et al.*, 2000; Stokkan *et al.*, 2001; Pezuk *et al.*, 2010).

1.1.6 Molecular clock architecture

At a cellular level, circadian rhythms are generated by an endogenous cellular transcriptional/translational feedback loop (TTFL) which runs with a period of approximately 24hrs (**Fig 1.4**). While many components are now known to be involved in the generation of these rhythms, the mammalian clock is centred on a few core genes and their corresponding proteins. Briefly, transcription factors BMAL1 and CLOCK form heterodimers that drive the activation of *Per(1-3)* and *Cry(1-2)* genes, by binding to E-box regulatory elements upstream of the transcription starts sites; this forms the positive arm of the feedback loop (Yoo *et al.*, 2005). PER and CRY accumulate in the cytoplasm and heterodimerise before translocating back into the nucleus where they inhibit CLOCK and BMAL1 activity; thus comprising the negative arm of the feedback loop. This in turn leads to a decrease in transcription of *Per* and *Cry* and renewal of the cycle. The speed of the molecular clock (i.e. period or tau) is dictated by the cycle rate of this feedback loop, and is therefore heavily influenced by synthesis and degradation rates of its key proteins. PER and

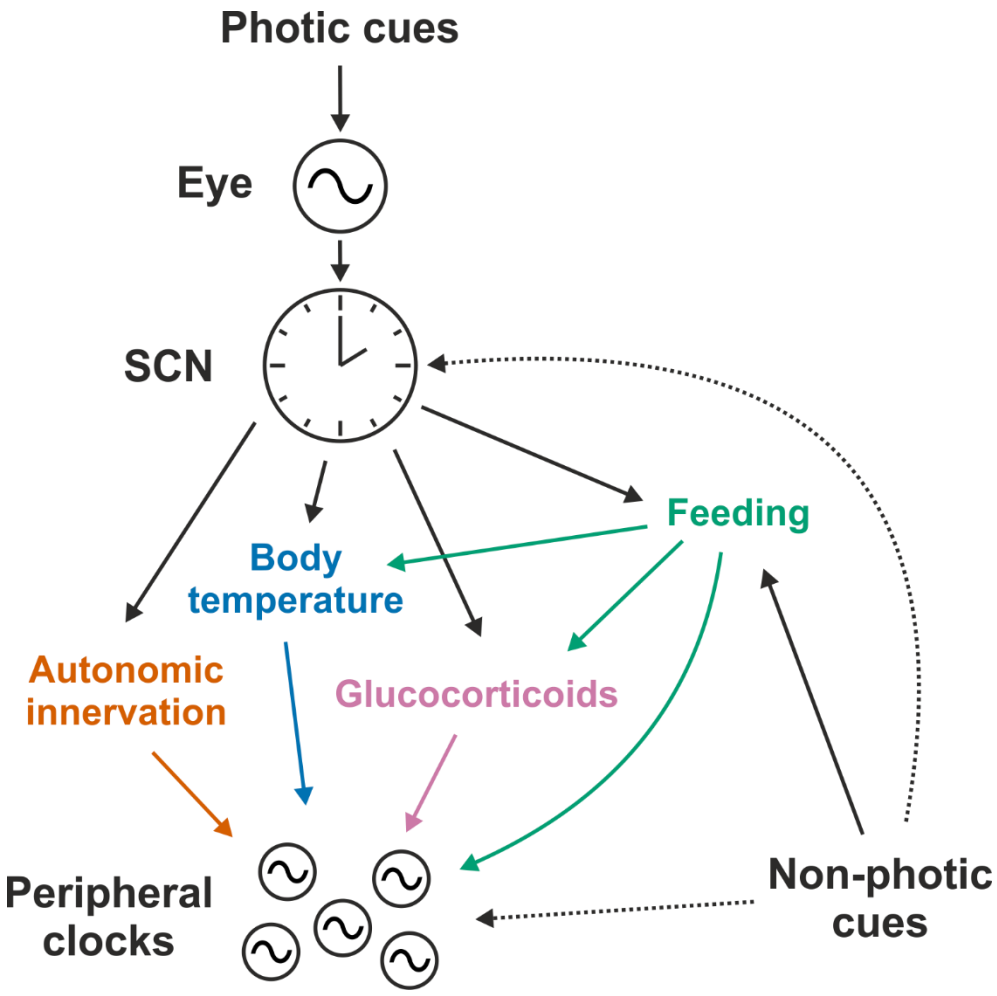

Figure 1.3. Hierarchical organisation of the mammalian circadian system. Photic cues entrain the SCN to the external environment via the eyes. The SCN then synchronises peripheral clocks via numerous avenues including autonomic innervation, GC secretion and dictating rhythms in body temperature. Feeding, an example of a non-photic cue, can entrain peripheral clocks independent of the SCN. The ability of other non-photic cues to entrain peripheral clocks have not yet been investigated. Non-photic cues can also entrain the SCN, although only in conditions where an LD cycle is not present. Figure adapted from (Mohawk *et al.*, 2012).

CRY protein stability is governed by post-transcriptional regulation. PER is targeted for degradation via phosphorylation by casein kinase (CK1ε/δ) which promotes polyubiquitination by the $SCF^{\beta\text{-}TrCP}$ E3 ubiquitin ligase complex, which in turn results in 26S proteasomal degradation (Akashi *et al.*, 2002; Reischl *et al.*, 2007). Similarly, CRY is phosphorylated by AMPK, ubiquitinated by the SCF^{FBXL3} E3 complex and degraded by the 26S proteasome (Lamia *et al.*, 2009; Takahashi, 2017). This degradation leads to disinhibition of BMAL1 and CLOCK, allowing the feedback cycle to continue (King and Takahashi, 2000; Eide *et al.*, 2005; Hastings *et al.*, 2008). A secondary feedback loop accompaniments the primary loop by direct regulation of *Bmal1* expression. Specifically, BMAL1:CLOCK heterodimers drive transcription of nuclear receptors *Reverb(α-β)* and *Ror(α-γ),* which in turn bind to retinoic acid-related orphan receptor response elements (ROREs) in the *Bmal1* promotor. Competitive binding of RORs and REVERBs causes transcriptional activation and repression of *Bmal1* respectively (Ko and Takahashi, 2006; Takahashi *et al.*, 2008). A third transcriptional loop involves BMAL1:CLOCK driven expression of DBP, HLF and TEF, which all in turn bind D-boxes alongside the repressor NFIL3 (driven itself by RORs/REVERBs) to regulate the expression of *Ror*, *Reverb* and *Per* genes (Mitsui *et al.*, 2001). The molecular clock imparts rhythmicity to physiology directly by controlling the expression of downstream clock controlled genes. Together, these loops can drive rhythmic expression of thousands of downstream genes with a range of phase profiles, dependent on the combination of *cis*-regulatory elements upstream of target genes (**Fig 1.4**) (Ueda *et al.*, 2005).

The molecular clockwork harbours a degree of redundancy, where removal of some clock genes does not result in abolition of rhythmic behaviour. For example, in *Clock* knockout animals, the *Clock* paralogue *Npas2* can compensate to retain a functional molecular clock (DeBruyne *et al.*, 2006, 2007; Landgraf *et al.*, 2016). *Bmal1* is the only clock component essential for clock function. As such, loss of *Bmal1* abolishes all rhythms in the molecular clockwork and results in behavioural arrhythmicity *in vivo* (Bunger *et al.*, 2000). Rhythms can also be disrupted by deletion of core genes and compensatory analogues (e.g. $Cry1^{-/-}$ $Cry2^{-/-}$ or $Per1^{-/-}Per2^{-/-}$) or by a mutation in the clock gene ($Clock^{\Delta 19/\Delta 19}$), resulting in non-functional BMAL1:CLOCK dimers which do not allow NPAS2 to compensate (Vitaterna *et al.*, 1994; Herzog *et al.*, 1998; Van Der Horst *et al.*, 1999; DeBruyne *et al.*, 2006).

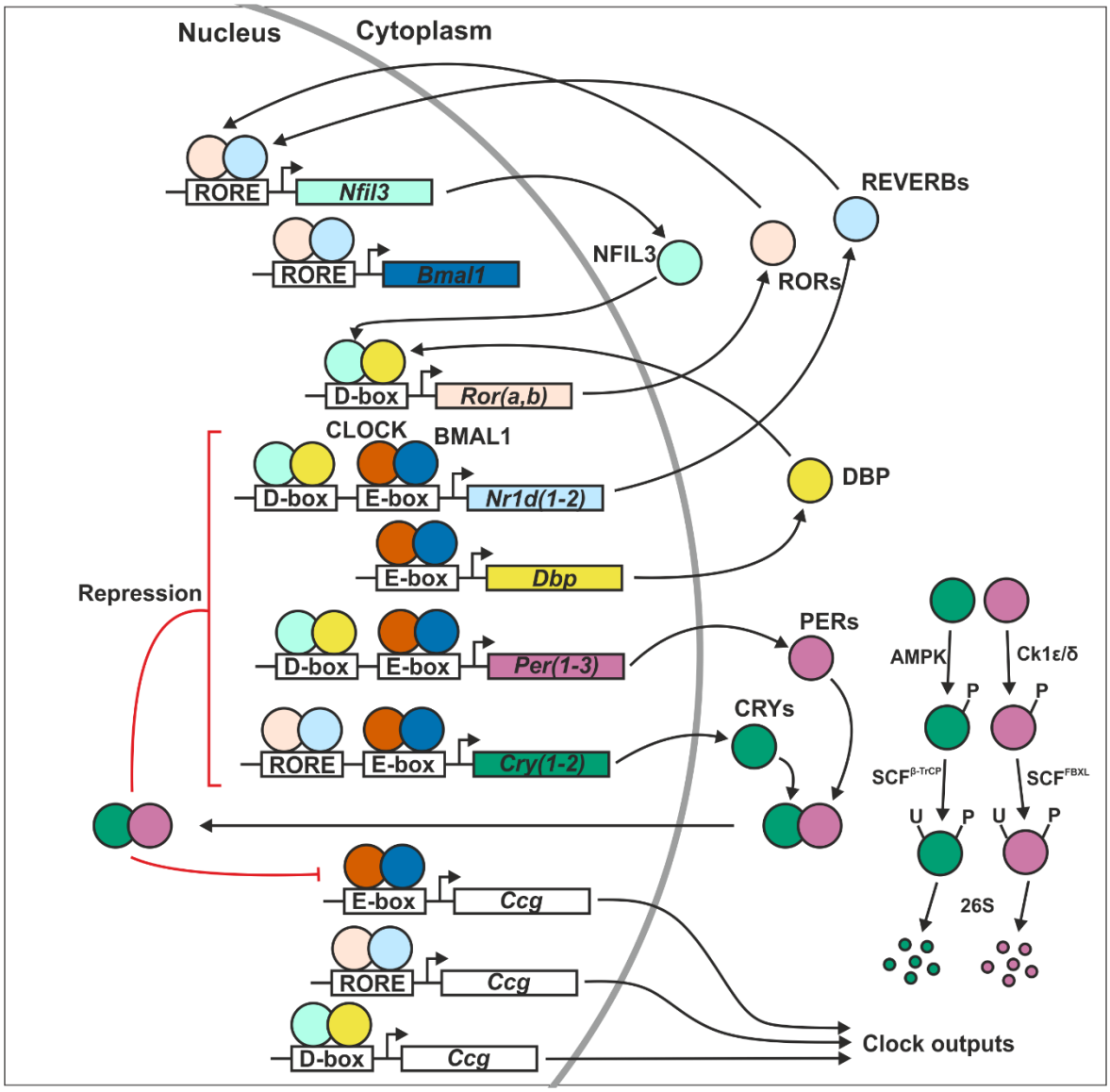

Figure 1.4. Molecular circadian architecture in the mammalian cell. At the core of the molecular circadian clock exists a transcriptional/translational feedback loop which runs with a period of approximate 24hrs. BMAL1 and CLOCK drives the expression of PERs and CRYs which in turn repress BMAL1 and CLOCK activity. PER and CRY stability, and thus the speed of the clock, is governed in part by E3 ubiquitin ligase pathways. BMAL1 and CLOCK also drive the expression of REVERBs (encoded by *NR1d1/2*) which functionally represses the transcription of *Nfil3* and *Bmal1*. NFIL3 and DBP (also driven by BMAL1 and CLOCK) serve to balance transcription of *Rorα/β*, as NFIL3 represses the function of DBP. RORs drive transcription and compete with REVERBs. Together these three loops form the core of the circadian clock, and can each drive rhythmic transcription of downstream clock controlled genes by binding to E-boxes, D-boxes and ROREs in regulatory regions. Figure adapted from (Takahashi, 2017).

1.1.7 Circadian oscillators in peripheral tissues

In the mid-twentieth century, multiple studies found that explanted tissues in culture still displayed daily rhythms in activity, including peristalsis in intestines (Bünning, 1958), actinomycin sensitivity in adrenal glands (Andrews and Shiotsuka, 1970), oxygen consumption in the liver (Langner and Rensing, 1972) and firing rate of cultured heart cells (Tharp, 1965). We now know that these rhythms are due to the molecular circadian architecture which is present in almost all cells in the body. This was 're-discovered' by Ueli Schibler's group in 1998 when they showed rhythmic mRNA expression and protein levels of core clock genes in isolated fibroblasts can be induced by a serum shock (Balsalobre *et al.*, 1998). Rhythms in clock gene expression of *ex-vivo* tissue can now be measured using bioluminescent reporters, such as the *Period1:Luciferase* transgene, or PERIOD2:LUCIFERASE fusion protein. As such, many tissues from animals with these reporters, when cultured, display rhythms in bioluminescence (Yamazaki *et al.*, 2000; Yoo *et al.*, 2004). The period of molecular oscillations can vary largely between tissues and rhythms decay over a few days, unlike the SCN.

The functional significance of clocks in peripheral tissues has now be investigated in many studies using tissue selective clock manipulations. *Bmal1* deletion in various tissues has highlighted profound influence of peripheral clocks in tissue function. For example, retinal *Bmal1* deletion results in loss of daily rhythm in electroretinogram b-wave amplitude and timing (Storch *et al.*, 2007), liver-specific deletion results in hypoglycaemia during fasting (Lamia *et al.*, 2008), Pancreatic-specific deletion causes impaired glucose tolerance and hyperglycemia (Marcheva *et al.*, 2010) and cardiomyocyte-specific deletion can result in age-related cardiomyopathy (Young *et al.*, 2014; Ingle *et al.*, 2015).

1.2 The mammalian cardiovascular system

1.2.1 Overview of heart anatomy

The heart is a vital organ which pumps blood around the body through vessels to distribute oxygen and nutrients and collect metabolic waste for expulsion, such as carbon dioxide through the lungs. The developed mammalian heart consists of 4 chambers: the left and right atria and ventricles (**Fig 1.5**). Oxygenated blood flows from the lungs into the left atrium via the pulmonary veins and is then pumped into the left ventricle. The left ventricle

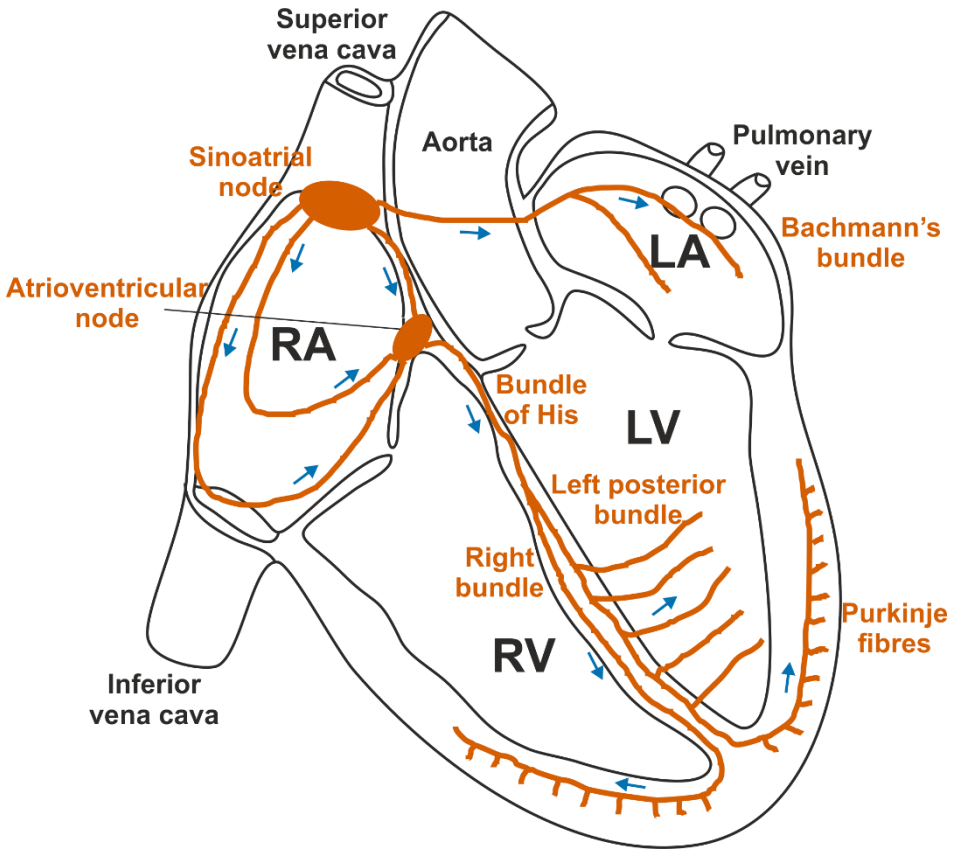

Figure 1.5. Anatomy of the human heart and cardiac conduction system. Oxygenated blood flows into the left atria (LA) through pulmonary veins and into the left ventricle (LV), before being pumped out of the heart to the body via the aorta. Deoxygenated blood returns to the right atria (RA) through superior and inferior venae cavae and is pumped into the right ventricle (RV) and out through the pulmonary artery to the lungs (not shown for clarity). Orange shows the cardiac conduction system, with direction of impulse shown with blue arrows. The electrical impulse originated at the SA node, travels through the atria (causing atrial contraction and blood to pump into the ventricles) to the AV node and down into the ventricles through the bundle of His, left and right bundles and Purkinje fibres resulting in ventricular contraction and pumping of blood to the body.

is surrounded by a thick myocardial wall required to generate sufficient force to deliver oxygenated blood around the body via the aorta. In the aorta also originate the coronary arteries which supply the heart with oxygenated blood. As oxygenated blood travels around the body it travels through arterioles, where oxygen diffuses from the bloodstream into nearby cells for utilisation and metabolic waste is collected for removal. Deoxygenated blood then drains through the venous system into the right atrium by the superior and inferior venae cavae before being pumped into the right ventricle. Finally, the pulmonary artery takes blood from the right ventricle to the lungs where gaseous exchange in alveoli replaces carbon dioxide for expulsion with oxygen. For this pumping process to occur, the heart creates an electrical impulse that propagates around the parts of the heart resulting in muscular contraction and pumping of blood.

In order for blood to be pumped into and out of the heart efficiently, contraction of heart chambers must be timed optimally. This is the function of the cardiac conduction system (**Fig 1.5**). An electrical impulse which initiates the heart beat (a contraction of first atria and then ventricles) is generated in the pace making sinoatrial (SA) node, which is seated in the upper wall of the right atrium between the opening of the superior vena cava and the crista terminalis; a well-defined crescent shaped fibromuscular ridge formed during development (Boyett *et al.*, 2000; Sánchez-Quintana *et al.*, 2002). The electrical impulse then propagates through the anterior, middle and posterior tracts driving depolarisation and contraction of the right atria, and progresses to the atrioventricular (AV) node, located as the base of the interatrial septum (Widran and Lev, 1951). Simultaneously, the left atrium depolarises via innervation of the conducting Bachmann's bundle which projects from right to left atria (James, 1963). At the AV node, the electrical impulse is slowed considerably to allow sufficient time for blood to flow from the atria into the ventricles. After this delay the impulse from the AV node to the bundle of His, then splits into right and left bundle branches, propagating down the interventricular septum to the apex of the heart. Here, Purkinje fibres conduct the impulse around the right and left ventricles, resulting in coordinated depolarisation and contraction of the ventricles from apex to base (James and Sherf, 1971). After contraction and pumping of blood out of the heart, the ventricles relax and repolarise ready to be filled again.

Electrical impulses are generated spontaneously at the SA node at a rate of ~100 beats per minute (bpm) in humans and SA pacemaker activity is modulated heavily by the sympathetic and parasympathetic branches of the autonomic nervous system which increase and decrease HR respectively. The autonomic nervous system is tonically active, and modulates signals in response to a number of factors including stress, exercise and blood pressure. As such, resting HR varies significantly between individuals, but is usually around 60-100bpm in humans and 500-700bpm in mice (van Dijk *et al.*, 1991; Janssen *et al.*, 2016). While displaying considerably different resting HRs, humans and mice have remarkably similar hearts with the same chamber and conduction system layout, albeit considerably smaller in mice.

1.2.2 The sinoatrial node

The SA node is a particularly complex structure which is responsible for spontaneously firing action potentials to generate the heartbeat. It is an electrophysiologically and anatomically heterogeneous structure with a unique set of ion channels that together are responsible for spontaneous action potential generation and pace making.

Anatomically, the SA node is a diffuse structure with a central region responsible for pacemaking and a 'paranodal' area forming a bridge between the SA node and surrounding atrial myocardium which primarily differs in its inability to spontaneously depolarise. The core SA of the node comprises small, irregularly organised myocytes surrounded by a mass of highly fibrous connective tissue, reflective of its lessened need for contraction compared to myocardium. The paranodal region is an intermediate between SA node and atrial myocardium, comprising both SA and atrial myocytes packed together in less connective tissue and displaying a pattern of ion channel expression somewhere between the two areas (Chandler *et al.*, 2009). The SA node receives blood supply from the sinoatrial nodal artery which passes through the core region (though this can vary largely between individuals), and drains directly into the right atrium via venules (Anderson *et al.*, 1979).

The cardiac action potential varies in morphology across species and throughout the regions of the heart due to differences in ion currents and ion channel expression (**Fig 1.6, Table 1.1**). The SA node is capable of spontaneous pace making due to a 'pacemaker potential' which is not present in myocardium. The pacemaker potential is generated by a

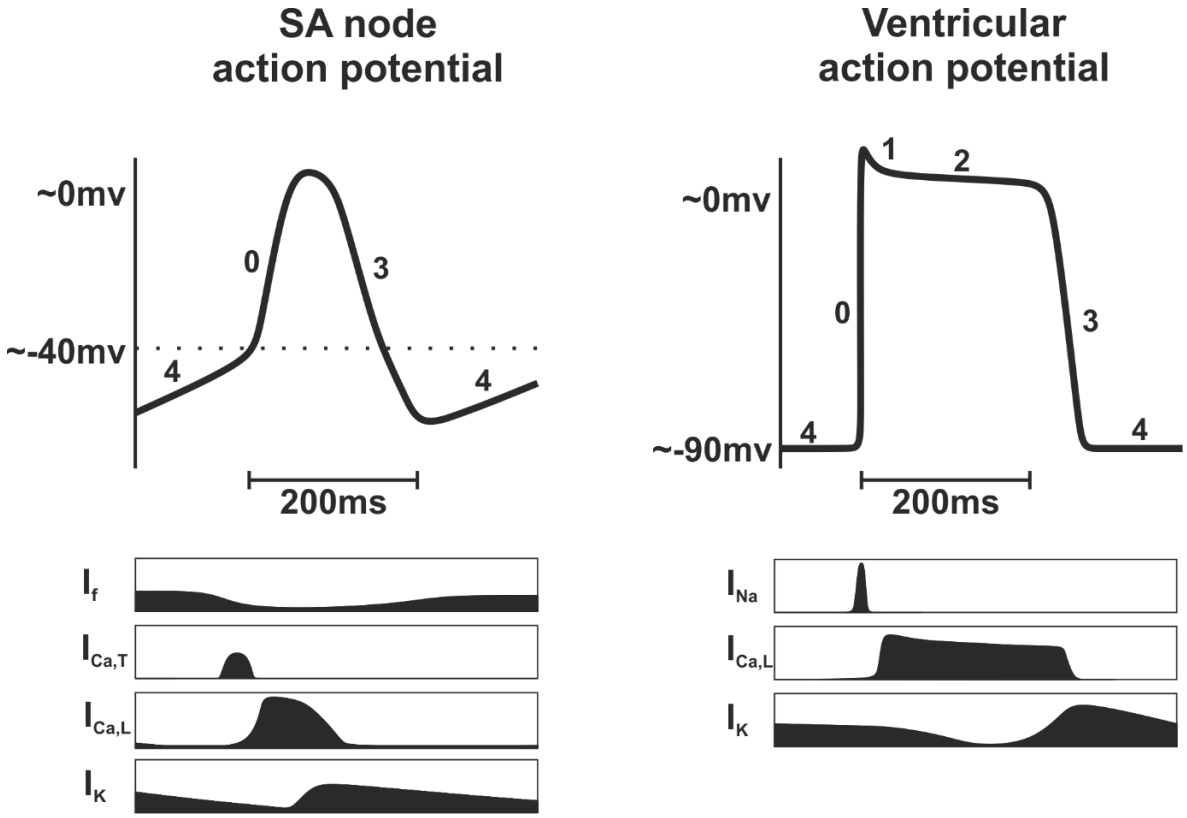

Figure 1.6. Differences between SA nodal and ventricular action potentials. SA nodal cells spontaneously gradually depolarise, predominantly because of the 'funny' current. When a threshold is reached, Ca^{2+} influx results in faster (but not rapid) depolarisation. K^+ efflux returns the action potential to baseline where the pacemaker potential starts to depolarise again. In contrast, the ventricular action potential remains stable until an electrical impulse reaches the cell at which point Na^+ channels open to allow rapid influx of Na^+ and thus depolarisation. Ca^{2+} influx then maintains a plateau in the action potential before K^+ efflux again hyperpolarises the membrane. Action potential phases are indicated by the inset numbers. The main ion currents are indicated below the action potential waveforms.

Current	Description	AP Phase	Gene	Protein
I_{Na}	Sodium current	0	*Scn5a*	$Na_v1.5$
$I_{Ca,L}$	L-type calcium current	2	*Cacna1c*	$Ca_v1.2$
$I_{Ca,T}$	T-type calcium current	2	*Cacna1g*	$Ca_v3.1/3.2$
$I_{to,f}$	Transient outward current, fast	1	*Kcnd2* *Kcnd3*	$K_v4.2$ $K_v4.3$
$I_{to,s}$	Transient outward current, slow	1	*Kcna4* *Kcna7* *Kcnc4*	$K_v1.4$ $K_v1.7$ $K_v3.4$
I_{Kur}	Delayed rectifier, ultra-rapid	1	*Kcna5* *Kcnc1*	$K_v1.5$ $K_v3.1$
I_{Kr}	Delayed rectifier, fast	3	*Kcnh2*	HERG
I_{Ks}	Delayed rectifier, slow	3	*Kcnq1*	KVLQT1
I_{K1}	Inward rectifier	3 & 4	*Kcnj2* *Kcnj12*	$K_{ir}2.1$ $K_{ir}2.2$
I_{KATP}	ADP activated K^+ current	1 & 2	*Kcnj11*	$K_{ir}6.2$
I_{KAch}	Muscarinic-gated K^+ current	4	*Kcnj3* *Kcnj5*	$K_{ir}3.1$ $K_{ir}3.4$
I_{KP}	Background current	0-4	*Kcnk1* *Kcnk6* *Kcnk3* *Kcnk4*	TWK-1 TWK-2 TASK-1 TRAAK
I_F	Pacemaker current	4	*Hcn2* *Hcn4*	HCN2 HCN4

Table 1.1. Currents and genes that make up the human cardiac action potential. Table displays all currents involved in generating the cardiac action potential. Some currents are not present across all components of the heart and thus the differences in action potential morphology across the heart. Figure adapted from (Grant, 2009).

slow influx of positively charged ions, resulting in gradual depolarisation from a hyperpolarised state until a threshold membrane potential is reached and an action potential is fired (Chandler *et al.*, 2009). The predominant drivers of the pacemaker potential are hyperpolarisation-activated cyclic nucleotide-gated (HCN) channels which allow for the influx of Na^+ and K^+ ions, resulting in a 'funny current', I_f, so called due to its mixed permeability, slow kinetics and activation by hyperpolarisation (Difrancesco, 2010). Another contributor to the pacemaker potential is known as the calcium clock and results from spontaneous release of Ca^{2+} form the sarcoplasmic reticulum within the cytoplasm via the ryanodine receptor (RYR2). In turn the increase in Ca^{2+} results in activation of the sodium-calcium exchanger (NCX) on the cell surface, removing 1 calcium ion from the cell in exchange for 3 Na^+ ions, further depolarising the cell (Joung *et al.*, 2009). During this time T-type calcium channels also open, allowing for an influx of Ca^{2+} ($I_{Ca,T}$) and further depolarisation. When membrane potential hits the threshold voltage, L-type calcium channels open resulting in further calcium influx to the cell ($I_{Ca,L}$). It is this L-type-dependent calcium current which drives the main depolarisation of the SA action potential. Upon maximal depolarisation, L-type calcium channels close and potassium channels open, resulting in fast ($I_{K,r}$) and slow ($I_{K,s}$) components of the delayed rectifier current which repolarise the myocyte. I_k decays after repolarisation, allowing for depolarisation by the pacemaker current and the cycle repeats (Monfredi *et al.*, 2010).

An essential feature of SA nodal conduction is that it must be able to drive depolarisation of tissue much larger than itself, without being influenced by electrical signals coming from the neighbouring atria. Mathematical modelling showed that the only way this was possible is by cells within the SA node being poorly coupled to one another compared to the nearby myocardium to buffer against large changes in potential difference (Joyner and van Capelle, 1986). Consistent with this hypothesis, the electrical conduction across the SA is slow (~0.05m/s, compared to ~1m/s in atrial myocardium) and the space constraint (the distance at which a signal decays propagating out from a current injection) is low in rabbit SA node compared to atrial myocardium (Boyett *et al.*, 2000). Gap junctions are proteins that are made up of linked hemichannels (connexins) which physically join neighbouring cells, creating an electrically coupled link. The distribution of connexins varies across the heart, which may be one factor in the weaker cellular coupling in the SA node. For example,

there are significantly fewer gap junctions on the surface of SA nodal cells compared to atrial cardiomyocytes, and Cx43, a connexin that is abundant in the working myocardium and has a high conductance, is expressed only in low levels in the SA node (Verheule and Kaese, 2013).

1.2.3 Cardiac myocardium

In contrast to myocytes located within the conduction system, the function of the myocytes located within the atrial and ventricular myocardium is to contract efficiently and collectively to pump blood around the body. Cardiomyocytes fuse together to form long fibres joined by intercalated discs, which contain gap junctions to allow for electrical coupling between cells, and propagation of the electrical impulse across myocardium (Kleber and Saffitz, 2014). Cardiomyocytes contain fibres of actin and myosin arranged in parallel, which together comprise myofibrils. Upon excitation, actin and myosin fibres slide past one another resulting in contraction. The energy (adenosine triphosphate, ATP) required for such contraction is provided by high numbers of mitochondria in the cytoplasm (Cretoiu *et al.*, 2018; Sweeney and Hammers, 2018). In gross organisation, cardiac muscle fibres run in parallel and wrap around the heart in a figure of 8 pattern so contraction does not simply occur in one dimension, but rather longitudinally, radially and in a twisting motion to maximise the volume of blood pumped in each heartbeat (Stöhr *et al.*, 2016). Myocardium also contains a large proportion of fibroblasts (although significantly less than are found in the conduction system) which are responsible for creating and maintaining the extracellular matrix which supports the cardiomyocytes. While fibroblasts are not excitable cells per se they have also been implicated in modulating cardiac conduction (Fahrenbach *et al.*, 2007; Thomsen and Calloe, 2016). Ventricular and atrial myocytes are broadly very similar in structure, although ventricular myocytes are larger and together form a significantly thicker muscle wall compared to the atria (Walden *et al.*, 2009).

The myocardial action potential differs from the SA action potential (**Fig 1.6**). In non-pacemaker cells the resting membrane potential does not spontaneously depolarise and instead remains at a steady state due to the balanced influx and efflux of ions between membrane leakage and active pumps maintaining ion gradients. Primarily, gradual spontaneous depolarisation present in pacemaking cells is opposed by an inward rectifier K^+ current ($I_{k,1}$), realised by $K_{ir}2$ channels, resulting in a stable resting membrane potential

(**Table 1.1**). Upon electrical activation, voltage-gates Na^+ channels open and allow for rapid influx of Na^+ ions (I_{Na}) and depolarisation of the membrane. Sodium channels are then quickly inactivated by closing of the intracellular inactivation gate. Transient outward potassium channels (I_{to1}) open temporarily, resulting in K^+ efflux and a small 'notch' in the action potential waveform. In the next phase many channels are involved, resulting in influx and efflux of different ions, ultimately resulting in no major change in membrane potential and a 'plateau' in the action potential, not observed in the SA action potential. The initial depolarisation drives opening of delayed rectifier channels (K^+ efflux), and L-type calcium channels (Ca^{2+} influx). Ca^{2+} binds to RYR2 receptors on the sarcoplasmic reticulum, driving release of further Ca^{2+}, and activates Ca^{2+}-dependent Cl^- channels (I_{to2}), resulting in Cl^- influx. NCX antiporters are also opened due to the increased Ca^{2+} concentration, alongside Na^+/K^+-ATPase due to increased Na^+. Finally, repolarisation occurs as a result of closure of L-type Ca^{2+} channels while slow delayed rectified ($I_{K,S}$) remain open, leading to a net efflux in K^+ and repolarisation of the membrane potential. This initial repolarisation leads to opening of rapid delayed rectifier ($I_{K,R}$) and inward rectifier (I_{k1}) channels and thus further repolarisation (Grunnet, 2010). These channels close once a sufficiently repolarised state has been reached, with the exception of I_{K1} which remains open to maintain resting membrane potential.

1.2.4 The atrioventricular node

The AV node resides within the atrial septum in the triangle formed by the ostium of the coronary sinus, tricuspid valve and tendon of Todaro, named the triangle of Koch (George *et al.*, 2017). The function of the AV node is to slow down the pace of the electrical conduction to allow time for blood to flow from the atria to the ventricles. The conduction speed across the AV node is significantly slower than surrounding myocardium because of poor electrical coupling due to fewer and smaller (and thus lower conductance) gap junctions (Temple *et al.*, 2013). The compact core of the AV node is distinct from the surrounding atrial myocardium, with smaller, less dense interweaving cells and low expression of the gap junction Cx43. In contrast, the neighbouring lower nodal bundle expresses higher levels of Cx43. Both of these AV nodal regions connect to the penetrating bundle which continues down to the bundle of His, but display markedly different conduction speeds, providing alternative pathways to propagate into the penetrating

bundle (Markowitz and Lerman, 2018). Similarly to the SA node, the AV node is surrounded by transitional cells which act as intermediates between nodal cells and atrial myocardial cells.

Cells in the AV node also have the ability to spontaneously depolarise like those in the SA node, likely attributed to the I_f current mediated by HCN channels and the calcium clock. The spontaneous pacing from AV node cells is however slower than that of the SA node, meaning under normal conditions they simply conduct at the frequency of the SA node. If the SA node fails however, the AV node can take over pacing responsibility, albeit at a slower rate. As such, the action potential from AV cells is similar to that of SA node due to this spontaneous depolarisation capability and lack of Na^+ channels resulting in a slower upswing compared to myocardial cells.

The AV node displays a unique property known as detrimental conduction: as the frequency that the node is stimulated increases, the conduction speed across the node decreases. Detrimental conduction is vital for stopping rapid conduction into the ventricle during fast atrial rhythms such as atrial fibrillation (Patterson and Scherlag, 2002).

1.2.5 The His-Purkinje system

The role of the His-Purkinje system is to propagate the electrical impulse quickly through the ventricular myocardium to drive coordinated contraction. The His bundle extends from the AV node down the interventricular septum where it bifurcates into left and right bundle branches. The left bundle divides again into anterior and posterior fascicles which subdivide into Purkinje fibres which sprawl across the left ventricular myocardium to innervate the muscle. Towards the bottom of the interventricular septum the left and right bundles further branch off into Purkinje fibres which turn at the apex before propagating into the outer ventricular myocardium. Together the Purkinje fibres form a dense network across the whole endocardium, with fibres merging and bifurcating to allow full coverage of the ventricular muscle (Vigmond and Stuyvers, 2016). Each fibre is a combination of multiple Purkinje cells running in parallel surrounded by a collagen sheath to insulate the conductive cells from the surrounding myocardium (Ono *et al.*, 2009).

Purkinje fibres are specialised for rapid conduction. Like other cardiac cells they connect to each other by gap junctions but Purkinje fibres exhibit a significantly larger proportion of

Cx40, the largest gap junction with highest conduction (Kanter *et al.*, 1993). Furthermore, they exhibit lower intracellular Ca^{2+} buffering capacity to allow faster Ca^{2+} conduction (Boyden *et al.*, 2010). Purkinje fibres also express many voltage-gated sodium channels which aids rapid conduction. Like the SA and AV nodes, Purkinje fibres can spontaneously depolarise, but at a rate slower than the rest of the conduction system (Dobrzynski *et al.*, 2013).

1.2.6 Excitation-contraction coupling

The process by which a cardiac action potential results in contraction is called excitation-contraction coupling and is heavily dependent on Ca^{2+} transport. In ventricular myocytes, during depolarisation Ca^{2+} enters the cell through L-type calcium channels which then triggers mass Ca^{2+} release from the sarcoplasmic reticulum (SR) (**Fig 1.7**) (Venetucci *et al.*, 2008). SR Ca^{2+} release is governed by ryanodine receptors (RyR), which form large organised structures of >100 receptors. These structures also recruit a variety of regulatory proteins to the junctional complex including calmodulin which regulates RyR function and FK-506 which couples neighbouring RyR tetramers. These complex arrays coordinate to allow large coordinated release of Ca^{2+} from the SR. Calcium can also be spontaneously released from the SR by smaller RyR clusters (6-20 units), resulting in calcium spikes, thousands of which are coordinated during electrically induced depolarisation. The rapid rise in cytoplasmic Ca^{2+} then drives binding to myofilament protein Troponin C to drive contraction before dissociating to stop contraction when cytoplasmic Ca^{2+} falls as predominantly SR Ca^{2+}-ATPases pump Ca^{2+} back into the SR (**Fig 1.7**). Phospholamban regulates Ca^{2+} transport into the SR by inhibiting the SR Ca^{2+}-ATPase. Phosphorylation of phospholamban by protein kinase A or calmodulin kinase II reduces this inhibition resulting in faster Ca^{2+} uptake into the SR and greater sarcoplasmic Ca^{2+} concentrations (Brittsan and Kranias, 2000). Higher SR Ca^{2+} concentrations results in a greater Ca^{2+} release following depolarisation, and therefore increases myofilament contraction. In contrast, myofilament Ca^{2+} sensitivity can be reduced by increased phosphate and Mg^{2+} concentrations, as well as by increased sympathetic signalling. Mg^{2+} may also have added effects by modulating SR Ca^{2+}-ATPase activity (Bers, 2002; Michailova *et al.*, 2004; Eisner *et al.*, 2017).

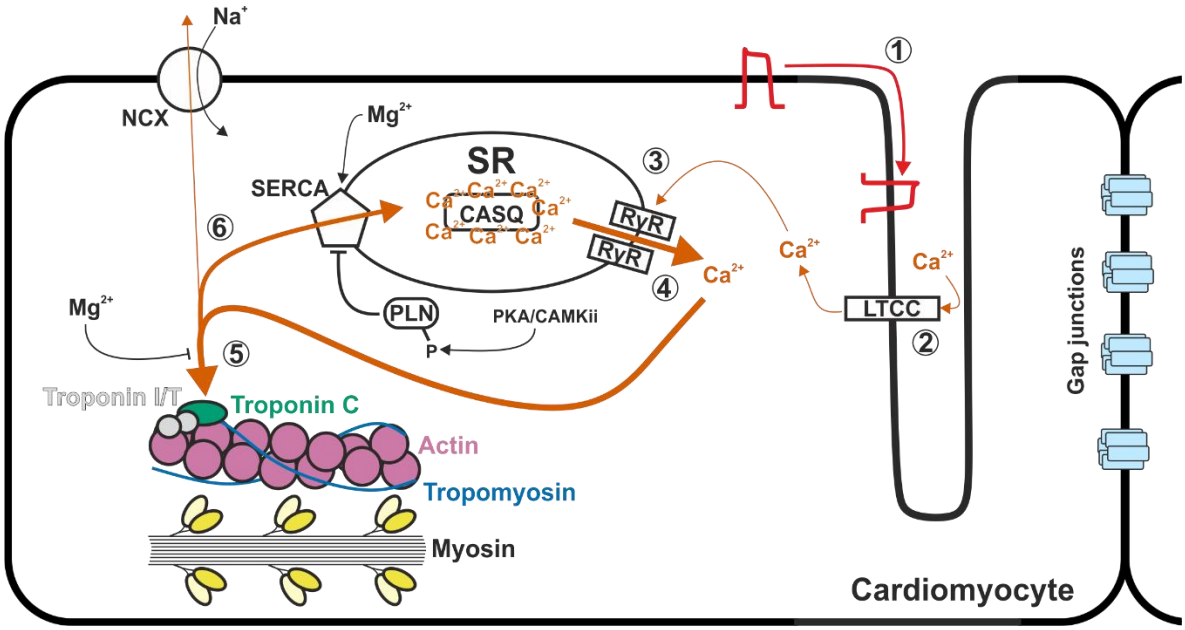

Figure 1.7. Excitation-contraction coupling mechanism in cardiomyocytes. 1. An action potential transverses the sarcolemma down into the T-tubule system, depolarising the membrane. **2**. L-type calcium channels (LTCC) open to allow influx of Ca^{2+}. **3**. Intracellular Ca^{2+} binds ryanodine receptors (RyR) on the sarcoplasmic reticulum (SR) to drive further Ca^{2+} release from calsequestrin (CASQ) through RyRs into the cytoplasm (**4**). **5.** Intracellular Ca^{2+} binds troponin C, part of the regulatory complex (troponins I,C,T) bound to tropomyosin. As Ca2+ binds to troponin C, a conformational change is induced resulting in troponin I exposing the myosin binding site on the actin molecule. Actin and myosin bind and further conformation change occurs to 'ratchet' the actin-myosin complex, shortening the sarcomere length. **6.** Ca^{2+} is taken up by SERCA (sarco-endoplasmic reticulum calcium-ATPase) and pumped back into the SR, reducing intracellular Ca^{2+}. To a lesser degree, Ca^{2+} is also removed from the cell by the sodium calcium exchanger (NCX). Phospholamban (PLN) inhibits SERCA activity while protein kinase A (PKA) and calmodulin kinase ii (CAMKii) phosphorylate PLN to reduce its inhibitory ability.

1.2.7 Autonomic innervation of the heart

The heart receives extensive input from both sympathetic and parasympathetic branches of the autonomic nervous system. Primary parasympathetic neurons synapse onto postganglionic neurons directly on the surface of the heart while sympathetic afferents project to sympathetic ganglia which in turns project to the heart and vasculature with longer postganglionic neurons. Sympathetic fibres innervate all parts of the heart and release noradrenaline which binds primarily to beta-adrenoceptors leading to increases in HR (positive chronotropy), contractility (inotropy), conduction velocity (dromotropy) and myocyte relaxation rate (lusitropy). In contrast the vagus nerves, the parasympathetic fibres that innervate the heart, innervate the SA and AV nodes strongly with weaker connections to atrial myocardium and sparse innervation of ventricular myocardium. Parasympathetic nerves release acetylcholine to activate M_2-muscarinic receptors in the heart and perform the opposite function of sympathetic nerves. Interestingly, M_2 receptors can also be found on terminals of sympathetic nerves and upon activation attenuate the release of noradrenaline, meaning parasympathetic activity can override sympathetic effects (Matkó *et al.*, 1994; Azevedo and Parker, 1999).

The origin of autonomic fibres can be found in the Medulla of the brainstem. Within the Medulla lies the nucleus tractus solitarius (NTS) which receives information directly from receptors on the vasculature such as baro- and chemoreceptors to form part of a feedback loop. The NTS projects to parasympathetic centres in the medulla, namely the dorsal vagal nucleus and nucleus ambiguus, in an excitatory manner, and the ventrolateral medulla, the sympathetic centre, in an inhibitory fashion. These parasympathetic and sympathetic centres also share reciprocal inhibitory connections. The medulla also receives input from both the hypothalamus and cortex (Zoccal *et al.*, 2014). Pre-parasympathetic and pre-sympathetic neurons in the SCN project and relay 24hr rhythmicity, while the cortex most likely informs the medulla of higher order brain activity such as stress or emotion (Buijs *et al.*, 2014; Myers *et al.*, 2017).

1.2.8 Electrocardiography

Cardiac electrophysiology can be measured non-invasively using surface electrodes attached to the skin, or marginally more invasively by sub-cutaneous electrode

implantation. At least 2 electrodes are required to calculate potential difference, although clinically often 10 are used surrounding the heart to garner a full picture of conduction dynamics across the heart. The electrodes detect small deflections in voltage, generated by cellular de- and repolarisation, moving towards or away from the electrode, resulting in a positive or negative deflection on the electrocardiogram (ECG). The ECG can therefore be used to calculate a range of parameters reflecting conduction dynamics. A standard, 1 lead ECG (potential difference across 2 electrodes either side of the heart) has a stereotypical pattern, with a P wave reflecting atrial depolarisation, QRS complex reflecting ventricular depolarisation and T wave reflecting ventricular repolarisation (**Fig 1.8**). Measuring each of these deflections and the time between them can provide information on SA nodal pace making, atrial depolarisation, AV nodal delay and ventricular dynamics. Furthermore, electrocardiography can also be used to determine position of heart chambers, any damage to parts of the heart and electrical abnormalities.

1.3 Rhythmic influences over cardiovascular function

1.3.1 Rhythms in physiology

The demand on the cardiovascular system varies significantly across the day. During physical activity, the required oxygen and nutrients transported by the blood are greater, resulting in the heart needing to work harder. To best adapt to these changing requirements across the day, the cardiovascular system exhibits daily rhythms in a range of parameters including blood pressure, endothelial function, thrombus formation and heart rate (Degaute *et al.*, 1991; Kollias *et al.*, 2009; Nosaka *et al.*, 2017). Indeed, whole heart sequencing studies reveal that, under LD conditions, a large proportion of cardiac transcriptome is rhythmic (10-13% of expressed transcripts) (Storch *et al.*, 2002; Martino *et al.*, 2004). Many of these transcripts are from pathways related to metabolism, such as mitochondrial function, reflecting the rhythmic energetic demand of the heart (Zhang *et al.*, 2020). Similarly, daily rhythms can be observed in 8% of the cardiac proteome (Podobed *et al.*, 2014a), reflecting the highly rhythmic nature of the molecular landscape in the heart across the day.

Daily rhythms can also be observed in many ECG parameters, reflecting the changes in electrical conduction, depolarisation and repolarisation mechanics. For example, in

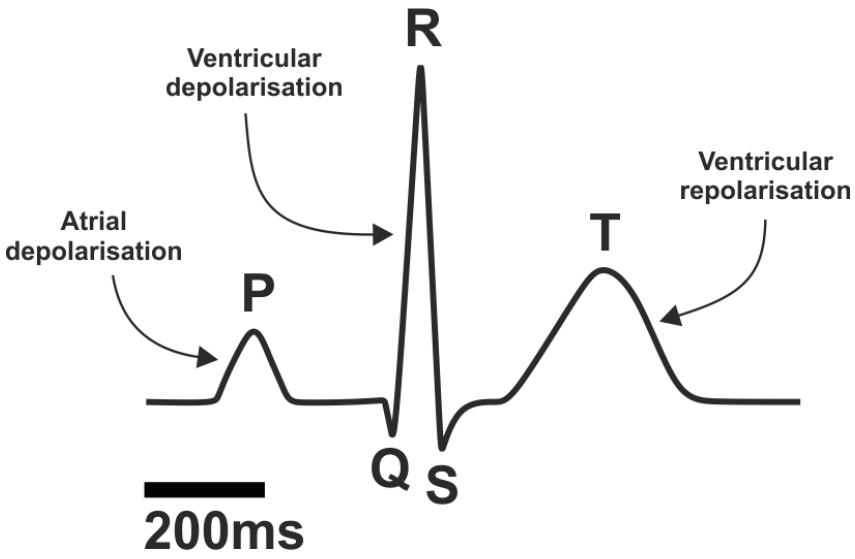

Figure 1.8. Human ECG waveform schematic. After the SA node initiates an impulse, the atria depolarise resulting in the occurrence of a P wave on the ECG waveform. After a delay at the AV node (reflected by the time between P and R waves), the ventricles depolarise which can be seen as the QRS complex. Finally the ventricles repolarise resulting in the T wave which is positive in humans (as in the figure) and negative in mice. Atrial repolarisation occurs around a similar time as ventricular depolarisation and therefore is likely lost within the QRS complex.

humans, diurnal rhythms can be observed in both corrected (for absolute HR) and uncorrected QT interval (Molnar *et al.*, 1996; Bonnemeier *et al.*, 2003a; Smetana *et al.*, 2003), PR interval and P wave morphology (Dilaveris *et al.*, 2001), QRS interval (Nakagawa *et al.*, 1998), RR interval and various measures of heart rate variability (HRV) (Boudreau *et al.*, 2012, 2013), with lengthened intervals occurring during the night when HR is at its lowest. In mice these same parameters have also been shown to display diurnal rhythmicity, but peaking during the light phase, again while HR is lowest (West *et al.*, 2017; Schroder *et al.*, 2021).

Abnormal ECG parameters can be indicative of cardiac disorders as mentioned previously, so changes across the day may impact incidence of adverse cardiac electrical events. Indeed, during the inactive phase in humans and rats (night and day respectively), incidence of bradycardic events such as sinus pauses are increased compared to the active phase (Otsuka *et al.*, 1986; Northcote *et al.*, 1989). In patients with implanted cardioverter defibrillators, risk of atrial arrhythmias, namely atrial flutter, fibrillation and tachycardia, also display a robust daily rhythm, peaking during the night (Shusterman *et al.*, 2012). Interestingly, the ventricular response during these fibrillation episodes (the change in firing rate of the ventricles while atria are in fibrillation), also exhibits a diurnal rhythm, but of greater magnitude during the day (Raeder, 1990). Diurnal variations also present in ventricular arrhythmias including incidence of premature ventricular complexes when recorded by 24hr Holter monitoring (Steinbach *et al.*, 1982), and in ventricular tachycardia and fibrillation in healthy individuals and across various disease states (Lucente *et al.*, 1988; Twidale *et al.*, 1989; Lampert *et al.*, 1994; Tofler *et al.*, 1995; Englund *et al.*, 1999; Kozák *et al.*, 2003). These ventricular arrhythmias occur most frequently during the day, predominantly in the morning similar to incidence of myocardial infarction (Muller *et al.*, 1985). Both ventricular arrhythmias and myocardial infarction contribute to sudden cardiac death, which again displays diurnal rhythmicity peaking in the morning (Muller *et al.*, 1987; Willich *et al.*, 1987).

In patients with congenital long QT syndrome, there are differences between the diurnal distributions and long QT subtype. Most notably, LQT1 results from a mutation in *Kcnq1*, resulting in disrupted I_{ks}, and is triggered most commonly by exercise (Wu *et al.*, 2016). Accordingly, LQT1 driven arrhythmias occur more frequently during the day. In contrast,

LQT3 results from mutations in *Scn5a* and causes defects in I_{Na} (Pérez-Riera *et al.*, 2018). LQT3 is most commonly trigged by bradycardia, and the frequency of LQT3-triggered arrhythmias do not display diurnal variation (Takigawa *et al.*, 2012). Given the widespread diurnal profiles of ventricular arrhythmias, it is currently unclear whether said rhythmic patterns are simply a result of changing conditions and influences on the heart across the day, or whether the circadian system is influential in governing cardiac arrhythmias.

While many studies have observed daily rhythms in adverse cardiac events in humans, little has been done to investigate whether similar rhythms are observed in animals, or to understand the underlying mechanisms. One study which has offered a potential link between the circadian system and arrhythmia susceptibility showed that *Klf15*, a transcription factor that modulated K^+ transport, is rhythmic across day/night and under circadian regulation by *Bmal1.* Importantly, when up- or downregulated in the heart, increased incidence to ventricular arrhythmias were observed (Jeyaraj *et al.*, 2012). As atrial arrhythmias peak seemingly in antiphase to ventricular arrhythmias, there may even be a fundamental difference in the circadian mechanisms governing different components of the heart.

It is important to stress that diurnal rhythms in cardiac measures could originate from a range of sources. Changes in locomotor activity, arousal state, lighting condition and temperature could all contribute to rhythms observed as well as central clocks directly via the autonomic nervous system or indirectly through neuroendocrine routes, or peripheral clocks directly within the heart. Particularly with some ventricular arrhythmias which peak in incidence around the same time that people get out of bed, resulting in a large change in blood pressure. As such, the impact of the circadian system on arrhythmogenesis is poorly understood.

1.3.2 Evidence for SCN input over cardiovascular function

While rhythms in cardiac function can be both dictated by the circadian system and passive to changes in behaviour across the day, studies have begun to investigate the roles of both central and peripheral clocks in cardiac electrophysiology. In humans, resting heart rate (measured while at rest in supine position after 2hr fast in darkness) follows a diurnal rhythm, and the magnitude of light-induced increases in HR (and decreases in HRV) also

varies by time-of-day, suggesting a role of the SCN in setting HR (Scheer *et al.*, 1999, 2004). In rats, surgical ablation of the SCN reduces the diurnal amplitude of HR rhythms, and abolishes rhythms in 'resting HR' (calculated after periods of inactivity) (Scheer *et al.*, 2001; Tong *et al.*, 2013). Of note, ablation of the SCN also abolishes behavioural rhythms, meaning that passive responses to behaviour cannot be separated from SCN influence. Selective genetic mutation of the SCN clock (*Vipr2*$^{-/-}$) also results in dampened rhythms in HR without abolishing behavioural rhythms in LD, suggesting a role for the SCN in contributing to rhythms in HR in mice (Sheward *et al.*, 2010). Pharmacological autonomic blockade reduces the diurnal amplitude of HR rhythms, further supporting the role of the autonomic nervous system in SCN control over HR (Tong *et al.*, 2013). However, how cardiac conduction dynamics around the rest of the heart are impacted by the SCN remain somewhat unclear, and as such is a topic of interest.

1.3.3 Impact of peripheral cardiomyocyte clock deletion

In addition to the SCN, local clock contribution to cardiac function has been demonstrated in a number of processes including metabolism (Durgan *et al.*, 2006; Tsai *et al.*, 2010; Young *et al.*, 2014) and ion transport (Jeyaraj *et al.*, 2012; Schroder *et al.*, 2013, 2015). Multiple genetic approaches have been used to study the roles of peripheral clocks on cardiovascular function by disrupting clock function in cardiomyocytes. Cardiomyocyte-specific clock mutations (*αMHC*^{cre}*Clock*$^{\Delta 19/\Delta 19}$*)* reduces heart rate and day-night amplitude, suggesting that the cardiomyocyte clock could be contributing to setting daily rhythms in HR, but other ECG parameters were unaffected (Bray *et al.*, 2008). However, neither mutant nor wild-type hearts when perfused *ex-vivo* in this study display any rhythms in HR. Cardiomyocyte-specific *Bmal1* knockout animals display decreased HR with no change to diurnal amplitude, lengthened QT and QRS intervals, although these results have not always been consistent between studies (Schroder *et al.*, 2013, 2015, 2021; Gottlieb *et al.*, 2021). Few studies have investigated the impact of cardiomyocyte clock disruption on arrhythmia sensitivity, although cardiomyocyte-specific *Bmal1* knockouts do display changes in action potential morphology and may be more susceptible to stretch induced premature ventricular complexes *ex vivo* (Schroder *et al.*, 2013; Gottlieb *et al.*, 2021). Changes in ECG morphology are accompanied by changes in ion channel gene expression, showing that the cardiomyocyte clock is clearly involved in determining conduction

dynamics around the heart, although clearly further research is needed to investigate the full involvement of the cardiomyocyte clock on cardiac function.

Cardiac metabolism is highly rhythmic across the day, with different processes peaking at different times to best adapt to the required needs of the heart. Glucose utilisation peaks during the active phase to meet the increased energetic demands, triglyceride synthesis peaks toward the end of the active phase to anticipate the upcoming sleep period and protein turnover peaks during the sleep phase to promote growth and repair (Young, 2016). All of these processes are influenced heavily by the cardiomyocyte clock. Glucose oxidation is rhythmic in *ex-vivo* wild-type hearts but abolished in $\alpha MHC^{cre}Clock^{\Delta 19/\Delta 19}$ hearts and markedly attenuated in $\alpha MHC^{cre}Bmal1^{f/f}$ hearts. Similarly, glycogen and triglyceride synthesis is rhythmic *ex-vivo* in wild-type, but not $\alpha MHC^{cre}Clock^{\Delta 19/\Delta 19}$ hearts (Tsai *et al.*, 2010; Durgan *et al.*, 2011a). Rhythms in protein synthesis persist *ex-vivo* and are elevated in $\alpha MHC^{cre}Bmal1^{f/f}$ hearts (He *et al.*, 2016). Clearly there is a significant influence of the cardiomyocyte clock over cardiac metabolism.

Cardiomyocyte *Bmal1* deletion is also detrimental to cardiac health. These animals routinely exhibit age-dependent cardiomyopathy with decreased lifespan compared to littermate controls (Young *et al.*, 2014; Ingle *et al.*, 2015). As *Bmal1* has extensive functions outside of its role as a circadian clock gene, it is yet unclear whether these health problems are due to circadian clock disruption or through its other functions (Rosenwasser, 2010). While few studies have been carried out to directly examine cardiovascular problems in $\alpha MHC^{cre}Clock^{\Delta 19/\Delta 19}$ mice, there is evidence that they exhibit decreased cardiac efficiency, decreased locomotor activity and increased hypertrophic markers (Bray *et al.*, 2008; Durgan *et al.*, 2011b; Ko *et al.*, 2011), observations associated with decreased cardiovascular health.

1.3.4 Shift work and cardiovascular health

Misalignment between the circadian system and behaviour occurs more and more frequently in modern society, from travelling between time zones to night time light exposure and shift work. While the impact of transient misalignment on health is poorly understood, chronic misalignment as present during long term shift work has clear impact to health and wellbeing. Working night shifts and rotating shifts is associated with

increased risk of cardiovascular disease, myocardial infarction and atrial arrhythmias (Vyas *et al.*, 2012; Torquati *et al.*, 2018; N. Wang *et al.*, 2021). These adverse cardiac outcomes may be partially due to altered autonomic signalling. For example, during circadian misalignment it has been reported that the balance between sympathetic and parasympathetic input to the heart is disrupted, assessed using HRV metrics (Wehrens *et al.*, 2012; Grimaldi *et al.*, 2016; Skornyakov *et al.*, 2019). Disrupted HRV has also been associated with a wide range of adverse cardiovascular events including atrial fibrillation, cardiovascular disease, mortality following myocardial infarction and sudden cardiac death (Kleiger *et al.*, 1987; Kubota *et al.*, 2017; Sessa *et al.*, 2018; Khan *et al.*, 2019). While the mechanisms by which shift work detrimentally impacts cardiovascular health remain poorly understood, it is likely a result of a combination of both indirect shift-work related stressors (e.g. sleep disruption, poor eating habits) and circadian misalignment.

1.4 Thesis aims

The general aims of this thesis are to dissect the relative contributions of rhythmic influences over components of cardiac electrophysiology. We examine ECG parameters in humans across tightly controlled laboratory studies encompassing environmental manipulations to compare influences from the circadian system and behavioural state. In mice we use genetic, pharmacological and environmental manipulations to establish the contributions of central and local clocks over cardiac electrophysiology. We will also examine whether and how the circadian system contributes to diurnal variations in arrhythmia susceptibility.

1. ECG data can be used to assess cardiac conduction dynamics under normal conditions, but current ECG analysis software is not able to automatically calculate ECG parameters robustly across the day during periods of noisy data such as during locomotor activity. Chapter 2 will address this deficit by creating new analysis software in MATLAB which is fully automatic, fast and robust to noise, allowing for analysis of large datasets consisting of longitudinal ECG over multiple days and across multiple subjects.
2. Using raw ECG data from previously published, tightly controlled laboratory studies in humans, Chapter 3 aims to assess how behavioural state changes and the

circadian system interact to govern rhythmicity in components of cardiac electrophysiology. This is done using behavioural and environmental manipulations to separate behavioural state influences from other rhythmic inputs.

3. Chapter 4 will further explore these relative rhythmic influences over the cardiac conduction system using mouse models. Here we aim to untangle the direct influences of central and peripheral cardiomyocyte circadian clocks on cardiac conduction and arrhythmia susceptibility using environmental manipulations, pharmacological blockade of the autonomic nervous system, and genetic ablation of the cardiomyocyte clock.
4. Chapter 5 aims to investigate the molecular basis underlying the circadian influence over ventricular tachycardia susceptibility. In humans, ventricular arrhythmias can occur via numerous mechanisms including genetic mutations of ion channels or heart disease. In Chapter 5 we use RNA sequencing to identify possible mechanisms underpinning the circadian control over arrhythmogenesis.

Chapter 2: Development of automated longitudinal electrocardiographic analysis methods in human and mouse

2.1 Introduction

Electrocardiography (ECG) is a powerful, non-invasive method of measuring cardiac electrophysiology. Each component of the ECG reflects a distinct part of the cardiac cycle: the P wave reflecting atrial depolarisation, QRS complex ventricular depolarisation and the T wave ventricular repolarisation. As such, measuring different intervals from these waves can provide useful information, such as the offset of the P wave to the onset of the QRS complex reflecting delay across the AV node, and onset of QRS to the offset of the T wave reflecting ventricular de- and repolarisation. Historically, ECG was first measured using a capillary electrometer, a fine tube half filled with mercury and half of sulphuric acid, with electrode wires attached either end. When an electrical impulse was detected, the meniscus between fluids would move due to changes in surface tension, and resulting capillary pressure would drive vertical movement of the tubes, allowing for an attached motor to transcribe electrical impulses (Stock, 2004). Following mathematical correction of the waveform generated during each heartbeat (to address inertia and momentum in the capillary tube), a PQRST waveform similar to that observed on modern ECG recordings was made (AlGhatrif and Lindsay, 2012). Considerable developments occurred over the following years, with the design of alternative recording methods, and incorporation of additional electrodes placed around the heart to capture additional information. By 1954 the 12-lead ECG, essentially as used today, was finalised (Wilson *et al.*, 1954). While the 12-lead ECG can provide vital information on the three dimensional aspects of electrical activity and conduction through the heart, a single lead ECG is sufficient for the general assessment of cardiac conduction.

Measurements of ECG parameters and morphology are routinely used in clinical settings as they provide valuable diagnostic information and can highlight patients at risk of adverse cardiac effects. For example, lengthened QT interval is associated with increased risk of cardiac arrhythmias and sudden cardiac death (Algra *et al.*, 1991). Diagnostically, lengthened PR interval often reflects of various types of AV block, while elevation above baseline of the ST segment (the flat period between QRS complex and the T wave) is

indicative of myocardial infarction (Steg *et al.*, 2012; Kwok *et al.*, 2016). In both clinical and most research settings, ECG parameters and diagnostics are typically measured using computer assisted, manual assessment. This is problematic for large scale data sets such as longitudinal recording for circadian analyses due to the additional time required to manually verify parameters.

In the context of our studies, longitudinal measurement of ECG parameters are essential to provide information on how components of cardiac electrophysiology change across the day and night, and in response to environmental, behavioural and pharmacological manipulations. Due to the vast amount of data recorded across the many days required for these types of analysis (~100000 beats per day in humans, ~700000 in mice), manual calculations, even when computer-assisted, are not feasible. One major flaw in computer-assisted ECG measurement is the requirement for data to be very high quality with little background noise. In longitudinal settings, this is rarely the case due to locomotor activity inducing myographic and electrode contact noise (D'Aloia *et al.*, 2019). While there are current options available for automated human ECG analysis, they often are primarily focused on diagnostics, have limited use during noisy recording periods, are cost prohibitive, or are not manipulatable for specific purposes (Macfarlane *et al.*, 2017; Apandi *et al.*, 2020; Serhani *et al.*, 2020). In mice, there are options such as the Ponemah software (Data Sciences International), although significant time investment is still required for manual verification. To address these problems, here we develop a fully automated ECG analysis algorithm for single lead ECG recording from both human and mouse, with built-in quality control. The principal approach taken uses beat averaging to minimise noise and increase precision. This comes at the cost of losing some specific within beat dynamics. This chapter explains the methodology behind the algorithm, with example code, and compares automated results to manual measurements, conducted by an expert clinician.

All code described here is now publically available under the MIT Licence in the Github repository (https://github.com/EdHayter/Hayter-et-al.-ECG-analysis) (Hayter *et al.*, 2021b).

2.2 Method development and results

2.2.1 Overview

Source data was acquired from two human studies performed at the University of Surrey (study 1) and Washington State University (study 2) and mouse studies were performed in house (Wehrens *et al.*, 2010; Skene *et al.*, 2018). In study 1, a total of 25 participants (11 long term shift workers and 14 control individuals) were kept in a tightly controlled laboratory session with ECG recorded throughout using a wireless polysomnographic system (Siesta EEG/PSG recorder, Compumedics Ltd) at 256Hz. In study 2, 14 participants were also in a laboratory session with ECG recorded throughout using a Holter monitor (DMS 300-3A, Bravo) at 4kHz, but down sampled to 128Hz for analysis. 3- and 5-lead ECG was recorded in study 1 and 2 respectively, but only a single lead used for analysis. Additional study details are provided in (Wehrens *et al.*, 2010, 2012; Skene *et al.*, 2018; Skornyakov *et al.*, 2019) and section 3.2 of the following chapter. Mouse ECG was recorded using radiotelemetry (PhysioTel HD, Data Sciences International) at 1000Hz following surgical implantation of an ECG monitoring radiotelemeter (ETA-F20; **Fig 2.1A**). Further details of study design can be found in section 4.2. Human ECG was recorded continuously while mouse ECG was recorded as 10s sweeps every 5 minutes. All analysis was performed using bespoke written code using MATLAB R2018a/R2019a as described herein. Data was split into sweeps of 10000 data points for analysis (10s in mouse, ~39s in human study 1 and ~78s in human study 2; **Fig 2.1B**).

The first stage in creating the algorithm for automated ECG analysis was to design a pipeline which requires minimal changes between human and mouse data to ensure as much consistency in analysis as possible (**Fig 2.2**). During the filtering and template matching steps, we opted to take quality control parameters which were saved and evaluated in the quality control step. An overview of the pipeline is described: i) Sweeps were filtered to remove baseline variability; ii) Heartbeats were detected by amplitude thresholding; iii) Beat waveforms were scaled to account for differing R wave magnitudes; iv) Beat waveforms were compared to a template to exclude beats that differ considerably to the average; v) HR and HRV measures were calculated; vi) ECG features were detected and

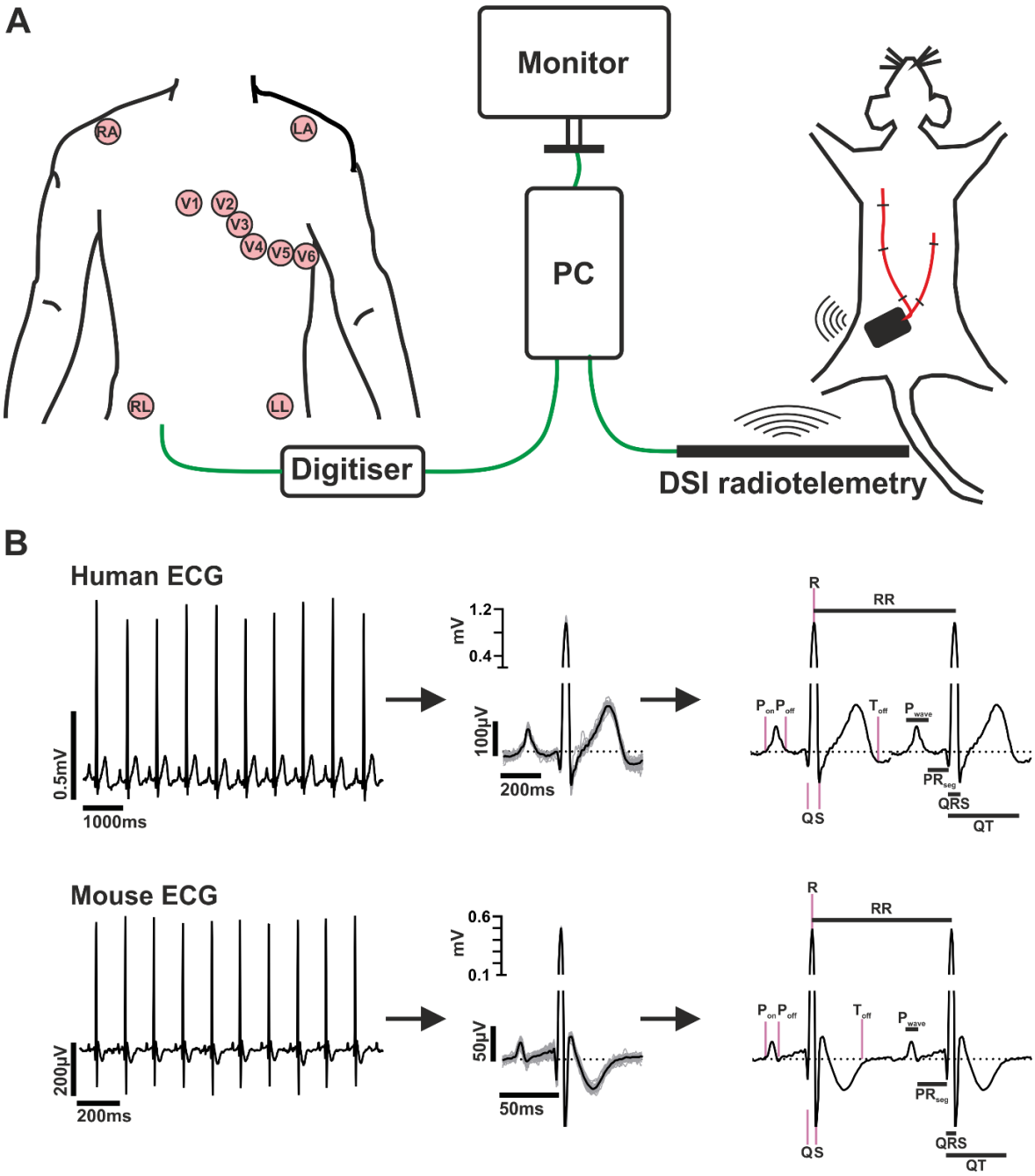

Figure 2.1. Electrocardiography acquisition in humans and mice. A. Schematic of ECG hardware and electrode placement for 12 lead ECG acquisition in humans (left) and location of radiotelemetry device in mice (right). lead I ECGs (as analysed in here) are collected in humans using right arm (RA) and left arm (LA) electrodes, with left leg (LL) to ground. **B.** Example ECG, average waveforms and calculated ECG parameters in human and mice. Note the differences in timescale and ECG morphology.

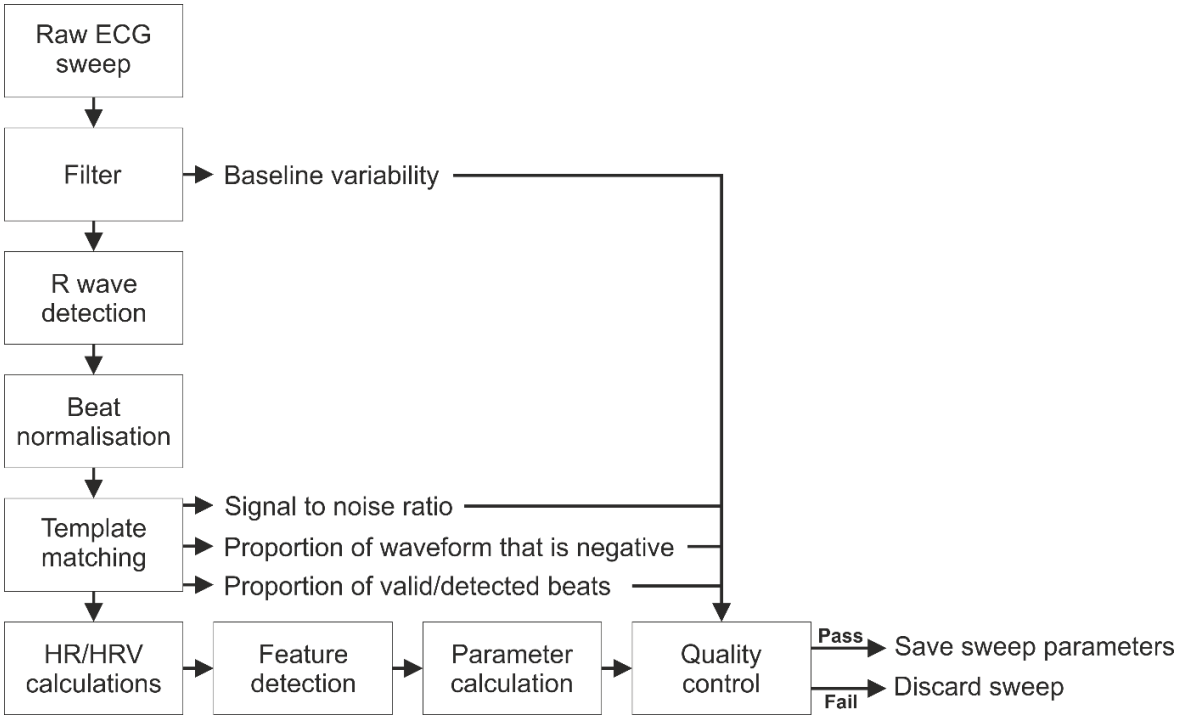

Figure 2.2. Diagram of ECG analysis procedure. Each ECG sweep is first filtered to establish baseline variability and clean the waveforms. R waves are then detected by amplitude thresholding and signal-to-noise and R wave to S wave magnitude ratios extracted. Beats are then normalised to R wave magnitude and a template derived from the average of all beats in the given sweep. Beats sufficiently different from the template are removed and proportion of valid beats calculated. ECG features and identified and parameters calculated. A final quality control step determines whether the sweep parameters are kept or discarded.

parameters calculated; vii) Quality control metrics were assessed; viii) Sweeps were either discarded or kept for further analysis (**Fig 2.2**). Each of these steps is described in further detail below.

2.2.2 Filtering

As ECG recording is highly sensitive to perturbations in electrical conduction, when recording ECG in a clinical setting care must be taken to avoid movement of the subject. Movement can introduce electromyographic (EMG) noise from muscles contracting, electrode contact noise from electrodes shifting position or becoming less firmly attached, and baseline wander due to respiration. The very nature of longitudinal ECG means that these factors cannot be fully controlled or excluded. While humans can be asked to remain still for short periods of time, over the course of many days movement will occur. In conscious mice, prevention of physical activity is not a viable option. One method to help minimise the impact of invasive noise is to filter the data. Therefore, a 0.5Hz highpass filter was used to remove low frequency oscillations including most baseline drift. An additional moving average filter (20ms for human ECG and 5ms for mice ECG) was added to smooth out high-frequency (likely EMG) noise (**Fig 2.3**). These values were chosen based on previous literature (Kher, 2019) and verified by visual inspection that they did not significantly dampen or distort the signal. Importantly, these settings have minimal impact on naturally clean ECG (often recorded during sleep or inactivity) but improve the reliability of noisy ECG considerably (**Fig 2.3**). The MATLAB code for this step can be found below.

```
function [data_filtered,wobble] = ECGfilt(data,Fs,smooth)
      data_filtered = highpass(data,0.5,Fs);
      window = round(smooth/1000*Fs);
      data_filtered = movmean(data_filtered,window);
      k=ones(500,1)./500;
      vs=convn(data_filtered,k');
      wobble = range(vs);
end
```

Here, `data` is the raw ECG, `Fs` represents the sampling rate in Hz and `smooth` is the desired smoothing window in milliseconds. In this step a measure of baseline variability, `wobble`, is also taken for use in the later quality control step. This is done by finding the range of values in the filtered data following a linear convolution to heavily smooth the data.

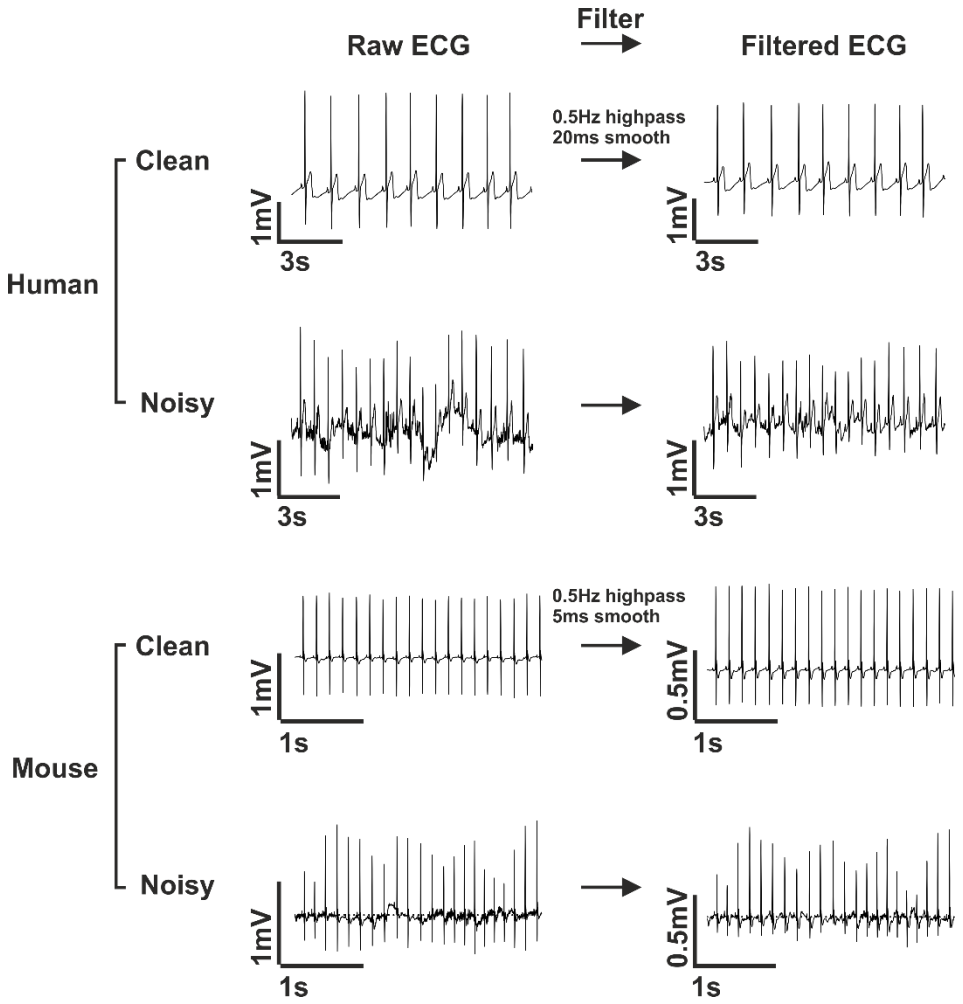

Figure 2.3. Example clean and noisy ECG sweeps pre- and post-filter. ECG is generally cleaner during inactivity and noisier during locomotor activity. Filtering the ECG using a 0.5Hz highpass filter and a moving mean of 5ms in mice and 20ms in humans reduces how much the baseline potential drifts from 0 and smooths high-frequency noise.

2.2.3 R peak detection

Next, R peaks are identified using a simple amplitude thresholding approach. The threshold is calculated by taking the 98th percentile of voltages across the entire sweep. This threshold reliably captures R waves while being high enough to avoid the peaks of P or T waves. In order to save the corresponding beat waveforms, we opted for a verbose 'for' loop, which loops over each valid data point in search of peaks above the threshold. Upon finding a peak, the algorithm saves the corresponding waveform in a matrix `beats` and peak timestamp in `bt`. `dp` is a variable which dictates how far away from the R peak to include while saving the waveform and is chosen manually, prior to running formal analyses, to ensure the start of P waves and end of T waves are reliably included in the waveform. As a default, 60 points prior to and 100 points following the R wave are selected (corresponding to 234ms and 390ms at 256Hz respectively). As detected R waves near the start or end of the sweep could be part of incomplete ECG waveforms, any R waves that were within the waveform limits (dictated by `dp`) to the start or end of the sweep were not analysed.

```
threshold = prctile(data_filtered,98);
dp = [60,100];
i = dp(1)+1;
while i < length(data_filtered)-dp(2)
    while data_filtered(i)<threshold & i < length(data_filtered)-
dp(2)
        i=i+1;
    end
    if i < length(data_filtered)-dp(2) %beat detected
        while data_filtered (i) < data_filtered (i+1) &
              i < length(data_filtered)-dp(2)
            i=i+1;
        end
        if data_filtered(i) > data_filtered(i-1) %valid peak
detected
           b = data_filtered(i-dp(1):i+dp(2)); %beat waveform
           pp = find(b==max(b),1);
           if pp==dp(1)+1
            beats=cat(2,beats,b); %save beat waveform
            bt=cat(1,bt,timestamp(i)); %save beat timestamp
           end
        end
    end
    i=i+1;
end
```

2.2.4 Beat normalisation and template matching

As the ECG can vary in amplitude, particularly during movement, beats need to be normalised. This step scales each beat waveform in `beats` to the height of the corresponding R peak.

```
bwf = beats./beats(dp(1)+1,:);
```

In the absence of cardiac health defects, ECG waveform morphology remains relatively stable between neighbouring beats (Liu *et al.*, 2014). Any detected beats which vary significantly from neighbouring beats is therefore not likely to be a true heartbeat, or be noisy and therefore difficult to extract accurate parameters from. As such, after the beats have been normalised, each waveform is assessed in a template matching step (**Fig 2.4**). During this step an average waveform of all normalised beats in the sweep is taken to generate a template, and for each beat a mean squared deviation, `msd`, is calculated. To calculate mean squared deviation for each beat, the template is subtracted from the beat waveform and difference squared. The average of these squared values is the mean squared deviation and provides a metric for how far a given waveform deviates from the template. Beats are rejected if the mean squared deviation is above predefined thresholds: 7.5x the median mean squared deviation in the sweep, or an absolute value of 0.012. These are arbitrary threshold values which were initially estimated by manual inspection of random beat waveforms. To investigate how these thresholds impact performance we executed sensitivity analysis on 100 sweeps of ECG data from an individual in study 1 across a wide range of possible thresholds (**Fig 2.5**). Under the majority of tested combinations, average deviation in RR interval from our default parameters was under 1ms. Only when the thresholds were set low (i.e. rejecting most beats) was a considerable change observed. By changing our default thresholds by 50% in any direction resulted in a maximal average change in RR interval of only 1.2ms, considerably less than a single data point at 256Hz recording (~3.9ms), providing confidence that our thresholds are robust.

When recording an ECG, the upper and lower limits of voltage measured are determined by the hardware and recording format. These limits are not generally reached in biological signals but are sometimes hit during noisy periods of recording. This saturation value `maxamp` is manually determined when new data is being analysed, or can be set lower if

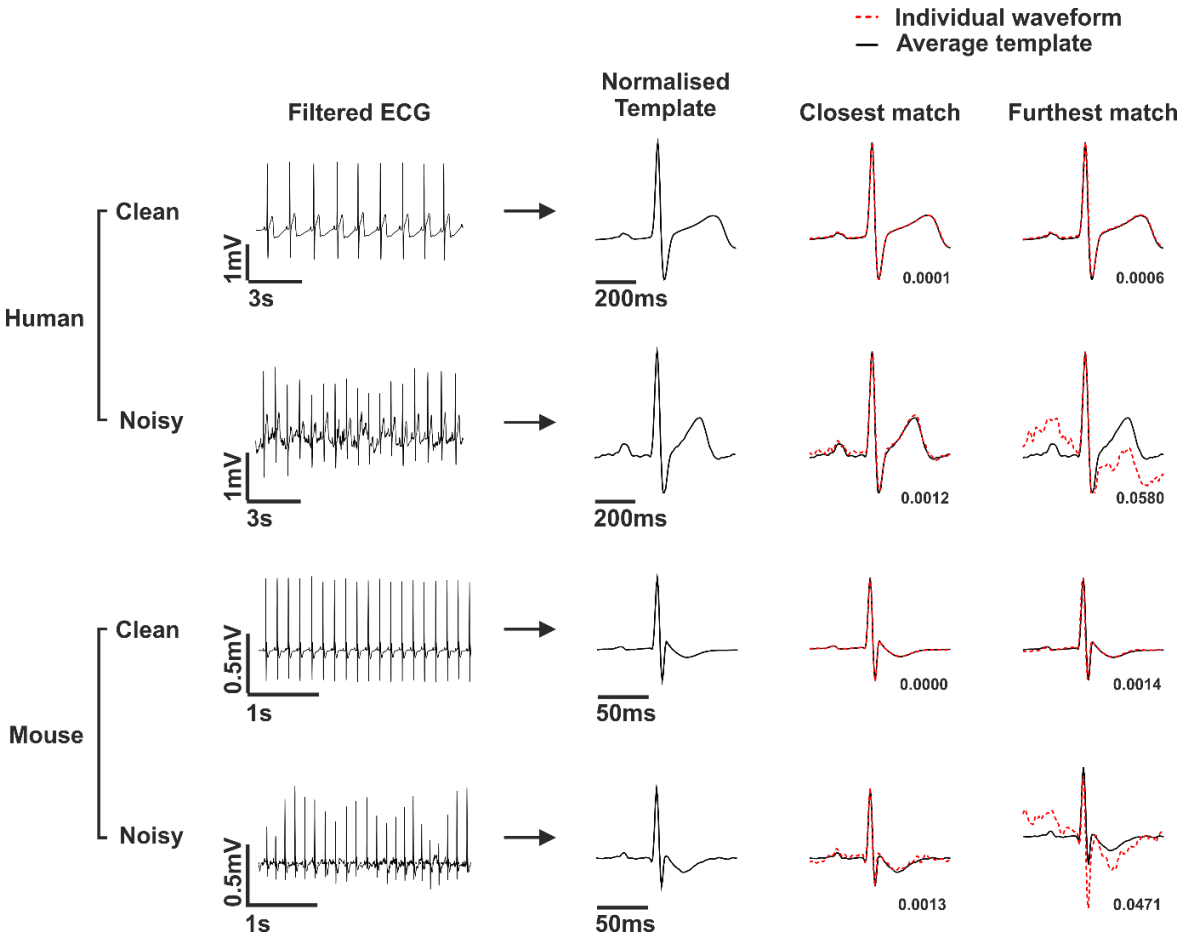

Figure 2.4. Templates derived from filtered ECG. For each ECG segment templates are made from the average of all detected beats. Each measured beat is then compared to the template waveform and removed if it differs significantly. Red dotted lines show the closest and furthest individual beat in the example sweep from the template. Inset values indicate mean squared deviation between template and red dashed waveforms.

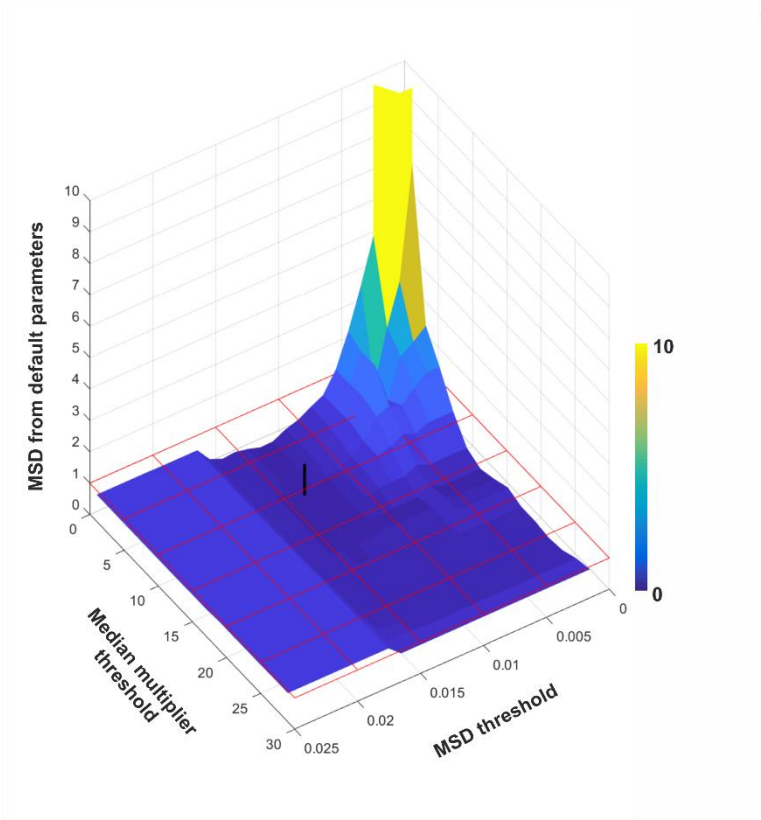

Figure 2.5. Sensitivity analysis for threshold determination in template matching. 100 sweeps of data from a human individual in study 1 were analysed a total of 375 times with selected combinations of thresholds for absolute mean squared deviation (0.001-0.025) and multiple of the sweep median (1-30). The Z axis and colour bar shows the mean squared deviation between RR intervals measured across the 100 sweeps at given parameters (X, Y axes) compared to the default parameters, shown as a vertical black line. To penalise analyses in which RR interval could not be measured (i.e. all beats were rejected), an RR interval value of 0 was given resulting in a large mean squared deviation. The horizontal hashed red platform indicates an average deviation of 1ms for visual context.

there is significant high-amplitude noise which does not reach saturation point. The maximum and minimum voltages in each beat are compared to this limit and if they are equal or greater in magnitude the beat is excluded.

```
mwf=mean(bwf); %normalised mean
bwf=bsxfun(@minus,bwf,mwf).^2; %squared deviation
msd=mean(bwf,2); %mean sq.
upper=max(beats);%beat maxima
lower=min(beats);%beat maxima
idx=isnan(upper)==0 & upper<maxamp & lower>-maxamp &
      (msd<median(msd)*7.5|msd<0.012)';%exclude noise
total_beats = length(idx);%total beats
valid_beats = sum(idx);%valid beats
beats=beats(:,idx)';
bt=bt(idx,:);
```

During this template matching step valid inter-beat intervals are calculated as the difference in time between valid beats, excluding any intervals that are >1.8x the median inter-beat interval of the sweep. On average this corresponds to an instantaneous HR (calculated from a single inter-beat interval) of ~35bpm in humans and ~300bpm in mice. These skipped beats can occur when a beat is rejected in the previous step, resulting in an inter-beat interval measured from the previous valid beat to the next valid beat. Three additional measures are taken for quality control: i) proportion of valid beats compared to total detected; ii) a measure of signal to noise ratio and iii) the proportion of the waveform with below 0mv, an approximation of the isoelectric line. In human ECG the proportion of the waveform that is negative is usually small but in mice the negative Q and S deflections can be pronounced and can make feature detection more difficult. In most cases the algorithm could calculate parameters from these waveforms well, unless the R peak was smaller in amplitude than Q or S. In this case the sweep was normally excluded using this quality control measure. These measures, and baseline variability (`wobble`) from the previous filtering step, are scaled using arbitrary scaling to within 0 and 1, 1 being the highest quality signal and 0 being the lowest. This scaling allows for an unbiased average to be taken for an overall quality measure and for ease of comparison between quality measures. They are stored in the variable `Q`, alongside the overall quality measure for use during the later quality control step.

```
ibis=diff(bt);%find interbeat intervals
idx=ibis<median(ibis)*1.8; %skipped beats;
valid_intervals=sum(idx); %valid intervals
f(2:sum(idx)+1)=find(idx==1)+1; %index of valid intervals
```

```
f(1)=f(2)-1;
beatwf=mean(beats(f,:));
max_amp=max(beatwf);%max amp
min_amp=-min(beatwf);%min amp
Q(1)=(valid_intervals+1)/valid_beats; %valid intervals
Q(2)=1-wobble; %wobble
Q(3)=max_amp/(prctile(data_filtered,95)*5); %SNR
Q(4)=max_amp/(min_amp*3); %negative spikes
Q(Q>1)=1;
Q(Q<0)=0;
Q(5)=mean(Q(1:4));
```

2.2.5 HR and HRV calculations

Next, using the valid intervals data from the previous step, HR is calculated using the average inter-beat interval and measures of HRV are also calculated. Here we use the publically available HRV analysis package HRVtool (Vollmer, 2019) to calculate the standard deviation of valid RR intervals (SDNN), low to high frequency power ratio (LF:HF) and a geometric measure based on relative RR intervals (rrHRV), discussed more in section 3.4 (Vollmer, 2015). In humans, spectral frequency bands to calculate LF and HF power are 0.04-0.15Hz and 0.15-0.4Hz respectively (von Rosenberg *et al.*, 2017). In mice these must be adjusted to 0.4-1.5Hz and 1.5-4Hz within `HRV.fft_val_fun` (Gehrmann *et al.*, 2000).

```
mibi=mean(ibis(idx));
HR = 60/mibi;
HRV(1) = HRV.SDNN(ibis(idx));
[~,~,LFHF] = HRV.fft_val_fun(ibis(idx),Fs);
HRV(2) = LFHF;
HRV(3) = HRV.rrHRV(ibis(idx));
```

2.2.6 Feature detection and parameter calculation

For each valid beat within the sweep ECG features are determined and recorded (**Fig 2.6**). The example code shown below is wrapped in a 'for' loop which loops over every valid beat, `btcurr`, which is omitted for clarity. As such the code here identifies the ECG features from the first valid beat only. Table 2.1 summarises the feature detection strategies. First, Q is identified as the first negative deflection after the first positive deflection moving backwards from the R wave.

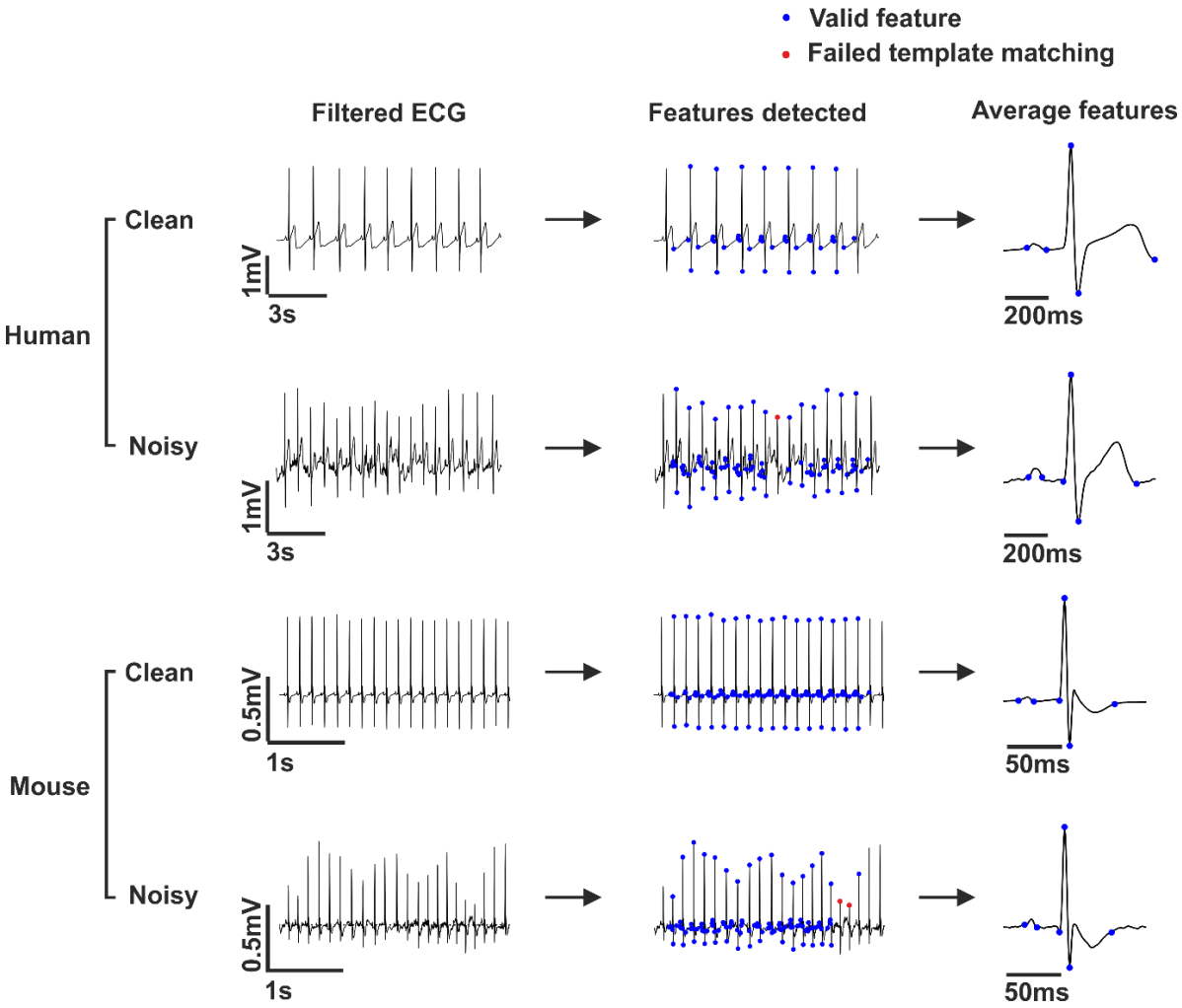

Figure 2.6. ECG feature detection and parameter calculation. P wave onset and offset, Q, R, S and T offset are identified for each beat that passes the template matching step (indicated by blue points in centre waveforms). Detected beats that fail template matching are labelled in red. For each feature the average is taken (right) and ECG parameters calculated.

Feature	Method	Search window	
		Start	End
Q onset	Counting backwards from R peak, first –ve deflection after first +ve deflection		
P peak	Maximal point	R peak - 234/60ms (human/mouse)	Q onset
Isoelectric line	Median voltage across search window	P peak	Q onset
P onset	Counting back from P peak, first point to cross the isoelectric line	P peak – 117/30ms	P peak
P offset	Counting forward from P peak, first point to cross the isoelectric line	P peak	P peak + 117/30ms
S peak	Counting forward from R peak, first +ve deflection		
J peak (mouse)	Counting forward from S peak, first –ve deflection		
T peak (human)	Maximal point	S peak	S peak + 352ms
T peak (mouse)	Minimal point	J peak	Next P wave
T offset	Counting forward from T peak, first point to cross the isoelectric line	T peak	Next P wave

Table 2.1. Feature detection strategies. Description of how each ECG feature was calculated during analysis. Any features that were not identified in the search window were labelled 'NA' and ECG parameters derived from these features were not calculated for that beat.

```
tctr=btcurr;
while tctr>btprev && data_filtered(tctr)>data_filtered(tctr-1)
    tctr=tctr-1;
end
while data_filtered(tctr)<data_filtered(tctr-1)
    tctr=tctr-1;
end
qcurr=tctr;
```

Next, the peak of the P wave is identified as the maximal point between Q and the start of the beat window (234ms and 60ms for human and mouse ECG respectively). An approximation of the isoelectric line for the beat is then calculated as the median voltage of all data points between P peak and Q. P onset and offset are calculated as the first points that cross this isoelectric line to either side of the peak of the P wave. Here there are limits set in place so if the waveform does not cross the isoelectric line within 117ms or 30ms in human and mouse respectively, P onset and offset are deemed incalculable.

```
pcurr=find(data_filtered(qcurr-
dp(1):qcurr)==max(data_filtered(qcurr-
dp(1):qcurr)),1,'last')+qcurr-dp(1);
iso = median(data_filtered(pcurr:qcurr));
tctr = pcurr-1;
while data_filtered(tctr)>iso
    tctr=tctr-1;
    if tctr == pcurr-30
        pon = [];
        break
    end
end
if ~isempty(pon), pon = tctr; end

tctr = pcurr+1;
while data_filtered(tctr)>iso
    tctr=tctr+1;
    if tctr == pcurr+30
        poff = [];
        break
    end
end
if ~isempty(poff), poff = tctr; end
```

Next, the S deflection is identified as the first positive deflection after the R wave.

```
tctr=btcurr+1;
while data_filtered(tctr)>data_filtered(tctr+1)
    tctr=tctr+1;
end
scurr=tctr;
```

Mice display an extra J wave after the S deflection, reflecting heterogeneities in early repolarisation (Boukens *et al.*, 2014). The J wave is identified as the first negative deflection after the S peak as described below. As this J wave is not present in humans, this section of code is omitted during human analyses.

```
tctr=scurr+1;
while data_filtered(tctr)<data_filtered(tctr+1)
    tctr=tctr+1;
end
jcurr=tctr;
```

The morphology of the T wave varies significantly between species so the analysis strategy differs. Human ECGs display a large positive wave while mice ECGs display a shallower negative wave. The offset of T is usually calculated as the point at which T returns to the isoelectric line. In our human ECG data the end of the T wave occurred at a point below the isoelectric line (**Fig 2.1B**) so a modified approach was taken; the first positive deflection after the peak of the T wave that crossed the isoelectric line. Peak T was identified as the maximal point between the S wave and the end of the beat waveform.

```
tcurr=find(data_filtered(scurr:scurr+90)==max(data_filtered(scurr:s
curr+90)),1,'last')+scurr

tctr=tcurr+10;
while data_filtered(tctr)>iso
    tctr=tctr+1;
    if tctr == btnxt || tctr == length(val)
        tctr = length(ts);
        break
    end
end
try while data_filtered(tctr)>data_filtered(tctr+1)
        tctr=tctr+1;
        if tctr == btnxt || tctr == length(val)
            tctr = length(ts);
            break
        end
    end

catch
    tctr = length(ts);
end
if tctr ~= length(ts)
    tend=tctr;
else
    tend = [];
end
```

In mice, a similar approach is taken but the peak of the T wave is the minimal point in the time window and T offset is the first point above the isoelectric line.

```
tctr = find(data_filtered(jcurr:jcurr + 90) ==
min(data_filtered(jcurr:jcurr+90)),1,'last') + jcurr;
if data_filtered(tctr) > iso
    toff = [];
else
    try
        while data_filtered(tctr) < iso && tctr < 10000
            tctr=tctr+1;
        end
        toff = tctr;
    catch
        toff=[];
    end
end
```

At any point during the analysis when a given feature is not identified within the search window (**Table 2.1**), the feature is labelled 'NA' for that beat and ECG parameters derived from those features were not calculated. Finally, ECG parameters are calculated for each valid beat with available feature data and averaged across the sweep (**Fig 2.6**). In instances where ECG parameters could not be reliably determined due to lack of feature identification, those ECG parameters were left blank for the sweep.

2.2.7 Quality control

The final step of the analysis is to filter sweeps which do not meet predefined inclusion criteria. The overall quality of a sweep is assessed as an average of the 4 QC measures, and is removed if this value falls below a chosen threshold. Comparing the proportion of sweeps that are excluded as this threshold is gradually increased revealed a steep decline in sweeps kept at around a threshold of 0.75, suggesting that sweeps are easily separated between high and low quality (rather than a continuum) (**Fig 2.7**). As most sweeps were of high quality we chose a final threshold of 0.66 which retains most sweeps, rejecting ~4% in mouse studies and ~2% in human study 1 (**Table 2.2**). In study 2 there was a large discrepancy in proportion of sweeps kept between night (91%) and day (44%), likely due to less posture management allowing individuals to move around freely as desired and possibly noisier data acquisition (as night time sweeps kept was lower than in study 1). Regardless, it shows that our algorithm correctly identifies clean sweeps and can utilise noisy data to still extract ECG parameters.

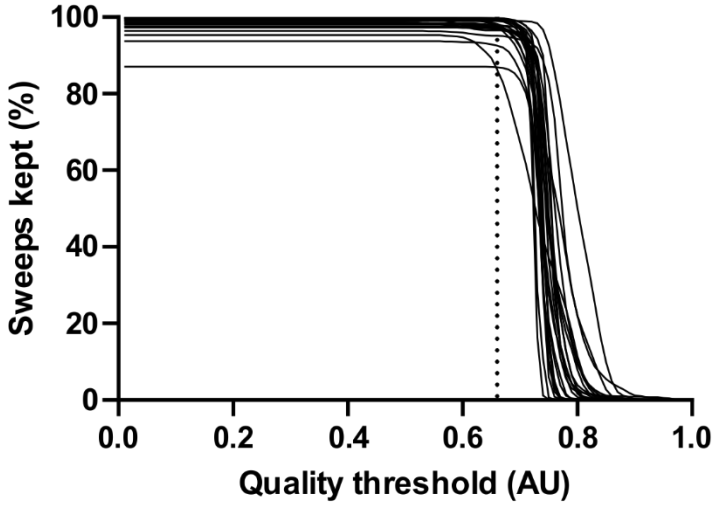

Figure 2.7. Impact of quality control threshold on sweep retention. Proportion of sweeps that would be kept in human study 1 across a range of quality control thresholds from 0 to 1. Each line is an individual, n=25. Vertical dashed line indicates final quality control threshold, chosen to retain as many sweeps as possible without inclusion of low quality data.

				Valid beats (%)	Baseline amp (µV)	Signal to noise ratio (dB)	Negative spikes	Sweeps kept (%)
Mouse			**Night**	90.7 ± 1.3	83.6 ± 12.8	16.0 ± 2.9	2.4 ± 0.8	96.9 ± 5.4
			Day	94.5 ± 1.5	61.5 ± 12.6	15.9 ± 2.7	2.2 ± 0.6	96.5 ± 5.8
Human	**Study 1**	**Control**	**Night**	99.4 ± 0.4	97.5 ± 52.0	16.0 ± 3.0	7.3 ± 2.8	98.3 ± 3.6
			Day	98.8 ± 1.0	109.8 ± 67.9	16.1 ± 4.0	7.0 ± 2.9	98.7 ± 3.0
		Shift	**Night**	98.4 ± 1.9	119.5 ± 76.5	15.5 ± 3.8	6.4 ± 2.0	97.3 ± 4.3
			Day	98.9 ± 0.9	84.2 ± 22.0	14.6 ± 4.2	5.3 ± 2.7	99.6 ± 0.6
	Study 2		**Night**	91.5 ± 6.5	178.1 ± 145.7	9.9 ± 3.3	6.6 ± 2.0	90.9 ± 10.7
			Day	77.6 ± 14.7	299.3 ± 256.0	9.2 ± 3.7	5.7 ± 2.3	44.2 ± 24.6

Table 2.2. Quality control variables across day and night for each group. Valid beats described the proportion of beats that pass the template matching step in each sweep. Baseline amplitude described the variability of the baseline. Signal to noise ratio quantifies the amplitude of the signal compared to the noise. Negative spikes compared the positive R wave deflection to the negative S wave. Lower numbers indicate a more negative waveform. Sweeps kept shows the proportion of sweeps kept in the windows assessed. Mouse quality parameters were averaged across 2 days. Human study 1 parameters were averaged across the dark phase and 4hr posture fixed window during the baseline day and study 2 assessed 4hr mid-dark and mid-light windows on day 1. Full details of study design can be found in section 3.2. These quality control parameters have not been scaled as per the text and instead calculated as interpretable values.

The quality control step occurs after all sweeps have been analysed for an individual. As such, the variable `Q` is a matrix of size `[n,5]` where n is the number of sweeps. This section compares the average quality parameter of each sweep to a predefined threshold (`Qrng`). If the user does not chose a threshold the value of `Qrng` is set to `[-1,-1]` and all sweeps are included.

```
if max(Qrng)>-1
    idx=Q(:,5)>=Qrng(1) & Q(:,5)<=Qrng(2);
else
    idx=ones(size(Quality,1),1);
end
```

This step is also carried out for each ECG parameter using the same approach with valid thresholds given in the form `[lower_limit, upper_limit]`. The variable `idx` contains a binary vector of whether each sweep meets the inclusion criteria, denoted by a 1 (true) or 0 (false).

2.2.8 Performance

After each new experiment analysed we randomly selected sweeps from each individual and plotted the features identified by the algorithm for manual verification. If features from ECG waveforms from any given individual were systematically incorrect (e.g. T offsets which could not be accurately determined), that feature was noted and subsequent parameters not calculated for further analysis. This occurred for 2 individuals in human study 1 (QT excluded) and <10% of mice. We also plotted random sweeps and beats that were included and excluded from each individual for manual verification to determine whether the quality control was functioning as intended. Finally, we assessed the performance of the algorithm by blind comparison of automatically calculated ECG parameters (PR interval, QRS duration and QT interval) to those calculated by a clinical and academic cardiologist, Dr Luigi Venetucci. For this assessment a random sweep from 12 human individuals from study 1 were taken and analysed. ECG parameters were averaged across the sweep and compared to manual measurement of the average waveform of the sweep. As the difference between the two measurement approaches may depend on the absolute value of the ECG parameter, we used Bland-Altman analysis to compare the methods (Bland and Altman, 1986) (**Fig 2.8**). Using this approach we observed only a minor,

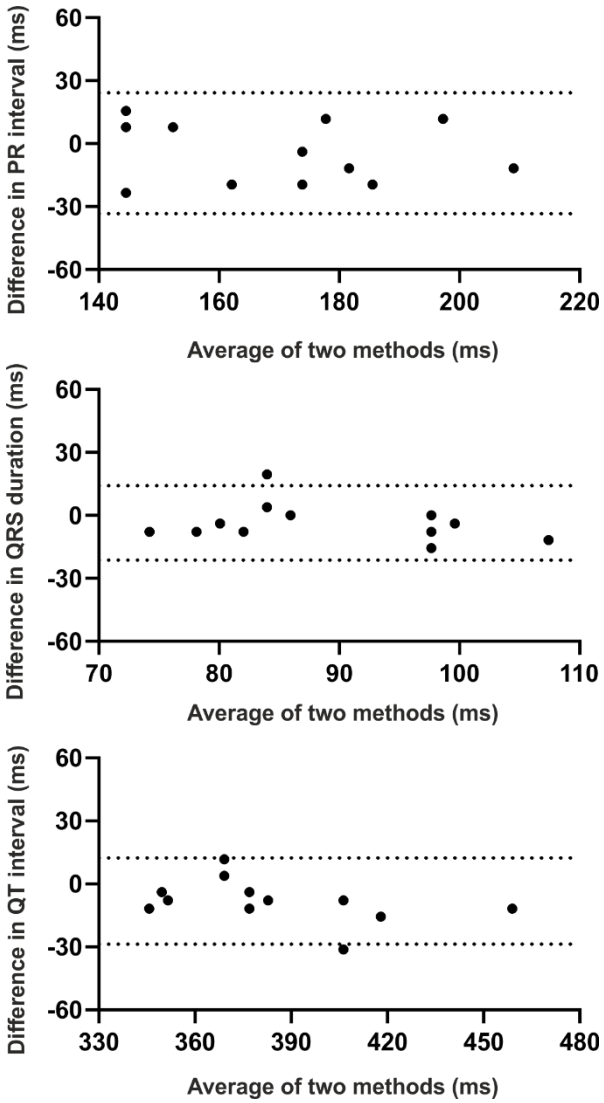

Figure 2.8. Bland-Altman plots comparing automatic parameter calculation and blinded manual calculation. Algorithm-derived PR interval, QRS duration and QT interval were not statistically different from manual measurement by a cardiologist. Data from human study 1, 2 individuals removed due to incalculable T offset. Automatic measurements were averaged across a randomly chosen sweep and manual measurements calculated from the average waveform from that sweep. Two way RM ANOVA, n=12, all parameters $p>0.05$. Bland-Altman 95% limits of agreement: -33.36 to 24.24, -21.30 to 14.14 and -28.65 to 12.37ms.

and not statistically significant, systematic deviation between methods, with average biases of -4.56ms (95% limits of agreement: -33.36 to 24.24), -3.58ms (-21.30 to 14.14) and -8.14ms (-28.65 to 12.37) for PR interval, QRS duration and QT interval respectively, giving us strong confidence in the performance of our algorithm compared to manual analyses (**Fig 2.8**).

2.3 Discussion

Here we describe a robust, computationally inexpensive algorithm for ECG feature detection and parameter calculation from both human and mouse recordings. Parameters calculated are statistically similar to expert manual measurements and take a fraction of the time to measure. For mouse data recorded at 1000Hz for 10 second sweeps every 5 minutes, it takes approximately 4 seconds per mouse per day to calculate all parameters and run quality control steps, while human data recorded continuously at 256Hz runs in less than 30 seconds per individual per day. This level of automation was instrumental in allowing for high fidelity analysis of longitudinal ECG data shown in chapters 3 & 4.

Similar approaches to automated feature detection as described above have been and are currently used in clinical settings for short term ECG parameter calculation. In these settings the patient must be as stationary as possible and only then a single average measure for PR interval, QRS duration, RR interval and QT interval are calculated. Even these semi-automated methods can under or overestimate parameters such as QT interval so manual measurement is often preferred (Postema and Wilde, 2014). Our algorithm minimises errors in calculation by averaging parameters across many beats. In our studies, electrode placement is fixed so wave morphology did not change significantly across the recording period for each individual. As such, we were able to manually verify random waveforms from each individual to confirm accurate measurements without needing to assess every sweep. Longitudinal studies also benefit from large amounts of data so noisy periods of recording can be removed from analysis with little impact on the results. With the exception of study 2, in our data on average less than 4% of sweeps were discarded due to noise and more than 90% of beats in each sweep were used to calculate average parameters. In study 2 a significantly lower proportion of sweeps were kept (~60% across

day/night) but sweeps kept were still of high quality (78% beats used for average calculations).

More recent studies have designed more advanced algorithms to extract ECG features in humans (Serhani *et al.*, 2020). Nearly all of these studies follow similar pre-processing steps to those described above: cleaning of the signal, removal of baseline wander, smoothing and beat detection. Where these models differ considerably is during feature extraction. Many rely on some level of machine learning to identify features. One example is to use discrete wavelet transformation which is a process that uses successive high- and low-pass filters to break down a signal into frequency parts which can then be used with artificial neural networks or support vector machines to extract features (Qibin and Liqing, 2005; Tamil *et al.*, 2008). Other wavelet transformations can be done in the time domain where an optimal wavelet (a brief oscillating signal) is chosen and used to decompose the signal before thresholding to identify P,R and T features (Castro *et al.*, 2000; Mohamed and Deriche, 2014). These methods, while accurate at feature detection (e.g. identifying the P wave) and good at identifying irregular waveform morphologies, have not yet been used for ECG parameter calculation.

In mice, options for ECG parameter determination are considerably fewer. ECGenie from Mouse Specifics Inc, provide an ECG monitoring and analysis system but only for short term recordings. Data Sciences International offer an ECG module in their Ponemah software which can be used for longer term recording. However, we found it was not particularly accurate, cost prohibitive for many situations, and also requires a heavy investment in time for manual validation.

Our algorithm accurately identified ECG parameters, in both human and mouse, quickly without the need for complex, slower machine learning methods and extracted more information than current methods (such as P wave duration and PR segment). It does however have some limitations to consider. Firstly, ECG parameters are partially influenced by electrode placement. As our algorithm only uses single lead ECG data, if electrodes are placed differently between individuals there may be slight variations in parameter determination. As we predominantly compare individuals across time and electrodes placement remains fixed for the study this issue is minimal. Secondly, if wave morphology is irregular due to individual variability or electrode placement, the algorithm may be

unable to accurate detect onsets or offsets. In this case individuals should be excluded from further analysis. Lastly, as our algorithm averages beats across each sweep, individual beat by beat analysis is not currently possible. Minor modifications would allow for this sort of analysis but additional validation would be necessary.

Chapter 3: Differential control of human cardiac electrophysiology by the circadian system and acute changes in behavioural routine.

3.1 Introduction

Many features of the cardiovascular system display pronounced time of day variation, including cardiac electrophysiology. Daily rhythms in HR and many ECG parameters can be observed in humans across normal, LD conditions, to allow the heart to adapt to the changing requirements across the day (Zhang *et al.*, 2020). These daily rhythms are not simply a reflection of behavioural state or sleep rhythms, but are also driven in part by the body's internal circadian clock (Scheer *et al.*, 1999; Guo and Stein, 2003). The endogenous circadian system is orchestrated by the SCN of the hypothalamus; small nuclei of approximately 10000 neurons per hemisphere which constitute the body's master clock and control global rhythms in physiology such as body temperature, hormone and sleep rhythms. While there is evidence for both circadian and acute external influences governing daily rhythms in HR (Scheer *et al.*, 1999), the heart is a heterogeneous structure with many components making up the cardiac conduction system, which may respond differentially to circadian input compared to external influences. As such, the relative contributions of the endogenous clock and acute external influences such as arousal state, light exposure and locomotor activity on dictating rhythms in aspects of cardiac electrophysiology remain poorly understood.

Longitudinal and continuous ECG recording is a useful, non-invasive method for determining cardiac conduction dynamics across time and in response to environmental or behavioural manipulations. As well as describing HR and HRV, ECG information, such as measured parameters, can also define activity across all components of the cardiac conduction system as described in Chapter 2. ECG parameters are of particular importance as many have important diagnostic value. For example, in both healthy individuals and in patients with cardiovascular disease, changes in HR and HRV have been associated with increased cardiovascular risk (Abildstrom *et al.*, 2003; Thayer *et al.*, 2010; Fujita *et al.*, 2012; Shaffer *et al.*, 2014). Prolonged PR and QT intervals are associated with potentially fatal conduction disturbances, namely heart block and sudden cardiac death respectively (Algra *et al.*, 1991; Kwok *et al.*, 2016).

In this chapter we assess human cardiac electrophysiology in controlled laboratory sessions during baseline days and across imposed changes in behavioural routine such as acute sleep deprivation and subsequent recovery nap, and inversion of behavioural schedule. We find that many components of cardiac conduction display robust diurnal rhythmicity, but with differential rhythmic control across components of the heart. For example, the SA node is heavily influenced by acute changes in arousal state while the AV node is insensitive to such changes, yet remains robustly rhythmic.

3.2 Methods

ECG data used in this chapter was collected during laboratory sessions at the University of Surrey and Washington State University and provided by Professors Debra Skene and Hans Van Dongen. HR, HRV and Non-ECG data from both laboratory sessions has been published previously (Wehrens *et al.*, 2010, 2012; Skene *et al.*, 2018; Skornyakov *et al.*, 2019).

3.2.1 Ethics

Human research studies were carried out at the University of Surrey (study 1) and Washington State University (study 2) and complied with all current ethical requirements and guidelines from those institutions. Protocols were approved by their respective institutional ethics committees and data stored anonymously in compliance with the Data Protection Act (1998). Studies also conformed to the Declaration of Helsinki (2004) and the Universal Declaration of Human Right and Covenants on Human Rights (UN General Assembly, December 1948). Participants gave written, informed consent and met predefined inclusion criteria described below for each study.

3.2.2 Study one

Male shift and non-shift workers aged between 25 and 45 were recruited for this study. Shift workers were required to have cumulative recent shift work history of at least 5 years working permanent night shifts or at least three night shifts per month on a rotating schedule. Non-shift workers were required to have worked less than 6 months shift work in total. Waist and hip circumferences were measured, a general health questionnaire filled out and written consent also gathered from the participants' general practitioner confirming the participants' suitability to take part. A further four validated questionnaires

were completed: Horne-Östberg, Pittsburgh Sleep Quality Index, Beck's depression inventory and Epworth Sleepiness scale. Shift workers also completed the Standard Shift work Index to determine current shift duration and pattern. Participants were free from medications and medical conditions and had normal haematological and biochemical screening. They also did not smoke, consumed less than 15 units of alcohol per week and tested negative for substances of abuse at the time of recruitment. In total 14 non-shift and 11 shift workers were recruited for the study.

Prior to the laboratory session participants were asked to maintain a self-selected regular sleep cycle for 8 days with 7.5-8 hours sleep per night and keep a daily sleep diary. Participants' also wore two actiwatches to record activity and light exposure, and called the laboratory voicemail within 10 minutes of going to bed and waking. Participants were asked to get 15 minutes outdoor light exposure within 1.5hrs of wake to strengthen their circadian rhythms. Participants were asked to not consume alcohol or caffeine, or carry out heavy exercise for 2 days prior to the laboratory session.

During the laboratory session, participants were kept in tightly controlled conditions for 4 days with the same sleep schedule selected prior to entering the laboratory. All analyses were done relative to the participants' wake time. After a day of adaptation and baseline recording, participants were kept awake for 1 night and allowed a subsequent 4-h recovery nap that afternoon, centred 12hr away from usual sleep centre. This was followed by a normal recovery day. On non-sleep deprivation days (1, 2, and 4), subjects were posture fixed in a semi-recumbent position for the same 4 h window as the recovery nap on the sleep deprivation day. Light was fixed at a dim ~8 lux throughout wake periods and 0 lux during sleep periods. All participants were provided 3 daily meals, an evening snack at set times and water was available *ad libitum*. Blood samples were taken throughout the study via a cannula inserted on the baseline day. ECG was recorded at 256 Hz throughout using a wireless polysomnographic system (Siesta EEG/PSG recorder, Compumedics Ltd, Australia) via electrodes in two positions (right midclavicular and around 6 cm under the left armpit) using ProFusion PSG2 (version 2.1, Compumedics Ltd). Data were converted to the European data format for further analysis. Full details of this study can be found in (Wehrens *et al.*, 2010, 2012).

3.2.3 Study two

A combination of 10 male and 4 female healthy volunteers aged between 22 and 34 were recruited for study 2. Participants were psychologically and physically healthy and on no medical interventions, as confirmed by physical examinations, urinalysis, blood tests and questionnaires. They all reported 6-10 hours sleep per night with a get up time between 06:00 and 09:00. Based on the Composite Scale of Morningness questionnaire, none were extreme morning or evening types. Night time polysomnography and validated questionnaires (Pittsburgh Sleep Quality Index, Sleep Disorders Questionnaire and Epworth Sleepiness Scale) showed no evidence of sleep disorders. Participants had no history of drug or alcohol abuse and did not smoke. They had not travelled time zones or worked night shifts in the month prior to laboratory study.

One week prior to the laboratory session participants maintained a regular sleep cycle confirmed by wrist actigraphy, sleep diary and from participant calling a time stamped voicemail before bed and after waking. They were also asked to refrain from alcohol and drugs including caffeine, verified with urinalysis and breathalyser tests prior to entering the laboratory.

During the laboratory session, participants were randomly assigned to either the “day” or “night” shift conditions. Participants had fixed, 8-h windows of sleep opportunity. Both groups had 1 day of baseline recording with sleep between 22:00 and 06:00 h before the “night shift” group were, after a transition nap between 14:00 and 18:00 h, shifted to a 3-day period with a sleep window between 10:00 and 18:00 h. This was followed by a day in a tightly controlled constant routine protocol before a final recovery day. Lights were kept below 50 lux during wakefulness. Participants were given three meals a day for normal sleep/wake days and hourly isocaloric snacks throughout the constant routine protocol. Blood samples were taken prior to sleep on day 1 and periodically throughout the constant routine protocol. ECG was recorded at 4 kHz throughout except for an ~8-h window on the 3rd day using a Holter monitor (DMS 300-3 A; Bravo, Huntington Beach, CA, USA) with standard 5-lead electrode placement. Data were downsampled to 128 Hz for analysis. Full details of this study can be found in (Skene *et al.*, 2018; Skornyakov *et al.*, 2019).

3.2.4 ECG data handling

In both studies, raw ECG data was analysed as discussed in the chapter 3. Briefly, continuous ECG was split into sweeps of 10000 data points (~39 seconds in study 1, ~78 seconds in study 2) for analysis. For each sweep, after filtering R waves were detected and beat waveforms assessed in a template matching step. Beats that differed significantly from the template were removed. For each valid beat, ECG features were identified (P wave onset, offset, Q onset, R, S and T offset) and ECG parameters calculated (RR, PR, QT, QTc intervals, PR segment, P wave duration, QRS duration). ECG parameters were then averaged across all valid beats in each sweep. Sweeps were assessed for quality and excluded if they failed to reach a predefined inclusion threshold and a set of random sweeps from each individual were visually inspected for accuracy of automated feature detection and measurement.For subsequent analysis and plotting data was binned into 5 minute bins. In study 1, QT interval could not be measured for 4 individuals (2 in the control group, 2 in shift work group) as T offset could not be reliably determined.

Correlation analysis. For correlation analysis, Z-scored daily waveforms were generated for each individual across the baseline day. Within subject cross correlation was then performed comparing RR interval to QT interval and PR segment, and RR interval autocorrelogram also calculated as a control. For each individual, a phase delay was calculated by taking the mean of a Gaussian curve fit to the cross correlogram and compared to the RR autocorrelogram using a paired t-test.

RR interval dependency analysis. To calculate QT interval and PR segment dependency on RR interval, Z-scored ECG parameters from the baseline day were used. Changes in RR interval between 5 minute bins were binned by standard deviation (0.25σ) and corresponding changes in QT interval and PR segment identified. Within each bin, all changes in QT interval and PR segment were averaged for each animal. Data was then plotted as mean parameter change within each bin against change in RR interval bin centre.

HRV measurements. Primarily, a robust, unbiased geometric measure of HRV was used to assess HR dynamics (Vollmer, 2015). This measure, along with SDNN (standard deviation of valid RR intervals) and LF:HF (ratio of low to high frequency power) was calculated post hoc on a sliding window of 60 valid RR intervals across baseline and sleep

deprivation days using the MATLAB R2019b package HRVTool (Vollmer, 2019). Increasing the window of analysed RR intervals to 600 increased the absolute values of SDNN by ~38% and LF:HF by ~5%, and did not alter rrHRV. Importantly, the diurnal characteristics of all HRV measures remained unchanged. HRV measures were binned into 5 minute bins for plotting.

Cosinor analysis. To calculate rhythmic features (mesor, phase, amplitude), ECG parameters were assessed across the baseline day. A sine wave with wavelength constrained to 24hr was fit to each individual, and rhythmic parameters calculated and averaged across participants. To identify whether ECG parameters were rhythmic, a 24 hour-constrained sine wave was fit to the group data (all individuals) and the model compared to a horizontal line using the extra sum-of-squares F test. This test compares the goodness of fit of each model, and generates a P value based on the likelihood of the observing the true data, if the simpler model (horizontal line) was correct. A small P value indicates that the more complex model (sine wave) fits the data better than the simpler model and thus the ECG parameter analysed is rhythmic.

3.3 Results

3.3.1 Differential circadian regulation of SA and AV node function

To investigate rhythmicity of, and the effects of behavioural manipulations on ECG parameters we acquired longitudinal ECG data from laboratory sessions in which participants were subject to controlled LD schedules, posture maintenance and sleep manipulations (Wehrens *et al.*, 2010; Skene *et al.*, 2018). In study 1, long-term shift workers and age matched control participants (**Table 3.1**; n=11, 14 respectively) were subject to 2 days of baseline recording (adaptation day 1, baseline day 2), following which they were subject to a 30.5hr period of total sleep deprivation (TSD), a subsequent 4hr recovery nap and final normal recovery day (**Fig 3.1A**). During the 4hr TSD day nap window, on days 1,2 and 4 participants were posture fixed in a supine position. As participants were allowed to choose time of sleep to best match their personal preference, all data plotted has been aligned to 7.5 hours prior to wake time to allow for ease of viewing and standardised analysis. ECG data was collected throughout and ECG parameters (RR, QT, QTc, PR intervals, PR segment, P wave duration and QRS duration) analysed as described in chapter 3 and

	Non-shift workers (n=14)			Shift workers (n=11)		
	Mean	**SD**	**Range**	**Mean**	**SD**	**Range**
Shift work(years)	0.03	0.11	0-0.42	8.7	5.2	5.0-18.5
Time since last shift (months)	60	-	-	1.6	5.4	0.0-18.0
Age (years)	32.5	6.2	25-42	35.7	7.2	25-45
Weight (kg)	83.7	13.5	67.8-109.0	91.6	10.3	82.0-117.0
Height (m)	1.77	0.06	1.66-1.85	1.79	0.07	1.71-1.91
BMI (kg/m^2)	26.6	3.4	21.5-34.0	28.7	3.8	23.0-35.7
Waist circumference (cm)	91.2	9.4	76.0-107.0	98	6.7	90.0-110.0
Hip circumference (cm)	100	7.4	88.0-114.0	105.6	6.2	95.0-114.0
Waist-hip ratio	0.91	0.04	0.84-0.96	0.93	0.03	0.86-0.98
Cholesterol (mmol/L)	4.7	0.5	3.9-5.5	4.9	1.1	3.0-6.5
HDL (mmol/L)	1.3	0.2	0.8-1.6	1.4	0.4	0.9-2.4
Leptin (ng/ml)	9.2	1.6	1.1-20.1	10.5	1.3	5.6-17.4
Caffeinated drinks (units/day)	1.7	1.5	0.5-5.0	3	2.3	0.0-7.5
Currently smoke (units/day)	0	0	0.0-0.0	0	0	0.0-0.0
Past smoked (units/day)	3.6	5.8	0.0-15.5	4.5	5.7	0.0-15.0
Smoking duration (years)	2.6	4.4	0.0-14.0	4.4	6.3	0.0-20.0
Time since last smoked (years)	1.5	2	0.04-5.0	3.2	4.5	0.02-11.0

Table 3.1. Participant information from study 1. Data collected on screening day prior to laboratory session, adapted from (Wehrens *et al.*, 2010). No significant differences were found between groups in any parameter (unpaired t-test), with the exception of shift work duration ($p<0.001$). One individual in the control group had a short history of shift work 5 years prior. BMI: body mass index; HDL: High density lipoprotein.

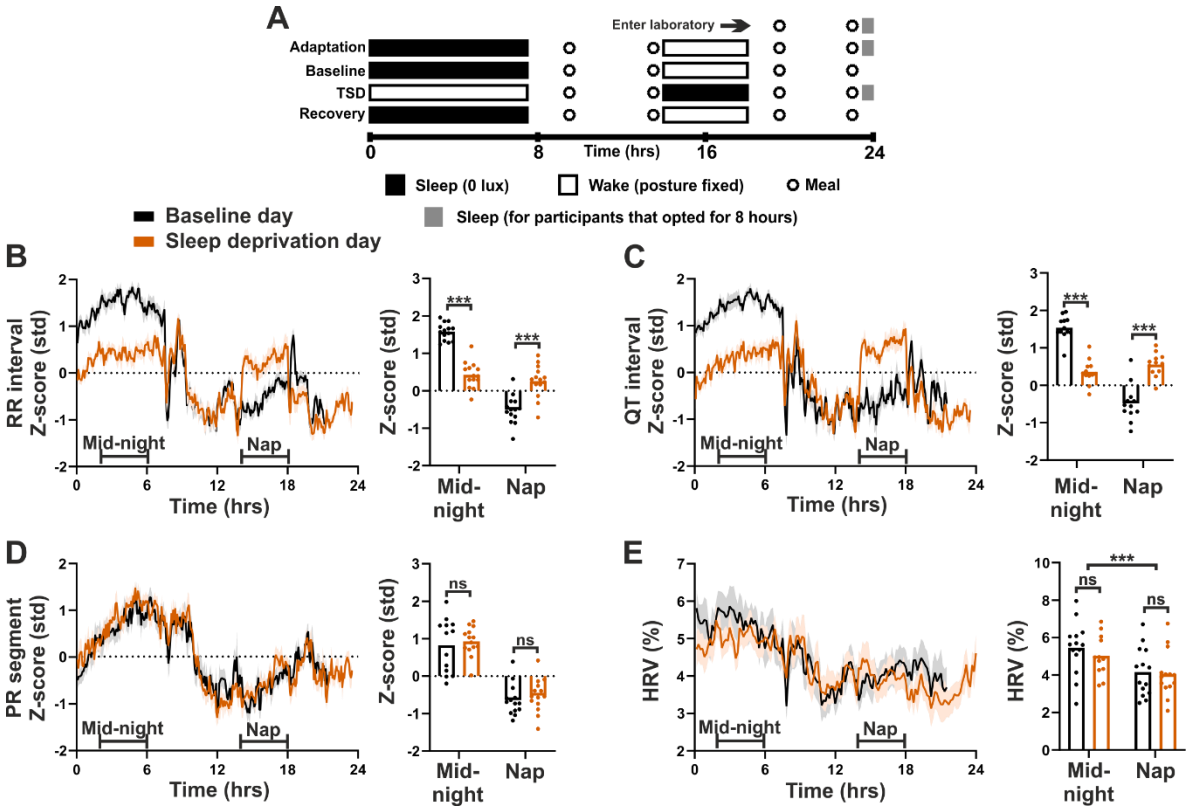

Figure 3.1. Differential circadian regulation of sinoatrial (SA) and atrioventricular (AV) node function, and decoupling by mistimed sleep. A. Schematic of 4-day laboratory session, adapted from (Wehrens *et al.*, 2010). Participants were allowed to self-select sleep duration of either 7.5 or 8 hours, and wake time. Interventions such as meals and posture fixed windows were aligned to each subjects wake time. Day 3 consisted of total sleep deprivation (TSD) followed by an afternoon recovery nap. (n=14 control). **B-E.** Z-scored ECG parameter profiles and HRV (**E**) in control participants under baseline (black) and TSD (orange) days, highlighting profound impact of mistimed sleep on RR and QT, but not PR segment. At baseline, all parameters were rhythmic based on cosinor analysis ($p<0.001$). Individual traces were excluded from waveform analysis where data coverage fell <70% of the 5 minute bins; n (baseline/TSD) = 13/14 (**B**), 11/12 (**C**), 12/14 (**D**), 12/14 (**E**). Mean ECG parameters were quantified across a 4hr mid-night and mid-day (equivalent to the nap window on day 3) analysis window on baseline and TSD days (bar graphs; two-way RM ANOVA/mixed model, n = 14 (**B,D,E**), 12 (**C**)). Data presented as group mean ± SEM; ns $p>0.05$, ***$p<0.001$.

binned into 5 minute bins for viewing and analysis. No significant differences were observed in any daily average ECG parameter, or rhythmicity characteristics between long-term shift workers and the control group (**Table 3.2**).

Robust diurnal rhythms in HR and many ECG parameters (including HRV, RR, QT, PR intervals and PR segment) were observed in both control (**Fig 3.1, 3.3**) and shift workers (**Fig 3.2, 3.4**) across the baseline day. In control individuals, sleep deprivation and subsequent recovery nap lead to significant responses in HR and RR intervals compared to the baseline day (**Fig 3.1B, 3.3**). QT interval, which reflects ventricular de- and repolarisation time, displayed similar diurnal patterns and response to sleep deprivation and recovery nap as RR interval (**Fig 3.1C**). The dependence of QT interval on HR is well documented and as such QT is often corrected to RR interval to compare values at any given heart rate. Correction of QT interval resulted in very shallow diurnal rhythms, suggesting that ventricular repolarisation time is not influenced heavily by the external influences and primarily reflects changes in heart rate (**Fig 3.3**). PR interval, reflecting atrial depolarisation and AV nodal delay, also displayed diurnal rhythmicity and a slight, though not significant, response to sleep deprivation and recovery nap (**Fig 3.3**). As PR interval reflects a combination of atrial depolarisation and AV nodal delay, we assessed P wave duration and PR segment separately. These measures approximately reflect atrial depolarisation and AV nodal delay, respectively. Interestingly, P duration was again slightly altered during TSD and recovery nap compared to baseline (though not significant), while PR segment was not changed, remaining robustly rhythmic across TSD day (**Fig 3.1D, 3.3**). Similarly, a robust, unbiased geometric measure of HRV (Vollmer, 2015) was also not influenced by changes in behavioural state, possibly suggesting that a diurnal variation in autonomic tone (thought to be largely responsible for the circadian rhythm in HRV (Boudreau *et al.*, 2013)) is not influenced by altered sleep/wake state (**Fig 3.1E**). Across all analyses, the long-term shift group exhibited similar ECG dynamics (**Fig 3.2, 3.4**). Thus, two critical aspects of cardiac conduction, pace making by the SA node and delay across the AV node exhibit robust diurnal rhythms, yet are differentially responsive to altered behavioural and sleep/wake state.

	Wehrens et al., 2012							
	Control group Baseline day		Shift group Baseline day		Control group TSD day		Shift group TSD day	
	Mean	SD	Mean	SD	Mean	SD	Mean	SD
Heart rate (bpm)	67.8	8.9	67.3	7.1	69.6[a]	9.3	69.8[a]	6.5
RR interval (ms)	917.7	128.0	915.8	93.8	887.6[a]	128.9	877.1[a]	79.6
QT interval (ms)	385.7	20.9	379.4	22.7	379.8	22.2	370.5[a]	20.1
QTc interval (ms)	397.6	11.7	391.7	10.4	396.9	8.5	389.3	11.8
PR interval (ms)	156.0	23.1	154.7	16.8	162.3	16.8	153.5	21.9
PR segment (ms)	71.9	18.3	64.4	17.9	71.0	18.0	65.6	19.6
P wave duration (ms)	82.0	13.9	87.6	6.5	87.1	9.5	82.5	14.3
QRS duration (ms)	90.0	8.5	97.2	11.6	89.5	11.1	95.3	11.5

	Wehrens et al., 2012							
	Control				Shift			
	Amplitude (ms)		Peak time (hrs)		Amplitude (ms)		Peak time (hrs)	
	Mean	SD	Mean	SD	Mean	SD	Mean	SD
RR interval	106.1	29.7	3.8	0.8	132.8	102.7	3.3	2.1
QT interval	25.3	8.4	2.9	1.9	24.7	9.2	3.3	1.6
PR segment	7.7	5.6	5.9	4.3	6.1	5.1	6.1	6.2

Table 3.2. ECG parameters in control subjects and experienced shift-workers across baseline and shift days in study 1. Top: ECG parameter means (and standard deviation, SD) across the baseline and total sleep deprivation (TSD) days. [a] Control group baseline vs TSD, $p<0.05$; Two-way ANOVA (RM where appropriate). **Bottom:** Rhythmic characteristics derived from baseline recording in control and shift-work groups. Amplitude and time of rhythm peak were calculated by cosinor analysis, with mean and SD taken between subjects (circular mean and SD for peak time). No parameters were significantly different.

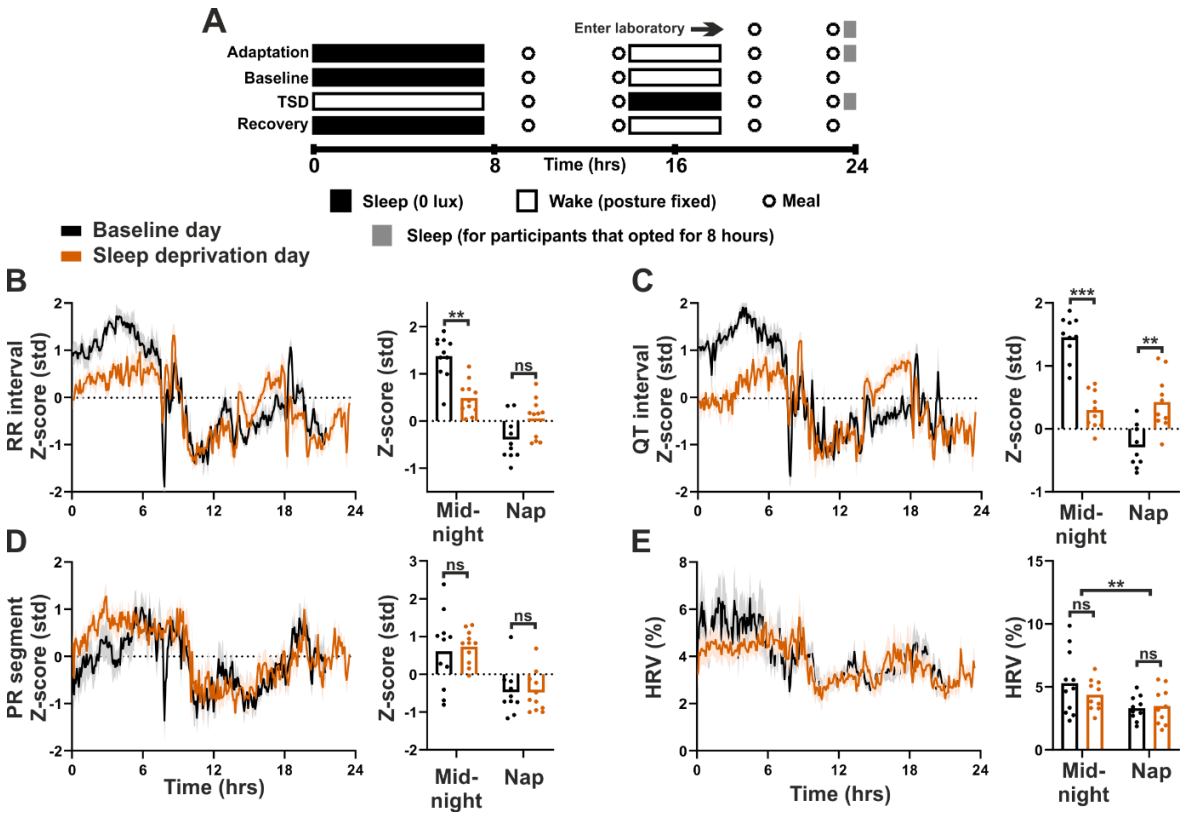

Figure 3.2. Differential circadian regulation of sinoatrial (SA) and atrioventricular (AV) node function, and decoupling by mistimed sleep in long-term shift workers. A. Schematic of 4-day laboratory session as in figure 4.1, adapted from (Wehrens *et al.*, 2010). Participants were allowed to self-select sleep duration of either 7.5 or 8 hours, and wake time. Interventions such as meals and posture fixed windows were aligned to each subjects wake time. Day 3 consisted of total sleep deprivation (TSD) followed by an afternoon recovery nap. (n=11 shift workers). **B-E.** Z-scored ECG parameter profiles and HRV (**E**) in long-term shift workers under baseline (black) and TSD (orange) days, highlighting profound impact of mistimed sleep on RR and QT, but not PR segment. At baseline, all parameters were rhythmic based on cosinor analysis ($p<0.001$). Individual traces were excluded from waveform analysis where data coverage fell <70% of the 5 minute bins; n (baseline/TSD) = 9/11 (**B**), 8/10 (**C**), 7/11 (**D**), 9/9 (**E**). Mean ECG parameters were quantified across a 4hr mid-night and mid-day (equivalent to the nap window on day 3) analysis window on baseline and TSD days (bar graphs; two-way RM ANOVA/mixed model, n = 11 (**B,D**), 10 (**C,E**)). Data presented as group mean ± SEM; ns $p>0.05$, ***$p<0.001$.

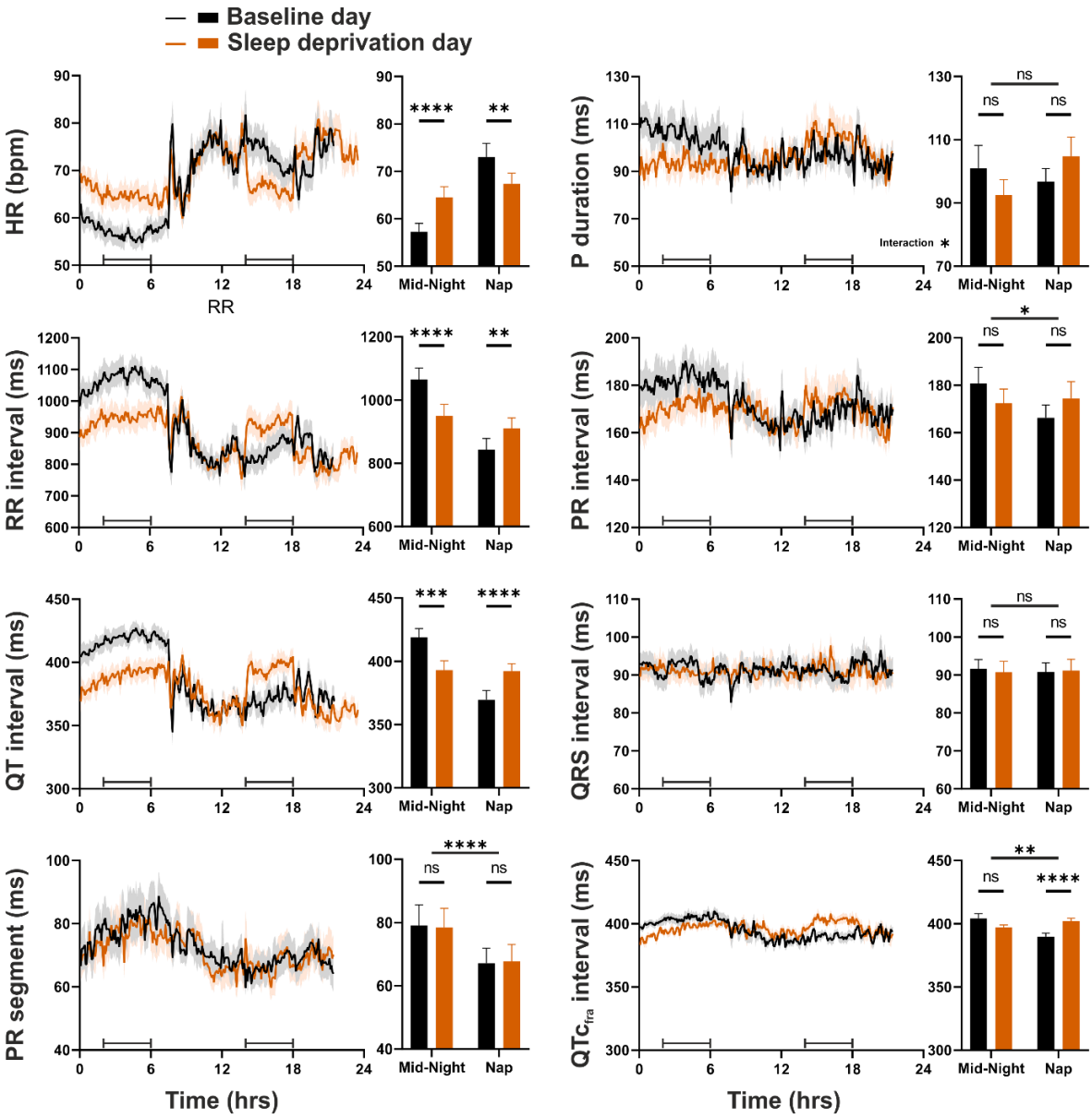

Figure 3.3. ECG parameters recorded in 4-day in-laboratory study in control (non-shift work) individuals. All calculated ECG parameters recorded over baseline (black) and total sleep deprivation (TSD, orange) days. Neighbouring bar charts reflect mean ECG parameters determined across 'mid-night' and 'nap' windows on baseline and sleep deprivation days (ns $p > 0.05$, *$p<0.05$, **$p<0.01$, ***$p<0.001$, ****$p<0.0001$, Two-way RM ANOVA/Mixed model). QTc was calculated using the Framingham correction formula (QTc = QT – 0.154(1-RR)). Shaded regions represent SEM. Individual traces were excluded from waveforms where data coverage fell <70% of the 5-min time bins; n (baseline/TSD) = 13/14 (RR, HR), 11/12 (QT), 13/14 (PR segment), 11/13 (P duration), 12/13 (PR interval), 12/14 (QRS), 11/12 (QTcFra). For mean night vs nap window analyses n = 14 (HR, RR, PR segment, P duration, PR interval, QRS), 12 (QT, QTc).

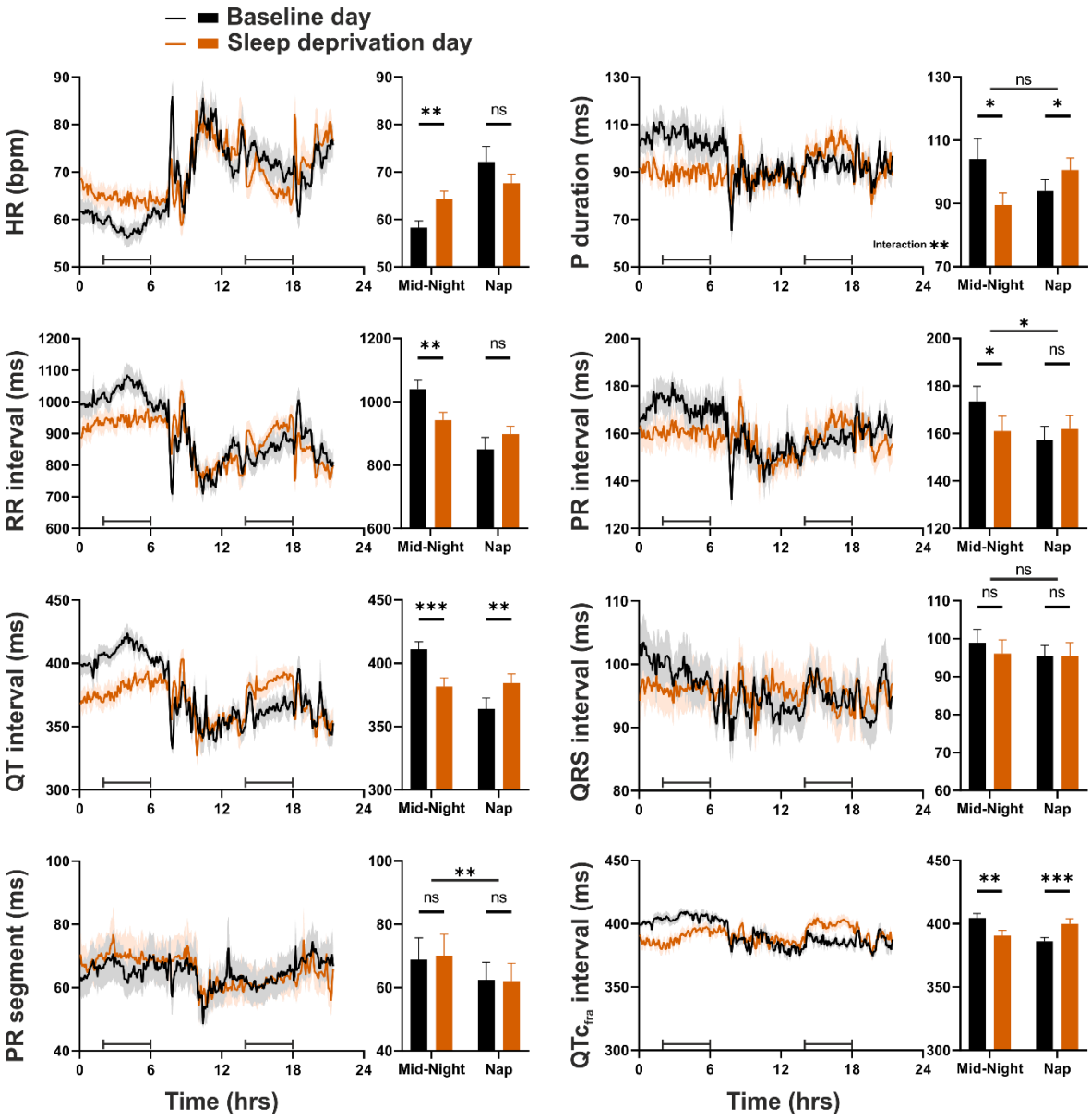

Figure 3.4. ECG parameters recorded in 4-day in-laboratory study in long-term shift work individuals. All calculated ECG parameters recorded over baseline (black) and total sleep deprivation (TSD, orange) days. Neighbouring bar charts reflect mean ECG parameters determined across 'mid-night' and 'nap' windows on baseline and sleep deprivation days (ns $p > 0.05$, *$p<0.05$, **$p<0.01$, ***$p<0.001$, ****$p<0.0001$, Two-way RM ANOVA/Mixed model). QTc was calculated using the Framingham correction formula ($QTc = QT - 0.154(1-RR)$). Shaded regions represent SEM. Individual traces were excluded from waveforms where data coverage fell <70% of the 5-min time bins; n (baseline/TSD) = 9/11 (HR, RR), 8/10 (QT), 9/11 (PR segment), 9/11 (P duration), 9/11 (PR interval), 9/11 (QRS), 8/10 (QTc_{Fra}). For mean night vs nap window analyses n = 11 (HR, RR, PR segment, P duration, PR interval, QRS), 10 (QT, QTc).

Given the temporal discordance in drivers of SA node, AV node and ventricular physiology, we next investigated the coordination between ECG parameters (RR, QT intervals and PR segment) over both long (24hr) and short (5min) time intervals (**Fig 3.5**). Across the baseline day, RR and QT interval profiles remained closely matched in both control and shift-work groups (**Fig 3.5A**). In contrast, PR segment displayed a marked phase delay from that of RR interval, as confirmed by a shift in PR segment x RR interval cross correlogram (**Fig 3.5B**). Across shorter timescales we investigated whether changes in RR interval across consecutive 5 minute bins were coordinated with changes in QT intervals or PR segments. Indeed, changes in RR interval were closely accompanied by changes in QT interval, but not PR segment (**Fig 3.5C**).

Together these findings indicate that AV nodal delay is robustly rhythmic, but acutely decoupled from heart rate under these conditions, and much less sensitive to changes in behavioural state, in stark contrast to SA pacemaking and ventricular repolarisation. Clearly the AV node is robustly rhythmic, but either buffered against acute and rhythmic changes, or receives a differential input from the SA node, for example differences in autonomic innervation.

3.3.2 Heart rate variability and effects of mistimed sleep

Given the possibility that there may be a segregation of acute and rhythmic autonomic inputs to the heart, we investigated the effects of changing behavioural state on HRV. HRV is often broadly used to assess cardiac autonomic tone (Acharya *et al.*, 2006; Billman, 2011) and can be measured in a number of ways, generally falling into three categories: i) time domain measures which reflect the instability of beats across time, ii) frequency domain measures which quantify oscillatory power across certain frequency bands and iii) non-linear methods which encompass other measures outside of time and frequency domains, often centred on geometric indices. All measures of HRV have advantages and drawbacks, and can provide qualitatively different information. Time domain measures are heavily influenced by absolute HR and changes in HR, and frequency domain measures are highly sensitive to outliers and noise, therefore requiring careful recording and interpretation. Geometric measures, such as the Poincaré plot, are excellent for visualisation, but measurements are still often sensitive to outliers. As such, we favour a geometric method

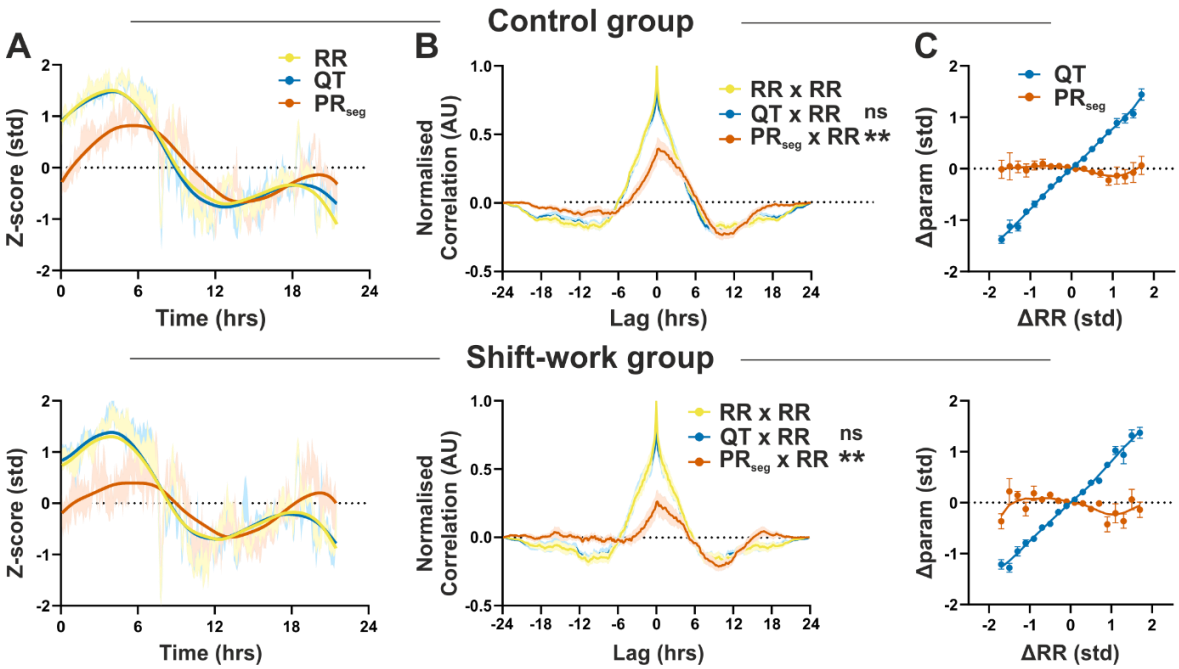

Figure 3.5. Coordination and dependence of QT interval and PR segment on HR in control and long-term shift work groups. **A,B**. Under baseline conditions, LOWESS fit of ECG profiles (**A**) and cross-correlation (**B**; Yellow: RR vs RR, blue: QT vs RR, orange: PR segment vs RR) revealed a significant phase delay in PR segment rhythm relative to that of RR (Gaussian fit with one sample T-test, **p<0.01) in both groups (control top, shift-work bottom). Shaded regions represent SEM of Z-scored data (**A**). QT remained highly coordinated with RR interval. **C.** Acute changes in RR were mirrored by a concordant change in QT, but not PR segment duration (ΔRR reflects z-scored difference in RR between sequential 5-min analysis bins; Δparam reflects concurrent change in QT or PR).

(rrHRV) that is based on relative RR intervals to minimise impact of absolute HR, short-term HRV dynamics to avoid bias from changing HRs, and robust to outliers (**Fig 3.6**) (Vollmer, 2015). This method takes periods of RR intervals and calculates the relative change between neighbouring RR intervals (**Fig 3.6B**). These can be visualised in a return map to view quasi-periodic orbital of HRV dynamics (**Fig 3.6C**). The average 2D distance from each point on this return map to the centre is then calculated as the HRV (**Fig 3.6D**). HRV calculated in this way displays diurnal rhythmicity that is not impacted by sleep/wake state, suggesting a rhythmic influence from the autonomic nervous system that is insensitive to changes in behaviour.

For a broader view of HRV dynamics we also assessed measures in the time and frequency domains across short (60 beats) sliding windows to minimise the impact of outliers/noise. SDNN, the standard deviation of valid RR intervals, is calculated as the standard deviation of all RR intervals in the analysis window (**Fig 3.7B**) and displays diurnal characteristics similar to that of rrHRV (**Fig 3.6A**). The ratio of low to high frequency power (LF:HF) is calculated using the total power within frequency bands (LF 0.04-0.15Hz, HF 0.15-0.4Hz) after conversion into the frequency domain (**Fig 3.7D**), and primarily reflects sleep/wake state (**Fig 3.7C**). Together these data suggest that there may be differential inputs from the autonomic nervous system: a buffered, rhythmic input and an acute input reflective of behavioural state.

3.3.3 Delayed response in AV nodal delay following behavioural shift

To investigate the impact of a prolonged shift in behavioural routine, akin to a transatlantic flight or night shift work, we acquired longitudinal ECG data from a second laboratory study (Skene *et al.*, 2018). In this study, participants were assigned at random to a day shift or night shift condition (**Table 3.3**, n=7 per group). After a day of baseline recording in both groups, the night shift group were subject to a reversal of behavioural routine for 4 days while the day shift group maintained the same schedule as the baseline day (**Fig 3.8A**). A constant routine protocol was then carried out, during which all external influences are removed in order to identify circadian rhythmicity. As in the first study, diurnal differences in ECG parameters were identified in most ECG parameters across the baseline day (HR, RR, QT, QTc, PR intervals, PR segment, QRS duration; **Fig 3.8B, 3.9**). No differences in daily

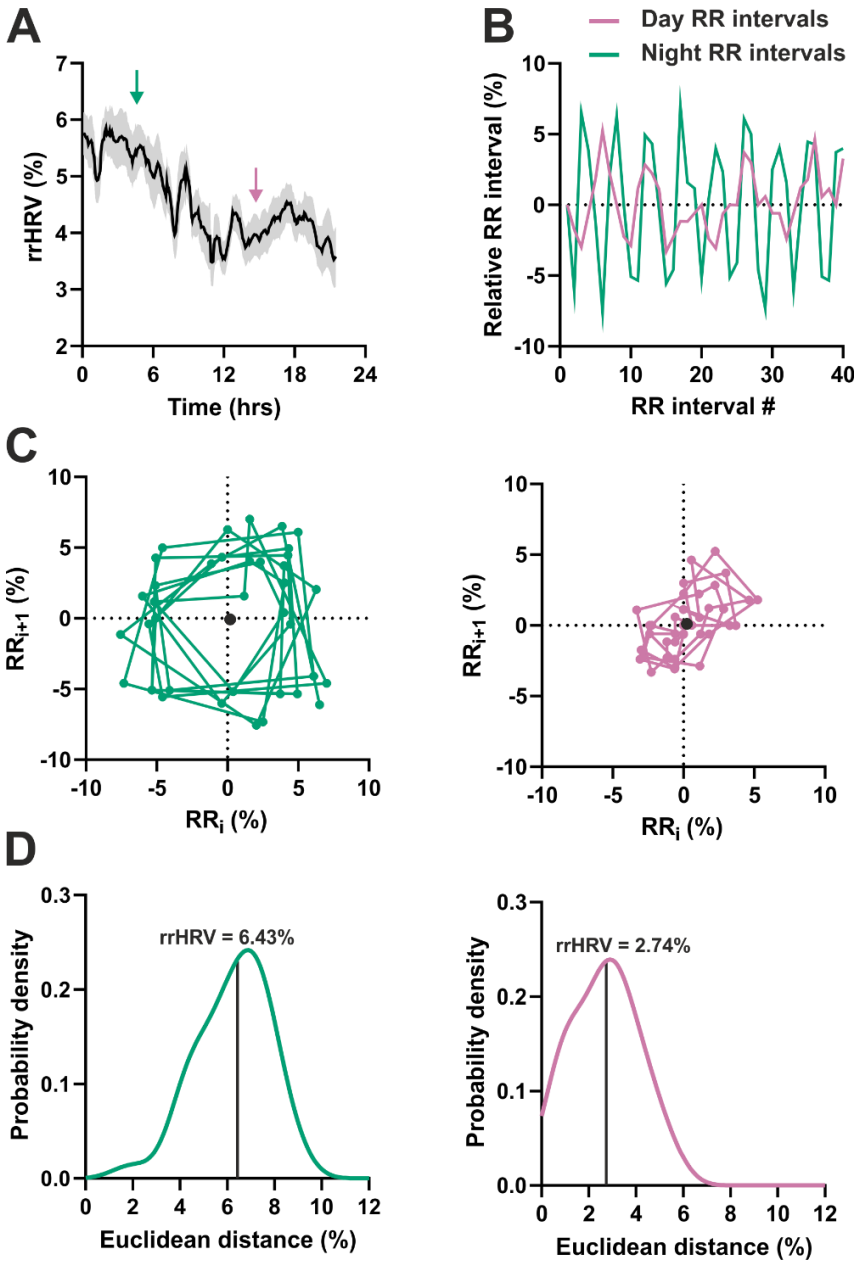

Figure 3.6. Calculation of an unbiased geometric measure of HRV based on relative RR intervals (rrHRV). Method from (Vollmer, 2015). **A**. rrHRV across baseline day in the control group. 40 beat sections of RR intervals were taken for further visualisation at times denoted by the green and pink arrows. **B.** Relative RR intervals from night and day. Using relative RR intervals rather than raw RR intervals removes bias from absolute, and acute changes in heart rate. **C**. Return map of relative RR intervals in night (left) and day (right) highlights quasi-periodic orbital nature of heart rate dynamics, to a greater degree at night. Black points identify the centre of the return map (approximately (0,0) during stable HR, but differs during changing HR). **D**. Probability density plot of Euclidean distance between each point in **C** and the return map centre. Horizontal line represents mean distance and final rrHRV calculation.

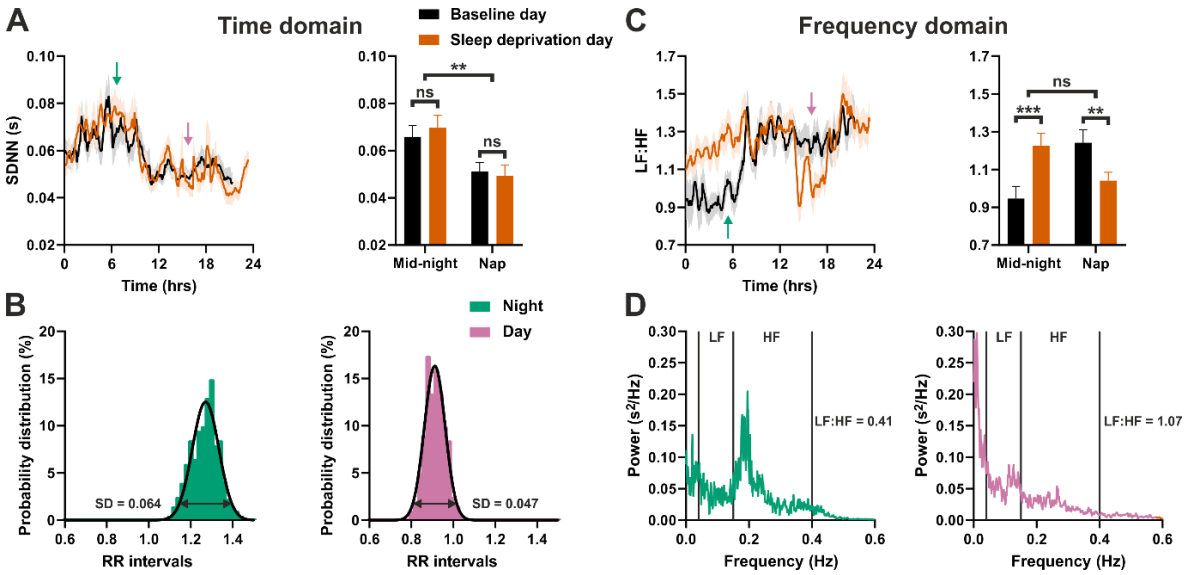

Figure 3.7. Differing HRV measures reflect differing aspects of cardiac dynamics. A. HRV measured in the time domain (SDNN: standard deviation of valid RR intervals) across baseline and TSD days (left: waveforms, right: average values across mid-night and nap windows as defined in figure 4.1) in control participants reflects diurnal dynamics that are insensitive to changes in arousal state (Two way RM ANOVA, n=14, ns p>0.05, **p<0.01). **B**. Probability histograms for periods of RR interval denotes by green (night) and pink (day) arrows in **A**, fit with a normal distribution. Inset text indicates SD of the distribution, and therefore the calculated SDNN. **C**. HRV measured in the frequency domain (LF:HF: low frequency to high frequency power ratio) across baseline and TSD days (left: waveforms, right: average values across mid-night and nap windows as defined in figure 4.1) in control participants reflects HR dynamics which are almost directly influenced by arousal state and not time of day (Two way RM ANOVA, n=14, ns p>0.05, **p<0.01, ***p<0.001). **D**. Example power frequency distributions across RR intervals taken from green and pink arrows in **C**. vertical black lines indicate thresholds for low and high frequency power and inset text shows the power ratio for the example data.

	Day condition (n=7)			Night condition (n=7)		
	Mean	**SD**	**Range**	**Mean**	**SD**	**Range**
Age (years)	24.0	2.2	22-28	27.6	3.2	24-34
Weight (kg)	80.9	12.3	59.0-98.0	90.6	19.6	62.6-108.4
Height (m)	1.77	0.08	1.65-1.88	1.87	0.12	1.66-2.04
BMI (kg/m2)	25.9	3.4	20.4-30.1	25.6	3.3	20.8-29.1

Table 3.3. Participant information from study 2. Day condition contained 4 males and 3 females, Night condition group contained 6 males and 1 female. Data from (Skene *et al.*, 2018). A slight difference between groups was observed in age (unpaired t-test, $p<0.05$), but no significant differences were found between groups in weight, height and BMI (unpaired t-test, $p>0.05$).

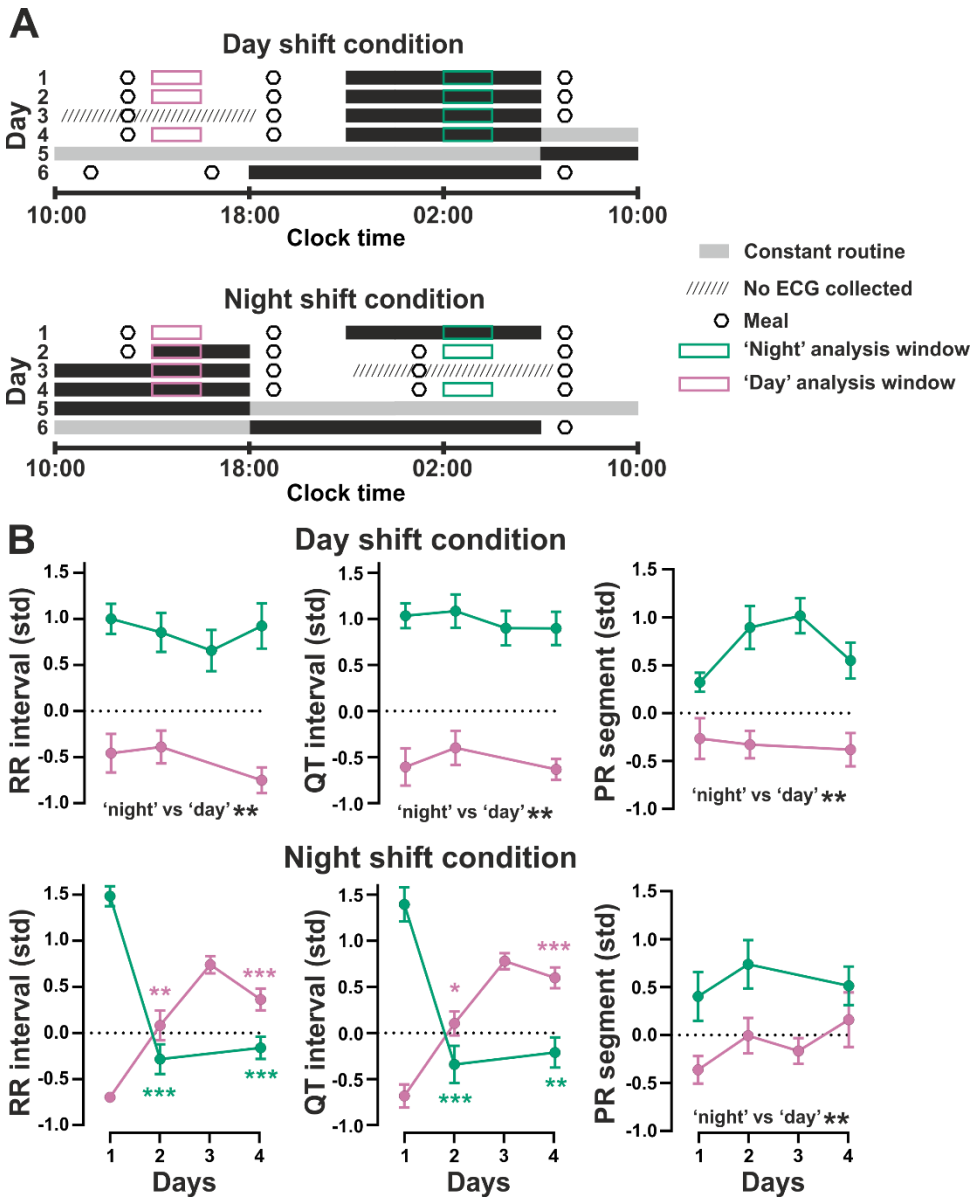

Figure 3.8. Altered behavioural routine results in long-term misalignment between SA and AV nodal function, highlighting differential regulation. **A.** Schematic of laboratory session, adapted from (Skene *et al.*, 2018). Participants entered the laboratory at 10:00, were assigned randomly to either the day shift or night shift group (n=7 per group) and maintained a controlled schedule throughout. The night shift group were subject to an inversion of behavioural schedules on day 2. Day 5 for both groups consisted of a 24hr constant routine protocol throughout which participants were posture fixed in dim light, kept awake and had hourly isocaloric snacks. 2hr mid-'night' and mid-'day' windows were used to calculate average ECG parameters, highlighted in green and pink respectively. **B**. ECG parameters were Z scored across the full laboratory session to allow direct comparison. The day shift group maintained similar ECG dynamics throughout while in the night shift group, RR and QT intervals rapidly adapted to the new schedule on day 2, whereas PR segment did not over the course of the 4 day laboratory session (Two way RM ANOVA, n=7 per group, day 3 omitted from analysis due to lack of ECG data, coloured asterisks indicate difference from day 1, *p<0.05, **p.0.01, ***p<0.001).

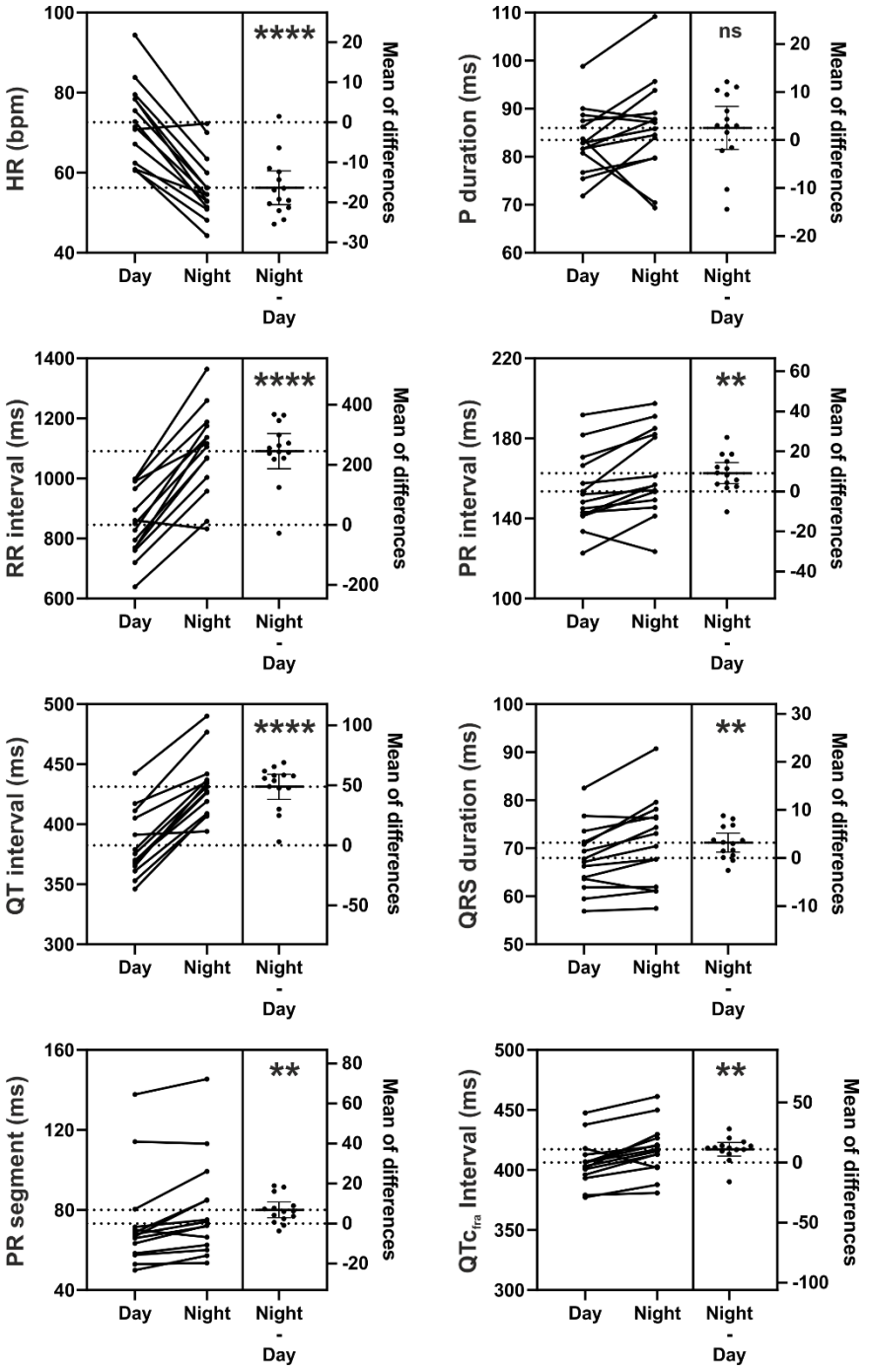

Figure 3.9. Diurnal rhythms in raw ECG parameters from study 2. Average ECG data from 4 hour day and night windows (12:00 – 16:00 and 00:00 – 04:00) during the baseline day, groups combined (n=14). Each black line represents an individual, and the differences between night and day plotted as a scatter in boxes on the right for each parameter. Horizontal dashed lines indicate day and night averages. Error bars indicate 95% CI. Inset asterisks indicate difference between day and night (paired t-test, ns $p>0.05$, ** $p<0.01$, **** $p<0.0001$).

average ECG parameters were observed between groups, or between baseline day and final day of shift routine (day 4, **Table 3.4**).

To assess changing diurnal ECG characteristics across the laboratory session, we took average parameters from 2hr 'night' and 'day' analysis windows, offset by 1 hour to avoid sleep-wake transitions during the shift (02:00 – 04:00 and 14:00 – 16:00 respectively) and compared z-scored parameters. ECG was not collected over this period on day 3. In the day-shift group that experienced no change in behavioural routine, RR, QT and PR segment retained strong time-of-day dependent profiles with lengthened intervals (and lower HR) during the 'night' window across all 4 analysis days (**Fig 3.8B**). In the night shift condition, RR and QT intervals rhythms rapidly switched to match the new behavioural routine, with parameters lengthening during the 'day' and shortening during the 'night' windows, thus matching the new sleep/wake pattern. In stark contrast, PR segment remained longer during the 'night' window across all 4 days of study. This behaviour is typical of slow circadian reentrainment to a new LD cycle and behavioural routine, which occurs over many days (Golombek and Rosenstein, 2010).

3.3.4 Constant routine reveals circadian rhythmicity

As behaviour is responsive to/driven by external influences such as light/dark cycles, daily physiological rhythms are often a consequence of a combination of endogenous circadian rhythms as well as exogenous factors. To identify circadian processes, protocols must be designed to control for external influences, the gold standard of which is a 'constant routine' protocol that holds constant external timing influences (hourly isocaloric meals, constant dim light) and behavioural rhythms (through sleep restriction and maintaining a semi-recumbent posture). On day 5 during the constant routine protocol, RR interval, QT interval and PR segment exhibited robust circadian rhythmicity in both day and night shift groups (**Fig 3.10A**). Circadian rhythms in these parameters exhibited a similar phase between day and night shift groups when aligned to external clock time but not when aligned to time in constant routine (**Fig 3.10B,C**), indicating that the mechanism that governs ECG circadian rhythmicity is unresponsive to acute changes in behaviour, and even opposes the direct influence of activity and sleep/wake state on cardiac electrophysiology.

	Skene et al., 2018							
	Day condition Day 1 (baseline)		Night condition Day 1 (baseline)		Day condition Day 4		Night condition Day 4	
	Mean	SD	Mean	SD	Mean	SD	Mean	SD
Heart rate (bpm)	67.0	9.6	65.4	4.8	68.7	9.4	66.0	8.1
RR interval (ms)	938.6	136.2	950.1	72.7	906.3	123.7	942.8	126.3
QT interval (ms)	402.2	30.3	402.0	18.3	397.7	31.4	398.7	19.6
QTc interval (ms)	411.7	21.8	409.7	17.9	412.1	19.4	407.6	20.4
PR interval (ms)	156.1	20.8	157.2	17.7	156.5	18.7	157.6	19.7
PR segment (ms)	71.3	18.2	80.1	29.0	71.4	16.1	79.9	32.6
P wave duration (ms)	85.3	9.1	83.7	5.5	85.2	8.8	84.6	5.7
QRS duration (ms)	67.9	5.4	69.9	9.3	67.9	5.7	71.4	11.1

Table 3.4. ECG parameters measured in study 2 under day- or night-shift conditions. ECG parameter means (and standard deviation, SD) measured across the baseline day (Day 1) and 4th day of shifted behavioural routine. No significant differences were observed between groups or in response to shifted routine (Two-way ANOVA with RM, $p>0.05$).

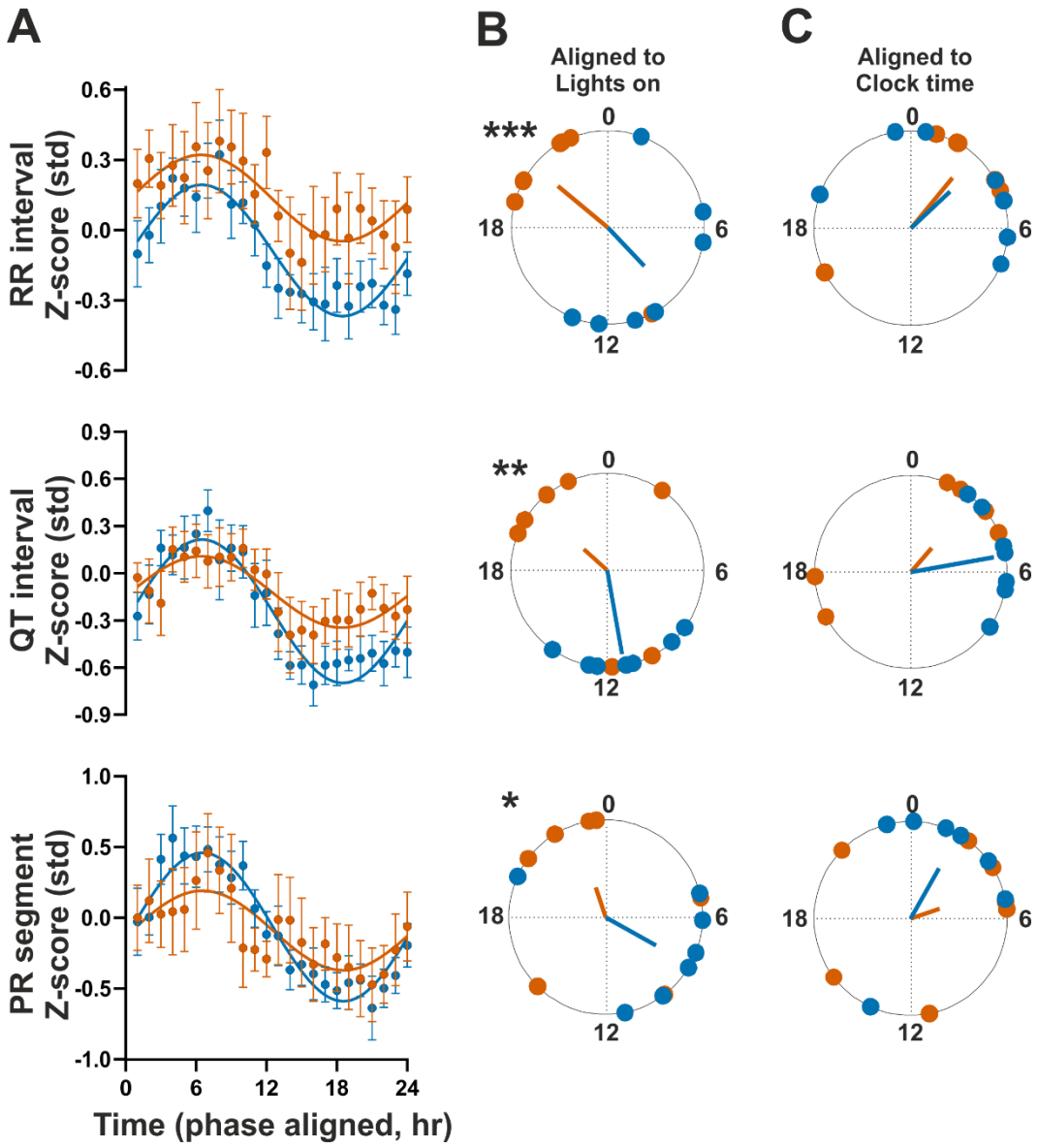

Figure 3.10. ECG parameters under constant conditions. A. Hourly binned z-scored group data and sinusoid fits from day- and night-shift conditions. Phases were aligned to account for individual differences in circadian phase. Data presented as group mean ± SEM. **B,C.** Timing (acrophase) of individual rhythm peaks relative to lights on (i.e. start of constant routine) (**B**) or external clock time (**C**). Asterisks indicate difference between groups (Watson-Williams test). *p<0.05, **p<0.01, *** p<0.001.

Together these data provide strong evidence that pace making at the SA node is influenced by the circadian system as well as changes in sleep/wake state and locomotor activity. Ventricular repolarisation may also be influenced by the circadian system and sleep/wake state, but is also heavily dependent on heart rate. In stark contrast, AV nodal delay remains insensitive to changes in sleep wake state and HR across 5 minute bins and within physiological circadian ranges (i.e. without exercise or other factors), yet remains robustly rhythmic as a result of the circadian system, indicating a fundamental discrepancy in the way components of cardiac electrophysiology are governed.

3.4 Discussion

This work highlights the profound rhythmicity of cardiac conduction across the day, and shows how components of the heart are differentially regulated on a circadian scale by the endogenous circadian clock and changes in behavioural routine. While previous work has implicated the SCN in setting rhythms in HR via the autonomic nervous system (Scheer *et al.*, 1999, 2004, 2010) and clearly changes in sleep and/or exercise impact HR, few studies have investigated how the circadian system interacts with additional factors to dictate other aspects of cardiac electrophysiology. Using longitudinal ECG recording and automated analysis alongside tightly controlled behavioural manipulations we untangle these influences and show how the SA and AV nodes can become decoupled on a diurnal scale following an acute shift in behavioural routine and/or mistimed sleep.

In humans, diurnal rhythms in HR and other ECG parameters have been documented previously, with lengthening of RR and PR intervals, QRS duration and both uncorrected and corrected QT intervals during the night (Nakagawa *et al.*, 1998; Dilaveris *et al.*, 2001; Bonnemeier *et al.*, 2003a). These changes reflect a slower HR and prolonged conduction across the AV node, His-Purkinje system and ventricular repolarisation respectively. Our data are in agreement with these findings, and for the first time show a remarkably robust rhythm in PR segment. There is some debate over whether corrected QT interval displays a diurnal rhythm (Molnar *et al.*, 1996; Ishida *et al.*, 1997), possibly in part due to the differences between correction formulae (Smetana *et al.*, 2003; Singh and Rabkin, 2021). From our tightly controlled laboratory sessions, our data do show a diurnal rhythm in QTc in humans, but with markedly reduced amplitude compared to uncorrected QT, showing

that ventricular repolarisation largely mirrors HR with only minor influence from external factors. Previous work has shown that the diurnal rhythm in HR is not only a result of external factors such as behavioural state, but also influenced by the endogenous circadian system (Scheer *et al.*, 1999, 2010; Vandewalle *et al.*, 2007). This has been most clearly shown using a forced desynchrony protocol in which behaviour is decoupled form the endogenous clock by forcing a behavioural rhythm shorter (or longer) than the limits of entrainment (Scheer *et al.*, 2010), and constant routine protocol in which all external factors are held constant (Vandewalle *et al.*, 2007). Our work confirms this finding and extends it to show that rhythms in QT and PR segment also persist under constant routine, highlighting that AV node conduction and ventricular repolarisation are also under control of the endogenous clock.

In contrast to SA node activity, which is influenced by the circadian system, arousal state, locomotor activity and light (Scheer *et al.*, 2003), our data show that AV node conduction is insensitive to behavioural manipulations and changes in HR but is strongly influenced by a rhythmic factor, most likely the circadian system. Upon first inspection this seems to be in conflict with published literature which shows that PR interval decreases with increasing HR during exercise (Atterhög and Loogna, 1977; Lee *et al.*, 1995). Importantly, these studies only investigate PR interval at HRs raised above baseline (rest) levels, while in our studies HRs are within a daily physiological range dictated by laboratory conditions with limited locomotor activity. It is reasonable to conclude that AV nodal delay remains robust to changes in HR within these ranges but may shorten in response to vigorous exercise to allow for the increased demand on the heart. However, when *ex-vivo* hearts are electrically paced at rates beyond baseline HRs, the AV node conduction velocity decreases in response to increased stimulation frequency, likely to protect from atrial arrhythmia or tachycardia propagating to the ventricles (Patterson and Scherlag, 2002). While this has not been demonstrated under physiological conditions, clearly there is a complex relationship between SA nodal pace making and AV nodal delay. Furthermore, PR interval reflects both atrial depolarisation and delay at the AV node. Our data show that P wave duration is disproportionately impacted by mistimed sleep, which could suggest that atrial depolarisation is more adaptive to HR while AV nodal delay is not. We believe that using

the P wave offset (PR segment rather than PR interval) provides a more robust measure of AV nodal delay due to the exclusion of atrial depolarisation.

The differential control over SA and AV nodal activity can render hearts susceptible to misalignment in response to relatively minor circadian manipulations. On an acute scale, sleep deprivation resulted in decreased RR with PR segment remaining similar compared to baseline day, and subsequent afternoon nap resulted in increased RR with constant PR segment. Across longer timescales after a reversal of behavioural routine similar to a transatlantic flight, a similar pattern occurs with RR switching quickly to the new schedule. This misalignment has not been previously documented so the consequent impact is currently not known. There is a possibility that differences of this magnitude are not pathologically relevant, particularly in the healthy population. However, in patients with pre-existing conditions they may become more functionally relevant. Shortened PR interval is observed in patients with pre-excitation syndromes such as Wolff-Parkinson-White (WPW) and Lown-Ganong-Levine (LGL), both of which are also associated with cardiac arrhythmias (Lown *et al.*, 1952; Benditt *et al.*, 1978; Benson and Cohen, 2017). Lengthened PR interval is associated with AV block, but whether lengthened PR interval is associated with arrhythmic events and mortality in the general population is debated (Cheng *et al.*, 2009; Aro *et al.*, 2014). While PR changes are a symptom of these disorders rather than a cause, clearly altered PR interval is associated with negative health outcomes. Further work is evidently necessary to understand how the relationship between SA and AV nodes impacts health. To speculate, when AV delay is short and SA pace making is slow there may not be optimal time to allow for blood to flow from the atria to the ventricles, resulting in decreased cardiac efficiency.

Previous studies have found that long-term shift work can influence ECG parameters such as QTc interval and measures of HRV (Meloni *et al.*, 2013; Souza *et al.*, 2015). In our study we observed no significant changes in ECG parameters between the control and shift group in terms of baseline values, features of rhythmicity (mesor, amplitude, phase) or response to behavioural manipulations. We did, however, observe a trend towards decreased PR segment diurnal amplitude in shift workers which was not significant but fits with the hypothesis that PR segment is predominantly driven by the circadian system and shift workers often have more disrupted circadian rhythms (Wright *et al.*, 2013). Generally to

understand differences in highly variable populations such as this, large n numbers are needed. Given our relatively small study (n=14 control, 11 shift workers) and that the shift work group were highly variable in duration of shift work, it is unsurprising no significant differences were observed. While we did not observe any significant differences in rrHRV between control and shift groups, a previous report from the same group who found a modest increase in baseline LF/HF ratio and a decrease in SDNN in shift workers at certain times of day (Wehrens *et al.*, 2012), which may be due to differences in HRV measures.

HRV can be measured in a multitude of ways. Methods usually fall into one of three categories: time domain, frequency domain and non-linear methods. HRV broadly reflects autonomic input to the heart but most measures have considerable limitations. Time domain measures rely on absolute differences between RR intervals and are therefore heavily influenced by heart rate. For example, a 100ms change would constitute a larger proportional change at 50bpm compared to 120bpm. Indeed, in many cases the prognostic value from time domain measures is simply down to changes in HR (Abildstrom *et al.*, 2003; Fujita *et al.*, 2012). Frequency domain measures require long periods of stable, noise free data and are heavily influenced by outliers. Traditionally frequency bands are separated into high and low, the power of which are treated as measures of parasympathetic and sympathetic tone respectively. As such, LF/HF ratio is sometimes used to describe autonomic balance. Direct vagal stimulation in anaesthetised dogs directly increases HF power (Hedman *et al.*, 1995) and increasing orthostatic tilt or other manoeuvres which increases sympathetic modulation drive increases in LF power and LF:HF ratio (Malliani *et al.*, 1991). In practice the relationship between the autonomic branches is more complex than a 'see saw'; sometimes the sympathetic or parasympathetic branch change independently of each other and sometimes they share a non-linear relationship (Billman, 2011; Shaffer and Ginsberg, 2017). Similarly, there is considerable evidence highlighting that frequency band analysis is severely oversimplified, particularly with interpretation of the low frequency band as reflecting both sympathetic and parasympathetic input (Eckberg, 1997; Billman, 2011; Reyes del Paso *et al.*, 2013). Non-linear HRV methods typically quantify distinct mathematical properties of unpredictability generally describe variability in within HR measures. These methods can circumvent some of the limitations with time and frequency domain measures but underlying physiological mechanisms can

be difficult to interpret. A good example of a nonlinear method is rrHRV; a geometric method based on relative RR intervals which is robust to artefacts, absolute HR and changing HR (Vollmer, 2015). Given these limitations interpretations of HRV should be considered carefully. As such we chose this method to simply reflect variations in relative HR dynamics.

Previous reports have shown diurnal rhythms in frequency domain (Boudreau *et al.*, 2012, 2013), time domain (Bonnemeier *et al.*, 2003b; Vandewalle *et al.*, 2007) and using a variety of non-linear methods (Vandeput *et al.*, 2012; Sammito *et al.*, 2016). Our data support these conclusions and highlight how changes in arousal state impact frequency domain measures of HRV (LF:HF) but do not impact time domain and non-linear measures. That different HRV measures respond differently supports the idea that there are differential components of autonomic innervation to the heart: potentially one that imparts time-of-day information and one that provides information on arousal state.

Chapter 4: Dissecting the relative contributions of central and local circadian clocks on cardiovascular electrophysiology in mice.

4.1 Introduction

Significant work has described circadian rhythms in mouse cardiac physiology, including endothelial function, thrombus formation, blood pressure and heart rate (Kollias *et al.*, 2009; Sheward *et al.*, 2010). Additionally, the onset of many types of cardiac arrhythmias and other adverse events display time-of-day rhythmicity (Crnko *et al.*, 2019). Results from our previous studies suggest differential impact of diurnal rhythmicity and behaviour on aspects of cardiac electrophysiology in humans. Here we examine the underlying mechanisms regarding the relative contributions of behaviour and central and local circadian clocks in mice.

Diurnal and circadian rhythms have been identified in mouse ECG parameters such as QT interval, PR interval and QRS duration (Jeyaraj *et al.*, 2012; Gottlieb *et al.*, 2016; West *et al.*, 2017; D'Souza *et al.*, 2021). Moreover, it is clear that at least some day/night differences in ECG parameters (e.g. HR and QT) are not simply passive responses to external influences (such as light or activity), but are directly influenced by the circadian system (Scheer *et al.*, 2001; Jeyaraj *et al.*, 2012). Previous studies have shown that surgical ablation of the SCN results in abolished light-induced decreases in HR in rats (Scheer *et al.*, 2001; Tong *et al.*, 2013). Moreover, in humans, light-induced increases in HR are gated by time of day, indicating a role of the central clock in setting HR across the day (Scheer *et al.*, 1999). Genetic manipulations of the cardiomyocyte clock have also revealed a role of local clock function in setting cardiac electrophysiology, with influences over HR and QT interval (Bray *et al.*, 2008; Jeyaraj *et al.*, 2012; Schroder *et al.*, 2013, 2015; Young *et al.*, 2014; Martino and Young, 2015). Significant further research is needed to understand how central and peripheral clocks interact to dictate daily rhythms in electrophysiology.

Despite observational evidence that many humans arrhythmias display a diurnal rhythm in prevalence (Black *et al.*, 2019), to date no studies have shown conclusively that there is a circadian rhythm in arrhythmia susceptibility. Previous work has shown that the transcription factor *Klf15* is strongly regulated by the circadian system, and genetic up or

down-regulation of *Klf15* results in increased likelihood of spontaneous or induced VT respectively, suggesting a role for the circadian clock (Jeyaraj *et al.*, 2012). Clearly it is important to understand the contribution of the circadian system in time-of-day vulnerability in arrhythmia onset, and how the central SCN and local clocks may contribute.

Due to similarities in cardiac physiology between mouse and human, mice are often used as models to identify mechanisms underpinning cardiac function and electrophysiology, but care must be taken before extrapolating results to humans. A predominant difference between mice and humans is in behavioural rhythms: mice are nocturnal and humans' diurnal. As a result, when a light pulse is given to a human during the night, HR increases while in mice locomotor activity ceases and HR decreases (Scheer *et al.*, 1999, 2001; West *et al.*, 2017). While mouse hearts are similar in structure and function to human hearts, there are differences in electrophysiology. Most notably, in single lead ECG humans exhibit a large positive T wave deflection while mice have a significantly shallower negative deflection, and in mice this T wave is preceded by a positive 'J' wave due to early repolarisation events, not present in humans (Boukens *et al.*, 2014). Differences in repolarisation dynamics between species are due to differences in ionic currents responsible. Namely, in humans repolarisation is predominantly driven by I_{Kr} and I_{Ks} while mouse repolarisation is driven by the transient outward K^+ currents $I_{to,f}$ and $I_{to,s}$ and a smaller contribution from $I_{Ca,L}$ (Sabir *et al.*, 2008). In mice, the P wave comprises a significantly smaller proportion of the PR interval and cardiac action potentials display markedly different morphologies, with larger depolarisation events and a lack of prominent plateau phase compared to humans. Despite these differences, the fundamental mechanisms of the heart, and how they are represented in the ECG, are similar (e.g. PR segment still reflects delay across the AV node). Therefore, using mice and models for understanding our cardiac physiology provides many advantages including ability to genetically manipulate animals, and ease of environmental and pharmacological manipulations, but care must be taken while making comparisons to acknowledge differences in cardiac physiology.

Here, we use a combination of *in vitro*, *ex vivo* and *in vivo* studies, alongside pharmacological, genetic and environmental manipulations in mice to interrogate circadian control over cardiac conduction. Furthermore, we seek to untangle the relative impact of

the central clock input via the two branches of the autonomic nervous system, peripheral clocks in cardiomyocytes, and indirect regulation from behavioural state, on cardiac electrophysiology. We also examine time-of-day dependency in susceptibility to life-threatening arrhythmias, and the potential role of the cardiomyocyte clock in such events. Together, these results provide vital insight into how the cardiac conduction system is impacted by the circadian system and highlight a need for further investigation into the mechanism of arrhythmogenesis on a circadian scale.

4.2 Methods

4.2.1 Animals

All animal experiments were licensed under the Animals (Scientific Procedures) Act of 1986 (UK) and were approved by the animal welfare committees at the University of Manchester. C57BL6J mice were purchased from Charles River (UK) and other mouse lines (*αMHC^{cre}* (Agah *et al.*, 1997)*, Bmal1$^{f/f}$* (Storch *et al.*, 2007)*, αMHC^{cre}Bmal1$^{f/f}$, αMHC^{cre}Nr1d1:Stop$^{f/f}$Luc:Bmal1$^{f/f}$*, *αMHC^{cre}Nr1d1:Stop$^{f/f}$Luc)* were bred at the University of Manchester. *Nr1d1:Stop$^{f/f}$Luc* animals were generated at the University of Manchester Transgenic facility. Mice imported from Charles River were acclimatized to the local animal unit for at least 7 days prior to use. Mice were housed under a 12:12 hour light/dark cycle at ~400 lux during the light phase and 0 lux during the dark phase unless specified otherwise. Ambient temperature was maintained at 22 ± 2 °C and humidity 52 ± 7%. Food and water were available *ad libitum*. For all ECG experiments, mice were group-housed until the start of ECG recording, during which they were individually housed and kept in light-tight cabinets.

4.2.2 ECG device implantation

Animals were implanted with ETA-F20 radiotelemetry devices (Data Sciences International, USA) to record electrocardiography, body temperature and locomotor activity. Mice were first shaved across the abdomen then anaesthetised with isoflurane (5% induction, ~2% maintenance in medical air). Following confirmation of surgical plane anaesthesia (stable breathing, lack of pedal reflex), the surgical area was swabbed with iodine solution and a primary ~1cm incision made along the midline. Skin was bluntly dissected away from the underlying muscle and a small cut made into the intraperitoneal cavity. The body of the

radiotelemetry devise was inserted and muscle layer sutured with biopotential leads protruding. Leads were then fixed in place subcutaneously ~1cm right of the midline at upper chest level (negative lead) and ~1cm left of the midline at the xiphoid plexus (positive lead). The skin was then sutured together and mice given an intramuscular injection of buprenorphine (0.03mg/kg) for postoperative analgesia. Mice were allowed a recovery period of 7-10 days before beginning recording and recovery monitored daily.

4.2.3 ECG analysis

All ECG analysis was carried out using bespoke analysis software written in MATLAB (R2018a, Mathworks, USA). Full details of analysis procedure and example code can be found in Chapter 2. Briefly, for each ECG sweep R waves were detected via thresholding and an average beat waveform template created. Any individual beats that differed significantly from the template were removed and any sweeps that did not meet predefined quality control measures were removed. ECG features were identified for each beat and parameters calculated and averaged across the sweep. A set of random sweeps from each individual animal were visually inspected for accuracy of automated feature detection and measurement. For most studies, physiological parameters were collected every 5 minutes alongside a 10s ECG sweep, or continuously for autonomic blockade studies.

Impact of siesta calculations. To identify the impact of the mid-night rest period on ECG parameters, Z-scored ECG and locomotor activity were averaged across a 5 day baseline recording period. The average locomotor activity trace for each animal was manually inspected and the time at which locomotor activity ceased for a prolonged period (~2hrs) was identified as siesta onset. ECG parameters were then aligned to the siesta onset and a 2hr window prior to and during siesta was used to calculate average 'active' and 'rest' values respectively (Two way ANOVA, 'active' vs 'rest', n=10 mice).

Impact of locomotor activity. Using 5 days of baseline recording, periods of locomotor activity which were followed by 45 minutes of inactivity were identified. For each animal, Z-scored ECG parameters across such each occurrence were averaged together. Each time point was compared to the data point 40 minutes following locomotor cessation as a baseline as this was the peak RR interval (lowest HR) across the recording

window. To assess the impact of transient activity bouts on ECG parameters, periods were identified in which a single 5 minute bin of locomotor activity was preceded by 5 minutes and followed by 20 minutes of inactivity. Changes in ECG parameters pre and post activity were compared (Two-way ANOVA vs pre-activity baseline, n= 10 mice).

Correlation analysis. For correlation analysis, Z-scored daily waveforms were generated for each animal for each parameter across 5 days of baseline recording. Within subject cross correlation was then performed comparing RR interval to QT interval and PR segment, and RR interval autocorrelogram also calculated as a control. For each individual, a phase delay was calculated by taking the mean of a Gaussian curve fit to the cross correlogram and compared to the RR autocorrelogram using a paired t-test (n=10).

RR interval dependency analysis. To calculate QT interval and PR segment dependency on RR interval, parameters were Z-scored across 5 days of baseline recording. Changes in RR interval between 5 minute bins were binned by standard deviation (0.5σ) and corresponding changes in QT interval and PR segment identified. Within each bin, all changes in QT interval and PR segment were averaged for each animal. Data was then plotted as mean parameter change within each bin against change in RR interval bin centre (n=10).

4.2.4 *In vivo* bioluminescence imaging

αMHC^{cre}Nr1d1Stop$^{f/f}$Luc mice (male, n=1 at ZT8 and ZT20) were anaesthetised in isoflurane (5% induction ~2% maintenance in medial air) and shaved across the chest prior to *in vivo* luminescence imaging. Mice were placed in the centre of the *in vivo* imaging system (IVIS, Perkin Elmer) imaging window and luciferin given via i.p. injection. After 10 minutes, mice were imaged for an automatically detected exposure period. This timing (10 minute post-injection) was determined in initial studies as the peak in bioluminescence after acute luciferin injection.

For longitudinal *in vivo* bioluminescence recording, mPER2:LUC mice (n=4 male) were shaved across the back to maximise bioluminescence signal and singly housed in DD within LESA-biolumicorders (LESA technologies). Luciferin was given *ad libitum* in the drinking water (1mg/ml; Promega). Photon emissions were collected over 1 minute periods and recorded continuously. CK1δ/ε inhibitor CP709 (50mg/kg i.p.; Pfizer) or vehicle control was

given as a daily injection at projected ZT10. This experiment was conducted by Oscar Allen, a previous student in the group.

4.2.5 Heart weight measurements

For heart weight measurements, *αMHC^{cre}Bmal1$^{f/f}$* and *Bmal1$^{f/f}$* Mice (n=6/group, aged 10-17 weeks) were rapidly culled by cervical dislocation and hearts quickly excised at approximately the level of the aortic arch. Excess blood was drained by dabbing the hearts on absorbent material and hearts were weighed using a fine balance.

4.2.6 Autonomic blockade

Conscious, free-moving mice (C57Bl/6J, *αMHC^{cre}Bmal1$^{f/f}$* and *Bmal1$^{f/f}$*; male aged 12-14 weeks, n = 7-9/group) were given an i.p injection of metoprolol (10mg/kg, Sigma-Aldrich) to block the sympathetic nervous system. After 40-60 minutes when HR had stabilised, a further i.p injection of atropine (4mg/kg, Sigma-Aldrich) was given to achieve total autonomic blockade. This was confirmed by the marked reduction in HRV which was maintained across the following 30 minute analysis window.

4.2.7 In vivo arrhythmia induction

Mice (*αMHC^{cre}Bmal1$^{f/f}$* and *Bmal1$^{f/f}$*; male aged 12-14 weeks, n=5-6/group) were first implanted with ECG radio telemetry devices and left to recover as described previously. At ZT0 or ZT12, mice were injected with 120mg/kg caffeine (Fisher Scientific) and 2mg/kg adrenaline hydrochloride (Sigma Aldrich) in PBS solution. Following injection, animals were monitored closely for 15 minutes and culled by cervical dislocation. Stereotypically animals displayed tachycardia immediately following injection, followed by bradycardia, then premature complexes and irregular/skipped beats before some progressed to bidirectional ventricular tachycardia (BVT). Traces were analysed by visual inspection (blinded to genotype). Periods of widened QRS complexes of ventricular origin with alternating polarity lasting at least 4 beats were categorised as BVT. In most cases bouts lasted longer than 30 seconds.

4.2.8 Mathematical modelling of phase advance

To approximate a circadian only process across a 9hr phase advance, we generated a 24hr sine wave with mesor and amplitude matched to Z-scored RR interval, synchronised with

the 12:12 LD cycle. Following a phase advance in the light cycle the model shifted linearly towards the new LD cycle over the course of 6-7 days. This entrainment period was chosen based on the average time it took for mice to entrain to this stimulus, measured manually by finding the intercept between activity onset and lights off in the actogram of each animal. Across each day, for each parameter and model, average value during lights off was subtracted from average value during lights on and scaled so a normalised value of 1 represents longest ECG parameters during lights on and -1 represents longest ECG parameters during the lights off. A model (or parameter) that mirrors the light exactly would be 1 across all days of the shift.

4.2.9 Bioluminescence recordings

Bioluminescent reporter mice (*mPer2luc, Nr1d1Stop$^{f/f}$luc, αMHC^{cre}Nr1d1Stop$^{f/f}$Luc and αMHC^{cre}Bmal1$^{f/f}$Nr1d1Stop$^{f/f}$Luc*; male/female) were culled by cervical dislocation and tissues rapidly dissected into 37°C Hanks Balanced Salt Solution (Sigma-Aldrich H6648). Tissue samples were then transferred to a sterile hood and plated into a 35mm dish on culture membranes (Millipore PICM0RG50) in 1ml sterile recording media [Dulbeccos Modified Eagles Medium (Gibco), 1X B-27 (Thermofisher), 25mg/L Penicillin-streptomycin (Gibco, Invitrogen), 0.1mM D-luciferin (E1602, Promega)] and sealed with high-vacuum grease (Dow Corning #14-625-5D, Fisher) and a glass coverslip. Samples were incubated in a 32 channel Lumicycle (Actimetrics) at 37°C and bioluminescence recorded for 1 minute every 10 minutes. Tissue samples were synchronised with 100nM Dexamethasone (D4902 Sigma) after 2 days recording. A 24 hour moving mean was subtracted from the raw data to generate baseline subtracted values.

4.2.10 Sinoatrial node dissection

Mice (C57BL/6J, male aged 12-14 weeks, n=4/time point) were housed under a stable 12:12hr LD cycle for 2 weeks prior to microdissection. SA tissue was collected at six equal time points across a 24hr period. Mice were culled using cervical dislocation and hearts rapidly excised into sterile, ice cold PBS. Hearts were washed to remove blood. Under a dissection microscope, hearts were cut horizontally across the base of the atria and pinned onto a Sylgard (Sigma-Aldrich) plate. Following identification of the right atrial appendage and superior vena cava on top of the preparation, a rectangular section including the SA

node was dissected using fine scissors. The first incision was made from sulcus terminalis towards the inferior vena cava, second made towards the superior vena cava, third lateral of the sulcus terminalis and fourth along the root of the superior vena cava to fully excise the tissue (Fenske *et al.*, 2015). Tissues were then snap frozen on dry ice and stored at -80°C.

4.2.11 Gene expression analysis

Tissue was homogenised using TRIzol reagent (ThermoFisher) in a Bead Mill (Bead mill 24, Fisherbrand), then chloroform (Sigma-Aldrich) added to promote phase separation. Following 10 minute incubation at room temperature, samples were centrifuged at 12000G for 15 minutes at 4°C. The aqueous phase was then transferred to a clean tube and isopropanol added. Samples were then vortexed and added to a minicolumn over a collection tube (Reliaprep tissue, Promega) and centrifuged at 12000G for 1 minute at room temperature. As per manufacturers protocol, RNA wash solution was then added to column and centrifuged for 30s, followed by incubation of DNAse mix for 15 minutes at room temperature. Columns were then washed with column wash and RNA wash solutions before RNA eluted in nuclease-free water and frozen at -80°C for storage. RNA was then converted to cDNA using a High-Capacity cDNA Reverse Transcription Kit (Applied Biosystems) as per manufacturers' protocol. Quantitative PCR was performed on a 384 well thermal cycler (7900, Applied Biosystems) using GoTaq master mix (Promega). Relative gene expression was calculated using the ΔΔCt method using *Hprt*, *Ppib* and *Actb* as housekeeping genes (Livak and Schmittgen, 2001).

4.2.12 Langendorff heart perfusion

Animals ($\alpha MHC^{cre}Bmal1^{f/f}$ and $Bmal1^{f/f}$; male/female aged 12-15 weeks, n=7 per group) were culled and hearts rapidly removed into ice cold Krebs-Henseleit Buffer (KHB) solution (constituents in mM: 118 NaCl, 11 glucose, 1.8 $CaCl_2$, 4.7 KCl, 25 $NaHCO_3$, 1.2 $MgSO_4$, 1.2 KH_2PO_4). Excess tissue was removed and aorta cannulated and perfused with KHB under a dissection microscope. Successful dissection was confirmed when the cardiac vasculature cleared with perfusate with no visible air bubbles. The cannulated heart was then attached to a jacketed glass coil filled with oxygenated KHB and warmed to 37°C. The heart was then perfused at 4ml/min. The whole process from culling to perfusion took approximately 4

minutes. Any hearts that did not stabilise during a 10 minute stabilisation period were excluded (<10%). Custom-made silver chloride electrodes were used to record monophasic action potential from the left atrial appendage and ventricular myocardium. Signals were amplified using Bioamplifiers, digitised by Powerlab (4/35) and analysed in LabChart (v8, ADInstruments). Electrical stimulation was applied by a similar custom-made silver chloride electrode to the right atrial appendage. Electrode placement remained consistent between experiments and based on anatomical landmarks. Ventricular arrhythmias were induced using an S1S10 protocol. An S1 train consisting of 20 pulses at 100ms cycle length was immediately followed by an S2-S10 train of extra stimuli, initially at 90ms cycle length and decreasing with every iteration by 3ms, down to 18ms. Each stimulus iteration was separated by a 2s rest period. Ventricular tachycardia was characterised according to the Lambeth convention. At least 4 premature ventricular complexes following stimulation was characterised as ventricular tachycardia. This process was repeated twice and hearts that displaced evidence of VT on both trials were classified as susceptible to VT. Animals were culled and hearts removed between ZT0-1 and ZT11-12 to avoid any differences in light exposure immediately prior to and during culling.

4.2.13 Cardiomyocyte isolation and recording

Primary cardiomyocytes were isolated from P2-3 neonatal mice using a commercially available dissociation kit (Miltenyi Biotec). Animals (*Bmal1*$^{f/f}$) were culled and hearts removed into ice cold dissociation buffer (constituents in mM: 106 NaCl, 20 HEPES, 0.8 NaH_2PO_4, 5.3 KCl, 0.4 $MgS0_4$, 5 glucose). Hearts were diced into small sections and digested enzymatically. Solution was then filtered through a 70µm and placed in dishes for 2hr. Supernatant was collected and 1 x 10^5 cardiomyocytes were seeded onto a multielectrode array (MEA) coated with 10µg/ml fibronectin (Sigma-Aldrich). Five hours after seeing, DMEM high glucose media supplemented with 10% horse serum, 5% calf serum, Glutamax, Penecillin/streptomycin, Mycozap (Lonza) and 17% M199 (Thermofisher) was added and changed daily for 8 days before release into constant 37°C conditions. Twice daily, field potentials were recorded using an MEA recording device (MEA2100-1 x 60-system (MCS) for 5 minutes at 20kHz following 2 minutes equilibration. Data was recorded and analysed using the Multi-Channel experimenter and DataManager software. Data presented are from electrodes on a single MEA but repeated across multiple experiments.

For bioluminescence recordings, cardiomyocytes were seeded and grown to confluence and then synchronised using temperature cycles of 12:12hrs at 32°C:37°C for a minimum of three days. During recording, cells were plated with sterile recording media. Bioluminescence was recorded using ALLIGATORs (Cairn Research) for 29 minutes in 30 minute intervals at 37°C. Cardiomyocyte isolation/recording experiments were performed by Alessandra Stangherlin at the MRC Laboratory of Molecular Biology at the University of Cambridge.

4.3 Results

4.3.1 Diurnal rhythms in cardiac physiology

To investigate diurnal rhythmicity in mouse cardiac electrophysiology, i*n vivo* radio telemetry was used for long term, non-invasive recording of behavioural and physiology rhythms in male C57BL/6J mice. Averaging across 5 days of baseline recording under 12:12hr LD cycle, animals displayed robust diurnal rhythms in locomotor activity, body temperature and HR (**Fig 4.1**). Recoding ECGs across the daily cycle revealed robust rhythms in most ECG parameters (RR, QT and PR intervals, PR segment and QRS duration) with lengthened intervals during the animals inactive phase (daytime), while no significant day-night differences were observed in HR corrected QT (QTc) interval or P wave duration (**Fig 4.1**). We also observed diurnal variations in HRV measures across the time, frequency and non-linear domains (**Fig 4.2**). The diurnal rhythmicity of a geometric measure of HRV based on relative RR intervals (rrHRV), like in humans, was lower during the active phase (dark) compared to the inactive phase (light). In contrast, SDNN and LF:HF displayed dynamics disparate to those in humans relative to the active/inactive phase, instead showing increased SDNN and decreased LF:HF during the active phase. Therefore, light may drive these measures of HRV independently of behavioural state, possibly suggesting a fundamental similarity in some components of autonomic control over cardiac dynamics between humans and mice. Indeed, the phase of SCN firing between species is similar relative to the LD cycle, as are fractal dynamics of HRV between human and rat (Hu *et al.*, 2008).

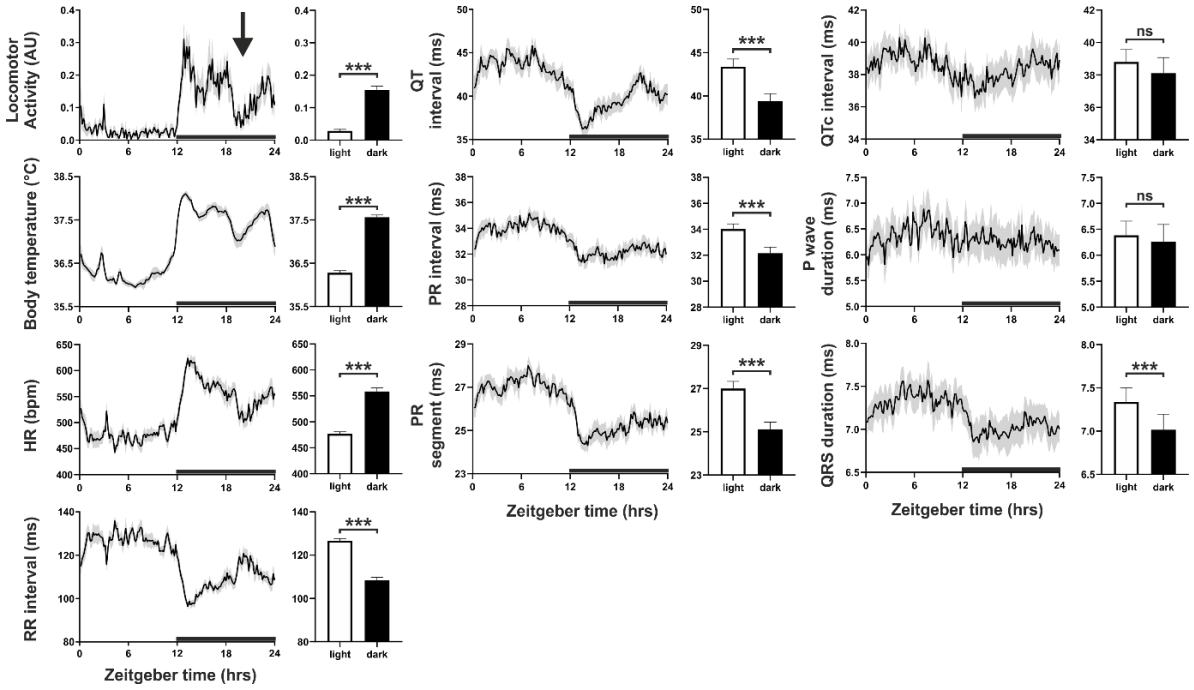

Figure 4.1. Diurnal rhythmicity in mouse physiology and cardiac conduction. Waveforms averaged for each mouse over 5 days of 12:12 LD recording. Vertical arrow highlights the siesta period during which mice sleep. Black bars inset in waveform panels indicate darkness. Neighbouring bar plots represent average parameter across light and dark phases. Paired t-test, ns $p>0.05$, ***$p<0.001$. Data plotted as mean ± SEM, n = 10 mice.

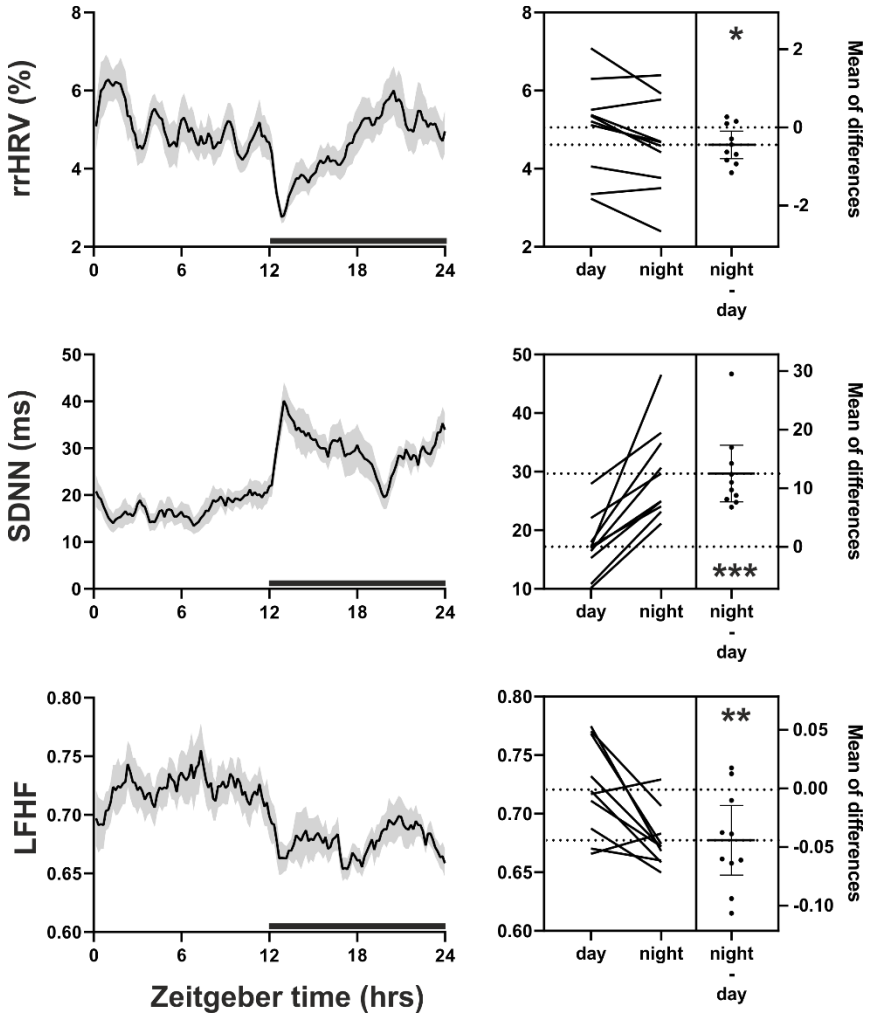

Figure 4.2. HRV measures across time, frequency and non-linear domains. Waveforms (left) averaged across 5 days and estimation plots (right) show individual differences between day and night and magnitude of change. Inset asterisks indicate differences between day and night (paired t-test, *p<0.05, **p<0.01, ***p<0.001). HRV measures calculated for all valid RR intervals across each sweep. Non-linear HRV is a non-biased geometric measure based on relative RR intervals (Vollmer, 2015). SDNN represents standard deviation of valid RR intervals and LF:HF is the ratio between low and high frequency power in the frequency domain.

4.3.2 Differential impact of sleep and locomotor activity on ECG parameters

An important observation in our human studies was the differential impact of changes in arousal state and locomotor activity on ECG parameters. Mice, in particular the C57BL/6J strain used here, typically exhibit a rest/sleep period in the second half of the dark period (Collins *et al.*, 2020). This was clearly observed in body temperature and locomotor activity recordings (**Fig 4.1**, arrow). We have therefore examined the impact of this altered resting state on ECG parameters. For this analysis, we aligned each animal to the onset of this 'siesta' period and compared 2hr windows prior to and during this relative rest period (**Fig 4.3A**). While locomotor activity calculated from radio telemetry devices may not be as sensitive as other methods (e.g. wheel running, passive infrared sensors), it was sufficient for the determination of siesta onset in our studies (see **Appendix A**). We observed a significant lengthening of RR and QT intervals during rest compared to preceding active period, but no change in PR segment (**Fig 4.3B**), indicating that PR segment is relatively insensitive to changes in behavioural state. We next identified periods of locomotor activity followed by 45 minutes of inactivity in each animal (across 5 days of recording) to assess how acute changes in locomotor activity impact ECG parameters. After aligning these periods averaging across events and animals, we found that RR and QT intervals showed a significant and pronounced response to changes in locomotor activity, while, although significant, the impact on PR segment much less pronounced (**Fig 4.3C**). Moreover, the impact of these activity bouts on PR segment was approximately 0.4std, substantially lower than the normal diurnal variation observed (~4std), suggesting that locomotor activity is not a major influence on the daily variations observed in PR segment. Indeed, transient bouts of locomotor activity (activity preceded by 5 minutes and followed by 20 minutes of inactivity) had little impact on PR segment (not significantly altered from baseline 10min prior to activity), while RR and QT intervals decreased significantly (**Fig 4.3D**).

As observed in our human studies, in mice, the daily rhythm in PR segment displayed a modest, but significant, phase delay compared to the rhythm in RR interval when assessed by cross-correlation analysis (**Fig 4.4A,B**). Rhythms in QT interval instead showed a slight phase advance compared to rhythms in RR interval. We next investigated whether changes in RR interval were accompanied by changes in QT interval and PR segment by binning changes in RR interval across consecutive 5 minute bins and comparing corresponding

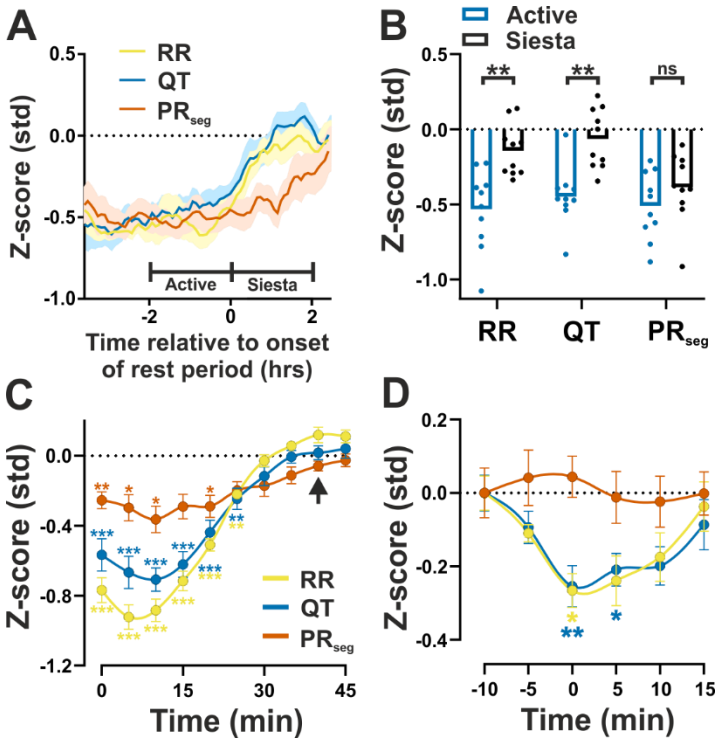

Figure 4.3. Influence of arousal state and locomotor activity on ECG parameters. A. RR, QT and PR segment aligned to the cessation of locomotor activity at the start of the dark phase 'siesta'. Black bars indicate 'active' and 'rest' periods used for analysis in **B**. Analyses based on 5 days of baseline recording. Z-scoring is based on the 5 day recording window for each mouse. **B**. Decreased locomotor activity during mid-night *siesta* was accompanied by a significant decrease in RR and QT intervals, but not in PR segment duration (2hr *siesta* period vs preceding 2hr of activity; two-way RM ANOVA). **C.** Periods of LA followed by >45min of complete inactivity were isolated and aligned to cessation of activity (time 0). RR, QT, and to a lesser extent PR segment showed a significant response to activity which decreased over subsequent inactivity (two-way RM ANOVA, Dunnet's post-hoc, difference from t=40). **D**. Transient bouts of LA (preceded and followed by inactivity) caused a significant response in RR and QT interval lengths, but not PR segment (two-way RM ANOVA, Dunnet's post hoc, difference from t=-10).

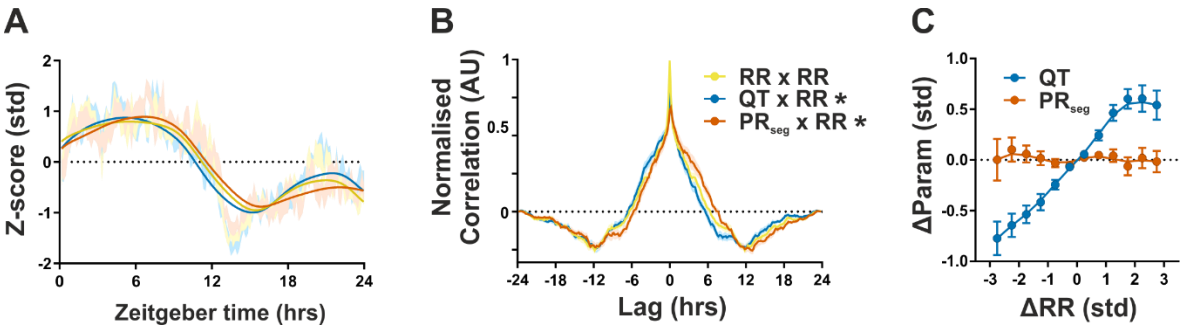

Figure 4.4. Correlations between ECG parameter waveforms and dependence on HR. A. LOWESS fit of RR (yellow), QT (blue) and PR segment (orange) averaged across 5 days baseline LD conditions. **B.** Phase shift revealed by cross-correlation analyses of RR vs QT and RR vs PR segment (Gaussian fit with one sample t-test). **C**. Acute change in RR (across 5-min analysis bins) were mirrored by changes in QT, but not PR segment. All data presented as mean ± SEM. N=10. ns $p>0.05$, *$p<0.05$.

changes in QT interval and PR segment. Indeed, changes in RR interval were closely accompanied by changes in QT interval, but not PR segment (**Fig 4.4C**). Together these data reveal that in contrast to QT interval, PR segment (reflecting AV nodal delay) is minimally influenced by arousal state, locomotor activity and changes in HR. These dynamics were similar to those observed in humans in section 3.3.

4.3.3 Phase advance results in misalignment between SA and AV nodes

To assess whether an abrupt change in external light/dark schedule impacted ECG parameters, mice were acclimatised to 12:12hr LD for 7 days, then subjected to a 9hr advance of the LD cycle (**Fig 4.5**). To this change in LD cycle, mice display slow re-entrainment, gradually shifting behavioural rhythms to match the new cycle over ~6-7 days (**Fig 4.5A**). Across this phase advance, daily rhythms in RR interval exhibited a rapid response to the shift, while rhythms in PR segment and body temperature (a physiological measure of the central circadian clock) did not (**Fig 4.5A,B,D**), instead gradually adjusting to the new schedule over many days. Remarkably, the rapid response in RR interval rhythm and the slower adaptation of rhythms in PR segment lead to a transient misalignment between the two profiles as evidenced by the inversion of light-dark averages on the day of shift in RR interval but not PR segment (**Fig 4.5D**) and waveforms from an individual animal (**Fig 4.5B,C**), revealing different sensitivity to behavioural input at the SA and AV nodes. That PR segment displayed a similar temporal response to the shift as observed body temperature rhythms (**Fig 4.5B,D**), suggests that PR segment is strongly influenced by an endogenous clock mechanism.

To estimate how a simple clock would entrain to a shift in behavioural cycle, we created a model in which a sine wave of period 24 hrs entrained linearly to the 9hr phase advance over 6-7 days (entrainment time estimated for each mouse based on body temperature profiles) (**Fig 4.5E**). Comparing the average value of the model with ECG parameter and body temperature rhythms relative to the prevailing LD cycle, we found that both body temperature and PR segment displayed a similar response to the model and to each other, in agreement with the view that rhythms in PR segment are set by a circadian clock. In contrast, RR interval remained closer to the baseline, suggesting a strong positive influence of activity (and potentially a negative masking impact of light) on shaping rhythms in HR (**Fig 4.5F**).

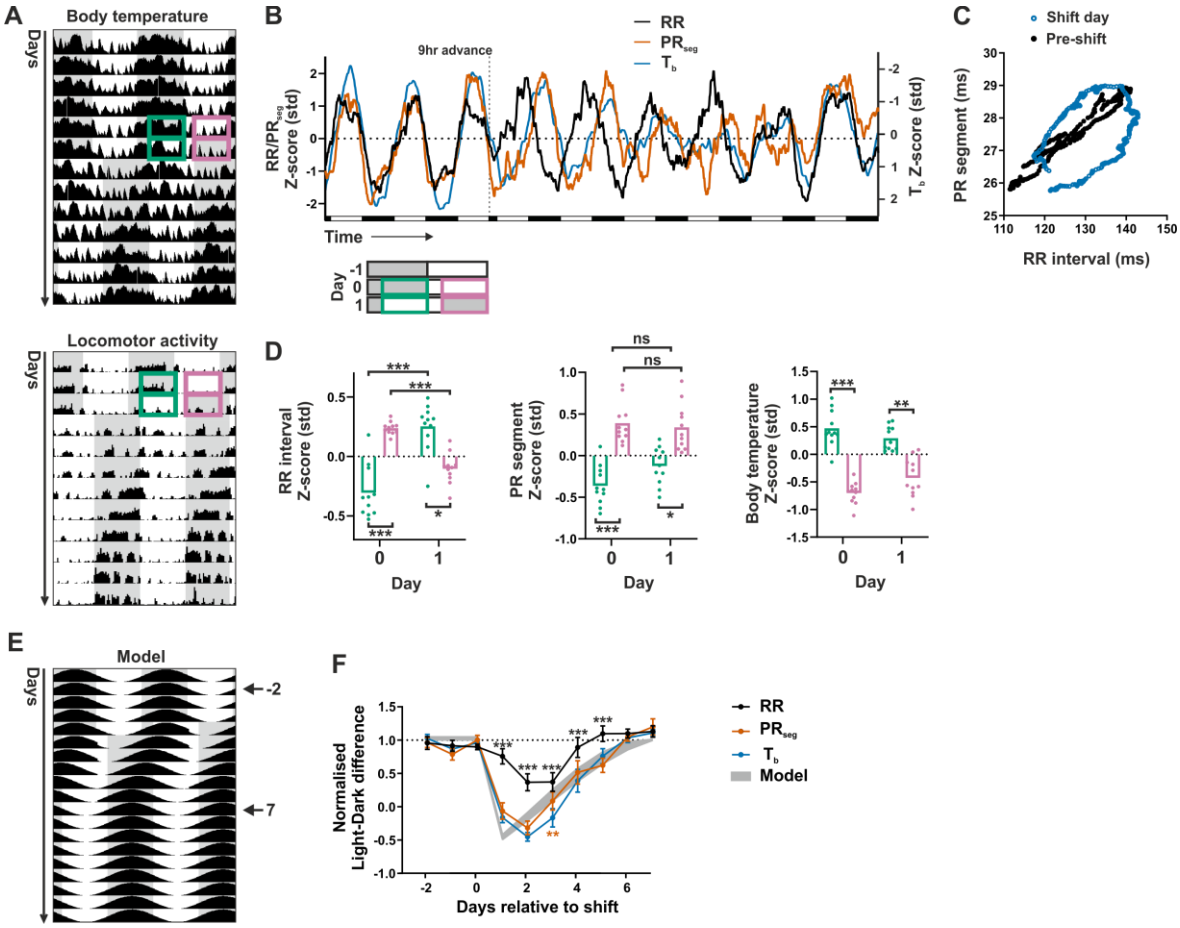

Figure 4.5. Impact of 9hr phase advance (akin to transatlantic flight) on physiology and conduction. **A**. Representative body temperature and locomotor activity profile recorded across a 9hr advance of the LD cycle (data are double plotted; shaded regions indicate periods of darkness). **B**. Representative Z-scored waveforms from an individual across 9hr phase advance in the lighting schedule. RR interval and PR segment are on the left Y axis and body temperature on the right, inverted for ease of comparison. **C**. Misalignment of RR and PR segment rhythms in response to the shift in LD cycles disrupts the normal temporal relationship of the two parameters. Data reflects group mean PR segment/RR on the day prior to shift (black) and the shift day (blue). **D.** Mean RR interval, PR segment and body temperature measured across dark (green) and light (pink) phases the day prior to shift (day 0) and equivalent times on the day of the shift (day 1; Two way RM ANOVA, n=11)**. E.** Schematic of mathematical model of a circadian process entraining over 6 days. Horizontal arrows indicate pre and post shift window plotted in **F. F**. Normalised light-dark difference of RR, PR segment, body temperature and the model. PR segment and body temperature closely match the model of a solely circadian process while RR does not. Coloured asterisks indicate differences from body temperature which is primarily under circadian control. All data presented as mean ± SEM. ns p>0.05, *p<0.05, **p<0.01, ***p<0.001.

4.3.4 Impact of pharmacological inhibition of *CK1δ/ε* on the circadian system

The speed of the circadian clock is heavily influenced by the rate of degradation of the core clock proteins (Zheng and Sehgal, 2012). Casein Kinase 1δ/ε (CK1δ/ε) phosphorylate PER proteins, which in turn targets them for degradation (Eide *et al.*, 2005). Influencing the activity of CK1δ/ε can thus impact the speed of the clock and inhibition of CK1δ/ε in mice can lead to phase delay and/or increased free running period (Meng *et al.*, 2010). We used the compound CP709 (gift from Pfizer), which is a potent inhibitor of CK1δ/ε, to investigate the impacts of CK1δ/ε inhibition on physiology and ECG parameters *in vivo*. Daily i.p. injections of 10mg/kg or 50mg/kg CP709 (at ZT10) in PER2:LUC mice resulted in a delayed onset of locomotor activity and body temperature rhythms under LD conditions, and a delay of whole animal PER2:LUC bioluminescence rhythms in DD, resulting in misalignment between the LD environment and internal clock (**Fig 4.6A,B**). The resulting phase delay was quantified on the final day of treatment (day 5 in LD or day 4 in DD) and revealed that the magnitude of the delay was dose dependent, with significant differences at doses of 10mg/kg and 50mg/kg when compared to vehicle controls (**Fig 4.6C**).

Comparing the daily acrophase of body temperature rhythms between vehicle and 50mg/kg CP709 groups prior to, during and after the treatment period revealed a significant phase delay in the circadian phase of the CP709 treated animals following treatment (**Fig 4.6D,E**). Interestingly, no such shift in acrophase was observed in RR interval, suggesting that while circadian phase is misaligned with the LD cycle, RR interval rhythms predominantly retain phase alignment with the LD cycle. Rhythms in PR segment, however, became clearly misaligned between groups, supporting our previous observations that AV nodal delay is under the control of the circadian system rather than the LD cycle or rhythms in HR. Unfortunately, during the day of the first injection the animals underwent a routine cage change by the animal care staff, resulting in a temporary increase in body temperature and heart rate (**Fig 4.6D**). As this was similar across all groups we believe it had minimal impact on the findings presented here. Together these data provide further evidence that circadian phase can be delayed via pharmacological inhibition of CK1δ/ε and such delays are apparent in AV nodal delay but no SA nodal pacemaking, suggesting that the nodes of the heart respond differently to incoming rhythmic signalling.

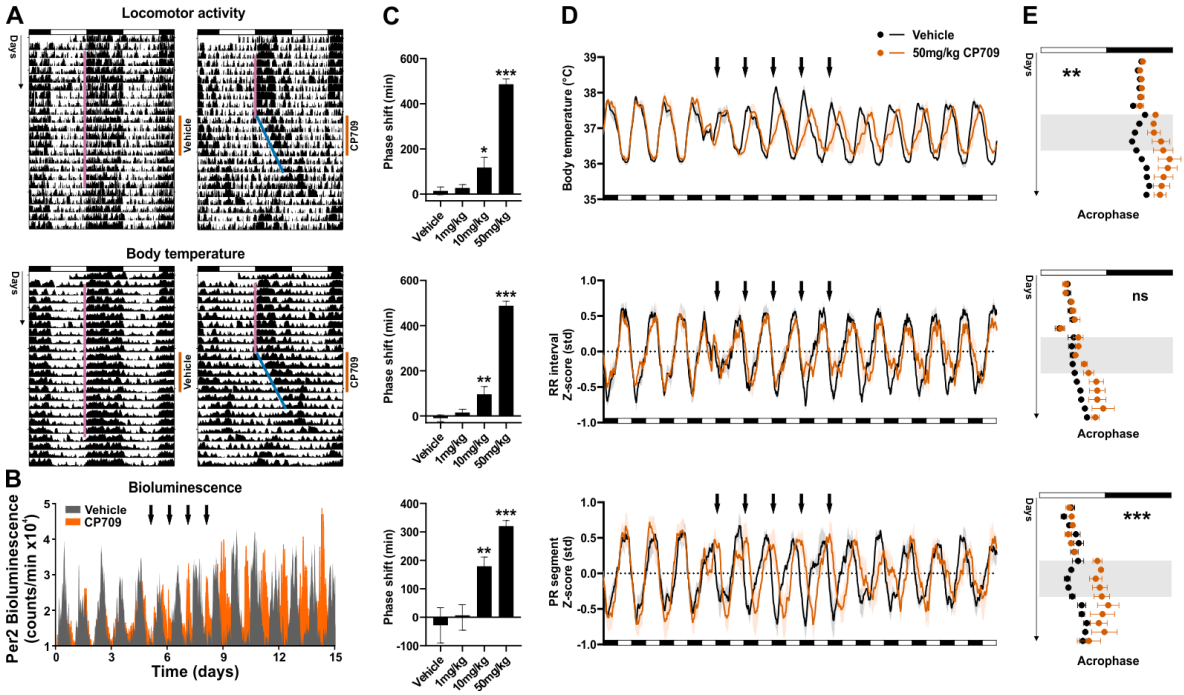

Figure 4.6. Effects of Ck1ε inhibitor CP709 on circadian phase and ECG phasing. A. Example actograms (top) and tempograms (bottom) of mice in LD with 5 daily vehicle injections (left) or 50mg/kg injections of CP709 (right), indicated by vertical orange bars. Coloured lines indicate onset of locomotor activity/temperature rise before (pink) and during (blue) CP709 treatment. **B.** Example bioluminescence traces across 15 days in DD from mice with daily vehicle or CP709 injections (denoted by arrows). **C.** Average phase shift in activity (top), temperature (middle) and bioluminescence (bottom) between pre-treatment and day 5 of treatment across a range of CP709 doses (vehicle, 1, 10 and 50mg/kg). Asterisks indicate difference from vehicle (One-way ANOVA, n=5-6/group and 3-4/group for **A** and **B** respectively). **D.** Average body temperature and z-scored RR and PR segment in vehicle and 50mg/kg CP709 groups across course of treatment denoted by arrows, n = 3/group. **E.** daily acrophase from parameters in **D** across the treatment, denoted by grey window. Inset asterisks indicate interaction term of Two-way RM ANOVA. Compared to vehicle injections, CP709 clearly misaligns body temperature and PR segment, but not RR interval. ns p>0.05, **p<0.01, ***p<0.001.

4.3.5 Cardiomyocyte targeting

To assess the role of circadian clocks local to the heart, we used Cre-Lox targeting to delete *Bmal1* specifically in cardiomyocytes. In these mice, Cre expression is driven by the *α* myosin heavy chain (*αMHC*) promotor which is only expressed in cardiomyocytes, and exon 8 of *Bmal1* was flanked by LoxP sites, resulting in a non-functional *Bmal1* in cardiomyocytes ($\alpha MHC^{cre}Bmal1^{f/f}$). Without *Bmal1* the circadian clock cannot function and when deleted globally results in behaviourally arrhythmic animals (Bunger *et al.*, 2000). This mouse line also expresses the PER2:LUC fusion protein. We first investigated whether tissues from these animals displayed rhythms in bioluminescence when cultured *ex vivo* and found that lung and atria samples displayed robust circadian rhythmicity in $Bmal1^{f/f}$ tissues (**Fig 4.7A**). Interestingly, this rhythmicity remained in the targeted $\alpha MHC^{cre}Bmal1^{f/f}$ tissues. We therefore assessed mRNA expression of clock related genes in whole ventricles collected at ZT0 and ZT12. Indeed, day-night variations in clock genes persisted in $\alpha MHC^{cre}Bmal1^{f/f}$ animals (with the exception of *Rorα*), although many showed a damped amplitude (**Fig 4.7B**). It is likely that the maintenance of rhythmicity in *Bmal1* targeted animals reflected clock function in other cell types such as fibroblasts. To address this, we generated a similar line of mice with a cre-dependent *Nr1d1* (clock gene *Reverbα*) bioluminescent reporter ($Nr1d1Stop^{f/f}Luc$, αMHC^{cre} $Nr1d1Stop^{f/f}Luc$ and $\alpha MHC^{cre}Bmal1^{f/f}$ $Nr1d1Stop^{f/f}Luc$). This should provide luciferase expression only in cardiomyocytes with intact *Bmal1* or *Bmal1* removed. Cultured lung and atria from global *Nr1d1:Luc* animals displayed robust rhythms in bioluminescence, phase inverted from PER2::LUC rhythms due to the phase differences between PER2 and REVERBα (**Fig 4.8A**). Importantly, in samples collected from the cre-dependent reporter line with intact *Bmal1*, rhythms were observed in the atria but not in lung samples (which do not express Cre). Finally, no robust rhythms in bioluminescence were observed in atria from $\alpha MHC^{cre}Bmal1^{f/f}Nr1d1Stop^{f/f}Luc$ animals (**Fig 4.8A**). We next imaged *in vivo* bioluminescence from animals with intact *Bmal1* ($\alpha MHC^{cre}Nr1d1Stop^{f/f}Luc$) using the IVIS imaging system and observed bioluminescence from only the thorax and that was brighter from an animal at ZT8 (aligning with peak *Nr1d1* expression) compared to ZT20 (**Fig 4.8B**). Together these data show that the *αMHC* targeting provides localised deletion of *Bmal1* in cardiomyocytes and thus removal of clock function in these cells.

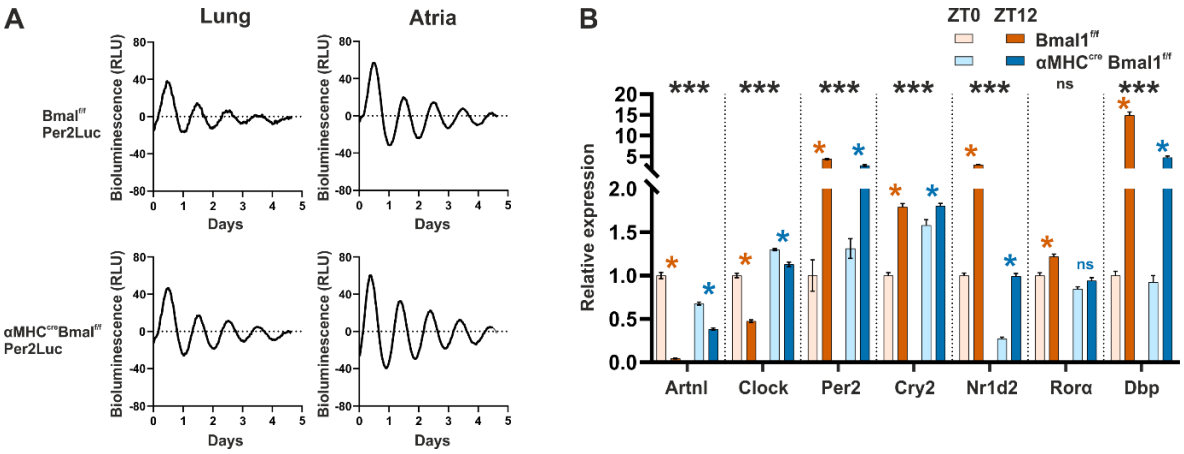

Figure 4.7. Rhythmic clock gene expression persists in hearts of cardiomyocyte-specific Bmal1 knockout animals. A. Representative PER2:LUC bioluminescence waveforms in control and knockout cultured atria and lung (control) samples. Traces are detrended by 7 day moving mean and are plotted from 100nM dexamethasone treatment (day 0). **B.** Panel of circadian clock gene expression *Bmal1$^{f/f}$* and *αMHC^{cre}Bmal1$^{f/f}$* animals. Coloured asterisks indicate differences between ZT0 and ZT12 ($p<0.05$) and black asterisks indicate a decrease in ZT0/ZT12 amplitude between *Bmal1$^{f/f}$* and *αMHC^{cre}Bmal1$^{f/f}$* groups. Data taken from RNA sequencing studies (chapter 6), n=6/group. ns $p>0.05$, ***$p<0.001$.

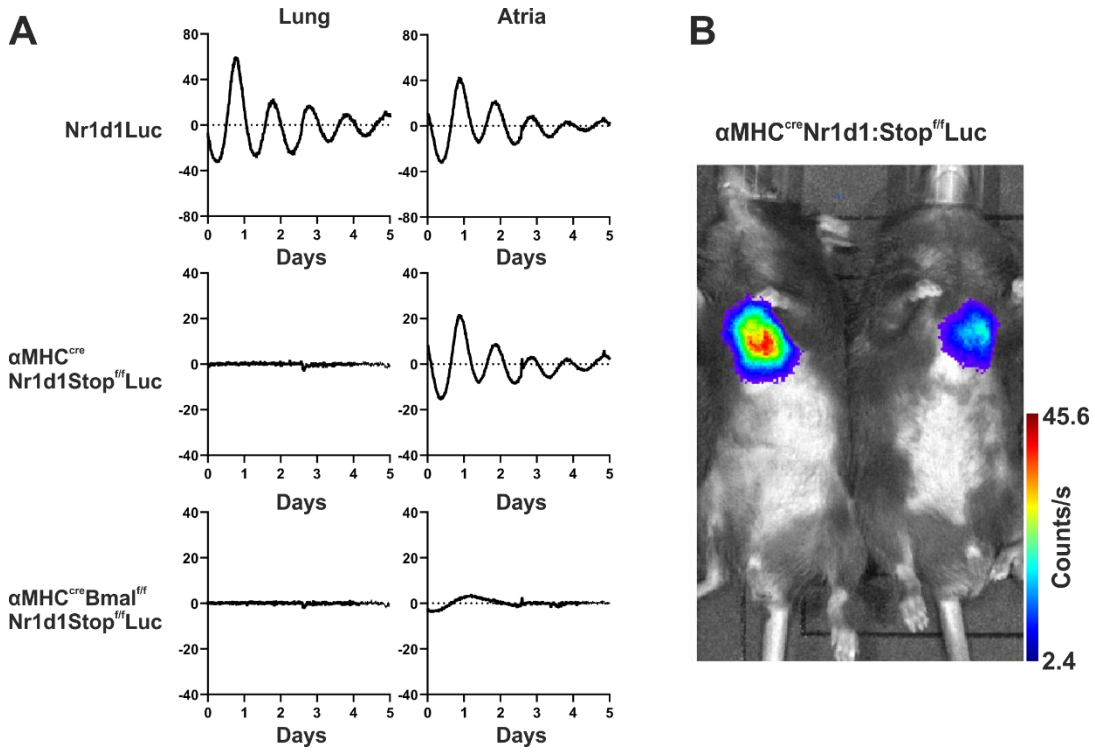

Figure 4.8. Cre-dependent Nr1d1 reporter reveals loss of circadian rhythmicity in cardiomyocytes. A. Representative bioluminescence traces from control (lung) and targeted (atria) tissue in positive control (*Nr1d1Luc*) and targeted animals. No rhythms were observed in lung of *αMHC^{CRE}Nr1d1:Stop$^{f/f}$Luc* but were found in atria, and no rhythms were observed in lung or atria of *αMHC^{CRE}Bmal1$^{Fl/Fl}$Nr1d1:Stop$^{f/f}$Luc.* Traces are detrended by 7 day moving mean and are plotted from 100nM dexamethasone treatment (day 0). **B.** In vivo bioluminescence imaging of mice with cardiomyocyte-specific *Nr1d1* reporting at ZT8 (left) and ZT20 (right) following i.p. injection of luciferin. Higher bioluminescence at ZT8 reflects peak *Nr1d1* expression.

The *αMHC^{cre}Bmal1$^{f/f}$* mouse line has been documented in the literature to exhibit age-dependent cardiomyopathy from ~28 weeks of age (Young *et al.*, 2014; Ingle *et al.*, 2015). To assess this potential phenotype in the mice used in our studies we compared cardiomyopathy-related genes expression in ventricles isolated from the two genotypes in 12 week old animals and found no significant differences (**Fig 4.9A**). Moreover, no significant differences in heart weights were observed in young and old mice (10 - 17 weeks) from *αMHC^{cre}Bmal1$^{f/f}$* and littermate controls (*Bmal1$^{f/f}$*) (**Fig 4.9B**), suggesting that the animals used in our experiments have not started to develop signs of cardiomyopathy.

We next sought to identify whether ECG parameters are impacted by cardiomyocyte-specific *Bmal1* deletion. We included founder line control animals (*αMHC^{cre}* and *Bmal1$^{f/f}$*) to confirm that differences observed in ECG parameters were not caused by inclusion of flox sites around *Bmal1* or cre recombinase expression *per se*. Cardiomyocyte-specific *Bmal1* knockout resulted in lengthened, but still rhythmic across the day/night, RR and QT intervals, and no differences were observed in 24hr mean or rhythmicity of PR segment (**Fig 4.10**). No differences were observed between the control groups in any parameters, 24hr mean or rhythmic profile (n=3-4/group). Interestingly, diurnal rhythms persisted in all parameters, suggesting the cardiomyocyte clock is not essential in setting daily rhythms in cardiac conduction, at least *in vivo* where behavioural rhythmicity persists.

On repeating *in vivo* ECG recordings (n=8-10/group), we observed similar results between *αMHC^{cre}Bmal1$^{f/f}$* and littermate controls (*Bmal1$^{f/f}$*). Cardiomyocyte-specific *Bmal1* deletion resulted in lengthened RR and QT intervals, with no changes to other ECG parameters under both LD and DD conditions (**Fig 4.11**). In addition, diurnal and circadian rhythmicity (12:12 LD and DD conditions respectively) were similar between genotypes with the exception of RR interval under DD which was greater in amplitude in *αMHC^{cre}Bmal1$^{f/f}$* compared to littermate controls (**Fig 4.11**).

4.3.6 Dissecting diurnal input between sympathetic and parasympathetic nervous system

To examine the source of circadian control over the SA and AV nodes, we next determined the impact of autonomic blockade on diurnal rhythms in ECG parameters. To this end, we employed sequential pharmacological autonomic blockade using metoprolol (to block

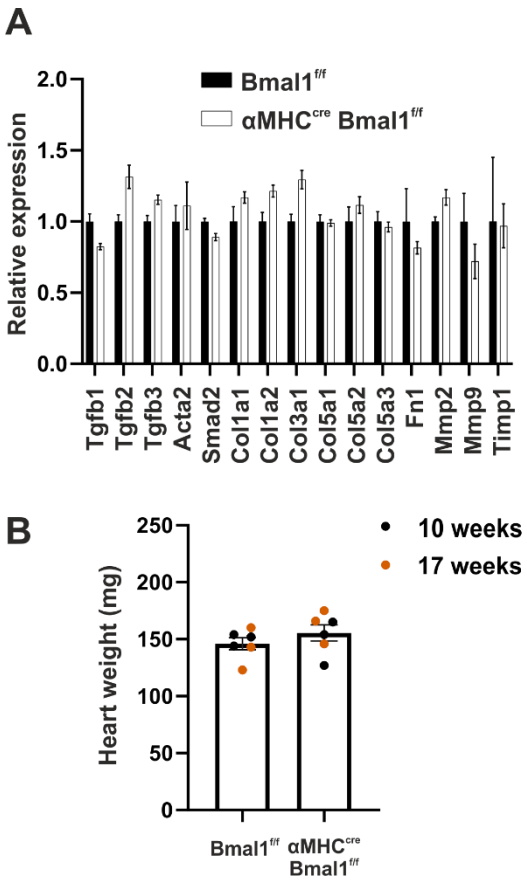

Figure 4.9. No evidence of fibrosis related gene enrichment or enlarged hearts in αMHC^{cre}Bmal1$^{f/f}$ animals. A. Panel of fibrosis-related genes in *αMHC^{cre}* and *αMHC^{cre}Bmal1$^{f/f}$* animals at ZT12. No significant differences were observed (multiple t-tests). Data taken from RNA sequencing studies (chapter 5), n=6/group. **B.** Heart weights of young (10 weeks) and old (17 weeks) *Bmal1$^{f/f}$* and *αMHC^{cre}Bmal1$^{f/f}$* animals. ns p>0.05

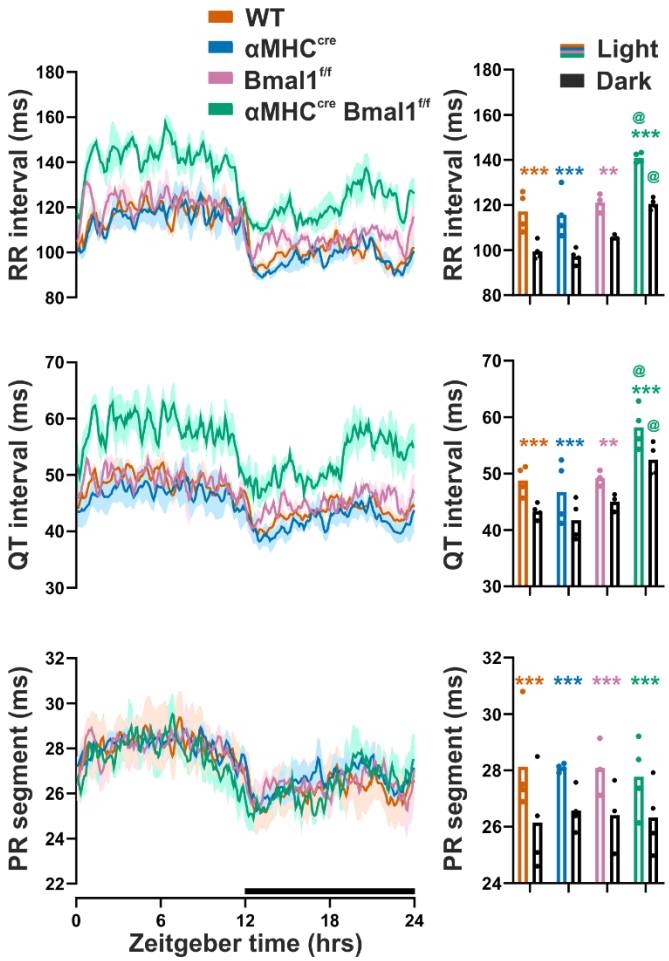

Figure 4.10. Specific targeting of cardiomyocytes using the αMHC promotor. Diurnal waveforms of RR, QT and PR segment from *αMHC^{cre}Bmal1$^{f/f}$* animals and multiple control groups (*αMHC^{cre}; Bmal1$^{f/f}$; WT)* (left) and quantification of night and day average in each group (right). Coloured asterisks indicate difference between day and night, @ indicates difference from WT group. All data presented as mean ± SEM. n = 3-4/group. ns p>0.05, **p<0.01, ***p<0.001, @p<0.05.

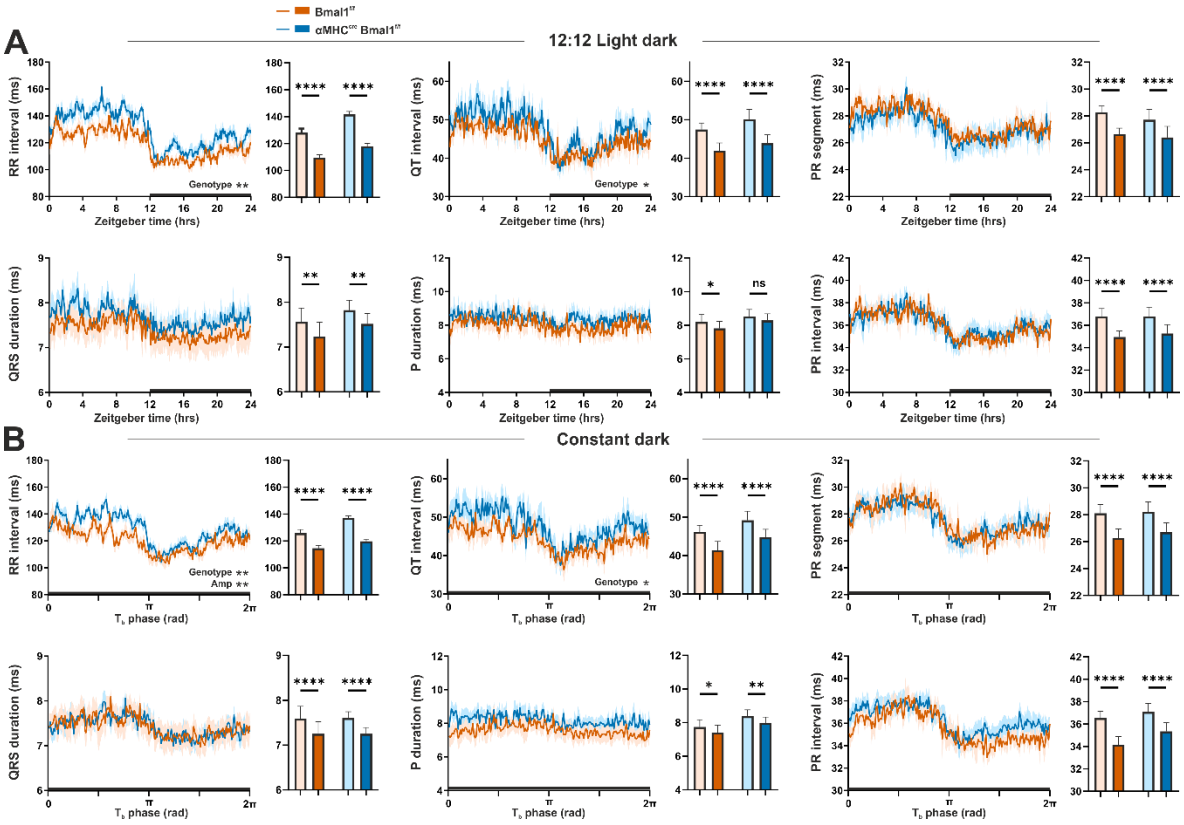

Figure 4.11. ECG parameters in control and *αMHC^{cre}Bmal1$^{f/f}$* animals under LD and DD conditions. waveforms averaged across 5 days of recording in 12:12 LD (**A**) and DD (**B**) in control (orange) and *αMHC^{cre}Bmal1$^{f/f}$* (blue) animals n = 8, 10respectively. Black bar indicates darkness. DD plots are relative to phase in body temperature to account for different circadian periods and phase. Neighbouring bars represent light and dark phase averages (**A**) or subjective day and night (**B**). Two way ANOVA. Inset asterisks indicate genotype difference in two-way ANOVA, and amplitude differences between genotypes (night – day, t-tests corrected for multiple comparison, Holm-Šídák). ns p>0.05, *p<0.05, **p,0.01, ***p<0.001.

sympathetic input) and atropine (to block parasympathetic input). Combined administration results in complete autonomic blockade, as was confirmed by a significant drop in HRV when calculated using the geometric measure rrHRV, or visually inspected in the Poincaré plot (**Fig 4.12A**). In wild-type C57Bl/6J animals (n=8 males aged 13 weeks), sympathetic blockade resulted in an increase in RR interval (decrease in HR) at ZT12, but had no impact at ZT0. Nevertheless, diurnal (ZT12 vs ZT0) differences in RR interval, QT interval and PR segment remained robust following metoprolol injection (**Fig 4.12B**). After atropine injection (i.e. when both sympathetic and parasympathetic branches were blocked), diurnal rhythms in PR segment were abolished. This suggests that the rhythm in AV nodal delay is predominantly driven by the parasympathetic branch of the autonomic nervous system. Interestingly, this also implies that there is a source of rhythmic parasympathetic input which is not impacted by changes in sleep or behavioural state (based on our previous findings related to PR segment rhythms).

In contrast to PR segment, diurnal differences in RR and QT intervals were maintained even amid total autonomic blockade, although lower in amplitude, suggesting that a circadian clock local to the heart is contributing to setting the rhythm in heart rate. To test this directly, we performed a similar autonomic blockade in cardiomyocyte-specific *Bmal1* knockout animals and littermate controls. In the control group (n=7 $Bmal1^{f/f}$, n=9 $\alpha MHC^{cre}Bmal1^{f/f}$, males ages 12-14 weeks), time-of-day dependent differences remained in RR and QT intervals, but were lost in PR segment (**Fig 4.12C**). However diurnal rhythms in all parameters were abolished in the cardiomyocyte-specific *Bmal1* knockout animals, confirming the contribution of the cardiomyocyte clock in setting rhythms in heart rate.

To highlight the relative influence of the cardiomyocyte clock over HR, we plotted RR interval distribution across 24hr in these animals (**Fig 4.12D**). These plots suggest that the cardiomyocyte clock confers a time-of-day dependent rhythm in excitability within the SA node, onto which autonomic regulation is imposed. The cardiomyocyte *Bmal1* knockout animals displayed a loss of consolidation of RR intervals across the light period, with a greater tendency for lower HRs, suggesting that the cardiomyocyte clock may also modulate sensitivity of the heart to parasympathetic input across the day (**Fig 4.12D**).

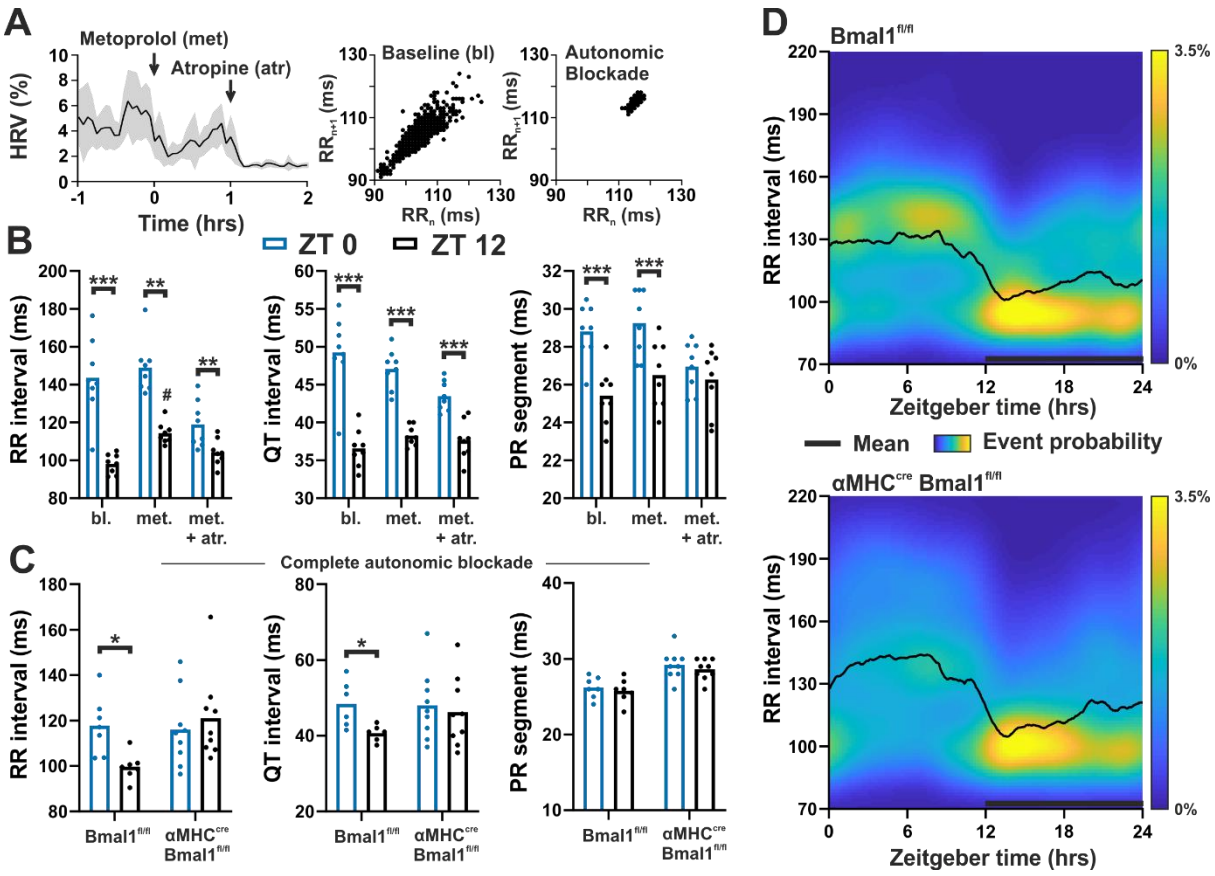

Figure 4.12. Relative contribution of autonomic nervous system input and local cardiac clock in setting RR and PR segment in mice. A. Heart rate variability (HRV) during autonomic blockade (with metoprolol and atropine) in conscious free moving mice (left panel: geometric measure of HRV, right panels: Poincaré plots pre-blockade and under complete block). **B.** Complete autonomic blockade (met + atr) reduced, but did not remove, time of day dependent differences in RR or QT intervals (blue: ZT0; black: ZT12; n=8). In contrast, no time of day difference was observed in PR segment under complete autonomic blockade (Two-way RM ANOVA, Sidak's post-hoc). **C**. In contrast to *Bmal1$^{f/f}$* control mice, no time of day differences in RR or QT intervals were evident in *αMHC^{cre}Bmal1$^{f/f}$* mice following complete autonomic blockade (n=7 *Bmal1$^{f/f}$*, 9 *αMHC^{cre}Bmal$^{f/f}$*; Two-way RM ANOVA, Sidak's post-hoc). **D.** 24 hr distribution of RR intervals in control (*Bmal1$^{f/f}$*; top) and littermate cardiomyocyte-specific *Bmal1* knockout mice (*αMHC^{cre}Bmal1$^{f/f}$*; bottom). Heatmap shows occurrence of RR interval distribution across 5 days of recording; black line reflects group mean. Substantial RR interval lengthening and variability were evident in the day and late night. All data presented as mean ± SEM. *p<0.05, **p<0.01, ***p<0.001 between time, $^{\#}$p<0.05 between treatment.

4.3.7 Ion channel expression rhythms in SA node

Given that our data suggests the clock influences excitability within the SA node, we performed microdissection of the SA node of wild-type animals across the circadian cycle and assessed gene expression using qPCR (**Fig 4.13**). Robust rhythms in clock genes (*Bmal1*, *Reverbα*) were observed, revealing the clock function at this site. Interestingly, rhythms were also observed in potassium channel genes and a related transcription factor (*Kcnq1*, *Kcnh2*, *Klf15*), T-type calcium channels (*Cacna1g*, *Cacna1h*), and a sodium channel subunit (*Scn5a*), all in approximately the same phase peaking around ZT12, the time of highest heart rate in the mice. Interestingly, no significant rhythms were observed in HCN channels, including the pacemaker channel *Hcn4*. Widespread transcriptional rhythmicity in the SA node has recently been reported, which also did not find significant rhythmicity in *Hcn4* expression (Y. Wang *et al.*, 2021). Together these data further suggest that the cardiomyocyte clock imposes rhythms in excitability/pacemaker function within the SA node, which contributes to the diurnal rhythms in HR.

4.3.8 Electrophysiological rhythms in Langendorff-perfused hearts

To remove all systemic cues and assess cardiac electrophysiology inherent to the heart, we recorded atrial and ventricular action potentials from Langendorff-perfused (retrograde through the aorta) control and cardiomyocyte *Bmal1* knockout hearts collected at ZT0 and ZT12 (n=7/group, male/female aged 12-15 weeks) (**Fig 4.14**). As observed *in vivo* during autonomic blockade, inter-beat interval was significantly lower in control hearts collected at ZT12 than ZT0, and no time-of-day difference was observed in $\alpha MHC^{cre}Bmal1^{f/f}$ hearts (**Fig 4.14B**), further implicating a role for the cardiomyocyte clock in determining pacemaker cell excitability. The time between atrial and ventricular action potential onset, a measure of AV nodal delay similar to PR segment, was not significantly different between ZT0 and ZT12 hearts in either genotype, confirming *in vivo* observations related to PR segment.

To examine directly how cardiomyocyte excitability varies across the day, we recorded spontaneous firing rate in isolated neonatal ventricular cardiomyocytes. These studies were performed by our collaborator Alessandra Stangherlin (LMB, Cambridge). Isolated cells exhibited a robust rhythm in PER2::LUC bioluminescence in culture (**Fig 4.14E**) indicating a functional clock. Even in culture, cardiomyocytes displayed a pronounced daily

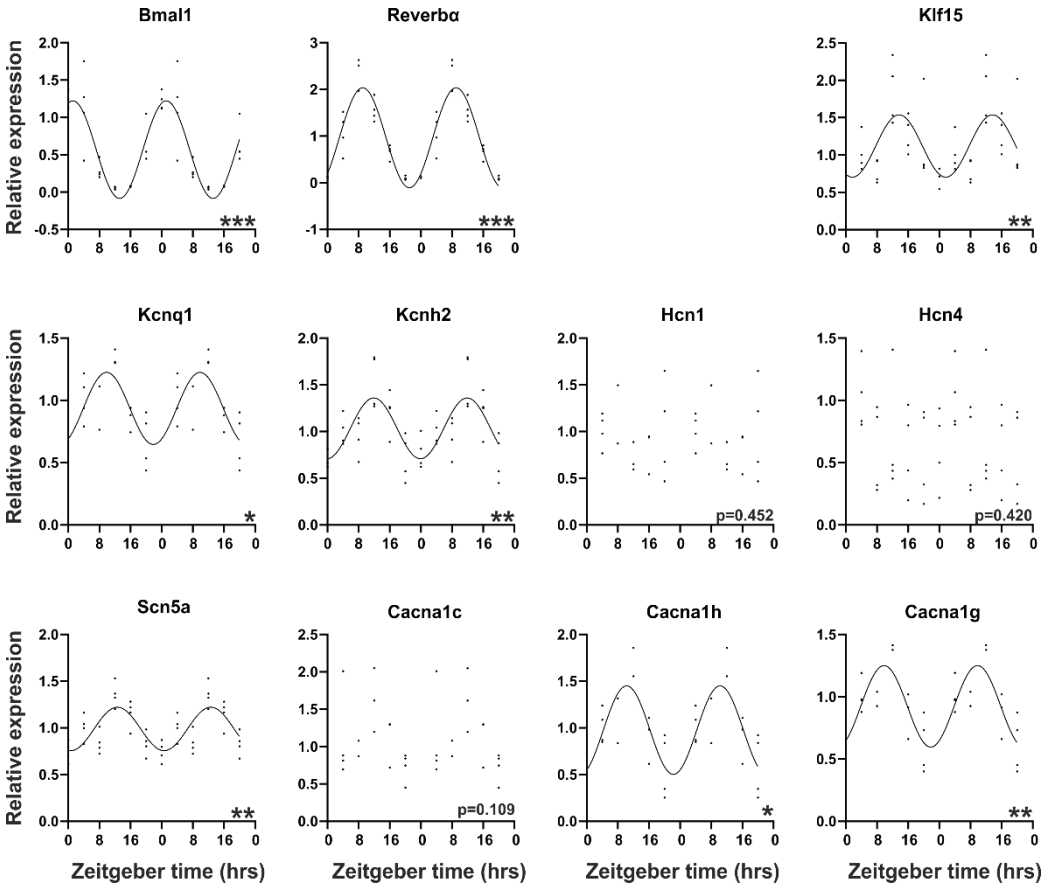

Figure 4.13. Diurnal rhythms in SA node gene expression. qPCR of clock genes (*Bmal1* and *Reverbα*) and ion channels across 24 hr reveals widespread rhythms in gene expression. The sodium channel Scn5a, potassium channels (*Kcnq1*, *Kcnh2*) and related transcription factor (*Klf15*) and T-type calcium channels (*Cacna1h*, *Cacna1g*) all display robust rhythmicity, determined by cosinor analysis (24 hr constrained sine wave vs horizontal line). Data presented as mean ± SEM. *p<0.05, **p<0.01, ***p<0.001. Data have been double plotted for visualisation only.

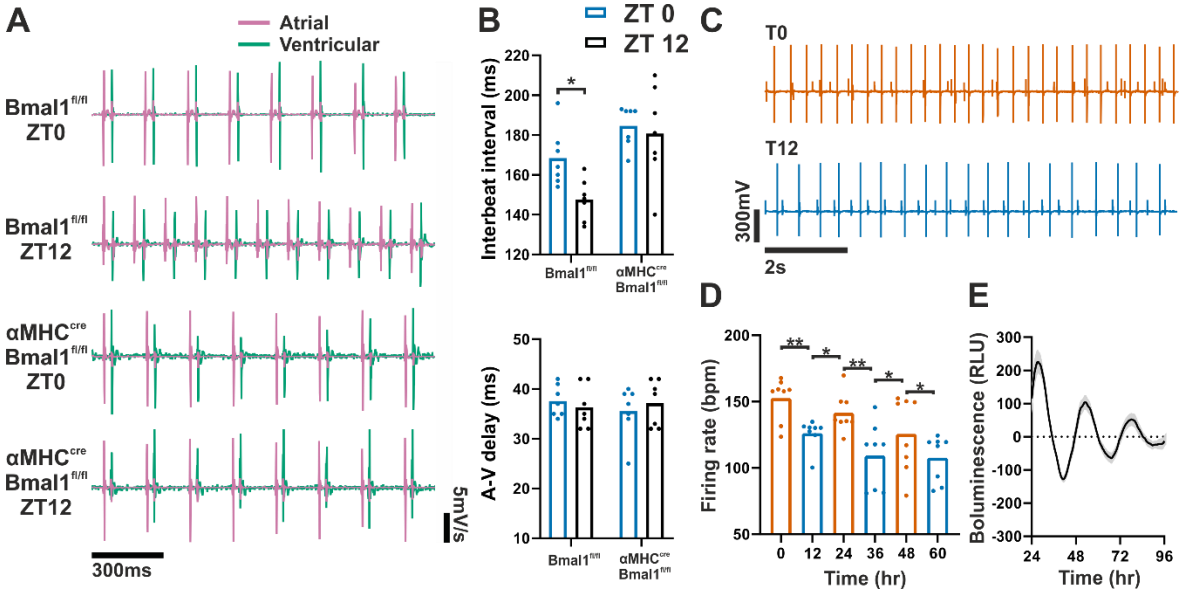

Figure 4.14. A local heart clock drives time-of-day dependent rhythms in cardiomyocyte excitability. **A**. Representative recordings of spontaneous atrial and ventricular electrograms recorded in *ex-vivo* Langendorff-perfused hearts collected from control (*Bmal1$^{f/f}$*) and *αMHC^{cre}Bmal1$^{f/f}$* mice at ZT0 or ZT12. **B**. Interbeat interval showed a time-of-day difference in control but not *αMHC^{CRE}Bmal1$^{Fl/Fl}$* hearts; A-V conduction delay in isolated hearts did not vary by time of day (n=7/group, Two-way RM ANOVA, Sidak's post hoc). **C.** Representative multielectrode array recording of spontaneous action potential firing in primary cardiomyocytes. **D-E**. Spontaneous firing rate in isolated cardiomyocytes showed robust circadian variation in constant culture conditions (**D,** n=8 active electrodes, one-way RM ANOVA), which followed rhythms of mPER2::LUC bioluminescence recorded in parallel cultures (**E**).

rhythm in spontaneous firing rate, which is likely dictated by a circadian clock local to the heart (**Fig 4.14C,D**).

Given this inherent rhythm in spontaneous firing rate, we next tested whether there is also an inherent rhythm in susceptibility to pacing-induced cardiac arrhythmia. To this end, we performed electrical stimulation of the ventricles of langendorff-perfused hearts (n=7/group, male/female aged 12-15 weeks) in an S1S2-S10 protocol (Clasen *et al.*, 2018). This pattern of stimulation consists of 20 stimulated beats separated by 100ms (equivalent of 600bpm), followed by a 9 beat burst of gradually decreasing cycle lengths from 90ms to 18ms in steps of 3ms. Each stimulation train was separated by a 2s pause. Directly following stimulation, beats of ventricular origin are identified and assessed as premature ventricular complexes (PVCs) based on frequency and morphology. A train of 4 or more PVCs were categorised as ventricular tachycardia (VT) as per the Lambeth convention guidelines (Walker *et al.*, 1988)(**Fig 4.15A**). We repeated this process twice and hearts that displayed evidence of VT on both trials were identified as susceptible to VT. Control hearts isolated at ZT12 were significantly more likely to display VT than hearts taken at ZT0 (**Fig 4.15B**; 6/7 vs 2/7 respectively). This aligns well with the observation that cellular excitability is highest at ZT12, and with the increased likelihood of cardiac arrhythmias and sudden cardiac death in humans during the start of our active phase (Muller *et al.*, 1987; Willich *et al.*, 1987). $\alpha MHC^{cre}Bmal1^{f/f}$ hearts did not display a circadian variation in VT susceptibility and showed pronounced resistance to electrically induced arrhythmias. This suggests that the cardiomyocyte clock drives rhythms in excitability to best adapt to the changing demands of the heart across the day, but at the cost of increased susceptibility to ventricular arrhythmias.

4.3.9 Arrhythmia susceptibility varies across the day in vivo

To extend our examination of arrhythmia susceptibility, and additionally test the contribution of time-of-day-differences in adrenergic sensitivity, we challenged mice (n=6/group $Bmal1^{f/f}$, n=5 $\alpha MHC^{cre}Bmal1^{f/f}$, male aged 12-14 weeks) with a single injection of 120mg/kg caffeine and 2mg/kg adrenaline at ZT0 or ZT12 (**Fig 4.16A**). This is a well-documented method for interrogating susceptibility to VT in mice, often used to assess susceptibility in arrhythmia-prone animals (Cerrone *et al.*, 2005; Liu *et al.*, 2009). In wild-type animals, this catecholamine challenge has low prevalence of VT induction

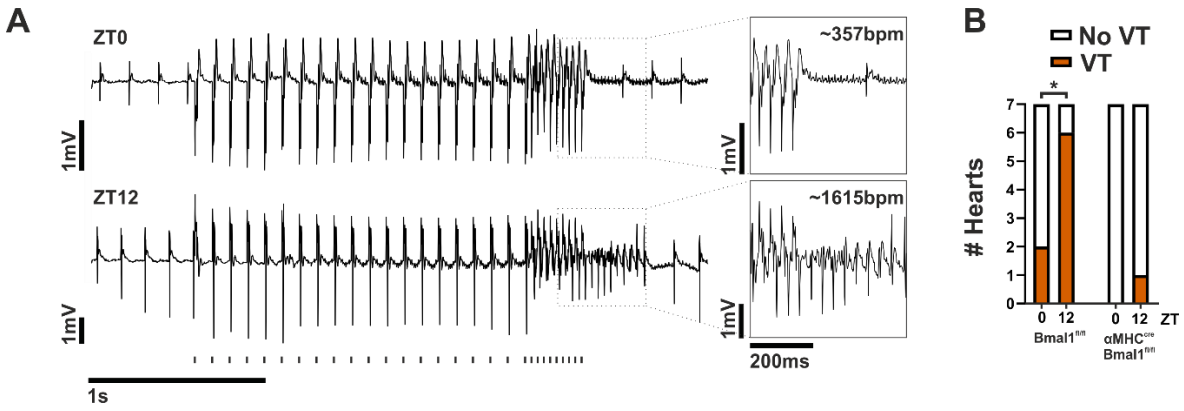

Figure 4.15. Langendorff-perfused hearts exhibit time of day variation in arrhythmia susceptibility. A. Representative ventricular traces and pacing protocol (stimulation train shown below recording). Inset showing recovery to normal sinus rhythm (top) and induced ventricular tachycardia (VT; bottom). **B.** Control hearts showed a significant time-of-day susceptibility to VT (ZT0: 2/7, ZT12: 6/7 tested; Chi-square) whereas only 1/14 *αMHC^{CRE}Bmal1$^{Fl/Fl}$* were susceptible. All data presented as mean ± SEM. *p<0.05, **p<0.01.

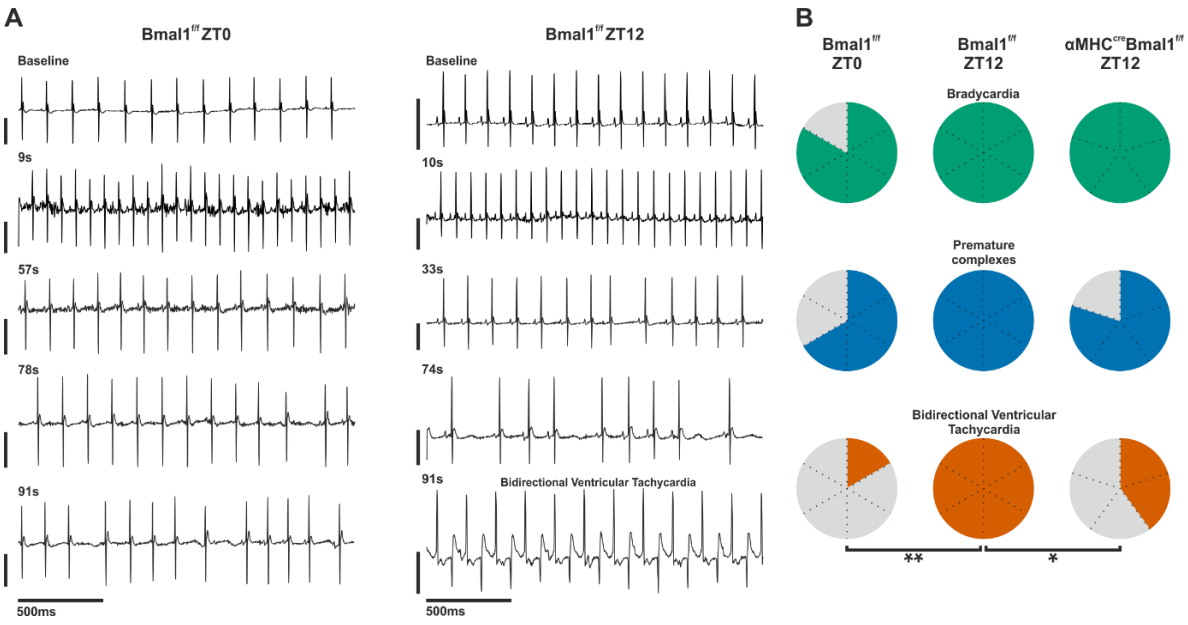

Figure 4.16. ***In vivo*** **propensity for catecholamine-induced bidirectional VT displays diurnal rhythmicity. A.** Typical ECG traces before (baseline) and after injection of caffeine and adrenaline. Animals displayed rapid tachycardia, typically followed by bradycardia and sinus pauses and/or premature complexes, with some progressing into bidirectional VT (bottom right). Vertical scale bars represent 0.5 mV and inset times are time from returning to cage after injection. **B.** Proportion of animals that display evidence of each stage of VT progression. At ZT12, all control animals (6/6) displayed robust evidence of bidirectional VT, compared to only 1 of 6 mice tested at ZT0. Only 2 of 5 $\alpha MHC^{CRE}Bmal1^{f/f}$ mice displayed bidirectional VT at ZT12. *p<0.05, **p<0.01, Chi-square.

(Alvarado *et al.*, 2019). Indeed, when performed at ZT0, despite most animals displaying stereotypical tachycardia, followed by bradycardia and premature complexes/skipped beats, only 1/6 control animals progressed to display signs of sustained bidirectional VT (BVT). Remarkably, at ZT12, all 6/6 control animals displayed robust, sustained BVT, in most cases lasting for >30 seconds (**Fig 4.16B**), revealing a pronounced impact of time of day on arrhythmia susceptibility. On testing $\alpha MHC^{cre}Bmal1^{f/f}$ animals at ZT12 only 2/5 animals displayed BVT, further supporting our previous findings in electrically induced arrhythmias in Langendorff-perfused hearts.

4.4 Discussion

Here we show that components of cardiac conduction are differentially influenced by circadian and non-circadian factors. SA node pacemaking and ventricular repolarisation time is heavily influenced by changes in behavioural state (encompassing arousal state, locomotor activity and lighting condition) while AV nodal delay is less sensitive, yet remains robustly rhythmic. While we never directly tested the effects of lighting condition, it is well documented that HR is heavily influenced by acute light exposure, both directly and indirectly through cessation of locomotor activity (Scheer *et al.*, 2001; Paul *et al.*, 2020). Interestingly, light exposure during the subjective night decreases HR while during light exposure during the subjective day, or under general anaesthesia, increases HR, indicating a possible gating of light-governed changes in HR by the SCN (Thompson *et al.*, 2008). AV nodal delay also remains insensitive to changes in HR, while ventricular repolarisation matches closely, similar to our observations across human electrophysiology in Chapter 3. While ventricular repolarisation is heavily dependent on HR, there is some debate regarding whether is it also influenced by the circadian system (Molnar *et al.*, 1996; Smetana *et al.*, 2003; Singh and Rabkin, 2021). Furthermore, we show that the rhythm in AV nodal delay is dictated primarily by the parasympathetic branch of the autonomic nervous system while rhythms in SA node pacing are generated from a combination of the autonomic nervous system, local cardiomyocyte clocks and indirectly through changes in behavioural state. Together this renders rhythms in SA and AV node activity susceptible to misalignment, on a circadian scale, in response to a phase advance of the LD cycle, akin to a transatlantic flight. Finally we show that local cardiomyocyte clocks contribute to daily rhythms in cellular excitability. This change in excitability imposes an inherent rhythm in

susceptibility to electrically and catecholaminergically induced ventricular arrhythmias, which removal of the cardiomyocyte clock offers protection against.

Previous reports have shown a diurnal rhythm in HR, locomotor activity and body temperature, as well as most ECG parameters (Studholme *et al.*, 2013; West *et al.*, 2017). These rhythms also persist in constant dark conditions, revealing that they are of circadian origin and not simply reflecting a passive response to the ambient LD cycle (Arraj and Lemmer, 2006; D'Souza *et al.*, 2021). While there is considerable evidence that the circadian system influences HR in rodents, fewer studies have investigated whether this influence is from the central SCN clock, or peripheral clocks. Previous reports have found marked reductions in diurnal HR amplitude after lesioning the SCN or under long-term autonomic blockade, and show disrupted rhythms in ion channel gene expression, suggesting a role for the central clock in determining cardiac electrophysiology (Tong *et al.*, 2013). Similarly, there is a circadian rhythm in HR that is not influenced by locomotor activity, which is abolished in SCN lesioned rats (Scheer *et al.*, 2001). Genetic knockout of the VIP receptor also abolishes diurnal and circadian rhythms in HR (Sheward *et al.*, 2010). Interestingly, there are similarities in rhythms in some measures of HRV (fractal dynamics) between rat and human, both peaking during the light phase when SCN is at maximum firing rate. These rhythms are too abolished in rats after SCN ablation (Hu *et al.*, 2008). Furthermore, there is evidence of polysynaptic neural pathways between the SCN and the heart (Scheer *et al.*, 2001), consistent with our previous work that shows chemogenetic inhibition of SCN VIP neurons can impact heart rate in a time of day dependent manner (Paul *et al.*, 2020). Older studies have shown that rhythms in HR are ablated by infusion of guanethedine (which blocks ganglionic transmission), suggesting the rhythm is imposed by the sympathetic nervous system, although guanethedine also severely reduces acetylcholine release from parasympathetic nerve terminals (Vizi and Knoll, 1971; Warren *et al.*, 1994). *Ex vivo* studies have also loosely suggested an impact of a local clock on setting rhythms in HR (Bray *et al.*, 2008). Deletion of the clock in cardiomyocytes has been shown to disrupt ion channel expression and ion currents (Schroder *et al.*, 2013, 2015, 2021). Recent studies have also highlighted a role of the local clock in dictating rhythms in I_f current which in turn contribute to setting rhythms in HR (D'Souza *et al.*, 2021). Our work supports this hypothesis that the rhythm in HR is dictated by both the SCN (via the

autonomic nervous system) and a local clock, and extends the knowledge of central and local clock control over rhythmicity to other aspects of cardiac conduction.

Other groups have previously described the physiology of the *αMHC^{cre}Bmal1$^{f/f}$* mouse line, often focussing on the impact of *Bmal1* deletion on cardiac metabolism (Tsai *et al.*, 2010; Durgan *et al.*, 2011b; Young *et al.*, 2014). These mice display an age-dependent onset cardiomyopathy, which we see little evidence of in the younger mice used in our experiments (Young *et al.*, 2014; Ingle *et al.*, 2015). Other groups have identified ion channel genes *Scn5a* and *Kcnh2* as genes which are regulated by the cardiomyocyte clock and subsequently impact electrophysiology in *αMHC^{cre}Bmal1$^{f/f}$* animals (Schroder *et al.*, 2013, 2015). These reports present lengthened RR and QT intervals in these animals, and further recent studies suggest that this QT interval prolongation is not simply dependent on RR prolongation, and that *Bmal1* knockout exacerbates *Scn5a* mutation induced long QT (Gottlieb *et al.*, 2021; Schroder *et al.*, 2021). There is also evidence (not using the *αMHC^{cre}Bmal1$^{f/f}$* line) that the cardiomyocyte clock regulates the transcription factor *Klf15*, which in turn influences K^+ ion currents and influences QT interval (Jeyaraj *et al.*, 2012). While we do not directly test these findings, our data are in agreement by showing prolonged RR and QT intervals, with minimal impact on other parameters, and also extends to show similar observations in constant dark conditions. We also show robust rhythms in *Klf15* (and potassium channels genes *Kcnq1* and *Kcnh2*) in the SA node, which may contribute to dictating rhythms in K^+ currents and thus electrophysiology within the pacemaking node.

As in Chapter 3 in humans, these data reveal differential control of diurnal rhythms in SA and AV node activity, rendering the rhythmicity of nodal activity susceptible to misalignment on a circadian scale. Activity of the SA node is influenced by behavioural routine, meaning that during an abrupt change in routine, the SA node will quickly adapt to the new schedule, as would be required due to the changing demands on the heart. In contrast, rhythmic activity at AV node buffers against changes in behavioural routine, and is dictated primarily by central clocks, closely mirroring rhythms in body temperature during an abrupt behavioural shift. As such, during a shift in routine, daily rhythms in SA and AV nodes become misaligned. Clearly further research is required to understand the full impact of this misalignment, but given the requirement that components of the

conduction system need to be coordinated for efficient contraction, it is likely that cardiac efficiency will be impaired, and there may be potential additional risk of arrhythmias.

Previous reports have directly showed the presence of a circadian clock within the SA node which dictates rhythms physiology (D'Souza *et al.*, 2021). Our data are broadly in agreement with these findings, although we report no rhythm in the pace making gene *Hcn4*. Indeed, the same group report RNA sequencing studies of the SA node and find no significant rhythm in *Hcn4* expression (Y. Wang *et al.*, 2021). We do, however, show widespread rhythmicity across ion channels within the SA node in agreement with this group, suggesting that rhythms in many ionic currents could contribute to rhythmicity in SA nodal physiology.

A remarkable observation of our studies is the inherent, circadian variation in susceptibility to ventricular tachycardia at the start of the animals' active phase. A well-documented increase in arrhythmia (and sudden cardiac death) propensity occurs in the morning in humans (Muller *et al.*, 1987; Willich *et al.*, 1987). These observations could be explained by the sudden increased demand on the heart in the morning when people wake and get out of bed, resulting in an increase in sympathetic drive. Indeed, people who take chronic propranolol, a non-specific β-adrenoceptor blocker, display no such rhythm in arrhythmias (Aronow *et al.*, 1995; Behrens *et al.*, 1997). However, our data suggest that this rhythm is in part due to the circadian system, either from the local cardiomyocyte clock, or a combination of both local clocks and altered sensitivity to autonomic signalling. We also show that $\alpha MHC^{cre}Bmal1^{f/f}$ mice are resistant to VT induction, suggesting that the cardiomyocyte clock drives rhythms in excitability to best adapt to the changing needs of the heart throughout the day, at the cost of increased susceptibility to ventricular tachycardias at the start of the active phase. We examine this directly in Chapter 5.

Chapter 5: Identification of potential mechanisms underlying diurnal patterns in arrhythmogenesis

5.1 Introduction

In humans, many types of cardiac arrhythmias display a morning peak in prevalence, including frequency of premature ventricular complexes (Steinbach *et al.*, 1982) and onset of ventricular tachycardia (Twidale *et al.*, 1989; Tofler *et al.*, 1995), ultimately resulting in increased prevalence of sudden cardiac death (Muller *et al.*, 1987; Willich *et al.*, 1987). The increased risk of arrhythmias in the morning may be driven by the circadian system, or simply be due to sudden physiological changes in blood pressure and/or autonomic tone between sleeping and waking. As such, the mechanism that governs diurnal risk of arrhythmogenesis remains poorly understood. A role for the local clock has been suggested previously. The transcription factor *Klf15* is highly regulated by *Bmal1* in the heart and in turn regulates potassium currents via modulation of *Kchip2*. Over or under expression of *Klf15* results in altered potassium currents, shortened or lengthened QT intervals respectively, and ultimately increased risk of arrhythmia, highlighting a potential link between the circadian system and arrhythmias (Jeyaraj *et al.*, 2012). Similarly, we showed that there are diurnal rhythms in arrhythmia susceptibility both *in vivo* and *ex vivo*, implicating the local cardiac clock in vulnerability to arrhythmias (Hayter *et al.*, 2021a).

Previous reports have also suggested that cardiomyocyte deletion of *Bmal1* influences arrhythmia susceptibility. These animals exhibit prolonged QT intervals and minor differences in action potential morphology compared to control animals, both of which are features associated with increased arrhythmia susceptibility (Gottlieb *et al.*, 2021; Schroder *et al.*, 2021). Perfused hearts from these animals may also be more likely to exhibit PVCs in response to increasing preload pressure, suggesting a greater risk of arrhythmias (Schroder *et al.*, 2013). However, when VT susceptibility was tested directly using electrical or pharmacological induction, cardiomyocyte *Bmal1* knockout animals are relatively protected against arrhythmias as shown in Chapter 4. The mechanism by which this protection occurs, particularly since they exhibit risk factors which have been associated with arrhythmias (such as long QT, stretch-induced PVCs), remains unclear.

Dysregulation of many ionic currents in cardiomyocytes can be responsible for ventricular arrhythmias. Indeed, genome wide association studies reveal links between a large number of ion channel and intracellular ion handling genes with arrhythmias in humans (Wilde and Bezzina, 2005; Hsiao *et al.*, 2013). Ventricular tachycardias can be broadly separated into two forms: abnormal impulse generation and electrical conduction disturbances, such as re-entry pathways (Landstrom *et al.*, 2017). Re-entry circuits require a physical substrate such as a channelopathy or heart disease (Delacretaz *et al.*, 2001; Lazzerini *et al.*, 2018), which allows for electrical impulses to re-enter the circuit to induce further contraction and, as such, are unlikely to be present in our studies. Abnormal impulse generation creates a spontaneous mistimed electrical impulse from somewhere other than the SA node, often the Purkinje fibres. Depending on whether these impulses occur during or after repolarisation they are termed early or delayed afterdepolarisations (EADs or DADs respectively). Given the integral role of calcium in excitation-contraction coupling in the heart it is perhaps unsurprising that dysregulation of intracellular calcium handling is a common cause of ventricular arrhythmias. Briefly, upon electrical activation of a cell Ca^{2+} ions activate ryanodine receptors on the surface of the sarcoplasmic reticulum, resulting in a rapid dump of Ca^{2+} ions previously sequestered by calsequestrin into the cytoplasm. These ions then bind to Troponin C, signalling to myofilaments to drive contraction of the muscle before being taken back up into the SR by SERCA2A, or pumped out of the cell by NCX exchangers. Possible mechanisms by which EADs and DADs can occur is through spontaneous release of Ca^{2+} from the SR, or through excess influx of Ca^{2+} via $I_{ca,L}$ which in turns drive SR release (Kistamás *et al.*, 2020). Alternatively, Ca^{2+} release can be driven by caffeine administration, and when given in combination with adrenaline (which results in slowed repolarisation via K^+ uptake and greater likelihood of EADs/DADs) can lead to arrhythmia induction as demonstrated in Chapter 4 (Struthers *et al.*, 1983; Veldkamp *et al.*, 2001; Kong *et al.*, 2008).

Here we use RNA sequencing to gain mechanistic insight into the circadian control of arrhythmia susceptibility and identify potential putative pathways and underlying genes.

5.2 Methods

5.2.1 Animals

All animal experiments were licensed under the Animals (Scientific Procedures) Act of 1986 (UK) and were approved by the animal welfare committees at the University of Manchester. Mouse lines (*Bmal1$^{f/f}$, αMHC^{cre}Bmal1$^{f/f}$)* were bred at in house at the University of Manchester. Mice were housed under a 12:12 hour light/dark cycle at ~400 lux during the light phase and 0 lux during the dark phase. Ambient temperature was maintained at 22 ± 2 °C and humidity 52 ± 7%. Food and water was available ad libitum. Male *Bmal1$^{f/f}$* and *αMHC^{cre}Bmal1$^{f/f}$* mice aged 12 weeks were culled at ZT0 or ZT12 (4 groups, n=6/group) and hearts rapidly extracted and washed in PBS to remove blood. Atria and excess tissue was removed and ventricles were snap frozen on dry ice.

5.2.2 RNA extraction

Tissue was first homogenised using TRIzol reagent (ThermoFisher) in a Bead Mill (Bead mill 24, Fisherbrand), then chloroform (Sigma-Aldrich) added to promote phase separation. Following 10 minute incubation at room temperature, samples were centrifuged at 12000G for 15 minutes at 4°C. The aqueous phase was then transferred to a clean tube and isopropanol added. Samples were then vortexed and added to a minicolumn over a collection tube (Reliaprep tissue, Promega) and centrifuged at 12000G for 1 minute at room temperature. As per manufacturers protocol, RNA wash solution was then added to column and centrifuged for 30s, followed by incubation of DNAse mix for 15 minutes at room temperature. Columns were then washed with column wash and RNA wash solutions before RNA eluted in nuclease-free water and frozen at -80°C for storage.

5.2.3 RNA sequencing pipeline

RNA libraries were built using TruSeq Stranded mRNA kits (Illumina) and sequenced using HISEQ4000 (Illumina) as paired-end, 76bp reads. Paired-end RNA sequencing reads were quality assessed using FastQC (v0.11.3) and FastQ Screen (v0.9.2). Sequencing reads were processed using Trimmomatic (v0.36) and mapped against a reference mouse genome (mm10) using STAR (v2.5.3). Counts per gene were calculated by STAR using annotation from GENCODE M22. Data was normalised using EdgeR ($\log_2$(CPM+c)) and K-means carried

out on the 2000 most variable genes (across all samples) using 4 clusters. Principal component analysis (PCA) was carried out and differentially expressed genes were calculated using DESeq2 with thresholds of 0.05 false discovery rate (FDR) and 1.3 fold change (corresponding to 30% increase or decrease in expression). The previous steps (normalisation, K-means, PCA and differential gene expression) were carried out in the web platform iDEP.92 (Ge *et al.*, 2018). Enriched Wikipathway (2019) pathways were identified in Enrichr (Kuleshov *et al.*, 2016) and pathways visualised using PathVisio (v3.3.0) (Kutmon *et al.*, 2015).

5.3 Results

5.3.1 RNA sequencing summary

We identified a robust diurnal rhythm in ventricular arrhythmia susceptibility, both in isolated hearts using electrical stimulation, and *in vivo* using a pharmacological catecholamine challenge (Hayter *et al.*, 2021a). We also showed that mice lacking *Bmal1* in cardiomyocytes were relatively protected against such arrhythmias suggesting an involvement of the local cardiomyocyte clock in arrhythmogenesis. To identify potential mechanisms underlying these observations, we performed RNA sequencing on ventricular myocardium collected from $Bmal1^{f/f}$ and $\alpha MHC^{cre}Bmal1^{f/f}$ animals at ZT0 and ZT12 (12 week old males, n=6/group). The quality of RNA sequencing was good, with all 24 samples passing basic FastQC quality control which assess a range of parameters including nucleotide identification quality, sequence GC content, sequence length distribution and adapter contamination (Andrews, 2010). Specifically, average total reads per sample were 29.8 ± 2.9 million (mean ± SD), of which 79.3 ± 0.8% were unique (**Fig 5.1A**). The number of unique reads did not differ significantly between groups (one way ANOVA, p = 0.4739). After within-sample count transformation using EdgeR (log(CPM+c)) all samples displayed a similar distribution (**Fig 5.1B,C**) and all pairs of samples were highly correlated ($R^2 > 0.98$), indicating that all samples were of similar condition and there were no technical differences between groups. Performing principal component analysis (PCA) reveals clear clustering within groups and separation between groups, with principal component 1 (PC1, 30% variance) correlating significantly with genotype ($p = 4.85 \times 10^{-13}$) and PC2 (14% variance) correlating with Zeitgeber time ($p = 8.28 \times 10^{-10}$; **Fig 5.1D**).

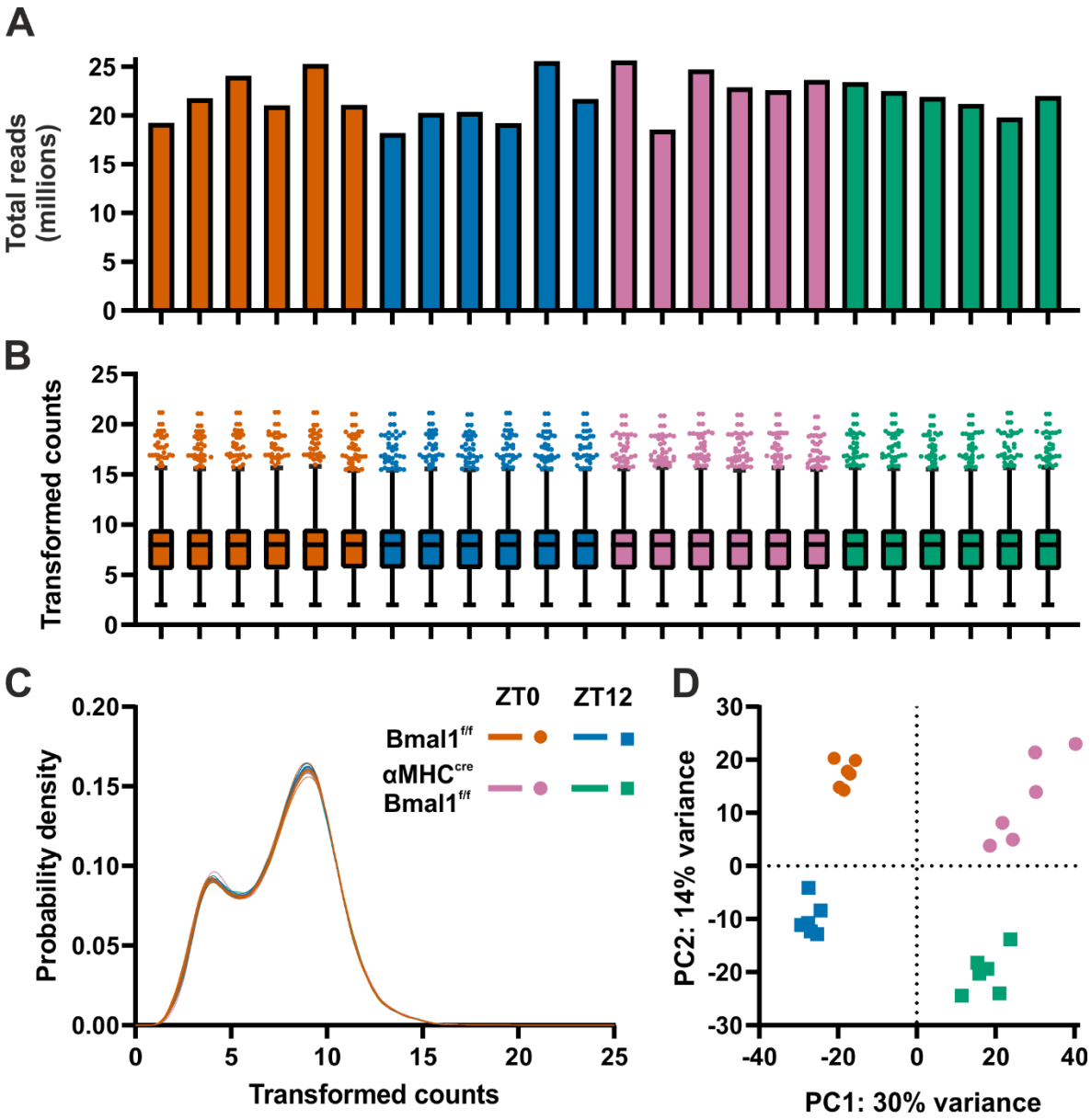

Figure 5.1. RNA sequencing counts and data normalisation. A. Total unique reads for each sample, separated by group. **B.** Box plot distribution of counts following transformation by EdgeR. **C.** Count density after transformation shows strong overlap between samples and no differences between groups. **D.** Principal component analysis of samples, coloured by group. PC1 approximates 30% of the variance and correlates with genotype while PC2 approximates 14% and correlates with zeitgeber time. Clear separation is observed between each group and samples cluster closely together.

Prior to statistical analyses, we used K means clustering (Steinley, 2006) on the 2000 genes with largest standard deviations (across all samples) to examine data clustering without bias via direct group comparison. We opted for 2000 genes as the default, but importantly including more or fewer genes resulted in clusters with similar patterns, again confirming that the biggest variation in the data comes from genotype and time. Using the default 4 clusters, K-means clustering identified approximately equal sized groups with unique expression profiles (**Fig 5.2**). Clusters A and D clearly relate to genes which were down- or upregulated in *αMHC^{cre}Bmal1$^{f/f}$* animals compared to the control group respectively, regardless of time of day, while clusters B and C identify gene groups which are time-of-day dependent, but do not differ between genotypes, with cluster B showing genes upregulated at ZT12 and C displaying genes downregulated at ZT12 compared to ZT0 (**Fig 5.2**).

5.3.2 Differential gene expression

We next identified significantly differentially expressed genes using cut off values of 0.05 false discovery rate (FDR) and 1.3 fold change (equivalent to 30% increase or decrease in expression). Interestingly, despite deletion of *Bmal1* resulting in a non-functional clock, there were approximately 40% more differentially expressed genes across time-of-day in *αMHC^{cre}Bmal1$^{f/f}$* animals compared to *Bmal1$^{f/f}$* animals (1453 vs 1052; **Fig 5.3A**). While many genes retained diurnal differences across genotypes (517; **Fig 5.3C**), a similar proportion also lost diurnal differences (535) and a greater proportion gained diurnal differences (936). That more differences are observed in *αMHC^{cre}Bmal1$^{f/f}$* animals compared to controls suggests the emergence of diurnal rhythms, with the imposition of rhythmicity on normally non-rhythmic genes. Of the 517 overlapping genes, almost all displayed diurnal differences in the same direction between genotypes (e.g. upregulated at ZT12 in both genotypes), with only 5 genes displaying downregulation at ZT12 in *Bmal1$^{f/f}$* and upregulation at ZT12 in *αMHC^{cre}Bmal1$^{f/f}$* (*Pdk4, Slc41a3, Pnpla3, Adra1b, Fut2*). The major dysregulation of *Adra1b* (encoding the α1b adrenoceptor) and *Slc41a3* (encoding a magnesium transporter) may suggest some disrupted autonomic signalling or intracellular magnesium handling respectively. In contrast, across genotype comparisons at ZT0 and ZT12, similar numbers of genes were differentially expressed (2058 vs 2093; **Fig 5.3B**) and

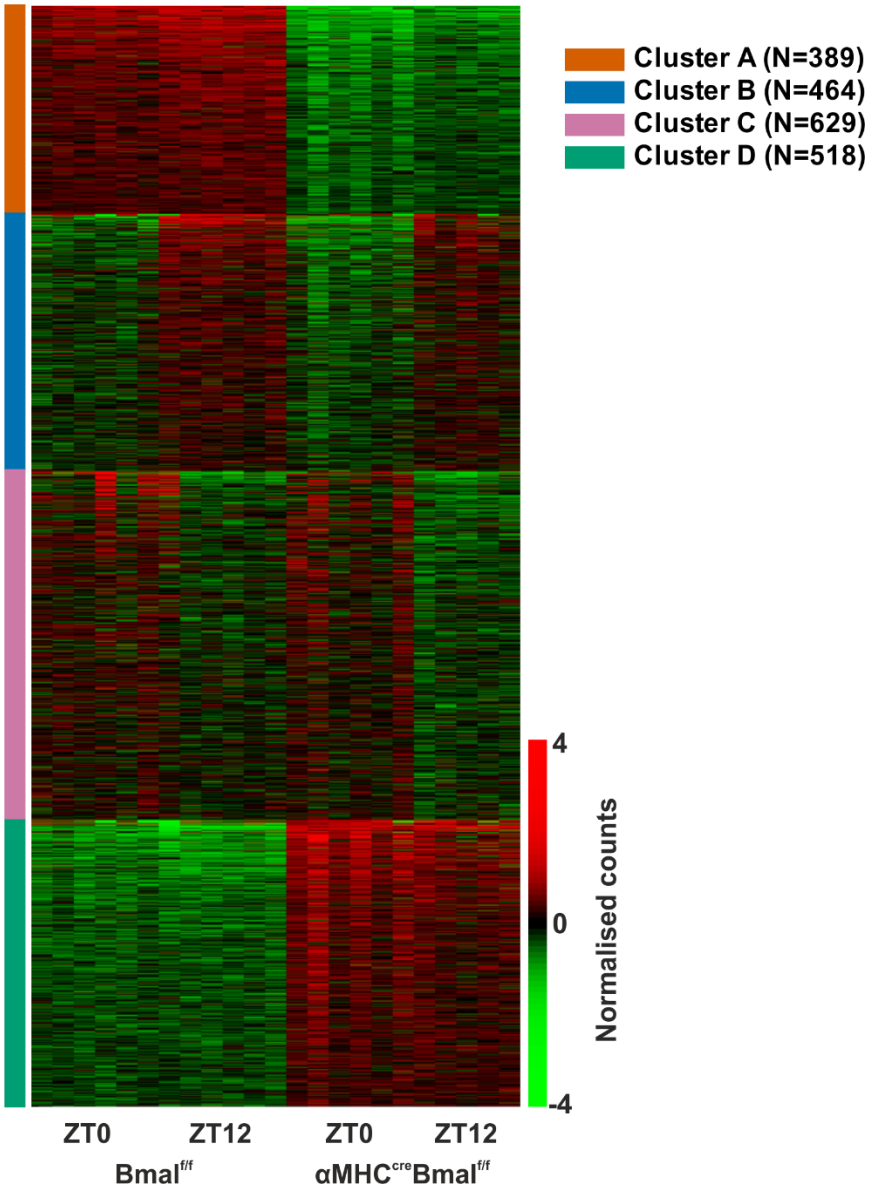

Figure 5.2. Unbiased K means clustering reveals distinct groups with physiological relevance. K means clustering of the top 2000 genes with highest standard deviation clusters genes into groups which are down- or upregulated in *αMHC^{cre}Bmal1$^{f/f}$* animals (orange, green respectively), and up or downregulated at ZT12 (blue, purple respectively). Heat map reveals clear distinction between groups.

while the majority of genes were differentially expressed at both time points (1236; **Fig 5.3D**), there remained a considerable proportion only dysregulated at ZT0 (822) or ZT12 (857). Of the 1236 overlapping genes, the majority changed in the same direction between comparisons, with only 2 genes displaying upregulation at ZT12 and downregulation at ZT0 (*Arntl*, *Adra1b*) and 2 genes displaying downregulation at ZT12 and upregulation at ZT0 (*Bhlhe41*, *Ier5*). *Arntl* (alias of *Bmal1*) and *Bhlhe41* (a circadian related gene) display robust rhythmicity which is dampened to an intermediate expression level in $\alpha MHC^{cre}Bmal1^{f/f}$ animals, while *Adra1b* again shows dysregulation implicating autonomic sensitivity.

As expected, many of the genes that were most changed between ZT0 and ZT12 in the control animals were related to the circadian clock (**Fig 5.3A**). Core clock genes (*Arntl*, *Per1*, *Per3)* and genes strongly associated with, or heavily influenced by, the clock (*Dbp*, *Tcap*, *Hspa1a*, *Hspa1b)* are among the stand out genes in the scatter plot. Interestingly, *Slc41a3*, a solute carrier involved in magnesium handling, displayed high counts and high amplitude time of day difference, being higher at ZT0 vs ZT12 in $Bmal1^{f/f}$ mice. In $\alpha MHC^{cre}Bmal1^{f/f}$ animals, many of these genes no longer stand out, instead being replaced with genes on which rhythmicity is imposed such as *Gdf15*, *Spon2*, *Nppb* and *Scd4* (**Fig 5.3A**, right). Some clock genes remain differentially expressed (*Per1*, *Dbp*) but at lower daily amplitude, likely due to the mixture of targeted and untargeted cell types in ventricular myocardium (predominantly cardiomyocytes and fibroblasts respectively). Between ZT0 and ZT12, some of the genes which showed major dysregulation in $\alpha MHC^{cre}Bmal1^{f/f}$ animals were differentially expressed at both ZT0 and ZT12 (**Fig 5.3B**). Among those downregulated in $\alpha MHC^{cre}Bmal1^{f/f}$ hearts were *Aldob* and *Ano4*, related to glycolysis/gluconeogenesis and glucose transport respectively, and *Ces1d* which is involved in lipid metabolism. Upregulated genes include *Kcnj14*, a gene which encodes a potassium channel involved in generating the inward rectifier current, *Slc17a7*, encoding a vesicular glutamate transporter, and *Casq1* which encodes the sarcoplasmic reticulum calcium buffering protein Calsequestrin. *Slc41a3*, the solute carrier gene identified as rhythmic previously, was also significantly upregulated in $\alpha MHC^{cre}Bmal1^{f/f}$ hearts.

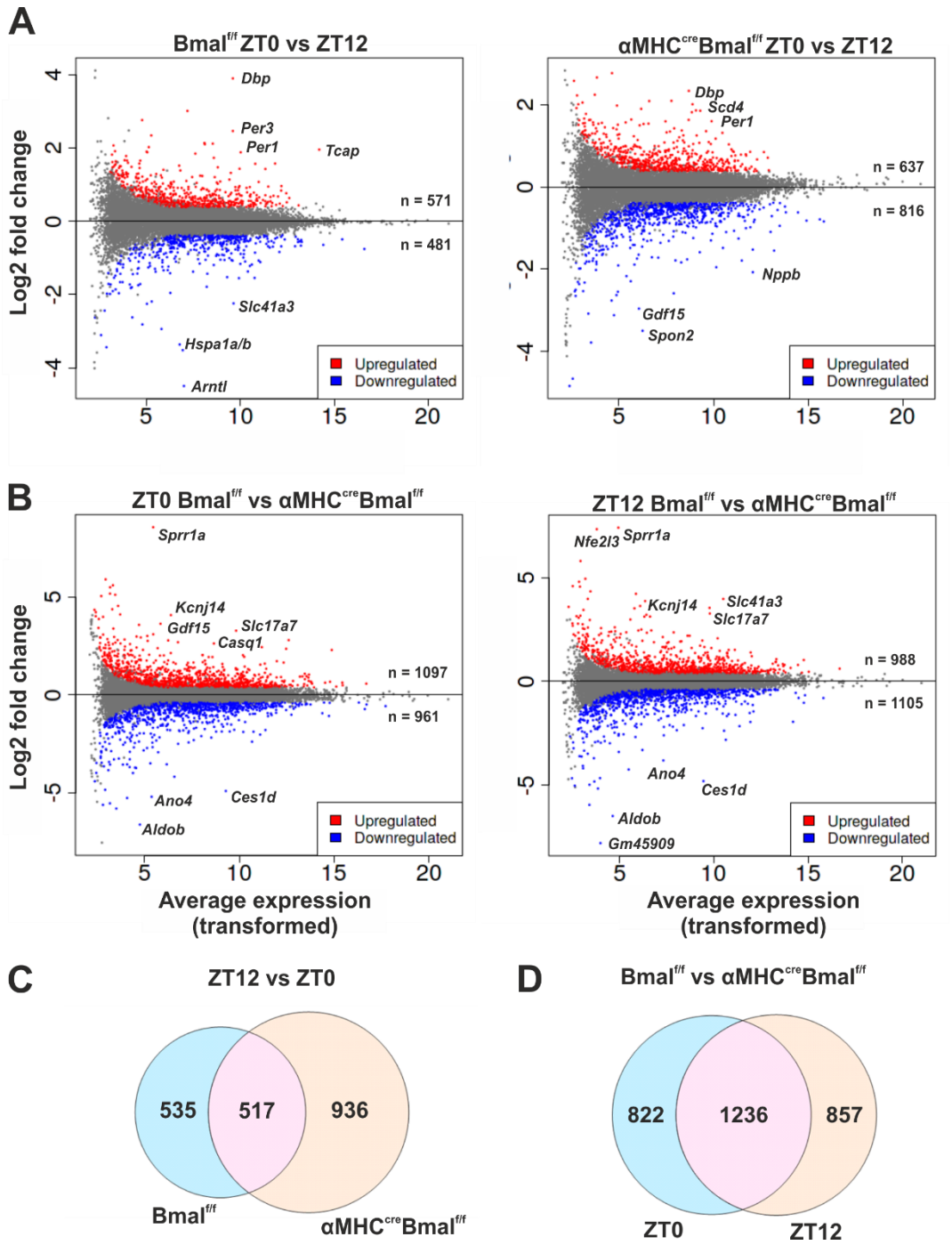

Figure 5.3. Differential gene expression across time and genotypes. A,B. MA plots of time-of-day comparisons (**A**) and genotype comparisons (**B**). Plots show log2 fold change against average normalised expression within each group. Statistical thresholds were set at 1.3 fold change 0.05 false discovery rate. Significantly up and downregulated genes are shown in red and blue respectively, with the most highly differentially expressed, and stand-out genes (highly dysregulated and of interest) labelled with text. Inset numbers indicate number of significantly up- (top) and downregulated (bottom) genes within each comparison. **C,D.** Venn diagrams showing overlap in differentially expressed genes between rhythmic genes in each genotype (**C**) and genotype differences at each time point (**D**).

5.3.3 Pathways implicated across time-of-day and between genotypes

To identify potential pathways altered by time and/or *Bmal1* expression in a non-biased manner, we performed pathway analysis on differentially expressed genes in each comparison condition. We first assessed pathways differentially expressed across time-of-day in each genotype (**Fig 5.4**). In each comparison a heat map of up- and downregulated genes highlights generally the minimal variability between samples across most genes and thus how robust the differential gene thresholds chosen were. Pathway analysis using Enrichr (Wikipathways 2019) was performed for up- and down-regulated genes separately. As expected, when comparing ZT0 and ZT12 in control hearts, the *Exercise-induced Circadian Regulation* pathway is implicated in both up and downregulated gene sets (**Fig 5.4**, top). Among other enriched pathways in the downregulated gene set were *Focal adhesion-P13k-Akt-mTOR-Signalling* and *MAPK Signalling*, suggesting a decrease in cellular proliferation and protein turnover at ZT12. Interestingly, upregulated at ZT12 was the pathway *Retinol metabolism*, which has been associated with the acceleration of development of ion channels responsible for $I_{Ca,L}$ and I_{to} currents (Gassanov *et al.*, 2008), in line with our previous observation of increased cellular excitability at ZT12. In $\alpha MHC^{cre}Bmal1^{f/f}$ animals comparing differentially expressed genes between ZT0 and ZT12, circadian pathways were no longer significantly enriched, while focal adhesion pathways remain time-of-day dependent in expression and downregulated at ZT12 (**Fig 5.4**, bottom).

We next established enriched pathways in the set of genes which lose (535) or gain (936) differences between ZT0 and ZT12 in $\alpha MHC^{cre}Bmal1^{f/f}$ ventricles (**Table 5.1**). As expected, *Exercise-induced Circadian Regulation* was among the highest scoring pathways that lost diurnal variation. Interestingly, *DNA replication, G1 to S cell cycle control* and *PluriNetWork* pathways also lost day-night variability in $\alpha MHC^{cre}Bmal1^{f/f}$ animals, possibly suggesting that the normal daily rhythms in cellular proliferation and differentiation (Chaix *et al.*, 2016) are disrupted. Of pathways that gain diurnal variation, *Inflammatory Response*, *TYROBP Causal Network* and *TGF Beta Signalling* suggest emergence of rhythms in inflammation. Indeed, the circadian clock and inflammation share a close relationship and disruption of the clock often leads to exacerbated inflammatory responses (Castanon-Cervantes *et al.*, 2010; Inokawa *et al.*, 2020; Xu *et al.*, 2021), suggesting a buffering of the circadian clock against rhythmic inflammatory cues.

Bmal$^{f/f}$ ZT0 vs ZT12

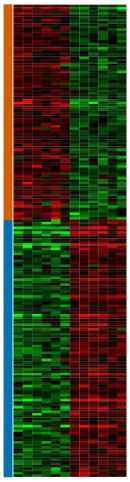

Downregulated at ZT12 (n=481)
Upregulated at ZT12 (n=571)

	Term	P-value	Odds Ratio	Combined Score
Up	Exercise-induced Circadian Regulation	0.000	6.623	62.952
	Irinotecan Pathway	0.032	8.411	28.879
	Retinol metabolism	0.005	4.967	26.216
	p53 signaling	0.003	3.949	22.706
Down	Robo4 and VEGF Signaling Pathways Crosstalk	0.009	19.819	94.374
	Exercise-induced Circadian Regulation	0.000	7.815	83.053
	Dysregulated miRNA Targeting in Insulin/PI3K-AKT Signaling	0.004	7.230	40.739
	Focal Adhesion-PI3K-Akt-mTOR-signaling pathway	0.000	2.964	32.023
	MAPK signaling pathway	0.000	3.584	31.202
	Endochondral Ossification	0.004	4.270	23.363

αMHC^{cre}*Bmal*$^{f/f}$ ZT0 vs ZT12

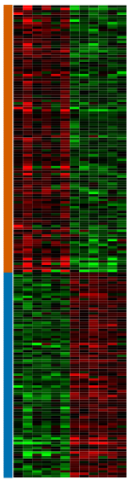

Downregulated at ZT12 (n=816)
Upregulated at ZT12 (n=637)

	Term	P-value	Odds Ratio	Combined Score
Up	Aflatoxin B1 metabolism	0.010	20.064	92.942
	Glutathione metabolism	0.003	7.543	42.785
Down	Hypertrophy Model	0.000	15.420	217.987
	Inflammatory Response Pathway	0.000	8.407	89.698
	Focal Adhesion	0.000	3.837	63.780
	Focal Adhesion-PI3K-Akt-mTOR-signaling pathway	0.000	3.143	57.867
	Spinal Cord Injury	0.000	4.486	56.614
	Endochondral Ossification	0.000	4.997	49.902
	Id Signaling Pathway	0.000	4.955	41.423
	Myometrial Relaxation and Contraction Pathways	0.000	3.303	35.436

Figure 5.4. Pathway analysis of significantly differentially expressed genes across time-of-day comparisons in control and cardiomyocyte Bmal1 knockout ventricles. Heat maps show expression patterns of up and downregulated genes (blue, orange respectively) highlighting consistency across samples. First 6 columns are ZT0 samples and last 6 are ZT12 samples in *Bmal*$^{f/f}$ (top) and *αMHC*^{cre}*Bmal*$^{f/f}$ (bottom) hearts. The top 10 enriched Wikipathways (dictated by combined score: a measure of P value and odds ratio. Right) were identified for each comparison and separated by up and downregulated pathways.

Loss/gain of rhythmicity	Term	P-value	Odds Ratio	Combined Score
Loss	Leptin Insulin Overlap	0.001	10.486	71.050
	Irinotecan Pathway	0.028	9.144	32.766
	Exercise-induced Circadian Regulation	0.002	5.133	32.272
	BMP Signalling Pathway in Eyelid Development	0.015	6.464	26.981
	DNA Replication	0.023	3.963	14.892
	Heart Development	0.029	3.665	12.926
	G1 to S cell cycle control	0.023	3.276	12.320
	Spinal Cord Injury	0.017	2.797	11.427
	Alpha6-Beta4 Integrin Signalling Pathway	0.033	2.958	10.070
	PluriNetWork	0.026	1.858	6.798
Gain	Hypertrophy Model	0.000	8.829	74.310
	Inflammatory Response Pathway	0.000	6.273	49.611
	TYROBP Causal Network	0.001	3.789	25.039
	Novel Jun-Dmp1 Pathway	0.006	4.898	24.826
	Spinal Cord Injury	0.001	3.126	22.836
	Focal Adhesion-PI3K-Akt-mTOR-signaling pathway	0.000	2.207	19.850
	Apoptosis	0.004	2.905	15.845
	MicroRNAs in Cardiomyocyte Hypertrophy	0.005	2.865	15.371
	TGF Beta Signalling Pathway	0.010	3.203	14.760
	Focal Adhesion	0.003	2.231	13.318

Table 5.1. Pathway analyses of differentially expressed genes which gain or lose time-of-day differences. Top 10 pathways for loss of rhythmicity (n=535 genes) and gain of rhythmicity (n=936 genes), ordered by combined score.

Pathways implicated in differentially expressed gene analyses between *Bmal1*$^{f/f}$ and *αMHC*^{cre}*Bmal1*$^{f/f}$ ventricles remained fairly consistent across ZT0 and ZT12 comparisons (**Fig 5.5**). Again, *Exercise-induced Circadian Regulation* was downregulated in *αMHC*^{cre}*Bmal*$^{f/f}$ ventricles at both time points (not in top 10 at ZT12: combined score of 17.1). Multiple pathways related to metabolism were downregulated in *αMHC*^{cre}*Bmal1*$^{f/f}$ animals, including *Amino Acid metabolism*, *Glutathione metabolism*, *Fatty Acid Biosynthesis* and *Fatty Acid Beta Oxidation*, highlighting the important role of the circadian clock in energy homeostasis and in agreement with previous work (Bray *et al.*, 2008; Young *et al.*, 2014; Young, 2016). When comparing pathways enriched from genes only dysregulated at ZT0 or ZT12 (**Table 5.2**), oxidative stress and metabolism were again prominent at ZT0 (*Mitochondrial LC-Fatty acid Beta-Oxidation, Oxidative damage, P53 signalling, Cholesterol metabolism*) while inflammatory pathways were more severely dysregulated at ZT12 (*Microglia Pathogen Phagocytosis, Macrophage Markers, IL-2, IL-5, & IL-6 signalling*), in agreement with the emergent rhythmicity outlined previously. Of particular interest, *Striated Muscle Contraction* and *Calcium Regulation in the Cardiac Cell* were robustly upregulated in *αMHC*^{cre}*Bmal1*$^{f/f}$ animals (**Fig 5.5**; *Calcium regulation in the cardiac cell*: combined score of 12.5 at ZT0), which may contribute to the relative protection against arrhythmias observed in *αMHC*^{cre}*Bmal1*$^{f/f}$ animals. Dysregulated genes in the *Calcium Regulation in the Cardiac Cell* pathway include those for Calmodulin Kinase (*Camk2b*, *Camk2d*), Calcium channels (*Cacna1a*, *Cacna1d*, *Cacnb1*), Connexin 43 (*Gja1*), Calsequestrin (*Casq1*, *Casq2*) and autonomic receptors (*Chrm2*, *Adra1b*).

5.3.4 Dysregulation of intracellular calcium handling

Given the well-documented involvement of dysregulated calcium handling in arrhythmogenesis, we examined this pathway in greater detail. Comparing *Bmal1*$^{f/f}$ to *αMHC*^{cre}*Bmal1*$^{f/f}$ animals at ZT12, the time point at which control animals were susceptible to arrhythmia induction, revealed widespread gene expression changes across the pathway (All changes shown, not only significantly differentially expressed; **Fig 5.6**). All beta adrenoceptors displayed lower expression in the knockout ventricles, in contrast to muscarinic acetylcholine receptors which exhibited higher expression, indicative of increased sensitivity to parasympathetic input and decreased sensitivity to sympathetic input. Two highly expressed (in *Bmal1*$^{f/f}$) potassium channel genes (*Kcnj3*, *Kcnj5*) were also

ZT0 *Bmal*$^{f/f}$ vs *αMHC*^{cre}*Bmal*$^{f/f}$

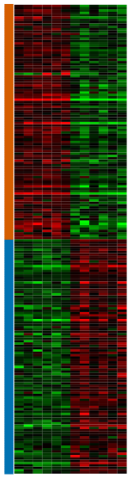

Downregulated in *αMHC*^{cre}*Bmal*$^{f/f}$ (n=961)
Upregulated in *αMHC*^{cre}*Bmal*$^{f/f}$ (n=1097)

	Term	P-value	Odds Ratio	Combined Score
Up	Striated Muscle Contraction	0.001	4.236	30.470
	Dysregulated miRNA Targeting in Insulin/PI3K-AKT Signaling	0.013	4.023	17.330
Down	Fatty Acid Biosynthesis	0.000	11.210	135.845
	Mitochondrial LC-Fatty Acid Beta-Oxidation	0.000	11.749	112.362
	Fatty Acid Beta Oxidation	0.000	8.186	103.289
	Amino Acid metabolism	0.000	3.992	44.747
	Fatty acid oxidation	0.011	8.367	37.912
	Macrophage markers	0.011	8.367	37.912
	Exercise-induced Circadian Regulation	0.002	3.822	23.074
	EPO Receptor Signaling	0.008	4.655	22.660

ZT12 *Bmal*$^{f/f}$ vs *αMHC*^{cre}*Bmal*$^{f/f}$

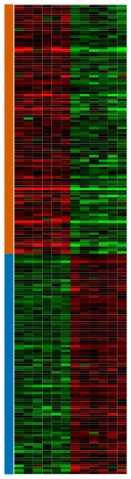

Downregulated in *αMHC*^{cre}*Bmal*$^{f/f}$ (n=1105)
Upregulated in *αMHC*^{cre}*Bmal*$^{f/f}$ (n=988)

	Term	P-value	Odds Ratio	Combined Score
Up	**Calcium Regulation in the Cardiac Cell**	**0.000**	**3.176**	**35.045**
	Striated Muscle Contraction	0.007	3.477	17.266
Down	Macrophage markers	0.000	25.368	308.101
	Microglia Pathogen Phagocytosis Pathway	0.000	10.910	241.839
	Fatty Acid Biosynthesis	0.000	7.895	70.117
	TYROBP Causal Network	0.000	5.409	69.144
	Glutathione metabolism	0.001	7.244	53.700
	IL-5 Signaling Pathway	0.002	3.213	20.883
	Amino Acid metabolism	0.001	2.932	20.847
	White fat cell differentiation	0.008	3.898	18.853

Figure 5.5. Pathway analysis of significantly differentially expressed genes across genotype comparisons at ZT0 and ZT12. Heat maps show expression patterns of up and downregulated genes (blue, orange respectively) highlighting consistency across samples. First 6 columns are samples from *Bmal*$^{f/f}$ hearts and last 6 from *αMHC*^{cre}*Bmal*$^{f/f}$ hearts taken at ZT0 (top) and ZT12 (bottom). The top 10 enriched Wikipathways (dictated by combined score: a measure of P value and odds ratio. Right) were identified for each comparison and separated by up and downregulated pathways.

DE at ZT0/12	Term	P-value	Odds Ratio	Combined Score
ZT0	Mitochondrial LC-Fatty Acid Beta-Oxidation	0.003	7.850	44.598
	Endochondral Ossification	0.001	4.015	28.209
	Cholesterol metabolism	0.004	3.933	22.151
	Dysregulated miRNA Targeting in Insulin/PI3K-AKT Signalling	0.020	4.280	16.684
	Serotonin and anxiety	0.035	4.704	15.746
	Factors and pathways affecting insulin-like growth factor (IGF1)-Akt signalling	0.036	3.486	11.552
	Prostaglandin Synthesis and Regulation	0.036	3.486	11.552
	Oxidative Damage	0.028	3.182	11.431
	p53 signalling	0.019	2.751	10.853
	Adipogenesis genes	0.022	2.112	8.089
ZT12	Microglia Pathogen Phagocytosis Pathway	0.000	11.817	248.865
	Macrophage markers	0.001	15.030	112.504
	TYROBP Causal Network	0.000	4.720	41.452
	Nucleotide GPCRs	0.013	7.505	32.744
	IL-2 Signalling Pathway	0.000	3.835	30.393
	IL-5 Signalling Pathway	0.001	3.838	28.130
	Heart Development	0.010	3.562	16.242
	IL-6 signalling Pathway	0.010	2.540	11.800
	Regulation of Actin Cytoskeleton	0.013	2.116	9.135
	MAPK signalling pathway	0.019	2.014	8.007

Table 5.2. Pathway analyses of differentially expressed genes which differ between genotypes at only ZT0 or ZT12. Top 10 pathways for ZT0 differences (n=822 genes) and ZT12 differences (n=857 genes), ordered by combined score.

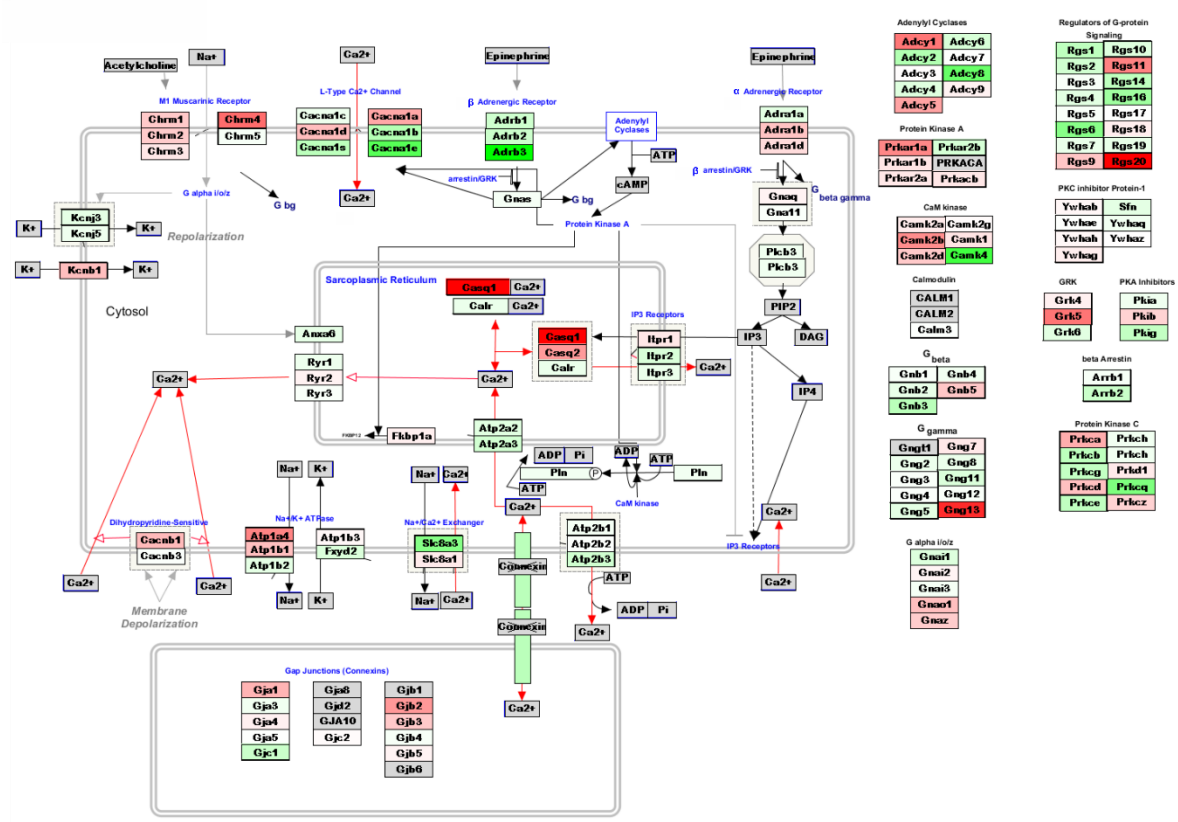

Figure 5.6. Comparison between genotypes at ZT12 for genes involved in *Calcium Regulation in the Cardiac cell*. Gene colours indicate up (red) or downregulation (green) of genes in *αMHC^{cre}Bmal1$^{f/f}$* animals compared to *Bmal1$^{f/f}$* animals at ZT12. Note the widespread changes across the whole pathway, from receptors receiving autonomic input to increased expression of genes involved in calcium sequestration in the sarcoplasmic reticulum.

downregulated, suggesting a potential general decrease in K^+ current into the cell. Many L-type calcium channel genes were also downregulated (including the most common *Cacna1c*) alongside *Atp2a2* and *Atp2a3* (encoding SERCA2a and SERCA3, proteins involved in pumping Ca^{2+} back into the SR following contraction), while *Casq1* and *Casq2* were highly upregulated, suggestive of decreased Ca^{2+} motility into and around the cell and greater sequestration within the SR. Also of interest, the gene for a gap junction highly expressed in ventricular myocardium (Cx43, *Gja1*) was markedly upregulated in in *αMHC^{cre}Bmal1$^{f/f}$* animals, which may indicate increased conduction velocity and connectivity between neighbouring cells. While it is unlikely that any one gene is responsible for the changes in physiology observed, together these data suggest an overall decrease in ion motility and cellular excitability which may underpin the protection against induced arrhythmias observed in *αMHC^{cre}Bmal1$^{f/f}$* animals.

5.4 Discussion

Here we show widespread changes in gene expression across the day/night and between cardiomyocyte *Bmal1* knockout and control animals and highlight potential mechanisms which may underlie the differences in cardiac electrophysiology (e.g. HR, QT interval), autonomic responses and arrhythmia induction sensitivity observed in the animals. Between genotypes, there may not be one clear mechanism, but rather a global decrease in ionic motility and excitability, with possibly increased sensitivity to parasympathetic input and decreased sensitivity to sympathetic input. This is consistent with previous findings which show inducible cardiomyocyte *Bmal1* knockout animals display decreased Na^+ and K^+ currents, lengthened QT intervals indicative of slower repolarisation and general decreased ion channel expression (Schroder *et al.*, 2013, 2015, 2021; Young *et al.*, 2014; Gottlieb *et al.*, 2021). Previous reports have not investigated autonomic sensitivity in these animals, though this observation is consistent with our physiological observations in cardiomyocyte *Bmal1* knockout animals (lower HR, greater prevalence of low HRs during the day and insensitivity to sympathetic arrhythmia generating stimuli).

Significant changes across the intracellular calcium regulation pathway were also observed in *αMHC^{cre}Bmal1$^{f/f}$* animals. While calcium dynamics have not been directly examined in these animals previously, calcium dysregulation is well-documented to be critical in

arrhythmia induction and maintenance (Landstrom *et al.*, 2017; Kistamás *et al.*, 2020). In particular, mutations in calsequestrin are associated with Catecholaminergic Polymorphic Ventricular Tachycardia (CPVT), a condition which often results in bidirectional ventricular tachycardia in response to increased sympathetic input (e.g. emotional stress or exercise) (Faggioni *et al.*, 2012). Indeed, at the level of gene expression we observed markedly increased levels of *Casq1* and *Casq2* in *αMHC^{cre}Bmal1$^{f/f}$* animals at ZT12, although it is unclear if this persists at the protein level and if it underlies the reduced risk of arrhythmogenesis in these mice. Also of note, we observed high counts of the skeletal isoform of calsequestrin (*Casq1*), despite it being commonly viewed that the heart only expressed the cardiac isoform (*Casq2*) (Woo *et al.*, 2020). However, there have been recent reports suggesting that *Casq1* is also expressed in cardiac muscle and is also relevant to arrhythmogenesis (Sun *et al.*, 2021).

We show dramatic changes in *Slc41a3*, a solute carrier involved in magnesium transport, both across time of day and between genotypes. Magnesium has previously been reported to offer protection against cardiac arrhythmias in humans (Orlov *et al.*, 1994; Guerrera *et al.*, 2009; Fairley *et al.*, 2017), likely due to Mg^{2+} competing with Ca^{2+} (Iseri and French, 1984). Intracellular Mg^{2+} concentration also displays robust circadian rhythmicity and feeds back to the clock by adjusting circadian period, indicating a close link between the circadian clock and magnesium homeostasis (Feeney *et al.*, 2016; van Ooijen and O'Neill, 2016). Previous work has showed that deletion of *Kvβ2* results in decreased *Slc41a3* expression, a loss of Mg^{2+} induced action potential duration shortening and increased arrhythmia susceptibility (Tur *et al.*, 2021). Indeed, decreased *Slc41a3* expression at ZT12 in control animals could result in decreased intracellular Mg^{2+}, less competition with Ca^{2+} and thus increased arrhythmia susceptibility. Inversely, the marked upregulation of *Slc41a3* in *αMHC^{cre}Bmal1$^{f/f}$* animals at both ZT0 and ZT12 could be responsible for the protection against arrhythmia observed in this genotype. Clearly this avenue of research is promising and could reveal a robust link between the circadian clock, magnesium homeostasis and cardiac arrhythmias.

In *αMHC^{cre}Bmal1$^{f/f}$* animals, robust diurnal differences are maintained despite lacking a functional clock in cardiomyocytes. The heart is made up of multiple cell types, predominantly cardiomyocytes and fibroblasts, but the role of fibroblasts in circadian

rhythmicity is not well studied. The retention of diurnal differences in our studies suggest that fibroblasts maintain an intracellular clock and may contribute to rhythmic physiological processes. Indeed, previous reports have shown that cardiac fibroblasts do have intrinsic clocks, and disruption of the myofibroblast clock leads to a profibrotic phenotype in lung tissue (Welsh *et al.*, 2004; Crnko *et al.*, 2019; Cunningham *et al.*, 2020). Another factor which may be driving the diurnal differences observed, and may explain why more genes show time-of-day differences in *αMHC^{cre}Bmal1$^{f/f}$* hearts compared to control hearts, is that of systemic diurnal signals. The local clock may, under normal circumstances, buffer against some systemic rhythmic inputs, and removal of the local therefore results in the emergence of diurnal rhythmicity. Indeed, the idea of emergent rhythms in tissues lacking a functional clock, and local clocks buffering against systemic rhythmic influences, has been reported previously (Kornmann *et al.*, 2007; Zhang *et al.*, 2019; Manella *et al.*, 2021).

Chapter 6: General discussion

This body of work interrogates the impact of the circadian system on cardiac electrophysiology using a range of models and techniques including environmental, behavioural, pharmacological and genetic manipulations to the circadian system in human and mice. ECG recording of de- and repolarisation of cardiac tissue across the heart beat can provide vital understanding about cardiac conduction dynamics. Here we have designed and implemented new, robust methodology for automated analyses of ECG recordings, which has allowed us to examine cardiac electrophysiology over many days, across behavioural interventions in humans and mice. Using these approaches we have made a number of observations:

- ECG measures of SA and AV nodal activity, and ventricular depolarisation, all display a robust circadian rhythm in function when measured under a constant routine protocol in humans.
- The SA node, and thus cardiac pacing, is highly rhythmic across the day, but this involves an integration of numerous rhythmic inputs. Circadian inputs from the brain via the parasympathetic nervous system and from the cardiomyocyte clock, and non-circadian, diurnal rhythms imposed by exogenous factors (for example locomotor activity, arousal state and lighting condition) all contribute to this rhythm.
- The AV node is highly rhythmic across the day, principally influenced by a clock of neural origin via the parasympathetic nervous system, and remains relatively insensitive to acute changes in behavioural routine.
- Differential circadian control over these two cardiac nodes can result in misalignment between diurnal rhythms in nodal activity following common circadian manipulations such as a 9hr advance in the lighting schedule, similar to a transatlantic flight.
- Observations regarding the decoupled rhythmic influences over SA and AV nodal activity appear robust across both mouse and human physiology.
- Ventricular arrhythmia susceptibility follows a diurnal pattern both *in vivo* by catecholaminergic challenge and in *ex vivo* mouse hearts by electrical stimulation, with greater susceptibility at the start of the active phase.

- Loss of the cardiomyocyte specific circadian clock via *Bmal1* deletion results in mice with lower HR, greater sensitivity to parasympathetic input and resistance to ventricular arrhythmias.
- Isolated cardiomyocytes exhibit circadian rhythms in spontaneous firing rate, which may underpin the rhythm in VT susceptibility.

Thus, overall we describe distinct circadian and rhythmic mechanisms that differentially control components of the heart, disruption of which can lead to misalignment between daily rhythms in SA and AV node activity. Furthermore we show how local clocks in the heart buffer inputs based on time-of-day, and dictate excitability across the day, likely to best adapt to the changing energy requirements of the heart, at the cost of increased susceptibility to arrhythmia during periods of high excitability (**Fig 6.1**).

6.1 Rhythmic neural control over cardiac electrophysiology

In humans under constant routine we show that ECG parameters reflecting HR, AV nodal delay and ventricular repolarisation are rhythmic and, although constant routine is not possible in mice, these parameters remain rhythmic under total autonomic blockade but with markedly reduced amplitude after parasympathetic blockade. As such, most parameters are under circadian control of neural origin through parasympathetic signalling. While this circadian signal is likely of central origin (rather than ganglionic), we are unable to conclude whether it originates in the SCN or downstream, such as in the brainstem. There is, however, significant evidence that the SCN partially dictates rhythms in cardiovascular electrophysiology, as discussed in chapter 4. Lesions of the SCN result in markedly reduced diurnal amplitude in HR and QT, abolished light-induced decreases in HR, and abolished daily variations in fractal dynamics of HRV (Scheer *et al.*, 2001; Hu *et al.*, 2008; Tong *et al.*, 2013). Multisynaptic pathways from the SCN to the heart, have been documented through multisynaptic retrograde tracing in the rat (Scheer *et al.*, 2001; Geerling *et al.*, 2010), and our previous work has shown that activation of VIP-expressing cells in the SCN can influence HR in a time-of-day dependent manner, likely via the PVN (Paul *et al.*, 2020) . Interestingly, there is also functional segregation between neurons that project to sympathetic neurons and neurons that project to parasympathetic neurons, with very few projecting to both, in the brainstem and further upstream into the paraventricular

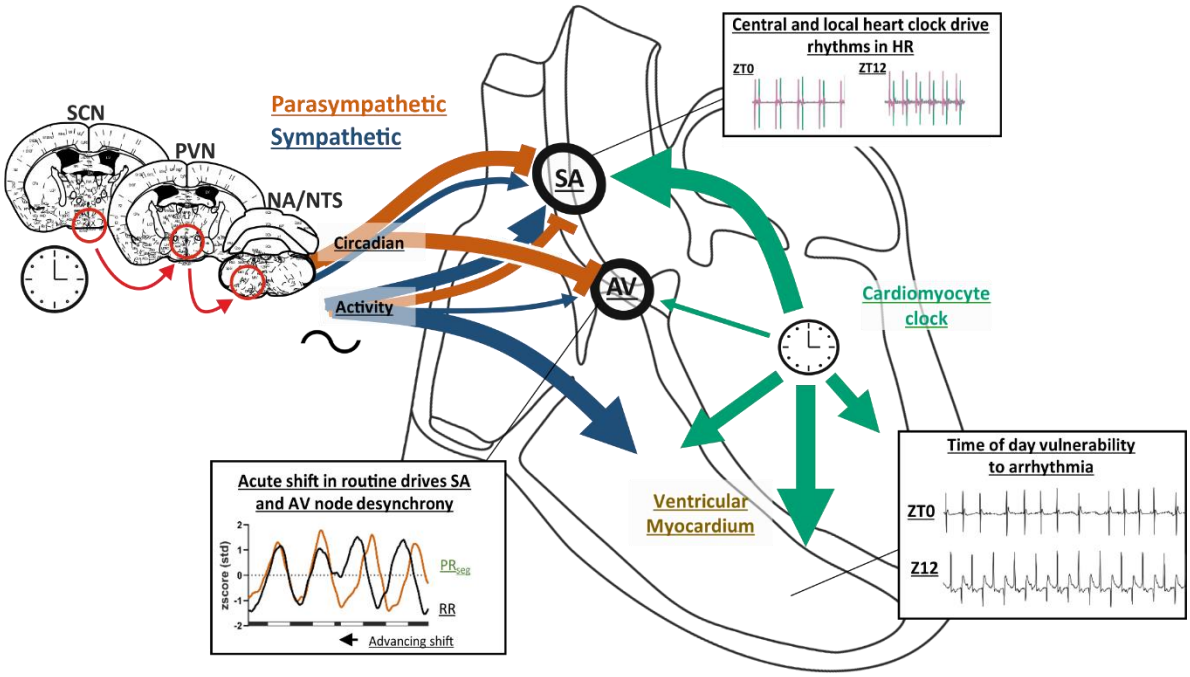

Figure 6.1. Schematic of circadian and non-circadian influences over cardiac electrophysiology. Local to the heart, the cardiomyocyte clock drives rhythms in firing rate and cellular excitability within the SA node and ventricular myocardium, resulting in a circadian component to ventricular arrhythmia susceptibility. Multiple distinct pathways from the brain, segregating acute arousal state changes from longer term circadian inputs deliver rhythmic information to the heart. Circadian cues from the brain likely originate in the SCN and project to the heart through autonomic signalling via the PVN and NA/NTS. While the SA node is influenced by arousal state and circadian inputs of neural and local origin, the AV node is disproportionately sensitive to the neural circadian input and relatively insensitive to arousal state.

and even the SCN, suggesting the SCN has a role in balancing autonomic tone (Buijs *et al.*, 2003). Together these findings demonstrate that the SCN is a source of circadian influence to the heart, and most likely via rhythmic drive to parasympathetic input. Nevertheless, robust endogenous clock function has also been identified in the NTS, a brainstem region which innervates the heart (Chrobok *et al.*, 2020). Therefore, the NTS could contribute to the oscillatory signal to the heart, for example by modulating signals from the SCN to shape the rhythms in cardiac electrophysiology. Indeed, brainstem regions have been shown to interact with the SCN in alternative physiological outputs, such as sleep/wake and feeding behaviours (Abbott *et al.*, 2013; Challet, 2019).

A key observation of our work is that there is functional segregation between rhythmic inputs to the SA and AV nodes. Our data suggest that while the SA node receives circadian input from the parasympathetic nervous system and predominantly acute input (e.g. activity, arousal state) via the sympathetic nervous system, the AV node is disproportionately driven by the parasympathetic nervous system. In the cat, dog and non-human primate, there are distinct parasympathetic ganglion located on the surface of the heart, located within epicardial fat pads at the junction of the inferior vena cava and inferior left atrium, and superior vena cava and right atrium, which independently control the AV and SA nodes (Randall *et al.*, 1986, 1987). Ablation of the left, inferior ganglion selectively abolishes changes in AV nodal conduction in response to vagal stimulation, while ablation of the right, superior ganglion selectively abolishes vagally-induced changes in HR (Billman *et al.*, 1989; Gatti *et al.*, 1995). This separation of inputs provides a possible avenue by which rhythmic inputs from the brain may control SA and AV node activity. Indeed, segregation of this parasympathetic input to the AV and SA nodes persists in the brainstem. The vast majority of neurons within the NTS that project monosynaptically to vagal preganglionic neurons project to either the SA or AV node innervating ganglion only (Blinder *et al.*, 1998). In the neighbouring nucleus ambiguus, activation of specific spatial populations of neurons can also decrease HR or AV conduction independently of the other (Gatti *et al.*, 1996). There is also evidence that sympathetic innervation is also segregated between SA and AV nodes at the level of the heart in dogs, though sympathetic innervation is more diffuse than parasympathetic so is harder to separate (Furukawa *et al.*, 1991). In our studies we observed that ECG measures of SA and AV node activity are differentially

impacted by changes in behavioural routine in humans and mice, and by sequential autonomic blockade in mice (**Fig 6.1**). These observations are consistent with anatomical/functional segregation of vagal inputs to the SA and AV nodes, and provide an extra hypothesis that circadian input may originate from an anatomically distinct pathway.

Acute autonomic control over cardiac electrophysiology is dictated by rapid changes in sympathetic and parasympathetic tone, and the relative contributions of each. There is a traditional view that autonomic control in larger animals, such as dogs or humans, is dominated by high basal parasympathetic tone, whereas in smaller animals, such as mice, higher basal sympathetic tone prevails (Gehrmann *et al.*, 2000; Janssen and Smits, 2002; Swoap *et al.*, 2008). In this case, heart rate would always decrease following total autonomic blockade in mice, as has been previously suggested by some groups (D'Souza *et al.*, 2014; Mesirca *et al.*, 2014). However, we believe this is a much too simplistic view; our data showed a significant decrease in HR at ZT12 but an increase at ZT0. Autonomic balance is controlled by a range of drivers including ambient and body temperature, mouse strain, arousal state of the animal, light exposure and time of day (Niijima *et al.*, 1993; Shusterman *et al.*, 2002; Mutoh *et al.*, 2003; Swoap *et al.*, 2004). Indeed, multiple studies have shown an increase or little change in HR from baseline to total autonomic blockade (Altman *et al.*, 1999; Lu *et al.*, 2009; Sebastian *et al.*, 2013; West *et al.*, 2017). A factor in these discrepancies likely lies in the method of ECG recording used. Radiotelemetry benefits from minimal additional stress to the animal during recording (thus keeping sympathetic tone at baseline) while other methods involve moving the animal to a new enclosure for ECG recording, likely introducing stress and elevating sympathetic input. Indeed, previous reports using the ECGenie system (which involves moving animals to a new enclosure for recording), report baseline HRs of ~750bpm at ZT12 in C57BL/6 mice, significantly higher than peak HR observed in our studies (~625bpm) (D'Souza *et al.*, 2014). Our data contribute to this ongoing discussion and highlight that both sympathetic and parasympathetic are fundamental in determining basal heart rate under laboratory conditions in C57Bl/6J mice. In our experiments sympathetic tone was minimal during the day but high during the night (as there was no change following metoprolol injection at ZT0, but a large change at ZT12), while parasympathetic tone remained at a moderate basal rate across the whole circadian

period (as HR increases following atropine at both ZT0 and ZT12), with an additional diurnal rhythm which drives cardiac electrophysiology.

6.2 Circadian misalignment: mechanisms and impact on cardiovascular health

Our data show that there are multiple rhythmic mechanisms at play in setting diurnal rhythms in cardiovascular electrophysiology: central and peripheral clocks, and rhythmic influence from diurnal behaviour. Circadian misalignment can therefore occur when two of these rhythmic influences are not synchronised, for example when SCN clocks are mistimed with peripheral clocks, or when behaviour is misaligned with the body clock (West and Bechtold, 2015). In our data, we show that acute shifts in behavioural routine can result in misalignment between rhythms in SA and AV node activity due to the differential rhythmic control over the nodes. We conclude that rhythms in AV nodal delay are dictated by a central circadian clock as they are abolished under autonomic blockade, and closely match rhythms in body temperature (which is dictated primarily by the circadian clock (Scheer *et al.*, 2005)) across phase advances. In contrast, rhythms in SA nodal pace making are dictated in part by behavioural rhythms as they adapt quickly to changes in behavioural routine, central circadian clocks as autonomic blockade severely dampens amplitude, and circadian clocks local to the heart as remaining rhythms under autonomic blockade (and *ex vivo*) are abolished in animals lacking a functional cardiomyocyte clock.

Across a phase shift, the SCN does not adapt quickly to the new schedule, instead taking days to entrain as evidenced by rhythms in body temperature across the 9hr phase advance in our mouse studies, by the constant routine phasing in our human studies, and previous literature (Golombek and Rosenstein, 2010). In contrast, behavioural routine adapts quickly as evidenced by the quick adaptation of HR to the new behavioural routine during the shift in mice, and during sleep deprivation/forced routine change in humans. As such, it is clear that behavioural rhythms are misaligned with the SCN clock across our experimental paradigms. However, we never directly tested whether central and peripheral clocks are misaligned. One possible mechanism by which peripheral and central clocks can become misaligned is when feeding is misaligned to the LD cycle, for example during long term night shift work. Peripheral clocks can entrain to feeding schedules while central clocks entrain to the LD cycle (Damiola *et al.*, 2000; Stokkan *et al.*, 2001). During our

studies, however, there were no long-term periods of LD cycles being misaligned to food availability in humans, and as such we do not believe there to be misalignment between central and local clocks in our studies. Nonetheless, our data open the intriguing possibility that misalignment between central and local clocks may result in misalignment between autonomic signalling and cardiomyocyte excitability, the impact of which is currently unknown. Indeed, intrinsic desynchony has been associated with accelerated development of cardiovascular risk factors, and may be one mechanism at play in the development of cardiovascular complications in long-term shift workers (Young and Bray, 2007; Arble *et al.*, 2010; Evans and Davidson, 2013).

Circadian misalignment has been shown to have stark impacts to physiology in animal models. Mice can entrain to LD cycles slightly shorter or longer than 24hr in period, but display phase offset rhythms in physiology and central clock activity (West *et al.*, 2017). At the limits of entrainment, mice can entrain to 22.5hr or 27hr LD cycles, but exhibit a phase delay, or advance, respectively. Such misalignment between the LD cycle and behaviour results in reduced energy efficiency (e.g. increased respiratory exchange rate and carbohydrate oxidation) and lengthening of ECG parameters suggesting disrupted autonomic signalling (West *et al.*, 2017). Similarly, hamsters with mutations resulting in a 22hr endogenous clock (+/*tau*), develop cardiomyopathy, extensive fibrosis, impaired contractility of the heart, renal dysfunction and premature death when housed under 24hr LD cycles. When housed under 22hr LD cycles, in synchrony with the endogenous clock, adverse cardiac and renal phenotypes are normalised, highlighting that the adverse physiological effects are due to misalignment between the SCN and behaviour (Martino *et al.*, 2008). Indeed, direct measures of circadian period and lifespan reveal a correlation between natural deviation from 24hr period and premature death in mice (Wyse *et al.*, 2010; Libert *et al.*, 2012).

Humans can also be subject to chronic misalignment between behaviour and LD cycle through long-term shift work, the implications of which are only beginning to be understood. Long-term shift work is associated with increased risk of a range of cardiovascular disorders including myocardial infarction, cardiovascular disease, ischaemic stroke and coronary heart disease, alongside non-cardiovascular disorders such as type 2 diabetes and cancer (Vyas *et al.*, 2012; Kecklund and Axelsson, 2016; Torquati *et al.*, 2018).

Long-term shift work has also been associated with disrupted ECG parameters, most notably lengthened QTc interval (a risk factor for arrhythmias and SCD) and increased risk of atrial fibrillation (Murata *et al.*, 1999; Meloni *et al.*, 2013; N. Wang *et al.*, 2021). That our work found no significant alterations in baseline ECG parameters between long-term shift work and the control individuals is perhaps unsurprising given the relatively small number of participants compared to large scale population studies. We do however, show that acute shift work results in marked misalignment between ECG parameters on a circadian scale. Whether acute alterations in cardiac electrophysiology present during mistimed sleep and shift-work routines influences susceptibility to adverse cardiac events such as arrhythmias is currently unclear. However, during ECG-based diagnosis and/or interventions it is likely of important relevance, as patient occupation, recent sleep-wake history and even current time of day could influence the outcome dramatically. Likewise, doctors of patients with pre-existing cardiac conditions who are routinely monitored for ECG parameters, or who have an implantable ICD device which monitors ECG constantly, may need to be aware of the involvement of the circadian system.

6.3 Endogenous rhythms in ventricular repolarisation

Ventricular repolarisation dynamics (measured by QT interval on the ECG) are an important risk factor for cardiac death (Algra *et al.*, 1991; Brüggemann *et al.*, 1997) and is highly dependent on HR (Batchvarov *et al.*, 2002). A number of previous studies, including our own, have observed diurnal rhythms in QT interval (Bonnemeier *et al.*, 2003a), but whether QTc interval (after HR has been corrected for) is rhythmic is a matter of debate, with many arguing that the rhythm is solely dictated by HR (Morganroth *et al.*, 1991; Ishida *et al.*, 1997; Yi *et al.*, 1998), and some arguing there is an additional circadian influence on ventricular repolarisation, although dependent on the QT interval correction formula used (Molnar *et al.*, 1996; Smetana *et al.*, 2003; Singh and Rabkin, 2021). Indeed, QT/RR relationships are highly variable between humans (Batchvarov *et al.*, 2002) and are complex in mice, differing under different conditions such as pharmacological challenge (Roussel *et al.*, 2016). As such, correction formulae may be appropriate in some circumstances and not in others. As such, a true circadian variation in ventricular repolarisation is difficult to establish. Despite these limitations, our data add to this body of literature and suggest, in both human and mouse, that there is a slight diurnal variation in QTc interval, but is

significantly lower in amplitude than uncorrected QT interval, suggesting that the majority of the rhythm is dictated by changes in HR.

6.4 Cardiac clocks and cellular excitability

An influence of cardiac clock on cardiac function has been established in rodents, with cardiomyocyte clock function regulating over 10% of the transcriptome in a rhythmic manner (Martino *et al.*, 2004; Bray *et al.*, 2008; Zhang *et al.*, 2014). Similarly, a recent study has shown that a large proportion of the transcriptome is rhythmic in the SA node (Y. Wang *et al.*, 2021). Genetic manipulation of the cardiomyocyte clock results in disrupted contractility, myocardial metabolism and protein turnover (Young *et al.*, 2014; Zhang *et al.*, 2020) and a body of previous literature has implicated local cardiac clocks in dictating cardiac electrophysiology (**Table 6.1**). The expression pattern of many genes is rhythmic across the day, including several important ion channels. This suggests a direct role of *Bmal1* and/or clock function *per se* on electrophysiology. Deletion of the cardiomyocyte clock also impacts electrophysiology, disrupting both sodium and potassium currents and expression of associated ion channel genes *Scn5a* and *Kcnh2*, alongside changes in HR and QT interval (Schroder *et al.*, 2013, 2015). In animals with genetically induced long QT interval ($Scn5a^{+/\Delta KPQ}$), deletion of the clock exacerbates QT lengthening, and lengthening of QT interval in cardiomyocyte *Bmal1* knockout animals is not dependent on changes in HR, suggesting the clock impacts ventricular repolarisation dynamics directly (Gottlieb *et al.*, 2021; Schroder *et al.*, 2021). *Bmal1* in the heart directly regulates the transcription factor *Klf15*, over- or underexpression of which results in abolished diurnal rhythms in QT interval and increased risk of ventricular arrhythmias (Jeyaraj *et al.*, 2012). Interestingly, mathematical modelling of cardiomyocytes reveals an inherent circadian variation in EAD likelihood, and 2D modelling reveals a rhythm in the break up propensity of spiral waves across myocardium, which occurs during ventricular fibrillation (VF), suggesting a role for the cardiomyocyte clock in setting rhythms in arrhythmogenesis (Diekman and Wei, 2021). Our data support these observations, highlighting rhythms in ion channel genes in the SA node which likely contribute to the rhythms observed in HR *in vivo* under complete autonomic blockade and *ex vivo* in isolated hearts. We also build on these findings to show that the cardiomyocyte clock directly dictates temporal rhythms in cellular excitability and

Model	ECG phenotype	Disrupted genes/ion currents	Reference
Cardiomyocyte clock mutant ($CLOCK^{\Delta19/\Delta19}$)	Decreased HR Decreased daily HR amplitude Decreased HR at ZT18 *ex vivo*	Disrupted rhythmicity / expression in variety of genes	(Bray *et al.*, 2008)
Klf15 knockout, *Klf15* overexpression. (*Bmal1* directly regulates *Klf15*)	Abolished daily QT rhythms Increased arrhythmia sensitivity Increased APD_{90} (*Klf15-null*) Decreased APD_{90} (*Klf15-Tg*)	Decreased expression / daily amplitude of *Kchip2* Increased $I_{to,fast}$ (*Klf15-Tg*) Decreased $I_{to,fast}$ (*Klf15-null*)	(Jeyaraj *et al.*, 2012)
Inducible cardiomyocyte *Bmal1* knockout	Lengthened RR Lengthened QRS Stretch induced PVCs	Disrupted rhythm in *Scn5a* Disrupted rhythm in *Kcnj2* Reduced I_{Na}	(Schroder *et al.*, 2013)
Cardiomyocyte clock mutant ($CLOCK^{\Delta19/\Delta19}$)		Disrupted rhythm in *Tcap*	(Podobed *et al.*, 2014b)
Inducible cardiomyocyte *Bmal1* knockout	Lengthened QT Increase daily QT amplitude	Disrupted rhythm in *Kcnh2* Reduced I_{Kr}	(Schroder *et al.*, 2015)
Wild-type	Diurnal rhythms in HR under AB abolished with I_f blocker	Diurnal rhythms in *Hcn4* Diurnal rhythms in I_f	(D'Souza *et al.*, 2021)
Computational cardiomyocytes	Circadian rhythm in EADs Circadian rhythm in spiral wave breakup (represents VF)		(Diekman and Wei, 2021)
Wild-type SA node		Widespread circadian rhythmicity in ion channel genes	(Y. Wang *et al.*, 2021)
Wild-type Cardiomyocyte *Bmal1* knockout	Diurnal difference in *ex-vivo* HR Diurnal difference in arrhythmogenesis Lengthened RR Lengthened QT Loss of daily ECG rhythmicity under AB Decreased arrhythmia sensitivity	Rhythm in spontaneous cardiomyocyte firing Diurnal rhythmicity in SA node ion channel gene expression Decreased expression of *Adrb1, Ryr2, Cacna1g, Cacna1h, Cacna1c, Kchip2, Kcnq1, Kcnh2, Kcnj2, Hcn4, Scn4b, Scn5a, Cx45, Klf15* Increased expression of *Casq1, Casq2, Kcne1*	(Hayter *et al.*, 2021a)
Inducible cardiomyocyte *Bmal1* knockout	Lengthened QT Exacerbates $Scn5a^{+/\Delta KPQ}$ induced long QT Rescues $Scn5a^{+/\Delta KPQ}$ induced HRV decrease	Disrupted rhythms in *Hcn4, Scn4b, Kcnj2, Kcnq1, Tbx5, Gata4* Reduced expression of *Klf15, Kchip2, Kcna5, Kcnb1*	(Schroder *et al.*, 2021)
Cardiomyocyte *Bmal1* knockout	Lengthened RR Lengthened QT & QTc Increased LF:HF Increased APD restitution Decreased frequency to induce alternans		(Gottlieb *et al.*, 2021)

Table 6.1. Papers with evidence for a role of the cardiomyocyte clock in dictating cardiac electrophysiology. Of note, there are many other papers which investigate the role of the cardiomyocyte clock on metabolism.

spontaneous firing rate. It seems likely that this increased excitability results in increased susceptibility to ventricular arrhythmias.

A recent paper suggests that a circadian clock with the SA node contributes to inherent time-of-day rhythms in HR through regulation of *Hcn4* and its associated current I_f (D'Souza *et al.*, 2021). Care must be taken when interpreting their data; firstly, the authors show no reduction in HR during a light pulse at ZT13, despite reduction of locomotor activity, in contrast with previous literature (Thompson *et al.*, 2008; West *et al.*, 2017). Secondly, they show a reduction in HR following autonomic blockade in anaesthetised animals, despite isoflurane (the anaesthetic used) severely dampening sympathetic signalling (Seagard *et al.*, 1983; Tanaka and Tsuchida, 1998; Lee *et al.*, 2002). Third, protein levels of HCN4 peak around ZT12, ~18hours after peak *Hcn4* mRNA, incongruent with known transcription-translation dynamics (Alberts *et al.*, 2002). Furthermore, between ZT0 and ZT12 (when they show differences in intrinsic HR/SA nodal pace making), there are no significant differences in HCN4 protein level or I_f dynamics. Finally, the authors use ivabradine and caesium ions to abolish I_f, while both of these interventions also alter off-target ion currents (Clay and Shlesinger, 1984; Haechl *et al.*, 2019). The same group also fail to show a significant rhythm in SA node *Hcn4* expression in later reports (Y. Wang *et al.*, 2021), in agreement with our studies. Instead, we believe that widespread diurnal rhythms in the ion channel landscape and autonomic sensitivity within the SA node likely underpin the changing cellular excitability across the day.

There may also be other mechanisms driving cardiomyocyte cellular excitability alongside oscillations in gene transcription. Protein translation oscillates across the day, dependent on mTORC signalling, resulting in rhythms in cytoplasmic protein concentration. Greater protein concentration is concurrent with macromolecular crowding within the cell, increasing osmolarity. To buffer against increasing osmolarity without changes in physical size, cardiomyocytes pump out intracellular ions such as K^+ and Na^+, decreasing cytosolic ion concentrations, maintaining osmotic homeostasis and ultimately imparting cell-autonomous daily variations in firing frequency (Stangherlin *et al.*, 2020). Indeed, increased mTOR expression and protein synthesis have been reported in cardiomyocyte *Bmal1* knockout animals (McGinnis *et al.*, 2017) which may result in decreased intracellular ion concentrations and cellular excitability, consistent with our findings and supporting the

view that alterations in overall protein synthesis contribute to the phenotype observed in our studies.

Given that the AV node is made up of similar cell types to the sinus node and rest of the heart (primarily cardiomyocytes and fibroblasts), it likely also contains a molecular circadian clock, although this remains to be directly tested. However, while we observed robust daily rhythms in AV nodal delay across all studies, this delay was primarily driven by the autonomic nervous system and not by a local clock. It is possible that a local AV node clock may contribute to other functions within this site. Indeed, RNA sequencing of ventricular tissue revealed that deletion of the cardiomyocyte clock alters the expression levels of muscarinic acetylcholine receptor and beta adrenergic receptor genes, suggesting that autonomic sensitivity may be altered, with increased sensitivity to parasympathetic signalling and decreased sensitivity to sympathetic signalling. Indeed, previous reports have shown a diurnal rhythm in baroreflex sensitivity in rats, which is abolished under autonomic, or ganglionic, blockade, indicating a rhythmic sensitivity to autonomic control across the day (Oosting *et al.*, 1997). Therefore, the rhythms observed in AV nodal physiology may derive from a combination of rhythmic autonomic signalling, and differing autonomic sensitivity across the day.

There may also be other aspects of conduction governed by the clock in the AV node outside of delay in healthy hearts. For example, previous studies have reported circadian rhythms in AV node refractoriness and degree of concealed AV conduction (i.e. not visible on the ECG) during atrial fibrillation (Raeder, 1990; Hayano *et al.*, 1998). These rhythms are blunted in patients with congestive heart failure and chronic atrial fibrillation, suggesting that their origin is cardiac and therefore may be under control of the local clock (Hayano *et al.*, 1998, 2002).

6.5 Circadian influences governing susceptibility to ventricular tachycardia

Our data show, for the first time, that ventricular arrhythmia susceptibility is inherently influenced by the circadian system. Using the same catecholamine challenge (i.p. injection of 120mg/kg caffeine and 2mg/kg adrenaline), previous reports have highlighted that wild-type mice are relatively resistant to induced arrhythmias (Cerrone *et al.*, 2005; Alvarado *et al.*, 2019). While not explicitly reported, these experiments most likely took part during the

day, in keeping with our observations. In contrast, during the night we observed a dramatic increase in progression to bidirectional VT in response to injection of caffeine and adrenaline. Similar heightened sensitivity is observed in animals with transgenic sensitivity to VT such as those with disrupted SR calcium retention (*Casq2*$^{R33Q/R33Q}$) or reduction in RYR function (*Ryr2*$^{P1124L/P1124L}$) (Rizzi *et al.*, 2008; Alvarado *et al.*, 2019). We also show that *ex vivo* hearts display a rhythm in VT susceptibility, again with higher incidence in hearts removed at ZT12, suggesting that a local circadian clock in the heart contributes to arrhythmogenesis. Surprisingly, in our studies, mice lacking a functional clock in cardiomyocytes are relatively protected against both catecholamine-induced VT *in vivo*, and electrically induced arrhythmias *ex vivo*. Previous work has identified that inducible cardiomyocyte *Bmal1* knockout animals display more numerous spontaneous sinus pauses, with >10% of RR intervals being longer than 150ms (corresponding to 400bpm), compared to ~5% in control animals (Schroder *et al.*, 2013) (although, such differences are expected given the lower baseline HR in these animals, and more sinus pauses would likely impact HRV measures, which the game group show are similar between the two genotypes (Schroder *et al.*, 2021)). These animals also exhibit greater susceptibility to stretch-induced conduction block *ex vivo* (measured by increasing preload) (Schroder *et al.*, 2013). Another recent report has shown that these animals are more susceptible to pacing-induced APD alternans (alternating APDs between beats), which is often associated with arrhythmia (Gottlieb *et al.*, 2021). While we demonstrate that cardiomyocyte *Bmal1* knockout animals are relatively protected against VT, the differences are likely a result of the mechanism underpinning the arrhythmia. Specifically, conduction block is a result of a loss of conduction, alternans are a result of differences in repolarisation, and VT is a result of spontaneous firing of the ventricular conduction system.

Given that cardiomyocyte deletion of *Bmal1* partially protects against arrhythmias in our studies, pharmacologic inhibition of *Bmal1* or disruption of other clock mechanisms may, in theory, be beneficial to humans therapeutically. Small-molecule modulators of clock function are becoming increasingly studied and it is feasible that some with suitable pharmacokinetic/dynamic profiles (e.g. inability to cross the blood brain barrier, long half-life) will soon become available (Doruk *et al.*, 2020; Ribeiro *et al.*, 2021). Removal of functional *Bmal1* would, however, result in a range of off-target effects, not only due to

removal of a functional clock in peripheral tissues, but through the non-clock related functions of *Bmal1* (discussed in **6.6.5**). In healthy individuals, the risk would surely outweigh any reduced risk of arrhythmia, but in high risk patients this strategy may be beneficial. Alternatively, a more appropriate approach may be to identify the mechanisms by which *Bmal1* exerts anti-arrhythmic effects, and pharmacologically target key components of these pathways. This approach may result in greater tissue-specificity, and fewer off-target effects, and would be of significant importance to follow up in future studies.

In humans there is a daily variation in VT susceptibility in healthy individuals and across various disease states, peaking in the morning (Lucente *et al.*, 1988; Twidale *et al.*, 1989; Lampert *et al.*, 1994; Tofler *et al.*, 1995; Englund *et al.*, 1999; Kozák *et al.*, 2003). Interestingly, this rhythm is not present in patients on beta adrenoceptor blocking drugs (Aronow *et al.*, 1995; Behrens *et al.*, 1997), implicating sympathetic signalling in the daily rhythm in arrhythmogenesis. Moreover, in a canine model of chronic heart failure, there is also a time-of-day variation in VT peaking in the morning (Zhu *et al.*, 2014). This variation is associated with disrupted HRV rhythms, implicating the autonomic nervous system. Indeed, we demonstrate robust rhythms in HRV from time, frequency and non-linear domains were observed in mice and humans. Furthermore, in our RNA sequencing studies, we found an apparent changes in gene expression relating to autonomic signalling in cardiomyocyte *Bmal1* knockout mice. Wild-type animals also display a robust time-of-day sensitivity to catecholamine-induced arrhythmias. Together this suggests that the autonomic nervous system may be influential in either driving arrhythmias in a time-of-day dependent manner, or by priming the heart for arrhythmias via rhythmic signalling.

One possible mechanism underpinning our observations regarding arrhythmia susceptibility is though circadian regulation of the transcription factor *Klf15*. *Bmal1* directly regulates *Klf15*, which in turn regulates KChIP2, a K_v channel-interacting protein which regulates potassium currents. Overexpression of Klf15 results in augmented potassium currents ($I_{to,f}$), shortened action potential duration and spontaneous ventricular arrhythmias. Knockout of *Klf15* instead results in dampened potassium currents and lengthened action potential durations, but also increased arrhythmia susceptibility (through electrical stimulation) (Jeyaraj *et al.*, 2012). These findings offer a possible link

between the cardiomyocyte clock and the time-of-day rhythm in arrhythmogenesis, although it is unclear whether the normal daily variation in *Klf15* is sufficient to drive rhythms in arrhythmia susceptibility. Indeed, in our studies we observe a robust diurnal variation in *Klf15* in control animals, and marked downregulation in cardiomyocyte *Bmal1* knockout animals. Another possible mechanism governing rhythms in arrhythmogenesis is through calcium handling. We observe widespread dysregulation of calcium handling genes between genotypes at ZT12, and calcium dysregulation is well-documented to be critical in arrhythmia induction and maintenance (Landstrom *et al.*, 2017; Kistamás *et al.*, 2020).

6.6 Technical considerations

6.6.1 Robust ECG measures from noisy longitudinal data

One of the challenges posed by longitudinal ECG data is the requirement for automated analysis. As the ECG signal can become noisy during locomotor activity, a robust, automated analysis procedure was required. To overcome this challenge and increase signal-to-noise ratio, we opted for an averaging approach. After taking sweeps of data, ECG parameters were calculated for all valid beats and averaged across the sweep. While this approach is robust to noisy data and provides accurate measures for the sweep, it does so at the cost of losing information about beat-by-beat interactions. For our studies, we believe that this is an acceptable compromise as we are interested in circadian dynamics across longer temporal timescales, though it is a limitation to be considered.

6.6.2 PR segment and interval

When investigating AV nodal delay, often the ECG parameter PR interval is used (Cheng *et al.*, 2009; Aro *et al.*, 2014). PR interval is measured from the onset of the P wave to the onset of the QRS complex, that is, the time between the SA node firing (generating the electrical impulse) and initiation of ventricular depolarisation. This measure therefore includes depolarisation time of the atria, AV nodal delay and his bundle depolarisation and is thus a complex measure and overestimation of the delay across the AV node. In reality, the impulse propagates around the atria and initially reaches the AV node at some time during the P wave, which cannot be measured without invasive techniques such as catheter electrodes inserted into the pulmonary, or femoral vein (Scherlac *et al.*, 1972). Likewise, the true time at which the impulse leaves the AV node cannot be measured using surface

ECG. As a result, we believe that PR segment, measured from the offset of the P wave to the onset of the QRS complex, is a more robust measure of AV nodal delay in our experimental approach. While PR segment likely underestimates the delay compared to when the impulse reaches the AV node, it minimises any impact of changing atrial dynamics (Verweij *et al.*, 2014). Indeed, in our human study 1, P wave duration was not significantly rhythmic across the baseline day, but was altered during mistimed sleep (**Fig 3.3**), suggesting an impact of arousal state changes on atrial depolarisation dynamics. As a result, PR interval lengthens during mistimed sleep where PR segment does not, yet PR segment remains robustly rhythmic. Importantly, our comparisons predominantly compare the same individuals across time, rather than comparing between individuals. Also, the contribution of the P wave to PR interval is significantly smaller in mice (~50% in humans and ~20% in mice), so any differences generated from measuring PR segment compared to PR interval are minimised in mice.

6.6.3 Atrioventricular delay and HR dependency

Previous reports have studied changes in AV nodal delay during exercise and found that as heart rate increases, AV nodal delay decreases linearly (Atterhög and Loogna, 1977; Lee *et al.*, 1995). Similarly, studies in humans have directly assessed the dependency of PR interval on heart rate and found a significant correlation, with some arguing that a HR correction should be applied to PR interval calculations for risk estimation measures, similar to that done for QT interval (Soliman and Rautaharju, 2012; Toman *et al.*, 2020). These results seem in conflict with our findings that AV nodal delay remains robustly rhythmic but insensitive to changes in HR. One key difference between our studies and these reports is the measure of PR interval compared to PR segment, discussed above. Importantly, these studies incorporate a wide range of RR intervals, from measures at rest compared to measures during high HRs induced by exercise. Our studies investigate the interdependence of PR segment and HR across a narrower range of intervals, covering the 'normal' physiological values with minimal exercise and predominantly across values within the range dictated by the circadian system. For example, in our human studies we rarely saw HR rise above 80-90bpm and the only rapid increase in HR (as would be present during exercise) was upon waking/getting out of bed. This spike in HR was mirrored in PR segment, but to a lesser degree relative to diurnal amplitude (**Fig 3.1**). Other than this minor physical

exertion the participants were mostly sedentary. Mice were much more likely to exhibit large bouts of activity, which may explain the significant response of PR segment to bouts of locomotor activity (**Fig 4.3**), although again minor relative to that of RR/QT intervals. Our data therefore does not preclude the findings that AV nodal delay is responsive to HR at ranges outside those measured here. Also of note, all of our comparisons have been binned for robustness in measurement, and to allow better comparison across the day. Consequently, we are unable to conclude how ECG parameters interact on a beat-by-beat basis, although we believe that robust correlations between parameters will persist across bins.

6.6.4 Differences between human and mouse electrophysiology

Humans and mice have similar heart anatomy and cardiac conduction systems. However, ECG waveforms are different in appearance between the two species. As mentioned previously, mice have significantly smaller P waves which contribute a smaller proportion of the PR interval than humans. In addition, the ventricular action potential differs largely between human and mouse, with mice lacking the long plateau phase and instead repolarising to a greater extent following initial depolarisation. These differences can be explained by differences in ionic currents shaping the action potential, predominantly from mice lacking I_{Ks} and I_{Kr} currents (slow and rapid components of the delayed rectifier K^+ current) and instead exhibiting slow, voltage-gated K^+ currents (Nerbonne and Kass, 2005; Liu *et al.*, 2008). As a result of this large repolarisation spike, mice exhibit a further positive J wave following the QRS complex and have a shallow, negative T wave rather than the large positive T wave observed in humans (Boukens *et al.*, 2014). While the presence of the J wave can obstruct the end of the QRS complex, making ventricular depolarisation times difficult to interpret, the end of the T wave remains a good measure of the end of ventricular repolarisation (Boukens *et al.*, 2013; Speerschneider and Thomsen, 2013). Of importance in the study of arrhythmias, mice exhibit differences in intracellular calcium handling dynamics compared to humans, displaying less prominent Ca^{2+} currents and instead displaying greater K^+ currents (Clauss *et al.*, 2019). However, autonomic innervation remains similar, and even arrhythmias that are primarily driven by dysregulated calcium handling (such as CPVT) can be modelled accurately in mice (Rizzi *et al.*, 2008; Dobrev and Wehrens, 2018). Thus, despite differences in cardiac electrical dynamics and ECG

measurements, the mouse is still an excellent model for human cardiac electrophysiology, though care must be taken with interpretation, particularly of QRS measurements. Mice and humans exhibit similar conduction systems and ECG parameters relating to equivalent electrical dynamics, and we show that the differential circadian control over components of the heart remains similar between the species.

6.6.5 Mouse genetics

Generally, all mouse lines used here have been well documented in literature, with the exception of the *Nr1d1:Stop$^{f/f}$Luc* reporter. While we have not yet studied any phenotype in animals with this reporter, in our studies they were only used for tissue samples to assess rhythmicity in cardiomyocytes. The expression of bacteriophage Cre recombinase under the *αMHC* promotor has the capability of being cardiotoxic after prolonged expression (Pugach *et al.*, 2015). As such, in all breeding lines Cre was kept heterozygous to keep Cre levels at a minimum, and all mice were used at the earliest convenience to avoid age-dependent phenotypes. We also opted to breed and phenotype *αMHC^{Cre}* animals with intact *Bmal1* expression and found no changes in ECG parameters, providing confidence that animals in our studies were healthy. Similarly, *αMHC^{Cre}Bmal1$^{f/f}$* animals are reported to start developing age-onset cardiomyopathy at around 28 weeks of age (Young *et al.*, 2014; Ingle *et al.*, 2015). From our RNA sequencing studies, we found minimal evidence of cardiomyopathy related genes in these animals, and heart weights did not differ significantly from control animals, providing confidence that in our studies these mice had not begun to develop cardiomyopathy. Animals with the *mPer2Luc* reporter are also reported to have slightly altered circadian behaviour, with slightly shorter circadian periods (~15 minutes) and activity dissociation in constant light (Ralph *et al.*, 2021). While many of our mouse lines (those without the *Nr1d1:Stop$^{f/f}$Luc* reporter*)* express the *mPer2Luc* reporter, we have not been investigating circadian dynamics of these animals in constant dark or light.

Importantly, *Bmal1* is a transcription factor that has functions outside of its role as a core clock gene. Global deletion of *Bmal1* results in myriad health defects including decreased body weight, infertility, insulin resistance, hair loss, arthropathy and premature death, all of which can be ameliorated if *Bmal1* is knocked out inducible in adulthood, suggesting a role for *Bmal1* in development (Bunger *et al.*, 2005; Kondratov *et al.*, 2006; Alvarez *et al.*,

2008; Yang *et al.*, 2016). As such, it is important to consider that phenotypes observed in cardiomyocyte specific *Bmal1* knockout animals may not be directly due to lack of circadian clock function. In our studies however, we primarily investigated circadian components of *Bmal1* knockouts such as time-of-day dependent changes in electrophysiology, rather than health deficits between genotypes, so we do not believe that non-circadian roles of *Bmal1* are of important consideration in our findings. We cannot yet, however, rule out the possibility that the protection against arrhythmias offered by this genetic manipulation, is not a result of a pleiotropic developmental effect.

6.7 Conclusions

In summary, we have developed robust methodology to analyse longitudinal ECG data collected from humans and mice and applied it to tightly controlled human laboratory studies and across a range of mouse experiments while performing environmental, pharmacological and genetic manipulations to unravel the relative influences of central and peripheral circadian clocks, and other rhythmic influences over cardiac electrophysiology. We show that daily rhythms in SA nodal pacemaking are dictated by central and peripheral clocks, and by acute changes in behaviour. In contrast, rhythms in AV nodal delay are governed primarily by central clocks (likely the SCN) via parasympathetic signalling. As such, rhythmic activity of the SA and AV nodes are sensitive to misalignment following an acute shift in behavioural routine, such as following a transatlantic flight. These observations appear robust across species. We also demonstrate that the cardiomyocyte clock contributes to daily rhythms in cellular excitability, likely to assist the heart in adapting to the changing energetic requirements across the day, at the cost of increased susceptibility to ventricular arrhythmias. Finally, we identify potential mechanisms which underpin the rhythms in VT sensitivity across the day, which may translate to further understanding of mechanisms involved in the generation of daily rhythms in human cardiac arrhythmogenesis, and thus offer important and logical new avenues for therapeutic investigation.

6.8 References

Abbott, S. M., Arnold, J. M., Chang, Q., Miao, H., Ota, N., *et al.* (2013) Signals from the Brainstem Sleep/Wake Centers Regulate Behavioral Timing via the Circadian Clock. *PLOS ONE*, **8**(**8**), e70481.

Abe, H., Honma, S. and Honma, K. I. (2007) Daily restricted feeding resets the circadian clock in the suprachiasmatic nucleus of CS mice. *American Journal of Physiology - Regulatory Integrative and Comparative Physiology*, **292**(**1**), 607–615.

Abildstrom, S. Z., Jensen, B. T., Agner, E., Torp-Pedersen, C., Nyvad, O., *et al.* (2003) Heart rate versus heart rate variability in risk prediction after myocardial infarction. *Journal of Cardiovascular Electrophysiology*, **14**(**2**), 168–173.

Abrahamson, E. E. and Moore, R. Y. (2001) Suprachiasmatic nucleus in the mouse: retinal innervation, intrinsic organization and efferent projections. *Brain Research*, **916**, 172–191.

Acharya, U. R., Joseph, K. P., Kannathal, N., Lim, C. M. and Suri, J. S. (2006) Heart rate variability: A review. *Medical and Biological Engineering and Computing*, **44**(**12**), 1031–1051.

Agah, R., Frenkel, P., French, B., Michael, L. H., Overbeek, P. and Schneider, M. D. (1997) Gene Recombination in Postmitotic Cells. *Journal of Clinical Investigation*, **100**, 169–179.

Akashi, M., Tsuchiya, Y., Yoshino, T. and Nishida, E. (2002) Control of Intracellular Dynamics of Mammalian Period Proteins by Casein Kinase I ε (CKIε) and CKIδ in Cultured Cells. *Molecular and Cellular Biology*, **22**(**6**), 1693–1703.

Alberts, B., Johnson, A., Lewis, J. and Al., E. (2002) From RNA to Protein. *Molecular Biology of the Cell*, 132–133.

AlGhatrif, M. and Lindsay, J. (2012) A brief review: history to understand fundamentals of electrocardiography. *Journal of Community Hospital Internal Medicine Perspectives*, **2**(**1**), 14383.

Algra, A., Tijssen, J. G. P., Roelandt, J. R. T. C., Pool, J. and Lubsen, J. (1991) QTc prolongation measured by standard 12-lead electrocardiography is an independent risk factor for sudden death due to cardiac arrest. *Circulation*, **83**(**6**), 1888–1894.

Altman, J. D., Trendelenburg, A. U., Macmillan, L., Bernstein, D., Limbird, L., *et al.* (1999) Abnormal regulation of the sympathetic nervous system in α2(a)- adrenergic receptor knockout mice. *Molecular Pharmacology*, **56**(**1**), 154–161.

Alvarado, F. J., Martijn Bos, J., Yuchi, Z., Valdivia, C. R., Hernández, J. J., *et al.* (2019) Cardiac hypertrophy and arrhythmia in mice induced by a mutation in ryanodine receptor 2. *JCI Insight*, **4**(**7**).

Alvarez, J. D., Hansen, A., Ord, T., Bebas, P., Chappell, P. E., *et al.* (2008) The circadian clock protein BMAL1 is necessary for fertility and proper testosterone production in mice. *Journal of Biological Rhythms*, **23**(**1**), 26–36.

Anderson, K. R., Ho, S. Y. and Anderson, R. H. (1979) Location and vascular supply of sinus node in human heart. *British Heart Journal*, **41**(**1**), 28.

Andrews, R. V and Shiotsuka, R. (1970) The Effect Of Actinomycin D On The In Vitro Adrenal Secretory Rhythm Of The Hamster. *Comp. biochem. Physiol*, **36**, 353–363.

Andrews, S. (2010) *FastQC: A Quality Control Tool for High Throughput Sequence Data*.

Apandi, Z. F., Ikeura, R., Hayakawa, S. and Tsutsumi, S. (2020) An analysis of the effects of noisy electrocardiogram signal on heartbeat detection performance. *Bioengineering*, **7**(**2**), 1–15.

Arble, D. M., Ramsey, K. M., Bass, J. and Turek, F. W. (2010) Circadian disruption and metabolic disease: Findings from animal models. *Best Practice and Research: Clinical Endocrinology and Metabolism*, **24**(**5**), 785–800.

Aro, A. L., Anttonen, O., Kerola, T., Junttila, M. J., Tikkanen, J. T., *et al.* (2014) Prognostic significance of prolonged PR interval in the general population. *European Heart Journal*, **35**(**2**), 123–129.

Aronow, W. S., Ahn, C., Mercando, A. D. and Epstein, S. (1995) Effect of propranolol on circadian variation of ventricular arrhythmias in elderly patients with heart disease and complex ventricular arrhythmias. *The American Journal of Cardiology*, **75**(**7**), 514–516.

Arraj, M. and Lemmer, B. (2006) Circadian rhythms in heart rate, motility, and body temperature of wild-type C57 and eNOS knock-out mice under light-dark, free-run, and

after time zone transition. *Chronobiology International*, **23**(**4**), 795–812.

Aschoff, J. (1965) Circadian Rhythms in Man. *Science*, **148**, 1427–1432.

Astiz, M., Heyde, I. and Oster, H. (2019) Mechanisms of communication in the Mammalian Circadian timing system. *International Journal of Molecular Sciences*, **20**(**2**), 343.

Atterhög, J. H. and Loogna, E. (1977) P-R interval in relation to heart rate during exercise and the influence of posture and autonomic tone. *Journal of Electrocardiology*, **10**(**4**), 331–336.

Azevedo, E. R. and Parker, J. D. (1999) Normal Ventricular Function Versus Congestive Heart Failure. *Circulation*, **100**, 274–279.

Balsalobre, A., Damiola, F. and Schibler, U. (1998) A serum shock induces circadian gene expression in mammalian tissue culture cells. *Cell*, **93**(**6**), 929–937.

Batchvarov, V. N., Ghuran, A., Smetana, P., Hnatkova, K., Harries, M., *et al.* (2002) QT-RR relationship in healthy subjects exhibits substantial intersubject variability and high intrasubject stability. *American Journal of Physiology - Heart and Circulatory Physiology*, **282**(**6**), 2356–2363.

Behrens, S., Ehlers, C., Brüggemann, T., Ziss, W., Dissmann, R., *et al.* (1997) Modification of the circadian pattern of ventricular tachyarrhythmias by beta-blocker therapy. *Clinical Cardiology*, **20**(**3**), 253–257.

Benditt, D. G., Pritchett, E. L. C., Smith, W. M., Wallace, A. G. and Gallagher, J. J. (1978) Characteristics of atrioventricular conduction and the spectrum of arrhythmias in Lown-Ganong-Levine syndrome. *Circulation*, **57**(**3**), 454–465.

Benson, D. W. and Cohen, M. I. (2017) Wolff-Parkinson-White syndrome: Lessons learnt and lessons remaining. *Cardiology in the Young*, **27**(**S1**), S62–S67.

Bers, D. M. (2002) Cardiac excitation–contraction coupling. *Nature 2002 415:6868*, **415**(**6868**), 198–205.

Berson, D. M., Dunn, F. A. and Takao, M. (2002) Phototransduction by retianl ganglion cells that set the circadian clock. *Science*, **295**(**2**), 953–9.

Biello, S. M., Janik, D. and Mrosovsky, N. (1994) Neuropeptide y and behaviorally induced phase shifts. *Neuroscience*, **62**(**1**), 273–279.

Billman, G. E., Hoskins, R. S., Randall, D. C., Randall, W. C., Hamlin, R. L. and Lin, Y. C. (1989) Selective vagal postganglionic innervation of the sinoatrial and atrioventricular nodes in the non-human primate. *Journal of the Autonomic Nervous System*, **26**(**1**), 27–36.

Billman, G. E. (2011) Heart rate variability - A historical perspective. *Frontiers in Physiology*, **2**(**11**), 1–13.

Black, N., D'Souza, A., Wang, Y., Piggins, H., Dobrzynski, H., *et al.* (2019) Circadian rhythm of cardiac electrophysiology, arrhythmogenesis, and the underlying mechanisms. *Heart Rhythm*, **16**(**2**), 298–307.

Bland, M. J. and Altman, D. G. (1986) Statistical methods for assessing agreement between two methods of clinical measurement. *The Lancet*, **327**(**8476**), 307–310.

Blinder, K. J., Gatti, P. J., Johnson, T. A., Lauenstein, J. M., Coleman, W. P., *et al.* (1998) Ultrastructural circuitry of cardiorespiratory reflexes: There is a monosynaptic path between the nucleus of the solitary tract and vagal preganglionic motoneurons controlling atrioventricular conduction in the cat. *Brain Research*, **785**(**1**), 143–157.

Bonnemeier, H., Wiegand, U., Brandes, A., Kluge, N., Katus, H. A., *et al.* (2003) Circadian profile of cardiac autonomic nervous modulation in healthy subjects: Differing effects of aging and gender on heart rate variability. *Journal of Cardiovascular Electrophysiology*, **14**(**8**), 791–799.

Bonnemeier, H., Wiegand, U., Braasch, W., Brandes, A., Richardt, G. and Potratz, J. (2003) Circadian profile of QT interval and QT interval variability in 172 healthy volunteers. *Pacing and clinical electrophysiology: PACE*, **26**(**1**), 377–382.

Boudreau, P., Yeh, W. H., Dumont, G. A. and Boivin, D. B. (2012) A circadian rhythm in heart rate variability contributes to the increased cardiac sympathovagal response to awakening in the morning. *Chronobiology International*, **29**(**6**), 757–768.

Boudreau, P., Yeh, W.-H., Dumont, G. A. and Boivin, D. B. (2013) Circadian variation of

heart rate variability across sleep stages. *Sleep*, **36**(**12**), 1919–1928.

Boukens, B. J., Hoogendijk, M. G., Verkerk, A. O., Linnenbank, A., Van Dam, P., *et al.* (2013) Early repolarization in mice causes overestimation of ventricular activation time by the QRS duration. *Cardiovascular Research*, **97**(**1**), 182–191.

Boukens, B. J., Rivaud, M. R., Rentschler, S. and Coronel, R. (2014) Misinterpretation of the mouse ECG: 'Musing the waves of Mus musculus'. *Journal of Physiology*, **592**(**21**), 4613–4626.

Boyden, P. A., Hirose, M. and Dun, W. (2010) Cardiac Purkinje cells. *Heart Rhythm*, **7**(**1**), 127–135.

Boyett, M. R., Honjo, H. and Kodama, I. (2000) The sinoatrial node, a heterogeneous pacemaker structure. *Cardiovascular Research*, **47**(**4**), 658–687.

Bray, M. S., Shaw, C. A., Moore, M. W. S., Garcia, R. A. P., Zanquetta, M. M., *et al.* (2008) Disruption of the circadian clock within the cardiomyocyte influences myocardial contractile function, metabolism, and gene expression. *AJP: Heart and Circulatory Physiology*, **294**(**2**), 1036–1047.

Brittsan, A. G. and Kranias, E. G. (2000) Phospholamban and cardiac contractile function. *Journal of Molecular and Cellular Cardiology*, **32**(**12**), 2131–2139.

Brown, T. M., Colwell, C. S., Waschek, J. A. and Piggins, H. D. (2007) Disrupted neuronal activity rhythms in the suprachiasmatic nuclei of vasoactive intestinal polypeptide-deficient mice. *Journal of Neurophysiology*, **97**(**3**), 2553–2558.

Bruce, V. G. and Pittendrigh, C. S. (1957) Endogenous Rhythms in Insects and Microorganisms. *The American Naturalist*, **91**(**858**), 179–195.

Brüggemann, T., Eisenreich, S., Behrens, S., Ehlers, C., Müller, D. and Andresen, D. (1997) Continuous QT interval measurements from 24-hour electrocardiography and risk after Myocardial Infarction. *Annals of Noninvasive Electrocardiology*, **2**(**3**), 264–273.

Buijs, F. N., Cazarez, F., Basualdo, M. C., Scheer, F. A. J. L., Perusquía, M., *et al.* (2014) The suprachiasmatic nucleus is part of a neural feedback circuit adapting blood pressure response. *Neuroscience*, **266**, 197–207.

Buijs, R. M., La Fleur, S. E., Wortel, J., Van Heyningen, C., Zuiddam, L., *et al.* (2003) The suprachiasmatic nucleus balances sympathetic and parasympathetic output to peripheral organs through separate preautonomic neurons. *Journal of Comparative Neurology*, **464**(**1**), 36–48.

Buijs, R. M., Escobar, C. and Swaab, D. F. (2013) *The circadian system and the balance of the autonomic nervous system*. 1st edn. *Handbook of Clinical Neurology*. 1st edn.

Bunger, M. K., Wilsbacher, L. D., Moran, S. M., Clendenin, C., Radcliffe, L. A., *et al.* (2000) Mop3 is an essential component of the master circadian pacemaker in mammals. *Cell*, **103**(**7**), 1009–17.

Bunger, M. K., Walisser, J. A., Sullivan, R., Manley, P. A., Moran, S. M., *et al.* (2005) Progressive arthropathy in mice with a targeted disruption of the Mop3/Bmal-1 locus. *Genesis*, **41**(**3**), 122–132.

Bünning, E. (1958) Das Weiterlaufen der phystologischen Uhr im Siiugerdarm ohne zentrale Steuerung. *Die Naturwissenschaften*, 68.

Castanon-Cervantes, O., Wu, M., Ehlen, J. C., Paul, K., Gamble, K. L., *et al.* (2010) Dysregulation of Inflammatory Responses by Chronic Circadian Disruption. *The Journal of Immunology*, **185**(**10**), 5796–5805.

Castro, B., Kogan, D. and Geva, A. B. (2000) ECG feature extraction using optimal mother wavelet. *21st IEEE Convention of the Electrical and Electronic Engineers in Israel, Proceedings*, 346–350.

Cerrone, M., Colombi, B., Santoro, M., di Barletta, M. R., Scelsi, M., *et al.* (2005) Bidirectional ventricular tachycardia and fibrillation elicited in a knock-in mouse model carrier of a mutation in the cardiac ryanodine receptor. *Circulation research*, **96**(**10**), 77–82.

Chaix, A., Zarrinpar, A. and Panda, S. (2016) The circadian coordination of cell biology. *Journal of Cell Biology*, **215**(**1**), 15–25.

Challet, E. (2019) The circadian regulation of food intake. *Nature Reviews Endocrinology*, 393–405.

Chandler, N. J., Greener, I. D., Tellez, J. O., Inada, S., Musa, H., *et al.* (2009) Molecular architecture of the human sinus node insights into the function of the cardiac pacemaker. *Circulation*, **119**(**12**), 1562–1575.

Cheng, S., Keyes, M. J., Larson, M. G., Elizabeth, L., Newton-cheh, C., *et al.* (2009) Long-term Outcomes in Individuals with a Prolonged PR interval or Firtst-Degree Atrioventricular Block. *Jama*, **301**(**24**), 2571–2577.

Chrobok, L., Northeast, R. C., Myung, J., Cunningham, P. S., Petit, C. and Piggins, H. D. (2020) Timekeeping in the hindbrain: a multi-oscillatory circadian centre in the mouse dorsal vagal complex. *Communications Biology*, **3**(**1**), 1–12.

Clapham, J. C. (2012) Central control of thermogenesis. *Neuropharmacology*, 111–123.

Clasen, L., Eickholt, C., Angendohr, S., Jungen, C., Shin, D. I., *et al.* (2018) A modified approach for programmed electrical stimulation in mice: Inducibility of ventricular arrhythmias. *PLoS ONE*, **13**(**8**), 1–17.

Clauss, S., Bleyer, C., Schüttler, D., Tomsits, P., Renner, S., *et al.* (2019) Animal models of arrhythmia: classic electrophysiology to genetically modified large animals. *Nature Reviews Cardiology*, 457–475.

Clay, J. R. and Shlesinger, M. F. (1984) Analysis of the effects of cesium ions on potassium channel currents in biological membranes. *Journal of Theoretical Biology*, **107**(**2**), 189–201.

Collins, B., Pierre-Ferrer, S., Muheim, C., Lukacsovich, D., Cai, Y., *et al.* (2020) Circadian VIPergic Neurons of the Suprachiasmatic Nuclei Sculpt the Sleep-Wake Cycle. *Neuron*, **108**(**3**), 486-499.e5.

Colwell, C. S., Michel, S., Itri, J., Rodriguez, W., Tam, J., *et al.* (2003) Disrupted circadian rhythms in VIP- and PHI-deficient mice. *American Journal of Physiology - Regulatory Integrative and Comparative Physiology*, **285**(**5 54-5**).

Cretoiu, D., Pavelescu, L., Duica, F., Radu, M., Suciu, N. and Cretoiu, S. M. (2018) Myofibers. in *Advances in Experimental Medicine and Biology*, 23–46.

Crnko, S., Du Pré, B. C., Sluijter, J. P. G. and Van Laake, L. W. (2019) Circadian rhythms and

the molecular clock in cardiovascular biology and disease. *Nature Reviews Cardiology*, **16**(**7**), 437–447.

Crosby, P., Hamnett, R., Putker, M., Hoyle, N. P., Reed, M., *et al.* (2019) Insulin/IGF-1 Drives PERIOD Synthesis to Entrain Circadian Rhythms with Feeding Time. *Cell*, **177**(**4**), 896-909.e20.

Cui, L. N., Coderre, E. and Renaud, L. P. (2001) Glutamate and GABA mediate suprachiasmatic nucleus inputs to spinal-projecting paraventricular neurons. *American Journal of Physiology - Regulatory Integrative and Comparative Physiology*, **281**(**4 50**-**4**), 1283–1289.

Cunningham, P. S., Meijer, P., Nazgiewicz, A., Anderson, S. G., Borthwick, L. A., *et al.* (2020) The circadian clock protein REVERBα inhibits pulmonary fibrosis development. *Proceedings of the National Academy of Sciences of the United States of America*, **117**(**2**), 1139–1147.

Cutler, D. J., Haraura, M., Reed, H. E., Shen, S., Sheward, W. J., *et al.* (2003) The mouse VPAC2 receptor confers suprachiasmatic nuclei cellular rhythmicity and responsiveness to vasoactive intestinal polypeptide in vitro. *European Journal of Neuroscience*, **17**(**2**), 197–204.

D'Aloia, M., Longo, A. and Rizzi, M. (2019) Noisy ECG signal analysis for automatic peak detection. *Information (Switzerland)*, **10**(**2**), 1–12.

D'Souza, A., Bucchi, A., Johnsen, A. B., Logantha, S. J. R. J., Monfredi, O., *et al.* (2014) Exercise training reduces resting heart rate via downregulation of the funny channel HCN4. *Nature Communications*, **5**.

D'Souza, A., Wang, Y., Anderson, C., Bucchi, A., Baruscotti, M., *et al.* (2021) A circadian clock in the sinus node mediates day-night rhythms in Hcn4 and heart rate. *Heart Rhythm*, **18**(**5**), 801–810.

Damiola, F., Le Minli, N., Preitner, N., Kornmann, B., Fleury-Olela, F. and Schibler, U. (2000) Restricted feeding uncouples circadian oscillators in peripheral tissues from the central pacemaker in the suprachiasmatic nucleus. *Genes and Development*, **14**(**23**), 2950–2961.

DeBruyne, J. P., Noton, E., Lambert, C. M., Maywood, E. S., Weaver, D. R. and Reppert, S. M. (2006) A Clock Shock: Mouse CLOCK Is Not Required for Circadian Oscillator Function. *Neuron*, **50**(**3**), 465–477.

DeBruyne, J. P., Weaver, D. R. and Reppert, S. M. (2007) CLOCK and NPAS2 have overlapping roles in the suprachiasmatic circadian clock. *Nature Neuroscience*, **10**(**5**), 543–545.

Degaute, J. P., Van De Borne, P., Linkowski, P. and Van Cauter, E. (1991) Quantitative analysis of the 24-hour blood pressure and heart rate patterns in young men. *Hypertension*, **18**(**2**), 199–210.

Delacretaz, E., Ganz, L., Soejima, K., Friedman, P., Walsh, E., *et al.* (2001) Multiple atrial macro-re-entry circuits in adults with repaired congenital heart disease: Entrainment mapping combined with three-dimensional electroanatomic mapping. *Journal of the American College of Cardiology*, **37**(**6**), 1665–1676.

Diekman, C. O. and Wei, N. (2021) Circadian Rhythms of Early Afterdepolarizations and Ventricular Arrhythmias in a Cardiomyocyte Model. *Biophysical Journal*, **120**(**2**), 319–333.

Difrancesco, D. (2010) The role of the funny current in pacemaker activity. *Circulation Research*, **106**(**3**), 434–446.

van Dijk, J. G., Koenderink, M., Zwinderman, A. H., Haan, J., Kramer, C. G. S. and den Heijer, J. C. (1991) Autonomic nervous system tests depend on resting heart rate and blood pressure. *Journal of the Autonomic Nervous System*, **35**(**1**), 15–24.

Dilaveris, P. E., Färbom, P., Batchvarov, V., Ghuran, A. and Malik, M. (2001) Circadian behavior of P-wave duration, P-wave area, and PR interval in healthy subjects. *Annals of Noninvasive Electrocardiology*, **6**(**2**), 92–97.

Dobrev, D. and Wehrens, X. H. T. (2018) Mouse models of cardiac arrhythmias. *Circulation Research*, **123**(**3**), 332–334.

Dobrzynski, H., Anderson, R. H., Atkinson, A., Borbas, Z., D'Souza, A., *et al.* (2013) Structure, function and clinical relevance of the cardiac conduction system, including the atrioventricular ring and outflow tract tissues. *Pharmacology and Therapeutics*, **139**(**2**),

260–288.

Doruk, Y. U., Yarparvar, D., Akyel, Y. K., Gul, S., Taskin, A. C., *et al.* (2020) A CLOCK-binding small molecule disrupts the interaction between CLOCK and BMAL1 and enhances circadian rhythm amplitude. *Journal of Biological Chemistry*, **295**(**11**), 3518–3531.

Durgan, D. J., Trexler, N. A., Egbejimi, O., McElfresh, T. A., Hee, Y. S., *et al.* (2006) The circadian clock within the cardiomyocyte is essential for responsiveness of the heart to fatty acids. *Journal of Biological Chemistry*, **281**(**34**), 24254–24269.

Durgan, D. J., Pat, B. M., Laczy, B., Bradley, J. A., Tsai, J. Y., *et al.* (2011) O-glcnacylation, novel post-translational modification linking myocardial metabolism and cardiomyocyte circadian clock. *Journal of Biological Chemistry*, **286**(**52**), 44606–44619.

Durgan, D J, Tsai, J., Grenett, M. H., Pat, B. M., William, F., *et al.* (2011) Evidence Suggesting that the Cardiomyocyte Circadian Clock Modulates Responsiveness of the Heart to Hypertrophic Stimuli in Mice, **28**(**3**), 187–203.

Eckberg, D. L. (1997) Sympathovagal balance: A critical appraisal. *Circulation*.

Eide, E. J., Woolf, M. F., Kang, H., Woolf, P., Hurst, W., *et al.* (2005) Control of Mammalian Circadian Rhythm by CKIε-Regulated Proteasome-Mediated PER2 Degradation. *Molecular and Cellular Biology*, **25**(**7**), 2795–2807.

Eisner, D. A., Caldwell, J. L., Kistamás, K. and Trafford, A. W. (2017) Calcium and Excitation-Contraction Coupling in the Heart. *Circulation Research*, **121**(**2**), 181–195.

Englund, A., Behrens, S., Wegscheider, K. and Rowland, E. (1999) Circadian variation of malignant ventricular arrhythmias in patients with ischemic and nonischemic heart disease after cardioverter defibrillator implantation. *Journal of the American College of Cardiology*, **34**(**5**), 1560–1568.

Evans, J. A., Suen, T. C., Callif, B. L., Mitchell, A. S., Castanon-Cervantes, O., *et al.* (2015) Shell neurons of the master circadian clock coordinate the phase of tissue clocks throughout the brain and body. *BMC Biology*, **13**(**1**).

Evans, J. A. and Davidson, A. J. (2013) Health consequences of circadian disruption in humans and animal models. *Progress in Molecular Biology and Translational Science*, **119**,

283–323.

Faggioni, M., Kryshtal, D. O. and Knollmann, B. C. (2012) Calsequestrin mutations and catecholaminergic polymorphic ventricular tachycardia. *Pediatric Cardiology*, **33**(**6**), 959–967.

Fahrenbach, J. P., Mejia-Alvarez, R. and Banach, K. (2007) The relevance of non-excitable cells for cardiac pacemaker function. *Journal of Physiology*, **585**(**2**), 565–578.

Fairley, J. L., Zhang, L., Glassford, N. J. and Bellomo, R. (2017) Magnesium status and magnesium therapy in cardiac surgery: A systematic review and meta-analysis focusing on arrhythmia prevention. *Journal of Critical Care*, **42**, 69–77.

Feeney, K. A., Hansen, L. L., Putker, M., Olivares-Yañez, C., Day, J., *et al.* (2016) Daily magnesium fluxes regulate cellular timekeeping and energy balance. *Nature*, **532**(**7599**), 375–379.

Fenske, S., Pröbstle, R., Auer, F., Hassan, S., Marks, V., *et al.* (2015) Comprehensive multilevel in vivo and in vitro analysis of heart rate fluctuations in mice by ECG telemetry and electrophysiology. *Nature Protocols*, **11**(**1**), 61–86.

Fujita, B., Franz, M., Goebel, B., Fritzenwanger, M., Figulla, H. R., *et al.* (2012) Prognostic relevance of heart rate at rest for survival and the quality of life in patients with dilated cardiomyopathy. *Clinical Research in Cardiology*, **101**(**9**), 701–707.

Furukawa, Y., Narita, M., Takei, M., Kobayashi, O., Haniuda, M. and Chiba, S. (1991) Differential Intracardiac Sympathetic and Parasympathetic Innervation to the SA and AV Nodes in Anesthetized Dog Hearts. *The Japanese Journal of Pharmacology*, **55**(**3**), 381–390.

Gardner, M. J., Hubbard, K. E., Hotta, C. T., Dodd, A. N. and Webb, A. A. R. (2006) How plants tell the time. *Biochemical Journal*, **397**(**1**), 15–24.

Gassanov, N., Er, F., Zagidullin, N., Jankowski, M., Gutkowska, J. and Hoppe, U. C. (2008) Retinoid acid-induced effects on atrial and pacemaker cell differentiation and expression of cardiac ion channels. *Differentiation*, **76**(**9**), 971–980.

Gatti, P. J., Johnson, T. A., Phan, P., Jordan, I. K., Coleman, W. and Massari, V. J. (1995)

The physiological and anatomical demonstration of functionally selective parasympathetic ganglia located in discrete fat pads on the feline myocardium. *Journal of the Autonomic Nervous System*, **51**(**3**), 255–259.

Gatti, P. J., Johnson, T. A. and Massari, V. J. (1996) Can neurons in the nucleus ambiguus selectively regulate cardiac rate and atrio-ventricular conduction? *Journal of the Autonomic Nervous System*, **57**, 123–127.

Ge, S. X., Son, E. W. and Yao, R. (2018) iDEP: An integrated web application for differential expression and pathway analysis of RNA-Seq data. *BMC Bioinformatics*, **19**(**1**), 1–24.

Geerling, J. C., Shin, J. W., Chimenti, P. C. and Loewy, A. D. (2010) Paraventricular hypothalamic nucleus: Axonal projections to the brainstem. *Journal of Comparative Neurology*, **518**(**9**), 1460–1499.

Gehrmann, J., Hammer, P. E., Maguire, C. T., Wakimoto, H., Triedman, J. K. and Berul, C. I. (2000) Phenotypic screening for heart rate variability in the mouse. *American Journal of Physiology - Heart and Circulatory Physiology*, **279**(**2 48**-**2**).

George, S. A., Faye, N. R., Murillo-Berlioz, A., Lee, K. B., Trachiotis, G. D. and Efimov, I. R. (2017) At the atrioventricular crossroads: Dual pathway electrophysiology in the atrioventricular node and its underlying heterogeneities. *Arrhythmia and Electrophysiology Review*, **6**(**4**), 179–185.

Golombek, D. A. and Rosenstein, R. E. (2010) Physiology of circadian entrainment. *Physiological Reviews*, **90**(**3**), 1063–1102.

Gooley, J. J., Lu, J., Fischer, D. and Saper, C. B. (2003) A broad role for melanopsin in nonvisual photoreception. *Journal of Neuroscience*, **23**(**18**), 7093–7106.

Gottlieb, L. A., Lubberding, A., Larsen, A. P. and Thomsen, M. B. (2016) Circadian rhythm in QT interval is preserved in mice deficient of potassium channel interacting protein 2. *https://doi.org/10.1080/07420528.2016.1225074*, **34**(**1**), 45–56.

Gottlieb, L. A., Larsen, K., Halade, G. V, Young, M. E. and Thomsen, M. B. (2021) Prolonged QT intervals in mice with cardiomyocyte-specific deficiency of the molecular clock. *Acta Physiologica*, **233**(**1**).

Grant, A. O. (2009) Cardiac ion channels. *Circulation: Arrhythmia and Electrophysiology*, **2**(**2**), 185–194.

Grimaldi, D., Carter, J. R., Van Cauter, E. and Leproult, R. (2016) Adverse Impact of Sleep Restriction and Circadian Misalignment on Autonomic Function in Healthy Young Adults. *Hypertension*, **68**(**1**), 243–250.

Grunnet, M. (2010) Repolarization of the cardiac action potential. Does an increase in repolarization capacity constitute a new anti-arrhythmic principle? *Acta Physiologica*, **198**(**676**), 1–48.

Guerrera, M. P., Volpe, S. L. and Mao, J. J. (2009) Therapeutic Uses of Magnesium. *American Family Physician*, **80**(**2**), 157–162.

Guo, Y. F. and Stein, P. K. (2003) Circadian rhythm in the cardiovascular system: chronocardiology. *American Heart Journal*, **145**(**5**), 779–786.

Haechl, N., Ebner, J., Hilber, K., Todt, H. and Koenig, X. (2019) Pharmacological profile of the bradycardic agent ivabradine on human cardiac ion channels. *Cellular Physiology and Biochemistry*, **53**(**1**), 36–48.

Hannibal, J. (2002) Neurotransmitters of the retino-hypothalamic tract. *Cell and Tissue Research*, **309**(**1**), 73–88.

Harmar, A. J., Marston, H. M., Shen, S., Spratt, C., West, K. M., *et al.* (2002) The VPAC2 receptor is essential for circadian function in the mouse suprachiasmatic nuclei. *Cell*, **109**(**4**), 497–508.

Hastings, M. H., Duffield, G. E., Ebling, F. J. P., Kidd, A., Maywood, E. S. and Schurov, I. (1997) Non-photic signalling in the suprachiasmatic nucleus. *Biology of the Cell*, **89**(**8**), 495–503.

Hastings, M. H., Maywood, E. S. and Reddy, A. B. (2008) Two decades of circadian time. *Journal of Neuroendocrinology*, **20**(**6**), 812–819.

Hatori, M., Le, H., Vollmers, C., Keding, S. R., Tanaka, N., *et al.* (2008) Inducible ablation of melanopsin-expressing retinal ganglion cells reveals their central role in non-image forming visual responses. *PLoS ONE*, **3**(**6**), e2451.

Hattar, S., Liao, H. W., Takao, M., Berson, D. M. and Yau, K. W. (2002) Melanopsin-containing retinal ganglion cells: Architecture, projections, and intrinsic photosensitivity. *Science*, **295**(**5557**), 1065–1070.

Hattar, S., Kumar, M., Park, A., Tong, P., Tung, J., *et al.* (2006) Central projections of melanopsin-expressing retinal ganglion cells in the mouse. *Journal of Comparative Neurology*, **497**(**3**), 326–349.

Hayano, J., Sakata, S., Okada, A., Mukai, S. and Fujinami, T. (1998) Circadian rhythms of atrioventricular conduction properties in chronic atrial fibrillation with and without heart failure. *Journal of the American College of Cardiology*, **31**(**1**), 158–166.

Hayano, J., Ishihara, S., Fukuta, H., Sakata, S., Mukai, S., *et al.* (2002) Circadian rhythm of atrioventricular conduction predicts long-term survival in patients with chronic atrial fibrillation. *Chronobiology International*, **19**(**3**), 633–648.

Hayter, E. A., Wehrens, S. M. T., Van Dongen, H. P. A., Stangherlin, A., Gaddameedhi, S., *et al.* (2021) Distinct circadian mechanisms govern cardiac rhythms and susceptibility to arrhythmia. *Nature Communications*, **12**(**1**), 1–13.

Hayter, E. A., Brown, T. M. and Bechtold, D. A. (2021) EdHayter/Hayter-et-al.-ECG-analysis: Hayter et al. ECG analysis. *GitHub*.

He, L., Hamm, J. A., Reddy, A., Sams, D., Peliciari-Garcia, R. A., *et al.* (2016) Biotinylation: A novel posttranslational modification linking cell autonomous circadian clocks with metabolism. *American Journal of Physiology - Heart and Circulatory Physiology*, **310**(**11**), 1520–1532.

Hedman, A. E., Hartikainan, J. E. K., Tahvanainan, K. U. O., Hakumaki, M. O. K., Hartikainen, J. E. K., *et al.* (1995) The high frequency component of heart rate variability reflects cardiac parasympathetic modulation rather than parasympathetic 'tone'. *Acta Physiologica Scandinavica*, **155**(**3**), 267–273.

Herzog, E. D., Takahashi, J. S. and Block, G. D. (1998) Clock controls circadian period in isolated suprachiasmatic nucleus neurons. *Nature Neuroscience*, **1**(**8**), 708–713.

Van Der Horst, G. T. J., Muijtjens, M., Kobayashi, K., Takano, R., Kanno, S. I., *et al.* (1999)

Mammalian Cry1 and Cry2 are essential for maintenance of circadian rhythms. *Nature*, **398**(**6728**), 627–630.

Hsiao, P.-Y., Tien, H.-C., Lo, C.-P., Juang, J.-M. J., Wang, Y.-H. and Sung, R. J. (2013) Gene mutations in cardiac arrhythmias: a review of recent evidence in ion channelopathies. *The Application of Clinical Genetics*, **6**, 1–13.

Hu, K., Scheer, F. A. J. L., Buijs, R. M. and Shea, S. A. (2008) The circadian pacemaker generates similar circadian rhythms in the fractal structure of heart rate in humans and rats. *Cardiovascular Research*, **80**(**1**), 62–68.

Ingle, K. A., Kain, V., Goel, M., Prabhu, S. D., Young, M. E. and Halade, G. V. (2015) Cardiomyocyte-specific Bmal1 deletion in mice triggers diastolic dysfunction, extracellular matrix response, and impaired resolution of inflammation. *American Journal of Physiology - Heart and Circulatory Physiology*, **309**(**11**), H1827–H1836.

Inokawa, H., Umemura, Y., Shimba, A., Kawakami, E., Koike, N., *et al.* (2020) Chronic circadian misalignment accelerates immune senescence and abbreviates lifespan in mice. *Scientific Reports*, **10**(**1**), 1–13.

Iseri, L. T. and French, J. H. (1984) Magnesium: Nature's physiologic calcium blocker. *American Heart Journal*, **108**(**1**), 188–193.

Ishida, A., Mutoh, T., Ueyama, T., Bando, H., Masubuchi, S., *et al.* (2005) Light activates the adrenal gland: Timing of gene expression and glucocorticoid release. *Cell Metabolism*, **2**(**5**), 297–307.

Ishida, S., Nakagawa, M., Fujino, T., Yonemochi, H., Saikawa, T. and Ito, M. (1997) Circadian variation of QT interval dispersion: Correlation with heart rate variability. *Journal of Electrocardiology*, **30**(**3**), 205–210.

James, T. N. (1963) The connecting pathways between the sinus node and A-V node and between the right and the left atrium in the human heart. *American Heart Journal*, **66**(**4**), 498–508.

James, T. N. and Sherf, L. (1971) Fine structure of the His bundle. *Circulation*, **44**(**1**), 9–28.

Janik, D. and Mrosovsky, N. (1994) Intergeniculate leaflet lesions and behaviorally-

induced shifts of circadian rhythms. *Brain Research*, **651**(**1**–**2**), 174–182.

Janssen, B. J. A. and Smits, J. F. M. (2002) Autonomic control of blood pressure in mice: Basic physiology and effects of genetic modification. *American Journal of Physiology - Regulatory Integrative and Comparative Physiology*, **282**(**6**), 1545–64.

Janssen, P. M. L., Biesiadecki, B. J., Ziolo, M. T. and Davis, J. P. (2016) The need for speed: Mice, men, and myocardial kinetic reserve. *Circulation Research*, **119**(**3**), 418–421.

Jeyaraj, D., Haldar, S. M., Wan, X., McCauley, M. D., Ripperger, J. A., *et al.* (2012) Circadian rhythms govern cardiac repolarization and arrhythmogenesis. *Nature*, **483**(**7387**), 96–99.

Johnson, R. F., Smale, L., Moore, R. Y. and Morin, L. P. (1988) Lateral geniculate lesions block circadian phase-shift responses to a benzodiazepine. *Proceedings of the National Academy of Sciences of the United States of America*, **85**(**14**), 5301–5304.

Joung, B., Ogawa, M., Lin, S.-F. and Chen, P.-S. (2009) The Calcium and Voltage Clocks in Sinoatrial Node Automaticity. *Korean Circulation Journal*, **39**(**6**).

Joyner, R. W. and van Capelle, F. J. (1986) Propagation through electrically coupled cells. How a small SA node drives a large atrium. *Biophysical Journal*, **50**(**6**), 1157–1164.

Kalsbeek, A., La Fleur, S., Van Heijningen, C. and Buijs, R. M. (2004) Suprachiasmatic GABAergic inputs to the paraventricular nucleus control plasma glucose concentrations in the rat via sympathetic innervation of the liver. *Journal of Neuroscience*, **24**(**35**), 7604–7613.

Kalsbeek, A., Palm, I. F., La Fleur, S. E., Scheer, F. A. J. L., Perreau-Lenz, S., *et al.* (2006) SCN Outputs and the Hypothalamic Balance of Life. *Journal of Biological Rhythms*, **21**(**6**), 458–469.

Kalsbeek, A. and Buijs, R. M. (2002) Output pathways of the mammalian suprachiasmatic nucleus: Coding circadian time by transmitter selection and specific targeting. *Cell and Tissue Research*, **309**(**1**), 109–118.

Kanter, H. L., Laing, J. G., Beau, S. L., Beyer, E. C., Saffitz, J. E., *et al.* (1993) Distinct patterns of connexin expression in canine Purkinje fibers and ventricular muscle. *Circulation Research*, **72**(**5**), 1124–1131.

Kecklund, G. and Axelsson, J. (2016) Health consequences of shift work and insufficient sleep. *BMJ*, **355**, 1–13.

Khan, A. A., Lip, G. Y. H. and Shantsila, A. (2019) Heart rate variability in atrial fibrillation: The balance between sympathetic and parasympathetic nervous system. *European Journal of Clinical Investigation*, **49**(**11**), 1–8.

Kher, R. (2019) Signal Processing Techniques for Removing Noise from ECG Signals. *Journal of Biomedical Engineering and Research*, **3**, 1–9.

King, D. P. and Takahashi, J. S. (2000) Molecular Genetics of Circadian Rhythms in Mammals. *Neurobiology*, **23**, 713–742.

Kistamás, K., Veress, R., Horváth, B., Bányász, T., Nánási, P. P. and Eisner, D. A. (2020) Calcium Handling Defects and Cardiac Arrhythmia Syndromes. *Frontiers in Pharmacology*, **11**, 1–25.

Kleber, A. G. and Saffitz, J. E. (2014) Role of the intercalated disc in cardiac propagation and arrhythmogenesis. *Frontiers in Physiology*, **5**(**10**), 1–9.

Kleiger, R. E., Miller, J. P., Bigger, J. T. and Moss, A. J. (1987) Decreased Heart Rate Variability and Its Association with Increased Mortality After Acute Myocardial Infarction. *Am J Cardiol*, **59**(**4**), 258–282.

Ko, C. H. and Takahashi, J. S. (2006) Molecular components of the mammalian circadian clock. *Human Molecular Genetics*, **15**(**2**), 271–277.

Ko, M. L., Shi, L., Tsai, J. Y., Young, M. E., Neuendorff, N., *et al.* (2011) Cardiac-specific mutation of clock alters the quantitative measurements of physical activities without changing behavioral circadian rhythms. *Journal of Biological Rhythms*, **26**(**5**), 412–422.

Kollias, G. E., Stamatelopoulos, K. S., Papaioannou, T. G., Zakopoulos, N. A., Alevizaki, M., *et al.* (2009) Diurnal variation of endothelial function and arterial stiffness in hypertension. *Journal of Human Hypertension*, **23**(**9**), 597–604.

Kondratov, R. V., Kondratova, A. A., Gorbacheva, V. Y., Vykhovanets, O. V. and Antoch, M. P. (2006) Early aging and age-related pathologies in mice deficient in BMAL1, the core component of the circadian clock. *Genes and Development*, **20**(**14**), 1868–1873.

Kong, H., Jones, P. P., Koop, A., Zhang, L., Duff, H. J. and Chen, S. R. W. (2008) Caffeine induces Ca2+ release by reducing the threshold for luminal Ca2+ activation of the ryanodine receptor. *Biochemical Journal*, **414**(**3**), 441–452.

Kornmann, B., Schaad, O., Bujard, H., Takahashi, J. S. and Schibler, U. (2007) System-driven and oscillator-dependent circadian transcription in mice with a conditionally active liver clock. *PLoS Biology*, **5**(**2**), 179–189.

Kozák, M., Křivan, L. and Semrád, B. (2003) Circadian variations in the occurrence of ventricular tachyarrhythmias in patients with implantable cardioverter defibrillators. *PACE - Pacing and Clinical Electrophysiology*, **26**(**3**), 731–735.

Kramer, A., Yang, F. C., Snodgrass, P., Li, X., Scammell, T. E., *et al.* (2001) Regulation of daily locomotor activity and sleep by hypothalamic EGF receptor signating. *Science*, **294**(**5551**), 2511–2515.

Kriegsfeld, L. J., LeSauter, J. and Silver, R. (2004) Targeted Microlesions Reveal Novel Organization of the Hamster Suprachiasmatic Nucleus. *Journal of Neuroscience*, **24**(**10**), 2449–2457.

Krout, K. E., Kawano, J., Mettenleiter, T. C. and Loewy, A. D. (2002) CNS inputs to the suprachiasmatic nucleus of the rat. *Neuroscience*, **110**(**1**), 73–92.

Kubota, Y., Chen, L. Y., Whitsel, E. A. and Folsom, A. R. (2017) Heart rate variability and lifetime risk of cardiovascular disease: the Atherosclerosis Risk in Communities Study. *Annals of Epidemiology*, **27**(**10**), 619–625.

Kuleshov, M. V., Jones, M. R., Rouillard, A. D., Fernandez, N. F., Duan, Q., *et al.* (2016) Enrichr: a comprehensive gene set enrichment analysis web server 2016 update. *Nucleic acids research*, **44**(**1**), 90–97.

Kutmon, M., van Iersel, M. P., Bohler, A., Kelder, T., Nunes, N., *et al.* (2015) PathVisio 3: An Extendable Pathway Analysis Toolbox. *PLoS Computational Biology*, **11**(**2**), e1004085.

Kwok, C. S., Rashid, M., Beynon, R., Barker, D., Patwala, A., *et al.* (2016) Prolonged PR interval, first-degree heart block and adverse cardiovascular outcomes: A systematic review and meta-analysis. *Heart*, **102**(**9**), 672–680.

Lamia, K. A., Sachdeva, U. M., Di Tacchio, L., Williams, E. C., Alvarez, J. G., *et al.* (2009) AMPK regulates the circadian clock by cryptochrome phosphorylation and degradation. *Science*, **326**(**5951**), 437–440.

Lamia, K. A., Storch, K.-F. and Weitz, C. J. (2008) Physiological significance of a peripheral tissue circadian clock. *Proceedings of the National Academy of Sciences of the United States of America*, **105**(**39**), 15172–7.

Lampert, R., Rosenfeld, L., Batsford, W., Lee, F. and McPherson, C. (1994) Circadian variation of sustained ventricular tachycardia in patients with coronary artery disease and implantable cardioverter-defibrillators. *Circulation*, **90**(**1**), 241–247.

Landgraf, D., Wang, L. L., Diemer, T. and Welsh, D. K. (2016) NPAS2 Compensates for Loss of CLOCK in Peripheral Circadian Oscillators. *PLoS Genetics*, **12**(**2**), 1–16.

Landstrom, A. P., Dobrev, D. and Wehrens, X. H. T. (2017) Calcium Signaling and Cardiac Arrhythmias. *Circulation Research*, **120**(**12**), 1969–1993.

Langner, R. and Rensing, L. (1972) Circadian Rhythm of Oxygen Consumption in Rat Liver Suspension Culture: Changes of Pattern. *Zeitschrift fur Naturforschung - Section B Journal of Chemical Sciences*, **27**(**9**), 1117–1118.

Lazzerini, P. E., Capecchi, P. L., El-Sherif, N., Laghi-Pasini, F. and Boutjdir, M. (2018) Emerging arrhythmic risk of autoimmune and inflammatory cardiac channelopathies. *Journal of the American Heart Association*, **7**(**22**), 1–19.

Leak, R. K., Card, J. P. and Moore, R. Y. (1999) Suprachiasmatic pacemaker organization analyzed by viral transynaptic transport. *Brain Research*, **819**(**1**–**2**), 23–32.

Lee, J. S., Morrow, D., Andresen, M. C. and Chang, K. S. K. (2002) Isoflurane depresses baroreflex control of heart rate in decerebrate rats. *Anesthesiology*, **96**(**5**), 1214–1222.

Lee, J. U., Kim, K. S., Kim, J. H., Lim, H. K., Lee, B. H. and Lee, C. K. (1995) PR interval behavior during exercise stress test. *The Korean journal of internal medicine*, **10**(**2**), 137–142.

Lehman, M. N., Silver, R., Gladstone, W. R., Kahn, R. M., Gibson, M. and Bittman, E. L. (1987) Circadian rhythmicity restored by neural transplant. Immunocytochemical

characterization of the graft and its integration with the host brain. *Journal of Neuroscience*, **7**(**6**), 1626–1638.

Libert, S., Bonkowski, M. S., Pointer, K., Pletcher, S. D. and Guarente, L. (2012) Deviation of innate circadian period from 24h reduces longevity in mice. *Aging Cell*, **11**(**5**), 794–800.

Liu, G. X., Zhou, J. and Koren, G. (2008) Single-channel properties of IK,slow1 and IK,slow2 in mouse ventricular myocytes. *Pflugers Archiv European Journal of Physiology*, **456**(**3**), 541–547.

Liu, N., Rizzi, N., Boveri, L. and Priori, S. G. (2009) Ryanodine receptor and calsequestrin in arrhythmogenesis: What we have learnt from genetic diseases and transgenic mice. *Journal of Molecular and Cellular Cardiology*, **46**(**2**), 149–159.

Liu, Y., Syed, Z., Scirica, B. M., Morrow, D. A., Guttag, J. V. and Stultz, C. M. (2014) ECG morphological variability in beat space for risk stratification after acute coronary syndrome. *Journal of the American Heart Association*, **3**(**3**).

Livak, K. J. and Schmittgen, T. D. (2001) Analysis of Relative Gene Expression Data Using Real-Time Quantitative PCR and the 2−ΔΔCT Method. *Methods*, **25**(**4**), 402–408.

Lown, B., Ganong, W. F. and Levine, S. A. (1952) The syndrome of short P-R interval, normal QRS complex and paroxysmal rapid heart action. *Circulation*, **5**(**5**), 693–706.

Lu, Y., Ma, X., Sabharwal, R., Snitsarev, V., Morgan, D., *et al.* (2009) The Ion Channel ASIC2 Is Required for Baroreceptor and Autonomic Control of the Circulation. *Neuron*, **64**(**6**), 885–897.

Lucente, M., Rebuzzi, A. G., Lanza, G. A., Tamburi, S., Cortellessa, M. C., *et al.* (1988) Circadian variation of ventricular tachycardia in acute myocardial infarction. *The American Journal of Cardiology*, **62**(**10**), 670–674.

Macfarlane, P. W., Mason, J. W., Kligfield, P., Sommargren, C. E., Drew, B., *et al.* (2017) Debatable issues in automated ECG reporting. *Journal of Electrocardiology*, **50**(**6**), 833–840.

Malliani, A., Pagani, M., Lombardi, F. and Cerutti, S. (1991) Cardiovascular neural regulation explored in the frequency domain. *Circulation*, **84**(**2**), 482–492.

Manella, G., Sabath, E., Aviram, R., Dandavate, V., Ezagouri, S., *et al.* (2021) The liver-clock coordinates rhythmicity of peripheral tissues in response to feeding. *Nature Metabolism*, **3**(**6**), 829–842.

Marchant, E. G., Watson, N. V. and Mistlberger, R. E. (1997) Both neuropeptide Y and serotonin are necessary for entrainment of circadian rhythms in mice by daily treadmill running schedules. *Journal of Neuroscience*, **17**(**20**), 7974–7987.

Marcheva, B., Ramsey, K. M., Buhr, E. D., Kobayashi, Y., Su, H., *et al.* (2010) Disruption of the clock components CLOCK and BMAL1 leads to hypoinsulinaemia and diabetes. *Nature*, **466**(**7306**), 627–631.

Markowitz, S. M. and Lerman, B. B. (2018) A contemporary view of atrioventricular nodal physiology. *Journal of Interventional Cardiac Electrophysiology*, **52**(**3**), 271–279.

Martino, T., Arab, S., Straume, M., Belsham, D. D., Tata, N., *et al.* (2004) Day/night rhythms in gene expression of the normal murine heart. *Journal of Molecular Medicine*, **82**(**4**), 256–264.

Martino, T. A., Oudit, G. Y., Herzenberg, A. M., Tata, N., Koletar, M. M., *et al.* (2008) Circadian rhythm disorganization produces profound cardiovascular and renal disease in hamsters. *American Journal of Physiology - Regulatory Integrative and Comparative Physiology*, **294**(**5**).

Martino, T. A. and Young, M. E. (2015) Influence of the cardiomyocyte circadian clock on cardiac physiology and pathophysiology. *Journal of Biological Rhythms*, **30**(**3**), 183–205.

Matkó, I., Fehér, E. and Vizi, E. S. (1994) Receptor mediated presynaptic modulation of the release of noradrenaline in human papillary muscle. *Cardiovascular Research*, **28**(**5**), 700–704.

McGinnis, G. R., Tang, Y., Brewer, R. A., Brahma, M. K., Stanley, H. L., *et al.* (2017) Genetic disruption of the cardiomyocyte circadian clock differentially influences insulin-mediated processes in the heart. *Journal of Molecular and Cellular Cardiology*, **110**, 80–95.

Meloni, M., Setzu, D., Del Rio, A., Campagna, M. and Cocco, P. (2013) QTc interval and electrocardiographic changes by type of shift work. *American Journal of Industrial*

Medicine, **56**(**10**), 1174–1179.

Meng, Q. J., Maywood, E. S., Bechtold, D. A., Lu, W. Q., Li, J., *et al.* (2010) Entrainment of disrupted circadian behavior through inhibition of casein kinase 1 (CK1) enzymes. *Proceedings of the National Academy of Sciences of the United States of America*, **107**(**34**), 15240–15245.

Mesirca, P., Alig, J., Torrente, A. G., Müller, J. C., Marger, L., *et al.* (2014) Cardiac arrhythmia induced by genetic silencing of 'funny' (f) channels is rescued by GIRK4 inactivation. *Nature Communications*, **5**(**1**), 1–15.

Meyer-Bernstein, E. L., Jetton, A. E., Matsumoto, S. I., Markuns, J. F., Lehman, M. N. and Bittman, E. L. (1999) Effects of suprachiasmatic transplants on circadian rhythms of neuroendocrine function in golden hamsters. *Endocrinology*, **140**(**1**), 207–218.

Michailova, A. P., Belik, M. E. and McCulloch, A. D. (2004) Effects of magnesium on cardiac excitation-contraction coupling. *Journal of the American College of Nutrition*, **23**(**5**), 514S-517S.

Mitsui, S., Yamaguchi, S., Matsuo, T., Ishida, Y. and Okamura, H. (2001) Antagonistic role of E4BP4 and PAR proteins in the circadian oscillatory mechanism. *Genes and Development*, **15**(**8**), 995–1006.

Moga, M. M. and Moore, R. Y. (1997) Organization of neural inputs to the suprachiasmatic nucleus in the rat. *Journal of Comparative Neurology*, **389**(**3**), 508–534.

Mohamed, M. A. and Deriche, M. A. (2014) An Approach for ECG Feature Extraction using Daubechies 4 (DB4) Wavelet. *International Journal of Computer Applications*, **96**(**12**), 36–41.

Mohawk, J. A., Green, C. B. and Takahashi, J. S. (2012) Central and Peripheral Circadian Clocks in Mammals. *Annual Review of Neuroscience*, **35**(**1**), 445–462.

Molnar, J., Zhang, F., Weiss, J., Ehlert, F. A. and Rosenthal, J. E. (1996) Diurnal pattern of QTc interval: How long is prolonged? Possible relation to circadian triggers of cardiovascular events. *Journal of the American College of Cardiology*, **27**(**1**), 76–83.

Monfredi, O., Dobrzynski, H., Mondal, T., Boyett, M. R. and Morris, G. M. (2010) The

anatomy and physiology of the sinoatrial node-A contemporary review. *PACE - Pacing and Clinical Electrophysiology*, **33**(**11**), 1392–1406.

Moore, R. Y. (2007) Suprachiasmatic nucleus in sleep-wake regulation. *Sleep Medicine*, **8**, 27–33.

Moore, R. Y. and Card, J. P. (1994) Intergeniculate leaflet: An anatomically and functionally distinct subdivision of the lateral geniculate complex. *Journal of Comparative Neurology*, **344**(**3**), 403–430.

Moore, R. Y. and Eichler, V. B. (1972) Loss of a circadian adrenal corticosterone rhythm following suprachiasmatic lesions in the rat. *Brain Research Bulletin*, **42**(**900**), 54–56.

Moore, R. Y. and Speh, J. C. (1993) GABA is the principal neurotransmitter of the circadian system. *Neuroscience Letters*, **150**(**1**), 112–116.

Morganroth, J., Brozovich, F. V., McDonald, J. T. and Jacobs, R. A. (1991) Variability of the QT measurement in healthy men, with implications for selection of an abnormal QT value to predict drug toxicity and proarrhythmia. *The American Journal of Cardiology*, **67**(**8**), 774–776.

Morin, L. P. (2013) Neuroanatomy of the extended circadian rhythm system. *Experimental Neurology*, **243**, 4–20.

Muller, J. E., Stone, P. H., Turi, Z. G., Rutherford, J. D., Czeisler, C. A., *et al.* (1985) Circadian variation in the frequency of onset of acute myocardial infarction. *N Engl J Med.*, **313**, 1315–22.

Muller, J. E., Ludmer, P. L., Willich, S. N., Tofler, G. H., Aylmer, G., *et al.* (1987) Circadian variation in the frequency of sudden cardiac death. *Circulation*, **75**(**1**), 131–138.

Murata, K., Yano, E., Shinozaki, T., Vano, E. and Shinozaki, T. (1999) Impact of shift work on cardiovascular functions in a 10-year follow-up study. *Scandinavian Journal of Work, Environment and Health*, **25**(**3**), 272–277.

Mutoh, T., Shibata, S., Korf, H. W. and Okamura, H. (2003) Melatonin modulates the light-induced sympathoexcitation and vagal suppression with participation of the suprachiasmatic nucleus in mice. *Journal of Physiology*, 15 February, 317–332.

Myers, B., Scheimann, J. R., Franco-Villanueva, A. and Herman, J. P. (2017) Ascending mechanisms of stress integration: Implications for brainstem regulation of neuroendocrine and behavioral stress responses. *Neuroscience and Biobehavioral Reviews*, 366–375.

Nakagawa, M., Iwao, T., Ishida, S., Yonemochi, H., Fujino, T., *et al.* (1998) Circadian rhythm of the signal averaged electrocardiogram and its relation to heart rate variability in healthy subjects. *Heart*, **79**(**5**), 493–496.

Nerbonne, J. M. and Kass, R. S. (2005) Molecular physiology of cardiac repolarization. *Physiological Reviews*, **85**(**4**), 1205–1253.

Niijima, A., Nagai, K., Nagai, N. and Akagawa, H. (1993) Effects of light stimulation on the activity of the autonomic nerves in anesthetized rats. *Physiology and Behavior*, **54**(**3**), 555–561.

Northcote, R. J., Canning, G. P. and Ballantyne, D. (1989) Electrocardiographic findings in male veteran endurance athletes. *Heart*, **61**(**2**), 155–160.

Nosaka, M., Ishida, Y., Kimura, A., Yamamoto, H., Kuninaka, Y., *et al.* (2017) Influence of Circadian Rhythm on Thrombus Formation of Murine Deep Vein Thrombosis Model. *Annals of Hematology & Oncology*, **4**(**9**), 7–9.

Ono, N., Yamaguchi, T., Ishikawa, H., Arakawa, M., Takahashi, N., *et al.* (2009) Morphological varieties of the purkinje fiber network in mammalian hearts, as revealed by light and electron microscopy. *Archives of Histology and Cytology*, **72**(**3**), 139–149.

van Ooijen, G. and O'Neill, J. S. (2016) Intracellular magnesium and the rhythms of life. *Cell Cycle*, **15**(**22**), 2997–2998.

Oosting, J., Struijker-Boudier, H. A. J. and Janssen, B. J. A. (1997) Autonomic control of ultradian and circadian rhythms of blood pressure, heart rate, and baroreflex sensitivity in spontaneously hypertensive rats. *Journal of Hypertension*, **15**(**4**), 401–410.

Orlov, M. Y., Brodsky, M. A. and Douban, S. (1994) A review of magnesium, acute myocardial infarction and arrhythmia. *Journal of the American College of Nutrition*, **13**(**2**), 127–132.

Oster, H., Damerow, S., Kiessling, S., Jakubcakova, V., Abraham, D., *et al.* (2006) The circadian rhythm of glucocorticoids is regulated by a gating mechanism residing in the adrenal cortical clock. *Cell Metabolism*, **4**(**2**), 163–173.

Otsuka, K., Ikari, M., Ichimaru, Y., Saito, H., Kawakami, T., *et al.* (1986) Experimental study on the relationship between cardiac arrhythmias and sleep states by ambulatory ecg-EEC monitoring. *Clinical Cardiology*, **9**(**7**), 305–313.

Patterson, E. and Scherlag, B. J. (2002) Decremental conduction in the posterior and anterior AV nodal inputs. *Journal of Interventional Cardiac Electrophysiology*, **7**(**2**), 137–148.

Patton, A. P. and Hastings, M. H. (2018) The suprachiasmatic nucleus. *Current Biology*, **28**(**15**), R816–R822.

Paul, S., Hanna, L., Harding, C., Hayter, E. A., Walmsley, L., *et al.* (2020) Output from VIP cells of the mammalian central clock regulates daily physiological rhythms. *Nature Communications*, **11**(**1**).

Paul, S. and Brown, T. M. (2019) Direct effects of the light environment on daily neuroendocrine control. *Journal of Endocrinology*, **243**(**1**), 1–18.

Pérez-Riera, A. R., Barbosa-Barros, R., Raimundo, R. D., Barbosa, M. P. da C. de R., Sorpreso, I. C. E. and Abreu, L. C. de (2018) The congenital long QT syndrome Type 3: An update. *Indian Pacing and Electrophysiology Journal*, **18**(**1**), 25.

Pezuk, P., Mohawk, J. A., Yoshikawa, T., Sellix, M. T. and Menaker, M. (2010) Circadian organization is governed by extra-SCN pacemakers. *Journal of Biological Rhythms*, **25**(**6**), 432–441.

Phillips, M. L. (2005) What makes life tick: Taking apart the living clock. *BioScience*, **55**(**11**), 928–933.

Pickard, G. E. (1982) The afferent connections of the suprachiasmatic nucleus of the golden hamster with emphasis on the retinohypothalamic projection. *Journal of Comparative Neurology*, **211**(**1**), 65–83.

Piggins, H. D., Antle, M. C. and Rusak, B. (1995) Neuropeptides phase shift the mammalian

circadian pacemaker. *Journal of Neuroscience*, **15**(**8**), 5612–5622.

Podobed, P., Alibhai, F. J., Chow, C. W. and Martino, T. A. (2014) Circadian regulation of myocardial sarcomeric Titin-cap (Tcap, telethonin): Identification of cardiac clock-controlled genes using open access bioinformatics data. *PLoS ONE*, **9**(**8**).

Podobed, P., Pyle, W. G., Ackloo, S., Alibhai, F. J., Tsimakouridze, E. V., *et al.* (2014) The day/night proteome in the murine heart. *AJP: Regulatory, Integrative and Comparative Physiology*, **307**(**2**), R121–R137.

Postema, P. and Wilde, A. (2014) Measurement of the QT interval. *Current Cardiology Reviews*, **10**, 287–294.

Pugach, E. K., Richmond, P. A., Azofeifa, J. G., Dowell, R. D. and Leinwand, L. A. (2015) Prolonged Cre expression driven by the α-myosin heavy chain promoter can be cardiotoxic. *Journal of Molecular and Cellular Cardiology*, **86**, 54–61.

Qibin, Z. and Liqing, Z. (2005) ECG feature extraction and classification using wavelet transform and support vector machines. *Proceedings of 2005 International Conference on Neural Networks and Brain Proceedings, ICNNB'05*, **2**, 1089–1092.

Raeder, E. A. (1990) Circadian fluctuations in ventricular response to atrial fibrillation. *The American Journal of Cardiology*, **66**(**12**), 1013–1016.

Ralph, M. R., Foster, R. G., Davis, F. C. and Menaker, M. (1990) Transplanted suprachiasmatic nucleus determines circadian period. *Science*, **247**(**4945**), 975–978.

Ralph, M. R., Shi, S. Q., Johnson, C. H., Houdek, P., Shrestha, T. C., *et al.* (2021) Targeted modification of the Per2 clock gene alters circadian function in mPer2luciferase (mPer2Luc) mice. *PLoS Computational Biology*, **17**(**5**), 1–31.

Randall, W. C., Ardell, J. L., Calderwood, D., Milosavljevic, M. and Goyal, S. C. (1986) Parasympathetic ganglia innervating the canine atrioventricular nodal region. *Journal of the Autonomic Nervous System*, **16**(**4**), 311–323.

Randall, W. C., Ardell, J. L., Wurster, R. D. and Milosavljevic, M. (1987) Vagal postganglionic innervation of the canine sinoatrial node. *Journal of the Autonomic Nervous System*, **20**(**1**), 13–23.

Refinetti, R. (2010) Entrainment of circadian rhythm by ambient temperature cycles in mice. *Journal of Biological Rhythms*, **25**(**4**), 247–256.

Reischl, S., Vanselow, K., Westermark, P. O., Thierfelder, N., Maier, B., *et al.* (2007) β-TrCP1-mediated degradation of PERIOD2 is essential for circadian dynamics. *Journal of Biological Rhythms*, **22**(**5**), 375–386.

Reyes del Paso, G. A., Langewitz, W., Mulder, L. J. M., van Roon, A. and Duschek, S. (2013) The utility of low frequency heart rate variability as an index of sympathetic cardiac tone: A review with emphasis on a reanalysis of previous studies. *Psychophysiology*, **50**(**5**), 477–487.

Ribeiro, R. F. N., Cavadas, C. and Silva, M. M. C. (2021) Small-molecule modulators of the circadian clock: Pharmacological potentials in circadian-related diseases. *Drug Discovery Today*, 1620–1641.

Rizzi, N., Liu, N., Napolitano, C., Nori, A., Turcato, F., *et al.* (2008) Unexpected Structural and Functional Consequences of the R33Q Homozygous Mutation in Cardiac Calsequestrin: A Complex Arrhythmogenic Cascade in a Knock in Mouse Model. *Circulation Research*, **103**(**3**), 298–306.

von Rosenberg, W., Chanwimalueang, T., Adjei, T., Jaffer, U., Goverdovsky, V. and Mandic, D. P. (2017) Resolving ambiguities in the LF/HF ratio: LF-HF scatter plots for the categorization of mental and physical stress from HRV. *Frontiers in Physiology*, **8**(**JUN**), 360.

Rosenwasser, A. M. (2010) Circadian clock genes: Non-circadian roles in sleep, addiction, and psychiatric disorders? *Neuroscience and Biobehavioral Reviews*, **34**(**8**), 1249–1255.

Roussel, J., Champeroux, P., Roy, J., Richard, S., Fauconnier, J., *et al.* (2016) The Complex QT/RR Relationship in Mice. *Scientific Reports*, **6**(**May**), 1–9.

Sabir, I. N., Killeen, M. J., Grace, A. A. and Huang, C. L. H. (2008) Ventricular arrhythmogenesis: Insights from murine models. *Progress in Biophysics and Molecular Biology*, **98**(**2**–**3**), 208–218.

Sammito, S., Sammito, W. and Böckelmann, I. (2016) The circadian rhythm of heart rate

variability. *Biological Rhythm Research*, **47**(**5**), 717–730.

Sánchez-Quintana, D., Anderson, R. H., Cabrera, J. A., Climent, V., Martin, R., *et al.* (2002) The terminal crest: Morphological features relevant to electrophysiology. *Heart*, **88**(**4**), 406–411.

Scheer, F. A. J. L., Ter Horst, G. J., Van Der Vliet, J. and Buijs, R. M. (2001) Physiological and anatomic evidence for regulation of the heart by suprachiasmatic nucleus in rats. *American Journal of Physiology - Heart and Circulatory Physiology*, **280**(**3 49**-**3**), 1391–1399.

Scheer, F. A. J. L., Pirovano, C., Van Someren, E. J. W. and Buijs, R. M. (2005) Environmental light and suprachiasmatic nucleus interact in the regulation of body temperature. *Neuroscience*, **132**(**2**), 465–477.

Scheer, F. A. J. L., Hu, K., Evoniuk, H., Kelly, E. E., Malhotra, A., *et al.* (2010) Impact of the human circadian system, exercise, and their interaction on cardiovascular function. *Proceedings of the National Academy of Sciences of the United States of America*, **107**(**47**), 20541–20546.

Scheer, F. A. J. L., van Doornen, L. J. P. and Buijs, R. M. (1999) Light and Diurnal Cycle Affect Human Heart Rate: Possible Role for the Circadian Pacemaker. *Journal of Biological Rhythms*, **14**(**3**), 202–212.

Scheer, F. A. J. L., Van Doornen, L. J. P. and Buijs, R. M. (2004) Light and diurnal cycle affect autonomic cardiac balance in human; possible role for the biological clock. *Autonomic Neuroscience: Basic and Clinical*, **110**(**1**), 44–48.

Scheer, F. A. J. L., Kalsbeek, A. and Buijs, R. M. (2003) Cardiovascular Control by the Suprachiasmatic Nucleus : Neural and Neuroendocrine Mechanisms in Human and Rat, **384**(**May**), 697–709.

Scherlac, B. J., Samet, P. and Helfant, R. H. (1972) His bundle electrogram. A critical appraisal of its uses and limitations. *Circulation*, **46**(**3**), 601–613.

Schroder, E. A., Lefta, M., Zhang, X., Bartos, D. C., Feng, H.-Z., *et al.* (2013) The cardiomyocyte molecular clock, regulation of Scn5a, and arrhythmia susceptibility. *AJP:*

Cell Physiology, **304**(**10**), 954–965.

Schroder, E. A., Burgess, D. E., Zhang, X., Lefta, M., Smith, J. L., *et al.* (2015) The cardiomyocyte molecular clock regulates the circadian expression of Kcnh2 and contributes to ventricular repolarization. *Heart Rhythm*, **12**(**6**), 1306–1314.

Schroder, E. A., Wayland, J. L., Samuels, K. M., Shah, S. F., Burgess, D. E., *et al.* (2021) Cardiomyocyte Deletion of Bmal1 Exacerbates QT- and RR-Interval Prolongation in Scn5a+/ΔKPQ Mice. *Frontiers in Physiology*, **12**, 853.

Seagard, J. L., Elegbe, E. O., Hopp, F. A., Bosnjak, Z. J., von Colditz, J. H., *et al.* (1983) Effects of isoflurane on the baroreceptor reflex. *Anesthesiology*, **59**(**6**), 511–520.

Sebastian, S., Ang, R., Abramowitz, J., Weinstein, L. S., Chen, M., *et al.* (2013) The in vivo regulation of heart rate in the murine sinoatrial node by stimulatory and inhibitory heterotrimeric G proteins. *American Journal of Physiology - Regulatory Integrative and Comparative Physiology*, **305**(**4**).

Serhani, M. A., El Kassabi, H. T., Ismail, H. and Navaz, A. N. (2020) ECG monitoring systems: Review, architecture, processes, and key challenges. *Sensors (Switzerland)*, **20**(**6**).

Sessa, F., Anna, V., Messina, G., Cibelli, G., Monda, V., *et al.* (2018) Heart rate variability as predictive factor for sudden cardiac death. *Aging*, **10**(**2**), 166–177.

Shaffer, F. and Ginsberg, J. P. (2017) An Overview of Heart Rate Variability Metrics and Norms. *Frontiers in Public Health*, **5**(**September**), 1–17.

Shaffer, F., McCraty, R. and Zerr, C. L. (2014) A healthy heart is not a metronome: an integrative review of the heart's anatomy and heart rate variability. *Frontiers in Psychology*, **5**(**September**), 1–19.

Sheward, W. J., Naylor, E., Knowles-Barley, S., Armstrong, J. D., Brooker, G. A., *et al.* (2010) Circadian control of mouse heart rate and blood pressure by the suprachiasmatic nuclei: behavioral effects are more significant than direct outputs. *PLoS ONE*, **5**(**3**), 1–9.

Shusterman, V., Usiene, I., Harrigal, C., Lee, J. S., Kubota, T., *et al.* (2002) Strain-specific patterns of autonomic nervous system activity and heart failure susceptibility in mice.

American Journal of Physiology - Heart and Circulatory Physiology, **282**(**6 51**-**6**).

Shusterman, V., Warman, E., London, B. and Schwartzman, D. (2012) Nocturnal peak in atrial tachyarrhythmia occurrence as a function of arrhythmia burden. *Journal of Cardiovascular Electrophysiology*, **23**(**6**), 604–611.

Silver, R., LeSauter, J., Tresco, P. A. and Lehman, M. N. (1996) A diffusible coupling signal from the transplanted suprachiasmatic nucleus controlling circadian locomotor rhythms. *Nature*, **382**, 810–813.

Singh, I. and Rabkin, S. W. (2021) Circadian variation of the QT interval and heart rate variability and their interrelationship. *Journal of Electrocardiology*, **65**, 18–27.

Singh, R., K. Sharma, P. and Malviya, R. (2012) Circadian Cycle and Chronotherapeutics: Recent Trend for the Treatment of Various Biological Disorders. *Recent Patents on Drug Delivery & Formulation*, **6**(**1**), 80–91.

Skene, D. J., Skornyakov, E., Chowdhury, N. R., Gajula, R. P., Middleton, B., *et al.* (2018) Separation of circadian- and behavior-driven metabolite rhythms in humans provides a window on peripheral oscillators and metabolism. *Proceedings of the National Academy of Sciences*, **115**(**30**), 7825–7830.

Skornyakov, E., Gaddameedhi, S., Paech, G. M., Sparrow, A. R., Satterfield, B. C., *et al.* (2019) Cardiac autonomic activity during simulated shift work. *Industrial health*, **57**(**1**), 118–132.

Smetana, P., Batchvarov, V., Hnatkova, K., Camm, A. J. and Malik, M. (2003) Circadian Rhythm of the Corrected QT Interval: Impact of Different Heart Rate Correction Models. *Pacing and Clinical Electrophysiology*, **26**(**1p2**), 383–386.

Soliman, E. Z. and Rautaharju, P. M. (2012) Heart rate adjustment of PR interval in middle-aged and older adults. *Journal of Electrocardiology*, **45**(**1**), 66–69.

Son, G. H., Chung, S., Choe, H. K., Kim, H. D., Baik, S. M., *et al.* (2008) Adrenal peripheral clock controls the autonomous circadian rhythm of glucocorticoid by causing rhythmic steroid production. *Proceedings of the National Academy of Sciences of the United States of America*, **105**(**52**), 20970–20975.

Souza, B. B., Monteze, N. M., De Oliveira, F. L. P., De Oliveira, J. M., De Freitas, S. N., *et al.* (2015) Lifetime shift work exposure: Association with anthropometry, body composition, blood pressure, glucose and heart rate variability. *Occupational and Environmental Medicine*, **72**(**3**), 208–215.

Speerschneider, T. and Thomsen, M. B. (2013) Physiology and analysis of the electrocardiographic T wave in mice. *Acta Physiologica*, **209**(**4**), 262–271.

Stangherlin, A., Wong, D., Barbiero, S., Watson, J., Zeng, A., *et al.* (2020) Compensatory ion transport buffers daily protein rhythms to regulate osmotic balance and cellular physiology. *bioRxiv*.

Steg, P. G., James, S. K., Atar, D., Badano, L. P., Lundqvist, C. B., *et al.* (2012) ESC Guidelines for the management of acute myocardial infarction in patients presenting with ST-segment elevation. *European Heart Journal*, **33**(**20**), 2569–2619.

Steinbach, K., Glogar, D., Weber, H., Joskowicz, G. and Kaindl, F. (1982) Frequency and Variability of Ventricular Premature Contractions—The Influence of Heart Rate and Circadian Rhythms. *Pacing and Clinical Electrophysiology*, **5**(**1**), 38–51.

Steinley, D. (2006) K-means clustering: A half-century synthesis. *British Journal of Mathematical and Statistical Psychology*, **59**(**1**), 1–34.

Stephen, F. K. and Irving, Z. (1972) Circadian Rhythms in Drinking Behavior and Locomotor Activity of Rats Are Eliminated by Hypothalamic Lesions. *Proceedings of the National Academy of Sciences of the United States of America*, **69**(**6**), 1583–1586.

Stock, J. T. (2004) Gabriel Lippmann and the capillary electrometer. *Bull. Hist. Chem*, **29**(**1**), 16–20.

Stöhr, E. J., Shave, R. E., Baggish, A. L. and Weiner, R. B. (2016) Left ventricular twist mechanics in the context of normal physiology and cardiovascular disease: a review of studies using speckle tracking echocardiography. *American Journal of Physiology - Heart and Circulatory Physiology*, **311**(**3**), H633–H644.

Stokkan, K. A., Yamazaki, S., Tei, H., Sakaki, Y. and Menaker, M. (2001) Entrainment of the circadian clock in the liver by feeding. *Science*, **291**(**5503**), 490–493.

Storch, K.-F., Lipan, O., Leykin, I., Viswanathan, N., Davis, F. C., *et al.* (2002) Extensive and divergent circadian gene expression in liver and heart. *Nature*, **417**(**6884**), 78–83.

Storch, K. F., Paz, C., Signorovitch, J., Raviola, E., Pawlyk, B., *et al.* (2007) Intrinsic circadian clock of the mammalian retina: importance for retinal processing of visual information. *Cell*, **130**(**4**), 730–741.

Struthers, A. D., Reid, J. L., Whitesmith, R. and Rodger, J. C. (1983) Effect of intravenous adrenaline on electrocardiogram, blood pressure, and serum potassium. *British Heart Journal*, **49**(**1**), 90–93.

Studholme, K. M., Gompf, H. S. and Morin, L. P. (2013) Brief light stimulation during the mouse nocturnal activity phase simultaneously induces a decline in core temperature and locomotor activity followed by EEG-determined sleep. *AJP: Regulatory, Integrative and Comparative Physiology*, **304**(**6**), 459–471.

Sujino, M., Masumoto, K., Yamaguchi, S., van der Horst, G. T., Okamura, H. and Inouye, S.-I. T. (2003) Suprachiasmatic Nucleus Grafts Restore Circadian Behavioral Rhythms of Genetically Arrhythmic Mice. *Current Biology*, **13**, 664–668.

Sun, Z., Wang, L., Han, L., Wang, Y., Zhou, Y., *et al.* (2021) Functional Calsequestrin-1 Is Expressed in the Heart and Its Deficiency Is Causally Related to Malignant Hyperthermia-Like Arrhythmia. *Circulation*, **144**(**10**), 788–804.

Sweeney, H. L. and Hammers, D. W. (2018) Muscle contraction. *Cold Spring Harbor Perspectives in Biology*, **10**(**2**), a023200.

Swoap, S. J., Li, C., Wess, J., Parsons, A. D., Williams, T. D. and Overton, J. M. (2008) Vagal tone dominates autonomic control of mouse heart rate at thermoneutrality. *AJP: Heart and Circulatory Physiology*, **294**(**4**), H1581–H1588.

Swoap, S. J., Overton, J. M. and Garber, G. (2004) Effect of ambient temperature on cardiovascular parameters in rats and mice: A comparative approach. *American Journal of Physiology - Regulatory Integrative and Comparative Physiology*, **287**(**2 56**-**2**), 391–396.

Takahashi, J. S., Hong, H. K., Ko, C. H. and McDearmon, E. L. (2008) The genetics of mammalian circadian order and disorder: Implications for physiology and disease. *Nature*

Reviews Genetics, **9**(**10**), 764–775.

Takahashi, J. S. (2017) Transcriptional architecture of the mammalian circadian clock. *Nature Reviews Genetics*, **18**(**3**), 164–179.

Takigawa, M., Kawamura, M., Noda, T., Yamada, Y., Miyamoto, K., *et al.* (2012) Seasonal and Circadian Distributions of Cardiac Events in Genotyped Patients With Congenital Long QT Syndrome. *Circulation Journal*, **76**.

Tamil, E. M., Kamarudin, N. H., Salleh, R., Idris, M. Y. I., Noor, M. and Tamil, A. M. (2008) Heartbeat Electrocardiogram (ECG) signal feature extraction using Discrete Wavelet Transforms (DWT). *Cspa (2008)*, 1112–1117.

Tanaka, S. and Tsuchida, H. (1998) Effects of halothane and isoflurane on β-adrenoceptor-mediated responses in the vascular smooth muscle of rat aorta. *Anesthesiology*, **89**(**5**), 1209–1217.

Temple, I. P., Inada, S., Dobrzynski, H. and Boyett, M. R. (2013) Connexins and the atrioventricular node. *Heart Rhythm*, **10**(**2**), 297–304.

Tharp, G. D. (1965) Rhythmic Changes In Rate Of The Mamalian Heart And Heart Cells During Prolonged Isolation. *University of Iowa ProQuest Dissertations publishing*.

Thayer, J. F., Yamamoto, S. S. and Brosschot, J. F. (2010) The relationship of autonomic imbalance, heart rate variability and cardiovascular disease risk factors. *International Journal of Cardiology*, **141**(**2**), 122–131.

Thompson, S., Lupi, D., Hankins, M. W., Peirson, S. N. and Foster, R. G. (2008) The effects of rod and cone loss on the photic regulation of locomotor activity and heart rate. *European Journal of Neuroscience*, **28**(**4**), 724–729.

Thomsen, M. B. and Calloe, K. (2016) Human atrial fibroblasts and their contribution to supraventricular arrhythmia. *Physiological Reports*, **4**(**3**).

Tofler, G. H., Gebara, O. C. E., Mittleman, M. A., Taylor, P., Siegel, W., *et al.* (1995) Morning Peak in Ventricular Tachyarrhythmias Detected by Time of Implantable Cardioverter/Defibrillator Therapy. *Circulation*, **92**(**5**), 1203–1208.

Toman, O., Hnatkova, K., Smetana, P., Huster, K. M., Šišáková, M., *et al.* (2020) Physiologic

heart rate dependency of the PQ interval and its sex differences. *Scientific Reports*, **10**(**1**), 1–17.

Tong, M., Watanabe, E., Yamamoto, N., Nagahata-Ishiguro, M., Maemura, K., *et al.* (2013) Circadian expressions of cardiac ion channel genes in mouse might be associated with the central clock in the SCN but not the peripheral clock in the heart. *Biological Rhythm Research*, **44**(**4**), 519–530.

Torquati, L., Mielke, G. I., Brown, W. J. and Kolbe-Alexander, T. (2018) Shift work and the risk of cardiovascular disease. A systematic review and meta-analysis including dose-response relationship. *Scandinavian Journal of Work, Environment and Health*, **44**(**3**), 229–238.

Tsai, J. Y., Kienesberger, P. C., Pulinilkunnil, T., Sailors, M. H., Durgan, D. J., *et al.* (2010) Direct regulation of myocardial triglyceride metabolism by the cardiomyocyte circadian clock. *Journal of Biological Chemistry*, **285**(**5**), 2918–2929.

Tur, J., Chapalamadagu, K. C., Manickam, R., Cheng, F. and Tipparaju, S. M. (2021) Deletion of kvβ2 (Akr6) attenuates isoproterenol induced cardiac injury with links to solute carrier transporter slc41a3 and circadian clock genes. *Metabolites*, **11**(**4**).

Twidale, N., Taylor, S., Heddle, W. F., Ayres, B. F. and Tonkin, A. M. (1989) Morning increase in the time of onset of sustained ventricular tachycardia. *The American Journal of Cardiology*, **64**(**18**), 1204–1206.

Ueda, H. R., Hayashi, S., Chen, W., Sano, M., Machida, M., *et al.* (2005) System-level identification of transcriptional circuits underlying mammalian circadian clocks. *Nature Genetics*, **37**(**2**), 187–192.

Vandeput, S., Verheyden, B., Aubert, A. E. and Van Huffel, S. (2012) Nonlinear heart rate dynamics: circadian profile and influence of age and gender. *Medical Engineering & Physics*, **34**(**1**), 108–117.

Vandewalle, G., Middleton, B., Rajaratnam, S. M. W., Stone, B. M., Thorleifsdottir, B., *et al.* (2007) Robust circadian rhythm in heart rate and its variability: Influence of exogenous melatonin and photoperiod. *Journal of Sleep Research*, **16**(**2**), 148–155.

Veldkamp, M. W., Verkerk, A. O., Van Ginneken, A. C. G., Baartscheer, A., Schumacher, C., *et al.* (2001) Norepinephrine induces action potential prolongation and early afterdepolarizations in ventricular myocytes isolated from human end-stage failing hearts. *European Heart Journal*, **22**(**11**), 955–963.

Venetucci, L. A., Trafford, A. W., O'Neill, S. C. and Eisner, D. A. (2008) The sarcoplasmic reticulum and arrhythmogenic calcium release. *Cardiovascular Research*, 285–292.

Verheule, S. and Kaese, S. (2013) Connexin diversity in the heart: insights from transgenic mouse models. *Frontiers in Pharmacology*, **4**, 1–14.

Verweij, N., Leach, I. M., Van Den Boogaard, M., Van Veldhuisen, D. J., Christoffels, V. M., *et al.* (2014) Genetic Determinants of P Wave Duration and PR Segment. *Circulation: Cardiovascular Genetics*, **7**(**4**), 475–481.

Vigmond, E. J. and Stuyvers, B. D. (2016) Modeling our understanding of the His-Purkinje system. *Progress in Biophysics and Molecular Biology*, **120**(**1**–**3**), 179–188.

Vitaterna, M. H., King, D. P., Chang, A. M., Kernhauser, J. M., Lowrey, P. L., *et al.* (1994) Mutagenesis and mapping of a mouse gene, clock, essential for circadian behavior. *Science*, **264**(**5159**), 719–725.

Vizi, E. and Knoll, J. (1971) The effects of sympathetic nerve stimulation and guanethidine on parasympathetic neuroeffector transmission; the inhibition of acetylcholine release. *Journal of Pharmacy and Pharmacology*, **23**(**12**), 918–925.

Vollmer, M. (2015) A robust, simple and reliable measure of heart rate variability using relative RR intervals. *Computing in Cardiology*, **42**(**6**), 609–612.

Vollmer, M. (2019) HRVTool - an Open-Source Matlab Toolbox for Analyzing Heart Rate Variability. *2019 Computing in Cardiology Conference (CinC)*, **45**, 1–4.

Vyas, M. V., Garg, A. X., Iansavichus, A. V., Costella, J., Donner, A., *et al.* (2012) Shift work and vascular events: Systematic review and meta-analysis. *BMJ*, **345**(**7871**), 1–11.

Walden, A. P., Dibb, K. M. and Trafford, A. W. (2009) Differences in intracellular calcium homeostasis between atrial and ventricular myocytes. *Journal of Molecular and Cellular Cardiology*, **46**(**4**), 463–473.

Walker, M. J. A., Curtis, M. J., Hearse, D. J., Campbell, R. W. F., Janse, M. J., *et al.* (1988) The lambeth conventions: guidelines for the study of arrhythmias in ischaemia, infarction, and reperfusion. *Cardiovascular Research*, **22**(**7**), 447–455.

Walmsley, L., Hanna, L., Mouland, J., Martial, F., West, A., *et al.* (2015) Colour As a Signal for Entraining the Mammalian Circadian Clock. *PLoS Biology*, **13**(**4**), e1002127.

Wang, N., Sun, Y., Zhang, H., Wang, B., Chen, C., *et al.* (2021) Long-term night shift work is associated with the risk of atrial fibrillation and coronary heart disease. *European Heart Journal*, **0**(**0**), 1–10.

Wang, Y., Anderson, C., Dobrzynski, H., Hart, G., D'Souza, A. and Boyett, M. R. (2021) RNAseq shows an all-pervasive day-night rhythm in the transcriptome of the pacemaker of the heart. *Scientific Reports 2021 11:1*, **11**(**1**), 1–18.

Warren, W. S., Champney, T. H. and Cassone, V. M. (1994) The suprachiasmatic nucleus controls the circadian rhythm of heart rate via the sympathetic nervous system. *Physiology and Behavior*, **55**(**6**), 1091–1099.

Watanabe, K., Vanecek, J. and Yamaoka, S. (2000) In vitro entrainment of the circadian rhythm of vasopressin-releasing cells in suprachiasmatic nucleus by vasoactive intestinal polypeptide. *Brain Research*, **877**(**2**), 361–366.

Webb, A. B., Angelo, N., Huettner, J. E. and Herzog, E. D. (2009) Intrinsic, nondeterministic circadian rhythm generation in identified mammalian neurons. *Proceedings of the National Academy of Sciences of the United States of America*, **106**(**38**), 16493–16498.

Wehrens, S. M. T., Hampton, S. M., Finn, R. E. and Skene, D. J. (2010) Effect of total sleep deprivation on postprandial metabolic and insulin responses in shift workers and non-shift workers. *Journal of Endocrinology*, **206**(**2**), 205–215.

Wehrens, S. M. T., Hampton, S. M. and Skene, D. J. (2012) Heart rate variability and endothelial function after sleep deprivation and recovery sleep among male shift and non-shift workers. *Scandinavian Journal of Work, Environment and Health*, **38**(**2**), 171–181.

Welsh, D. K., Yoo, S.-H. H., Andrew, L. C., Takahashi, J. S., Kay, S. A., *et al.* (2004)

Bioluminescence imaging of individual fibroblasts reveals persistent, independently phased circadian rhythms of clock gene expression. *Current Biology*, **14**(**24**), 2289–2295.

Welsh, D. K., Takahashi, J. S. and Kay, S. A. (2010) Suprachiasmatic Nucleus: Cell Autonomy and Network Properties. *Annual Review of Physiology*, **72**(**1**), 551–577.

West, A. C., Smith, L., Ray, D. W., Loudon, A. S. I., Brown, T. M. and Bechtold, D. A. (2017) Misalignment with the external light environment drives metabolic and cardiac dysfunction. *Nature Communications*, **8**, 417.

West, A. C. and Bechtold, D. A. (2015) The cost of circadian desynchrony: Evidence, insights and open questions. *BioEssays : news and reviews in molecular, cellular and developmental biology*, **37**(**7**), 777–88.

Widran, J. and Lev, M. (1951) The dissection of the atrioventricular node, bundle and bundle branches in the human heart. *Circulation*, **4**(**6**), 863–867.

Wilde, A. A. M. and Bezzina, C. R. (2005) Genetics of cardiac arrhythmias. *Heart*, **91**(**10**), 1352.

Willich, S. N., Levy, D., Rocco, M. B., Tofler, G. H., Stone, P. H. and Muller, J. E. (1987) Circadian variation in the incidence of sudden cardiac death in the framingham heart study population. *The American Journal of Cardiology*, **60**(**10**), 801–806.

Wilson, F. N., Kossmann, C. E., Burch, G. E., Goldberger, E., Graybiel, A., *et al.* (1954) Recommendations for standardization of electrocardiographic and vectorcardiographic leads. *Circulation*, **10**(**4**), 564–573.

Wirz-Justice, A., Daan, S., Folkard, S., Lewy, A., Lund, R. and Zulley, J. (2005) Rütger Wever: An Appreciation. *Journal of Biological Rhythms*, **20**(**6**), 554–555.

Woo, J. S., Jeong, S. Y., Park, J. H., Choi, J. H. and Lee, E. H. (2020) Calsequestrin: a well-known but curious protein in skeletal muscle. *Experimental & Molecular Medicine 2020 52:12*, **52**(**12**), 1908–1925.

Wright, K. P., Bogan, R. K. and Wyatt, J. K. (2013) Shift work and the assessment and management of shift work disorder (SWD). *Sleep Medicine Reviews*, **17**(**1**), 41–54.

Wu, J., Ding, W.-G. and Horie, M. (2016) Molecular pathogenesis of long QT syndrome

type 1. *Journal of Arrhythmia*, **32**(**5**), 381.

Wyse, C. A., Coogan, A. N., Selman, C., Hazlerigg, D. G. and Speakman, J. R. (2010) Association between mammalian lifesPan and circadian free-running period: The circadian resonance hypothesis revisited. *Biology Letters*, **6**(**5**), 696–698.

Xu, H., Huang, L., Zhao, J., Chen, S., Liu, J. and Li, G. (2021) The circadian clock and inflammation: A new insight. *Clinica Chimica Acta*, **512**, 12–17.

Yamaguchi, S., Isejima, H., Matsuo, T., Okura, R., Yagita, K., *et al.* (2003) Synchronization of Cellular Clocks in the Suprachiasmatic Nucleus. *Science*, **302**(**5649**), 1408–1412.

Yamazaki, S., Numano, R., Abe, M., Hida, A., Takahashi, R. I., *et al.* (2000) Resetting central and peripheral circadian oscillators in transgenic rats. *Science*, **288**(**5466**), 682–685.

Yang, G., Chen, L., Grant, G. R., Paschos, G., Song, W. L., *et al.* (2016) Timing of expression of the core clock gene Bmal1 influences its effects on aging and survival. *Science Translational Medicine*, **8**(**324**), 324ra16.

Yi, G., Guo, X. H., Reardon, M., Gallagher, M. M., Hnatkova, K., *et al.* (1998) Circadian variation of the QT interval in patients with sudden cardiac death after myocardial infarction. *American Journal of Cardiology*, **81**(**8**), 950–956.

Yoo, S.-H., Yamazaki, S., Lowrey, P. L., Shimomura, K., Ko, C. H., *et al.* (2004) PERIOD2::LUCIFERASE real-time reporting of circadian dynamics reveals persistent circadian oscillations in mouse peripheral tissues. *Proceedings of the National Academy of Sciences*, **101**(**15**), 5339–5346.

Yoo, S. H., Ko, C. H., Lowrey, P. L., Buhr, E. D., Song, E. J., *et al.* (2005) A noncanonical E-box enhancer drives mouse Period2 circadian oscillations in vivo. *Proceedings of the National Academy of Sciences of the United States of America*, **102**(**7**), 2608–2613.

Young, M., Brewer, R., Peliciari-garcia, R., Collins, H., He, L., *et al.* (2014) Cardiomyocyte-Specific BMAL1 Plays Critical Roles in Metabolism , Signaling , and Maintenance of Contractile Function of the Heart, **29**(**4**), 257–276.

Young, M. E. (2016) Temporal Partitioning of Cardiac Metabolism by the Cardiomyocyte Circadian Clock. *Experimental physiology*, **101**(**8**), 1035.

Young, M. E. and Bray, M. S. (2007) Potential role for peripheral circadian clock dyssynchrony in the pathogenesis of cardiovascular dysfunction. *Sleep Medicine*, **8**(**6**), 656–667.

Zhang, J., Chatham, J. and Young, M. E. (2020) Circadian regulation of cardiac physiology: rhythms that keep the heart beating. *Annual Review of Physiology*, **82**(**1**), 1–23.

Zhang, R., Lahens, N. F., Ballance, H. I., Hughes, M. E. and Hogenesch, J. B. (2014) A circadian gene expression atlas in mammals: Implications for biology and medicine. *Proceedings of the National Academy of Sciences*, **111**(**45**), 16219–16224.

Zhang, Z., Hunter, L., Wu, G., Maidstone, R., Mizoro, Y., *et al.* (2019) Genome-wide effect of pulmonary airway epithelial cell–specific Bmal1 deletion. *FASEB Journal*, **33**(**5**), 6226–6238.

Zheng, X. and Sehgal, A. (2012) Speed control: Cogs and gears that drive the circadian clock. *Trends in Neurosciences*, **35**(**9**), 574–585.

Zhu, Y., Hanafy, M. A., Killingsworth, C. R., Walcott, G. P., Young, M. E. and Pogwizd, S. M. (2014) Morning surge of ventricular arrhythmias in a new arrhythmogenic canine model of chronic heart failure is associated with attenuation of time-of-day dependence of heart rate and autonomic adaptation, and reduced cardiac chaos. *PLoS ONE*, **9**(**8**), e105379.

Zoccal, D. B., Furuya, W. I., Bassi, M., Colombari, D. S. A. and Colombari, E. (2014) The nucleus of the solitary tract and the coordination of respiratory and sympathetic activities. *Frontiers in Physiology*, **5**, 1–12.

6.9 Appendix A

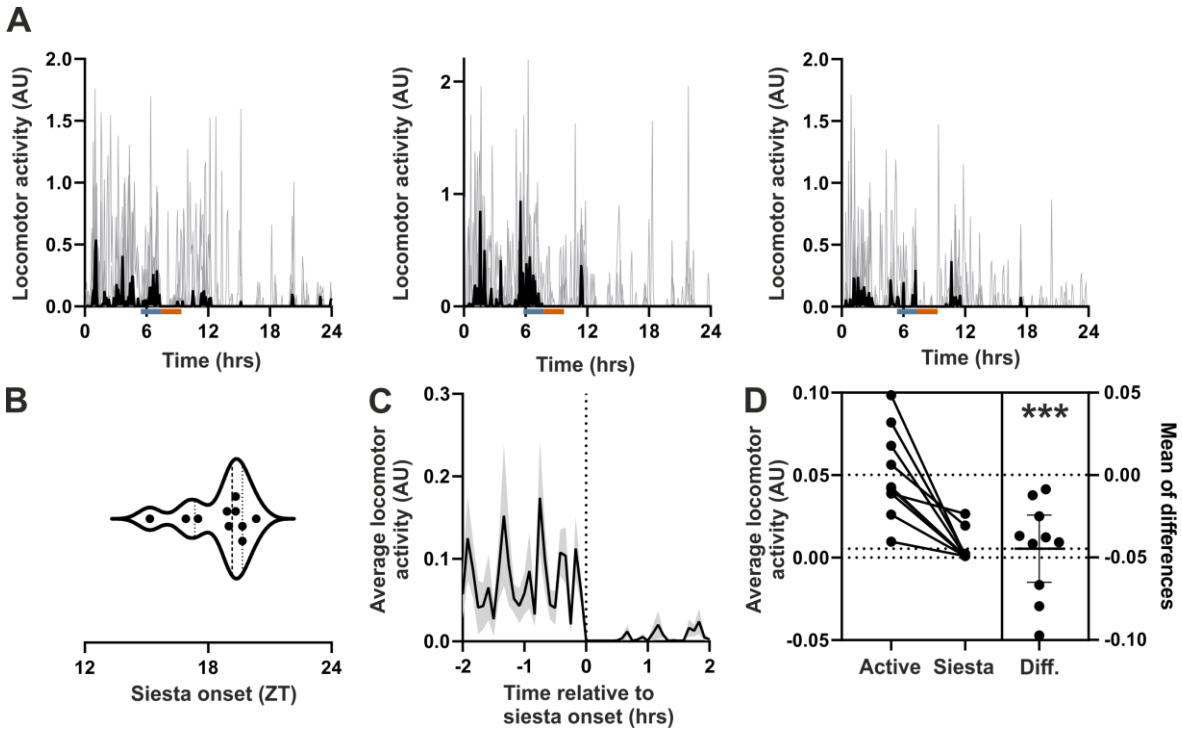

Figure A1. Mouse locomotor activity and siesta measured by DSI radio telemetry. A Representative locomotor activity traces of individual animals across 5 days baseline recording. Grey lines show individual days and black overlay represent the median across the recording period. Inset bars represent the calculated 2hr siesta recording period (orange) and preceding recording window of locomotor activity (blue). **B**. Violin plot of siesta onsets. Individual points represent single animals and vertical lines the median, 25th and 75th percentile. **C**. Average locomotor activity across animals relative to siesta onset. Grey shading represents SEM. **D**. Average locomotor activity during 'active' and 'siesta' windows. Paired T-test, $p<0.001$.